Phosphorus Cycling under different redox conditions

Yijun Xiong

Submitted in accordance with the requirements for the degree of
Doctor of Philosophy

The University of Leeds
Earth Surface Science Institute
School of Earth and Environment

April, 2018

The candidate confirms that the work submitted is his/her own and that appropriate credit has been given where reference has been made to the work of others.

Acknowledgement

Firstly, I must thank for Professor Simon Poulton's help. In this four years' PhD life, he not only gives a big help in my study, but also organizes a lot of amazing social activities to make my life colourful! Secondly, I must thank for Romain Guilboud. Although he is strict in the lab, without his help, I can not get so incredible data from the 'nasty' samples and design the complex experiments, similarly he teaches me as the artist to treat the lab work. Finally, I also thank for my last two supervsiors, Mike Krom and Caroline Peacock. When I face to the barrier in the work, you both give useful suggestions in time which sometimes are more helpful.

I also should thank for all the technical staff. As a chemist, I know that without you, the experiment and the heavy lab work can not be finished in such a short time. Leslsy always solves the problems of XRD for me, Steven measures lots of solutions for me, and Andy Connelly nearly solves all the difficulties in the lab for me!

Here, I know that without my friends' encourage and help, I also could not finish my PhD. My scientific 'sisters', Jennifer Thompson and Katherine Doyle, do a lot of supports both in my life and studies. My best scientific 'cousins', Aislinn Boylan and Andy Bray, always give me useful suggestions when I am struggling in my life and research. During these about 5 years' PhD life, I am appreciated that I have such important friends like you which make me not feel alone abroad.

I also should thank all the members in my family, especially for my parents and my uncles. Without the funding support from you, I even could not start my PhD research. I am very appreciated that all of you support my own dream without any complains, and now I am sure that I do not let you down. Finally, I would like to thank for my wife, Miao Cai, I always think that sending you to change my simple bachelor life is the best gift from god although it also delays my graduation time.

Finally, I would like to thank for my viva examiners, Christian März and Aubrey Zerkle. Your suggestions are very important for my current and future research, and I am very happy to have such an important discussion in my project during these four and a half hours.

Thank all of you very much!

Abstract

Phosphorus is a basic but essential nutrient element for life, as a major limiting nutrient, is also important for controlling primary productivity on geological timescales. However, P cycling is highly redox dependent through Earth history. The fate of P cycling in many environments is still not clear. This thesis is to investigate mineralogical controls on P cycling under different redox conditions. New geochemical data is reported in the low sulfate, euxinic Lake Cadagno, Switzerland, to investigate the behaviour of the phosphorus cycle. Sulfide-driven release of phosphorus from organic matter and Fe (oxyhydr)oxide minerals is re-trapped by Fe(II) phosphate to constrain the extent of P recycling, and this process is highly sulfate dependent. New experiments are designed to investigate what minerals control P cycling in the water column under different conditions. With the increase of P, Green rust is transformed to vivianite which shows that P concentrations exert first order controls on the mineralogy of Fe minerals, with strong implications for the availability of dissolved P in the water column. In order to quantify the extent of P cycling versus fixation in the sediments under different redox conditions, mass balance models are made based on 4 key redox scenarios. Analogous to those which were prevalent at various intervals in Earth history, under ancient episodes of ferruginous conditions, low flux of recycled P back to water column is controlled by both P re-uptake by Fe(III) (oxyhydr)oxide and the formation of Fe(II) phosphate. During the mid-Proterozoic and during Phanerozoic, under low sulfate euxinia, the flux of recycled P is constrained by Fe(II) phosphate formation. This study provides supporting evidence to the suggestion that the positive primary productivity feedback is constrained by these processes.

Table of Contents

Contents

List of Tables

List of Figures

Chapter 1 Introduction

1.1 Introduction to the phosphorus cycle

Phosphorus is a basic but essential nutrient element for life. It is irreplaceable in biochemical reactions of all organisms, for example, processes involving energy and genetic material transfer, and in the compounds which provide structural support to membranes and bone constituent (Westheimer, 1987). The availability of phosphorus is also important for biological productivity in both terrestrial and aquatic systems (e.g., Fogg, 1973; Bieleski and Ferguson, 1983 and Cembella et al., 1984a, 1984b). In general, it is difficult for P to be used by organisms via direct uptake, as particulate P which is locked in soils, lithified sediments and crystalline rocks cannot be used directly. However, the cycling of P is largely governed by biogeochemical reactions. In particular, the most abundant P-bearing mineral is apatite ($Ca_{10}(PO_4)_6(OH,F,Cl)_2$ (Ruttenberg, 2003) which is the most important source of P during continental weathering, allowing P to be transferred from terrestrial to oceanic settings, often as the result of microbial activity, such as the erosion of exposed minerals by naturally occurring acids (e.g., Cosgrove, 1977; and Likens et al., 1977 and Frossard et al., 1995).

In the marine system, there are four particularly important forms of P – organic P (P_{org}), authigenic Ca-P (P_{auth}), ferric iron bound P (P_{Fe}) and detrital apatite (P_{detr}) (e.g., Froelich et al., 1982; Filippelli, 1997a, b; Ruttenberg, 1993; Wheat et al., 1996). Furthermore, the first three particulate phases are reactive in the early diagenesis which is controlled by the biogeochemical processes, however, the detrital apatite is a refractory phase which is precipitated and does not undergo any biogeochemical reactions before deposition on the seabed. Over the last 3 decades, the extent to which bioavailable P may be trapped in the sediment or recycled back to the water column has been shown to be highly redox dependent (e.g., Slomp and Van Raaphorst, 1993; Ingall and Jahnke, 1994; 1997; Slomp et al., 1996 a, b; 2002; 2004; Dellwig et al., 2010). In addition, several recent studies have demonstrated that ferrous phosphate minerals may also be an important sink for reactive phosphorus during early diagenesis (e.g., Jilbert and Slomp, 2013; Dijkstra et al., 2014; 2016; Rothe et al., 2014; Joshi et al., 2015; O'Connell et al., 2015). Despite many studies focusing on the cycling of biogeochemical P in aquatic environments, the fate of P in some environments that might be considered analogous to ancient oceanic settings, such as under low sulfate euxinic conditions, is still not clear.

Furthermore, the fate of P in the redoxcline of anoxic water columns in general is not well understood. Finally, little quantitative information is available regarding the extent to which P may be fixed in the sediment or recycled back to the water column under different redox conditions.

Phosphorus transfers from the continents to the ocean through atmospheric, ground water and riverine fluxes. The deposition of atmospheric aerosols to surface ocean is considered relatively minor, while the ground water flux is poorly defined, but the riverine flux is considered the most important source for the transport of P from the continents to the ocean, with a global flux of $0.622 – 0.708 \times 10^{12}$ mol/y (Lerman et al., 1975; Richey, 1983; Mackenzie et al., 1993). The riverine phosphorus weathered from rocks and soils forms two basic forms – particulate P and dissolved P. Over 90% of the flux of P to the ocean is as particulate P, of which ~20 - 40% is organic, while the remaining inorganic P is partitioned between ferric oxyhydroxides and detrital apatite (Lucotte and D'Anglejan, 1983; Lebo, 1991; Berner and Rao, 1994; Ruttenberg and Canfield, 1994), or is carried by aluminium oxyhydroxides and clays (Lebo, 1991). For the dissolved P flux, more than 50% is present in organic forms, while the rest is inorganic (Meybeck, 1982).

The primary aim of this thesis concerns P cycling in different redox conditions in the water column and sediments. The thesis consists of three core data chapters. The first chapter investigates P cycling in a stratified lake with low sulfate concentrations. New data is provided to give ideas about the controls on P cycling, with the lake considered as a mid-Precambrian sulfidic ocean analogue. The second data chapter is based on laboratory experiments designed to evaluate chemical controls on the formation of vivianite versus green rust. The aim here is to evaluate potential controls on the nature of P cycling at the redoxcline of ancient anoxic water columns under different chemical conditions. The third data chapter involves modelling the nature of P cycling in sediments deposited under different water column redox conditions. This has led to consideration of global P cycling under oxic, nitrogenous (nitrate reducing), ferruginous (anoxic Fe-containing) and euxinic (anoxic and sulfidic) conditions. The remainder of this introduction provides an overview of the global P cycle, how P cycling is dependent on different redox conditions, and what is currently known about P cycling through Earth history.

1.2 Importance of the P cycle

P is a major limiting nutrient that has often controlled primary productivity in the oceans through Earth's history. The source of P to the ocean is generally considered more restricted than nitrogen, as it only originates from the weathering of continental material, whereas N is also supplied in great abundance via microbial fixation of atmospheric N_2 (Cosgrove, 1977; Frossard et al., 1995). Thus external P inputs are generally considered to control longer-term primary production in the global ocean, rather than N (Howarth, 1988; Tyrell, 1999).

There is a close connection between P and carbon in biogeochemical cycles. The link is through uptake of P during photosynthetic (Eq. 1) and release during respiration (Eq. 2) (Schindler, 1970; Tarapchak and Nawelajko, 1986; Hecky and Kilham, 1988):

$$106CO_2 + 64H_2O + 16NH_3 + H_3PO_4 \rightarrow C_{106}H_{179}O_{68}N_{16}P + 106O_2 \text{ (Eq. 1)}$$

$$C_{106}H_{179}O_{68}N_{16}P + 106O_2 \rightarrow 106CO_2 + 64H_2O + 16NH_3 + H_3PO_4 \text{ (Eq. 2)}$$

Specifically, carbon fixation during photosynthesis is accompanied with the utilisation of nutrient P and N. Phosphorus is then released through microbial respiration which is also called 'mineralization'. Furthermore, organic P is transformed into inorganic P such as phosphate, with oxygen acting as the electron acceptor used by microbial communities.

P, as the ultimate limited nutrient, plays a key role in controlling photosynthesis, which consumes surface oceanic CO_2 to form organic matter, thus controlling the concentration of the greenhouse gas CO_2 and exerting a control on climate, for example on more recent glacial-interglacial timescales (Broecker, 1982; Boyle, 1990; Ganeshram et al., 2002; Tamburini et al., 2003).

There is also a close link between P and oxygen cycling. As mentioned before, dissolved P plays a key role in oxygenic photosynthesis, which generally produces oxygen (Eq. 1). However, with increasing oxygen, unstable ferrous iron which may have been abundant in ancient ferruginous water columns (Poulton and Canfield, 2011) is oxidized to form ferric iron oxyhydroxide minerals. These minerals may then act as an important trap (via adsorption and co-precipitation) for dissolved P, which would thus impart a negative feedback on oxygenic photosynthesis. This could have helped to maintain the low levels of atmospheric O_2 envisaged for much of Earth's history (Kump, 1988; Berner and Canfield, 1989; VanCappellen and Ingall, 1994a, b; Colman et al., 1997; Petsch and Berner, 1998; Reinhard et al., 2017). As some oxygen was

required for early animal evolution, the size of the marine phosphate reservoir likely played an important role in the evolution of the biosphere (Holland, 2006). For example, the severe limits on eukaryote diversity and abundance through the Precambrian are commonly attributed to low levels of oxygen, partially caused by P limitation (Lyons et al., 2014). Indeed, the late emergence and diversification of metazoans has been attributed to very low atmospheric oxygen through the Mid-proterozic (Planavsky et al., 2014). Although many studies indicate that enhanced loss of N delays the oxidation of the atmosphere in the mid-Proterozoic (Anbar and Knoll, 2002; Fennel et al., 2005; Canfield et al., 2006; Scott et al., 2008; but also see Zerkle et al., 2006), recent isotopic studies of the mid-Proterozoic N cycle suggest that bioavailable nitrate was likely abundant in near-shore environments (Godfrey et al., 2013; Stüeken, 2013; Koehler et al., 2017), while research on modern ferruginous systems implies that large expanses of the mid-Proterozoic ocean were likely P, and not N, limited (Michiels et al., 2017).

In sum, P, as a major limiting nutrient, is important for controlling primary productivity on geological timescales. It limits the formation of organic carbon production and ultimately oxygenation, with strong links to biological evolution.

1.3 The global P cycle

Three components of the global phosphorus cycle are described here, including mass reservoirs and fluxes. These are the terrestrial phosphorus cycle, transport of P from continents to the ocean and the marine P cycle.

In the global terrestrial cycle, P is controlled by the weathering from solid P to dissolved P (e.g. Cosgrove, 1977; and Likens et al., 1977 and Frossard et al., 1995), the flux of which is 2.03×10^{12} to 6.45×10^{12} mol/yr (Lerman et al., 1975; Richey, 1983; Jahnke, 1992; Mackenzie et al., 1993). Here, the most abundant P-bearing mineral in crustal rocks is apatite which includes igneous fluorapatites and marine sedimentary carbonate fluorapatites (CFA) (McConnell, 1973; Jarvis et al., 1994; Jahnke, 1992). The dissolution rates of these two minerals are controlled by pH and CO_2 concentrations. Specifically, the dissolution rates decrease with increasing pH, and there is a negative relationship between dissolution kinetics and CO_2 concentration, with rates highest at low CO_2 concentrations (Guidry and Mackenzie, 2000). The uptake of P by terrestrial plants returns P to the soil through the decay of litterfall (e.g. Likens et al., 1977). Part of dissolved P in the soil is also controlled by oxide minerals, such as ferric iron and

aluminium oxyhydroxide. P sorption on these plays a key role in maintaining low levels of dissolved P (Lajtha and Harrison, 1995). With the cycling of P during burial, the reservoir fate of P also changes with time. At the beginning, P is commonly formed as phosphorus-bearing minerals; after long periods of biogeochemical cycling, more and more reactive phosphorus-bearing minerals are switched to organic P, thus the reservoirs for P change to organic P and refractory phosphorus-bearing minerals. (Walker and Syers, 1976). The reservoir size of P on the land is 3100×10^{12} - 6450×10^{12} mole, here the land ≈ total soil <60 cm deep (Lerman et al., 1975; Richey, 1983; Jahnke, 1992; Mackenzie et al., 1993).

The P transferred from the continents to the oceans via rivers includes both particulate and dissolved P from the weathering of continental rocks and soils (Ruttenberg, 2003). Due to the fact that dissolved P is highly particle reactive, over 90% of riverine P is present as particulate P, with a flux of $0.59 – 0.65 \times 10^{12}$ mol/yr (Meybeck, 1982; Jahnke, 1992; Mackenzie et al., 1993). Less than 10% of riverine P is dissolved, with a flux of $0.032 – 0.058 \times 10^{12}$ mol/yr (Lerman, et al., 1975; Meybeck, 1992; Jahnke, 1992), which includes more than 50% as dissolved organic P (Meybeck, 1982). Although the chemical form and the flux of P during river transport are controlled by the drainage basin geology, substrate weathering, and the native environment of the river, human impacts cannot be ignored. For example, over the past 20 years, the increased erosion of soil by forest clear-cutting and widespread cultivation has increased the flux of P from rivers to the oceans by a factor of 3 (Melack, 1995; Howarth et al., 1995).

The marine phosphorus cycle is divided into two large-scale environments – the hemipelagic ocean (sea above terrigenous-dominated shelf and slope) and the pelagic ocean (deep sea). As mentioned before, particulate P from riverine sources comprises refractory P (detrital apatite) and potentially bio-available P (reactive P), including organic P and adsorbed P. In hemipelagic sediments, detrital apatite represents a major source of P from the riverine particulate load. This P is refractory and is buried passively. In contrast, detrital P tends to be less important in pelagic sediments due to the limited physical transport of this heavy mineral (Ruttenberg, 2003). Furthermore, close to the shore where the water column is shallow, the burial rate of organic P is particularly high due to the high flux of nutrients from rivers and the low respiration in the water column (e.g., Filippelli, 1997a, b). In contrast, in deeper pelagic sediments,

organic P is more efficiently respired during settling through the water column (Ruttenberg, 1993).

At present, most of the world's oceans are well-oxygenated. Unstable Fe(II) is easily oxidized to Fe(III) to form iron (oxyhydr)oxide minerals at neutral pH, which readily scavenge dissolved P and deliver this to the sediment in both hemipelagic and pelagic ocean settings (e.g. Wheat et al., 1996). Using a sequential P extraction technique, Ruttenberg and Berner (1993) demonstrate that P released from organic matter and Fe (oxyhydr)oxide minerals is commonly transferred to authigenic carbonate fluorapatite (CFA), especially in pelagic sediments. Furthermore, CFA can also play a key role in the hemipelagic ocean. However, in the oxygen minimum zone (OMZ), CFA is highly restricted, in contrast, organic P is indicated as the most important precipitate for phosphorus (Kraal et al., 2012). Schenau et al. (2000) suggest that CFA is the dominant fraction of P deposted in the OMZ. However, not all CFA is formed during secondary diagenesis in the sediments, instead, a portion forms directly in the water column or is deposited by aeolian transport. This portion is defined as the unreactive CFA (Kraal et al., 2012). Finally, other redox conditions have been prevalent through Earth's history, and this greatly affects biogeochemical cycling of P, which is described below.

Phosphorus cycling in lakes is similar to that in ocean systems, yet due to the finite boundaries, lakes provide a more tractable study site. Caraco et al. (1989) suggest differences between lakes and oceans, more P can be released from the deep sediment in lakes which changes the sulfate concentrations in the lake systems changing the P behaviour in lakes. However, Ruttenberg (2003) argues that the redox conditions are the main factor for variations of P cycling.

1.4 P cycling under different redox conditions

The extent to which bioavailable P may be trapped in the sediment, as opposed to being recycled back to the water column, is highly redox dependent. Aquatic redox conditions are classified by utilization of different electron acceptors in a progression of metabolic pathways (Stumm and Morgan, 1970; Froelich et al., 1979; Berner, 1980). The electron acceptors are O_2, NO_2^-, NO_3^-, MnO_2, FeOOH, SO_4^{2-} and C (IV). The order in which these are consumed is based on the thermodynamics and energy requirements in respiration processes. Accompanied geochemical zones are formed with the progression of metabolic pathways as oxic, nitrogenous, manganous, ferruginous, sulfidic and methanic conditions (Canfield and Thamdrup, 2009). The scheme for geochemical

environments is showed in Figure 1.1. Nitrogenous and manganous redox zones tend to overlap in both the upper and lower bounds with other chemical zones (Fig. 1.1). In most natural environments, these two redox zones are much narrower than other zones because of changes the dominant respiration process due to changes in electron acceptor concentrations. For example, at the lower limit of the manganous redox zone, iron has accumulated to a much higher concentrations and becomes the dominant electron acceptor in what is then called the ferruginous zone (e.g., Murray et al., 1989, 1995; Schippers et al., 2005; Lam et al., 2007; Canfield et al., 1993a, b). Methane is produced when the sulfate is consumed to form sulfide, because the methane redox zone can only be formed when no electron acceptors react with methane. For example, sulfate can oxidize methane under anaerobic conditions through biologically mediated reactions to restrict the methanic redox zone (e.g., Iversen and Jøgensen, 1985). In terms of dominant ocean redox conditions, these have tended to be either oxic, ferruginous or euxinic (sulfidic) through Earth history (Poulton and Canfield, 2011) and thus these will be the dominant redox states considered here.

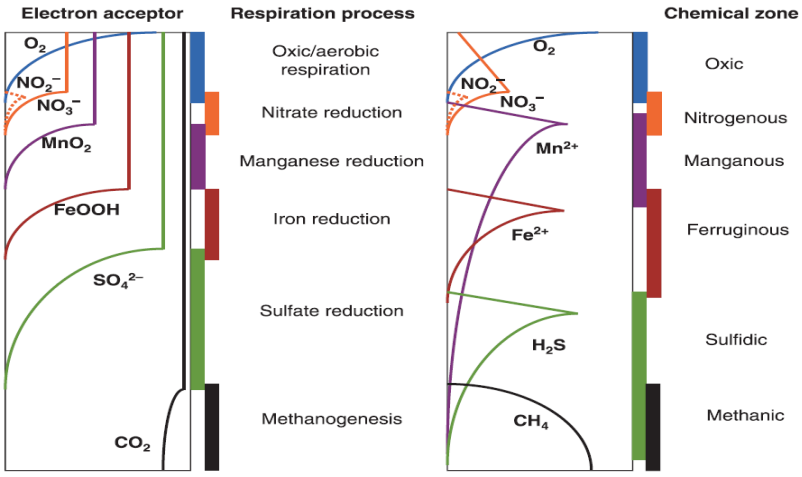

Figure 1.1 Scheme for geochemical redox environments. Adapted from Canfield and Thamdrup (2009). The left figure shows the depth distribution of electron acceptors. The middle part classifies the respiration process during organic matter mineralization. The right shows the depth distribution of chemical zones (redox conditions). The profile can be found both in the water column and sediments.

As mentioned above, beneath a well oxygenated water column, organic P and P adsorbed to iron (oxyhydr)oxides can be released in the sediments as dissolved P by the respiration of organic matter and the reduction of Fe (oxyhydr)oxide minerals, but this P is generally scavenged through re-adsorption to Fe (oxyhydr)oxide minerals close to the

sediment-water interface (Slomp and van Raaphorst, 1993; Slomp et al., 1996a, b) or biological sequestration of polyphosphates (Davelaar, 1993; Sannigrahi and Ingall, 2005), then transforming into CFA (Ruttenberg and Berner, 1993) (Fig. 1.2a). The polyphosphate is only formed through the microbial process by organisms living at the oxic-anoxic transition in the sediments (Schulz and Schulz, 2005; Sannigrahi and Ingall, 2005; Ingall et al., 2005). In a ferruginous water column, P is also delivered to the sediment in association with organic matter and Fe (oxyhydr)oxides (Fig. 1.2b). Again this P can be released from organic matter and Fe (oxyhydr)oxide minerals in the sediments, where some of it may be trapped as CFA (Fig. 1.2b). However, under ferruginous conditions there is greater potential for recycling of P back to the water column as the Fe (oxyhydr)oxide trap close to the sediment-water interface will generally be greatly diminished in comparison to oxic settings. In a sulfidic water column, Fe (oxyhydr)oxides forming in oxic surface waters or under ferruginous conditions in the upper chemocline are reduced by dissolved sulfide (e.g., Pyzik and Sommer, 1981; Dos Santos Afonso and Stumm, 1992; Peiffer et al., 1992; Poulton, 2003; Poulton et al., 2004a) deeper in the water column and in the sediments, releasing dissolved P (Fig. 1.2c). The reduced Fe(II) ultimately forms pyrite, to which P does not significantly adsorb (Krom and Berner, 1980; Anschutz et al., 1998). Thus, in the sediment under euxinic conditions, P is likely more extensively released to the water column from both organic matter remineralisation and Fe (oxyhydr)oxide reduction (Fig. 1.2c) (e.g., Ingall et al., 1993; Dellwig et al., 2010).

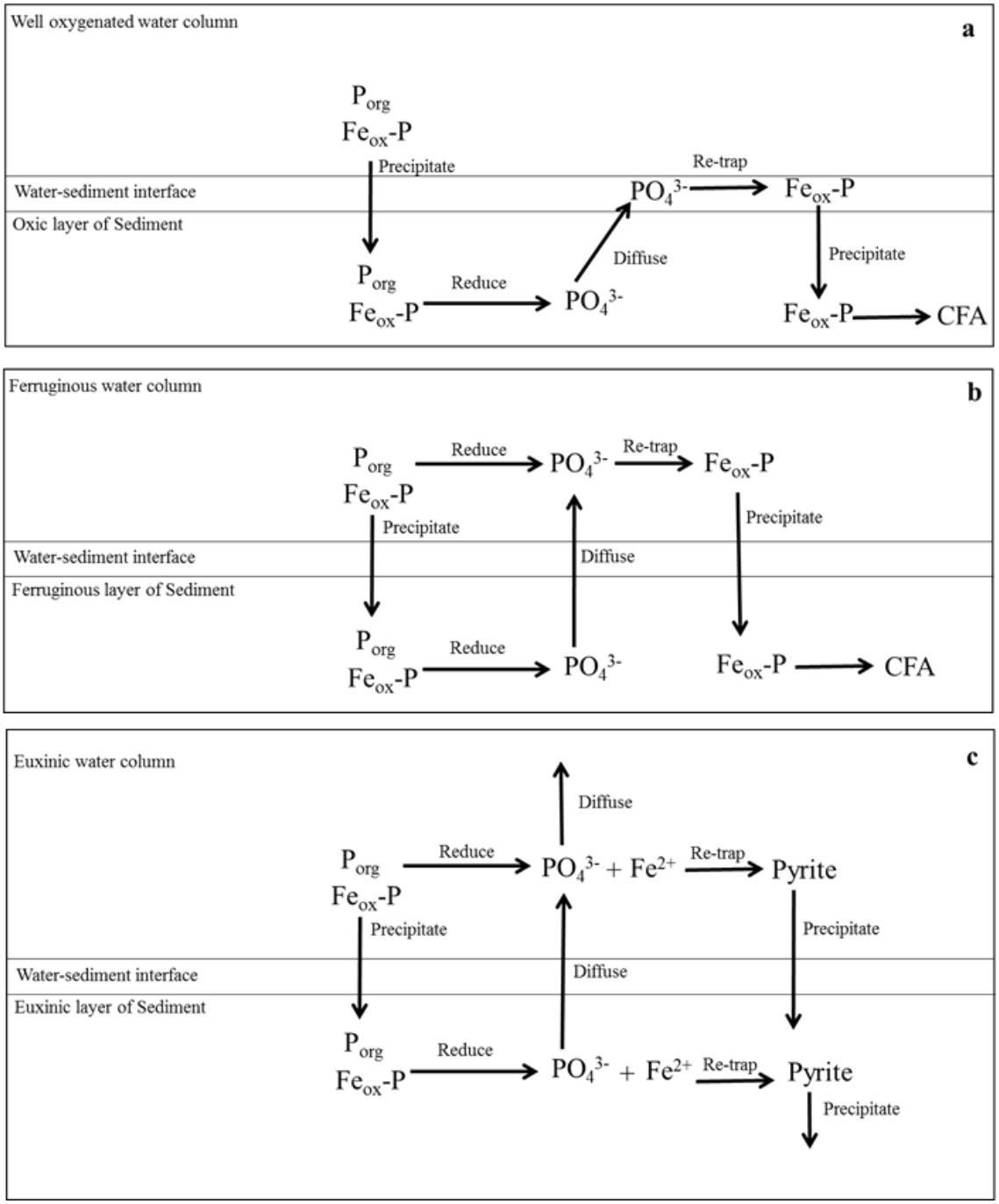

Figure 1.2 Scheme for P cycling under different redox conditions. a) well oxygenenated setting; b) ferruginous setting c) euxinic setting.

The ratio of C_{org} and P is also controlled by different redox conditions, corresponding to the behaviour of P mentioned above. Algeo and Ingall (2007) collect data from different aqueous systems to and reported that the C_{org}/P ratio is below 50 in the sediments beneath a well-oxygenated water column,; in suboxic to anoxic systems (maybe nitrogenous to ferruginous conditions), the median value of C_{org}/P ratio is close to 106; in sulfidic systems, the C_{org}/P ratio is much higher than 106.

1.5 P cycling over Earth history

As P cycling is highly redox dependent, the redox evolution of the water column through Earth history is important as it exerts a primary influence on P cycling. The redox state of the marine system through Earth's history (except for most of the Archean) varied temporally and spatially. During the early to late Archean (~3.8 to 2.7 Ga), based on the widespread deposition of banded iron formation (BIF), ocean redox conditions remained relatively stable, with anoxic ferruginous conditions in both deep and surface water, from proximal to distal settings (Fig. 1.3a; Poulton and Canfield, 2011). The main source of Fe^{2+} to the ocean during this time was via hydrothermal vents (Holland, 1984). During this epoch, atmospheric oxygen was less than 10^{-5} present atmospheric level (PAL) (Fig. 1.4; Farquhar et al., 2000; Pavlor and Kasting, 2002). Thus, a terrigenous source of Fe^{2+} was likely not the key dynamic controlling Fe^{2+} availability, because the low levels of atmospheric oxygen largely precluded significant oxidation of terrigenous pyrite (Kump, 2008 Furthermore, less dissolved Fe(III) can be formed as the Fe(II) is still constrained by greenalite during times of low PAL of oxygen (Tosca et al., 2016). Thus biogeochemical P availability may have been inhibited due to low concentrations of electron acceptors for organic remineralization (Kipp and Stüeken, 2017), even though some Fe(III) can be delivered to the ocean system, P is possibly removed through sorption onto, or incorporation into Fe (oxyhydr)oxide minerals (Bjerrum and Canfield, 2002; Jones et al., 2015; Reinhard et al., 2017).

From 2.7 Ga to 1.9 Ga (the Late Archean to Late Paleoproterozoic), redox conditions in the ocean systems changed. Roscoe (1969) originally modelled the evolution of atmospheric oxygen, suggesting a permanent increase in atmospheric oxygen sometime between ~2.4 Ga and 2.1 Ga (Figure 1.4). With new research, this model has been revised many times. Anbar et al. (2007) used Mo concentrations as a proxy to suggest atmospheric oxygen production at ~2.5 Ga. Here, 'whiffs of oxygen' (a slight increase in oxygen, but the duration and magnitude is not clear) occurred in the late Archean before the 'Great Oxidation Event (GOE)' (Figure 1.4). The first GOE is happened at ~2.3 Ga based on the loss of mass-independent fractionations of sulfur isotopes (Luo et al., 2016). Other studies have suggested that surface water was oxygenated or partially oxygenated by ~2.7 Ga (e.g., Reinhard et al., 2009; Kendall, et al., 2010; Scott et al., 2011), with possible atmospheric oxygen production as early as 3.0 Ga (Crowe et al., 2013). Due to oxygen production prior to the GOE, terrigenous pyrite was oxidized,

providing a source of sulphate to the ocean, which was then reduced as S(II) to form spatially restricted euxinic water column conditions (Fig. 1.3b; Reinhard et al., 2009; Kendall et al., 2010; Scott et al., 2011). However, during early oxidative weathering, a large proportion of sulfur was still locked in sulfide minerals, and in addition, a large Fe(II) source from hydrothermal vents through upwelling restricted euxinia to proximal oceanic waters through the process of precipitation with sulfide to form the pyrite (Fig. 1.3b; Reinhard et al., 2009; Kendall et al., 2010; Scott et al., 2011). Thus, in the pelagic ocean, deeper water remained ferruginous (e.g., Reinhard et al., 2009; Kendall et al., 2010).

After ~2.1 Ga, atmospheric oxygen fluctuated significantly between 10^{-3} and 10^{-1} PAL (Planavske et al., 2014; Zhang et al., 2016), but for most of the Precambrian remained at intermediate levels (Fig. 1.4). From ~1.84 to 1.0 Ga, euxinic conditions have been suggested to be pervasive and widespread, but restricted to productive continental margin settings and epicontinental seas (Fig. 1.3c; Canfield, 1998; Poulton et al., 2004; 2010; Scott et al., 2008; Poulton and Canfield, 2011). During this period, Reinhard et al. (2017) suggest that dissolved P in the ocean system stayed at low values due to adsorption on iron (oxyhydr)oxide minerals in the deeper ocean. However, these results are opposite to those suggested in some previous studies (Planavsky et al., 2010), and do not consider the P was recycled back to the water column under the widespread euxinic conditions that were prevalent during much of this period (Poulton, 2017).

After a stable period, oxygen increased again from ~0.8 Ga to 0.55 Ga (Fig. 1.4; Och and Shield-Zhou, 2012; Lyons et al., 2014). Because of this Neoproterozoic oxygenation, the deep sea water was also oxygenated in some places, at least for a limited period of time (Canfield et al., 2007; Sahoo et al., 2012; Lenton et al., 2014). However, other data point to different results. Through the early Neoproterozoic, global redox conditions began to transfer from widespread euxinic conditions to ferruginous conditions (Canfield et al., 2008; Johnston et al., 2010; Guilbaud et al., 2015; Sperling et al., 2015). The flux of sulfate was considered to be much lower than that of reactive Fe, due to a large amount of sulfate uptake by extensive continental evaporites on Rodinia (Guilbaud et al., 2015). Spear et al. (2014) adopted a new proxy based on fluid inclusions to also suggest that the concentration of SO_4^{2-} stayed at low values in Mid Neoproteozoic (~830 Ma) samples. Although ferruginous conditions were considered as the main redox conditions during the Neoproterozoic, euxinic conditions did occur in some Neoproterozoic basins (e.g., Canfield et al., 2008; Li et al., 2010; 2012; Sahoo et

al., 2012; Guilbaud et al., 2015; Thomson, et al., 2015; Och et al., 2016). In sum, through the Neoproterozoic, deep ocean redox conditions varied both temporally and spatially, but euxinic conditions were more restricted compared to the preceding mid-Proterozoic (Fig. 1.3c; Poulton and Canfield, 2011). Therefore, during the Neoproterozoic, a large amount of P might be expected to be trapped in association with iron (oxyhydr)oxides. However, most studies suggest high marine dissolved P during the latter half of the Neoproterozoic. For example, during the Cryogenian period (~0.75 – 0.62 Ga) (Planavsky et al., 2010; Reinhard et al., 2017) the extensive glaciations may have caused a high weathering influx of P during melting, which may have led to an increase in productivity and oxygen production (Canfield et al., 2007; 2008). After the glaciations, from ~0.635 – 0.541 Ga, dissolved P may have remained higher due to more expansive oxic water column conditions, with less P removal under ferruginous conditions (Fig. 1.3d; Reinhard et al., 2017).

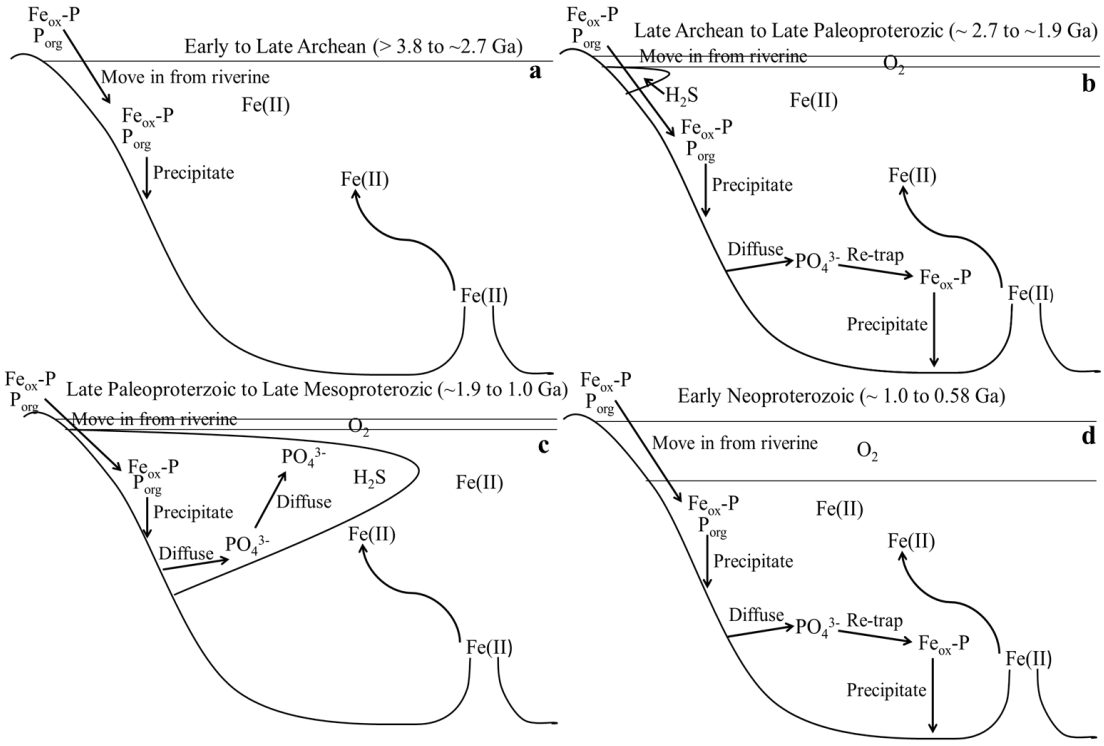

Figure 1.3 The evolution of redox conditions through Earth's history (from 3.8 Ga to 0.58 Ga; Poulton and Canfield, 2011; Guilbaud et al., 2015). Figure 1.3-a shows the situation of redox conditions during the early to late Archean. Figure 1.3-b shows redox conditions from the late Archean to the late Paleoproterozoic. Figure 1.3-c shows redox conditions from the late Paleoproterozoic to the late Mesoproterozoic. Figure 1.3-d shows redox conditions in the Neoproterzoic.

During the Phanerozoic (<541 Ma), oxygenation of the deep ocean was more and more common, with some notable exceptions. For example, during Phanerozoic oceanic anoxic events (OAEs), widespread euxinic conditions have been demonstrated (e.g. Jenkyns, 2010). In the case of the Cretaceous (145.5 Ma- 65.5 Ma) OAEs, however, euxinic intervals alternated with ferruginous intervals on orbital timescales (März et al, 2008; Poulton et al., 2015). These OAEs may often have been initiated by enhanced P influxes to the ocean due to higher rates of chemical weathering on land (Jenkyns, 2010). In addition, recycling of P under euxinic conditions may have exerted a positive productivity feedback, thus increasing the extent of ocean anoxia (Mort et al., 2007; Poulton et al., 2015).

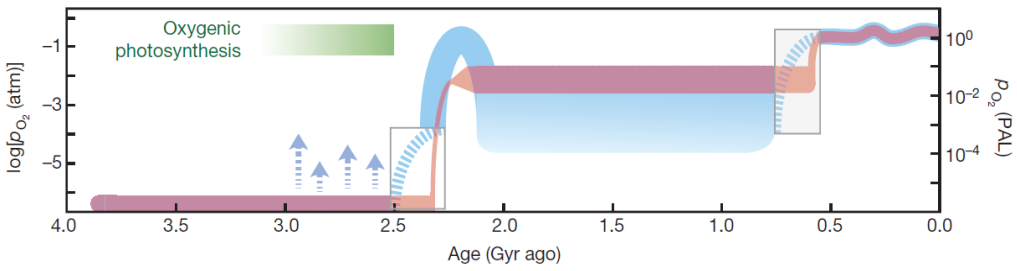

Figure 1.4 Evolution of Earth's atmospheric oxygen content through time. The red curve shows a classical model about the valuation of oxygen in atmosphere through time (Roscoe, 1969). The blue curve shows a modified model about the valuation of oxygen in atmosphere through time (graph is from Lyons, et al., 2014). Dark blue arrows indicate possible 'whiff' of oxygen in the late Archean.

1.6 Knowledge gaps

Although previous studies provide information on P cycling under different redox conditions through Earth history, the fate of P cycling in many environments is still not clear. Recent studies propose that Fe(II) phosphate (e.g., vivianite) may be an important sink for reactive P during early diagenesis, which is suggested to form in microenvironments within shallow sulfidic sediments (e.g. Jilbert and Slomp, 2013; Dijkstra et al., 2014, 2016; Egger et al., 2015; Joshi et al., 2015). März et al. (2008a) suggest that below the sulfate/methan transition zone, vivianite is formed as the long-term deposit of the P in the deep sea. Furthermore, Derry (2015) suggests that ferrous phosphate may have been an important sink rather than P adsorption on Fe (oxyhydr)oxide during the mid-Proterozoic, when the low oxygen level suppressed Fe

(oxyhydr)oxide formation. However, Kraal et al. (2017) demonstrated that in modern euxinic settings, P that has previously been attributed to vivianite is actually more likely associated with carbonate minerals. Therefore, the importance of vivianite formation as a sink for P remains unclear.

The fate of P that is recycled in the water column is also unclear. Several previous studies have suggested that phosphate is trapped by Fe(II) and Mn(II) in the redox-cline when P is recycled back to the water column, which ultimately suggests that vivianite may be an important trap for dissolved P (e.g. Dellwig et al., 2010; Turnewitsch and Pohl, 2010; Dijikstra et al., 2016, 2018). However, other minerals such as green rust may also be important. Green rust has been reported as a major iron mineral forming in the water column under anoxic ferruginous conditions (Zegeye et al., 2012).Therefore, the relative significance of these two minerals to P cycling under different redox conditions remains unclear.

Finally, although many studies of P cycling under different redox conditions have been conducted, a quantitative evaluation of the extent of P recycling back to the water column versus fixation in the sediment as secondary phases under different key redox states is currently lacking.

1.7 Aims and Objectives

The dominant aim in this research has been to investigate Fe mineralogical controls on P cycling under different abiotic conditions.

To reach this aim, several objectives were defined:

1. Report new P data on Lake Cadagno, Switzerland, including water column dissolved species, particulates and sediment cores from different parts of the basin, to investigate controls on P cycling in an environment considered analogous to ancient, low-sulfate, euxinic settings.

2. Investigate experimental controls on the formation of vivianite over green rust, to define the ratio of Fe and P under which each of these minerals may exert a major role on P cycling in the water column of anoxic basins.

3. Utilize mass balance models to quantify the extent of P recycling versus fixation in the sediment under different redox conditions, analogous to those which were prevalent at various times in Earth history.

1.8 Thesis Outline

The remainder of this thesis includes three data chapters and one conclusion chapter, focusing on Fe-P coupling in different environments. Chapter 2 reports new geochemical data to investigate controls on P cycling in Lake Cadagno. Chapter 3 involves new experiments to investigate what minerals control P cycling in the water column under different conditions. Chapter 4 utilises geochemical data from different redox environments in mass balance models to constrain P cycling. Finally, Chapter 5 provides an overall summary of the major findings of this work, and gives recommendations for future work.

Chapter 2 Phosphorus cycling in Lake Cadagno, Switzerland: A low sulfate euxinic ocean analogue

2.1 Introduction

Euxinic (sulfidic) water column conditions were an important feature during periods of ocean anoxia throughout much of Earth's history. Evidence for spatially and temporally restricted episodes of ocean euxinia stretch back to at least ~2.7 billion years ago (Ga), with such conditions early in Earth's history often being linked to an increased oceanic influx of sulfate due to oxidative weathering of pyrite as atmospheric oxygen rose (Reinhard et al., 2009; Kendall, et al., 2010; Scott et al., 2011). Euxinic conditions are generally considered to have become more widespread in the mid-Proterozoic, from ~1.84 to 1.0 Ga, with euxinia being particularly prevalent along productive continental margins and in epicontinental seas (Canfield, 1998; Poulton et al., 2004a; 2010; Scott et al., 2008; Poulton and Canfield, 2011). Euxinic episodes through the Neoproterozoic were more scarce, and instead anoxic ferruginous (Fe containing) water column conditions tended to dominate (Canfield et al., 2008; Johnston et al., 2010; Guilbaud et al., 2015; Sperling et al., 2015), although euxinic conditions did occur at certain times in some Neoproterozoic basins (e.g., Canfield et al., 2008; Li et al., 2010; 2012; Sahoo et al., 2012; Guilbaud et al., 2015; Thomson, et al., 2015; Och et al., 2016). Widespread euxinia has also been reported for certain intervals of the Paleozoic (e.g., Wignall and Twitchett, 1996; Wignall et al., 2010; Gill et al., 2011; Hammarlund et al., 2012), and during the oceanic anoxic events (OAEs) of the Mesozoic (e.g., Jenkyns, 2010).

A common feature of Precambrian euxinic episodes concerns the prevalence of relatively low marine sulfate concentrations compared to the modern ocean (~28 mM), which from the early Proterozoic to the terminal Neoproterozoic likely increased from the low micromolar range envisaged for much of the earlier Archean (Habicht et al., 2002; Crowe et al., 2014), to concentrations in the low millimolar range (Kah et al., 2004; Guilbaud et al., 2015). Similarly, a growing body of evidence suggests that sulfate concentrations were also much lower than at present during many Phanerozoic periods of euxinia (in the low millimolar range), at least through to (and including) the anoxic episodes of the Cretaceous (e.g., Adams et al., 2010; Newton et al., 2011; Song et al., 2013; Poulton et al., 2015).

Despite the significance of low-sulfate euxinic settings through time, relatively little is known about controls on P cycling under such conditions. P is commonly invoked as

the ultimate limiting nutrient on geologic timescales, with the behaviour of bioavailable P exerting a major control on primary productivity and hence organic carbon burial (e.g., Howarth, 1988; Tyrell, 1999). These factors ultimately exert a primary control on Earth's oxygenation history (e.g., Canfield, 2005), and it has been suggested that prior to Earth's first major rise in atmospheric oxygen (the Great Oxidation Event from ~2.45-2.32 Ga), bioavailable P was limited in the ocean due to removal via extensive adsorption to Fe (oxyhydr)oxides under anoxic ferruginous water column conditions (Bjerrum and Canfield, 2002; Jones et al., 2015; Reinhard et al., 2017; but see Konhauser et al., 2007; Planavsky et al., 2010).

After the Great Oxidation Event (GOE) at ~2.4-2.2 Ga, atmospheric oxygen levels are believed to have remained relatively stable (but with concentrations much lower than at present) under the more widespread euxinic water column conditions envisaged from ~1.84-1.0 Ga (Canfield, 2005; Lyons et al., 2014; Planavsky et al., 2014; Zhang et al., 2016; Daines et al., 2017). However, nutrient controls on productivity (and hence oxygen stability) across this mid-Proterozoic partially interval remain unclear. Limitation of the N cycle due to extensive Mo drawdown to the sediment coupled with enhanced loss of fixed N as N_2 (Anbar and Knoll, 2002; Fennel et al., 2005; Canfield et al., 2006; Scott et al., 2008; but also see Zerkle et al., 2006), or an increased contribution of anoxygenic photosynthesis to total primary production (Johnston et al., 2009), have been proposed as mechanisms to limit O_2 production in the mid-Proterozoic euxinic ocean. However, recent isotopic studies of the mid-Proterozoic N cycle suggest that bioavailable nitrate was likely abundant in near-shore environments (Godfrey et al., 2013; Stüeken, 2013; Koehler et al., 2017), while research on modern ferruginous systems implies that large expanses of the mid-Proterozoic ocean were likely P, and not N, limited (Michiels et al., 2017). In this regard, based on the total P content of shallow water marine shales through time, Reinhard et al. (2017) suggest that bioavailable P was maintained at extremely low concentrations throughout the mid-Proterozoic due to extensive stripping of water column P in association with Fe (oxyhydr)oxide minerals formed under deeper-water ferruginous conditions. Extremely low bioavailable P would ultimately maintain atmospheric oxygen at low levels throughout the mid-Proterozoic (Reinhard et al., 2017). However, this assertion assumes that the total P content of shallow marine shales tracks bioavailable P in the water column, with insignificant biogeochemical recycling of P from sediments back to the water column (Poulton, 2017).

The extent to which bioavailable P may be trapped in the sediment, as opposed to being recycled back to the water column (where it can fuel further productivity), is highly redox dependent. In organic-rich sediments deposited beneath oxic bottom waters, P is typically delivered to the sediment in association with organic matter and/or iron (oxyhydr)oxide minerals, in addition to detrital phases. During early diagenesis, organic matter and Fe (oxyhydr)oxide remineralisation (partially) releases P to pore waters (Krom and Berner, 1981; Froelich et al., 1988; Slomp et al., 1996b; Anschutz et al., 1998), with the potential either for recycling of some of this P to the overlying water column (Ingall and Jahnke, 1994; 1997; Slomp et al., 2002; 2004), or for the fixation of P in the sediment in association with other phases (i.e., sink-switching) (Van Cappellen and Ingall, 1994; Slomp et al., 1996a, b). Using a sequential P extraction technique, Ruttenberg and Berner (1993) demonstrated that a large proportion of the released P may be fixed as authigenic carbonate fluorapatite (CFA), and this is believed to typically account for ~50% of P burial in modern marine sediments deposited beneath oxic bottom waters. In addition, some of the recycled porewater P may be trapped in the sediment via re-adsorption to Fe (oxyhydr)oxide minerals close to the sediment-water interface (Slomp and Van Raaphorst, 1993; Slomp et al., 1996a, b; Dellwig et al., 2010).

Although these processes may begin in the oxic water column via the oxic degradation of organic matter, water column P recycling and the release of P from sediment porewaters tends to be particularly significant under euxinic conditions. In particular, the Fe (oxyhydr)oxide sink for P is greatly diminished under such conditions due to the reductive dissolution of Fe (oxyhydr)oxide minerals by dissolved sulfide (e.g., Pyzik and Sommer, 1981; Dos Santos Afonso and Stumm, 1992; Peiffer et al., 1992; Poulton, 2003; Poulton et al., 2004b) and the ultimate formation of pyrite, to which phosphate does not significantly adsorb (Krom and Berner, 1980; Anschutz et al., 1998). The effect of diminishing this sink under euxinic conditions is exacerbated by the preferential release of P from organic matter during microbial remineralisation (e.g., during the production of sulfide via bacterial sulfate reduction), which ultimately results in high organic C/P ratios relative to the Redfield Ratio (e.g., Ingall et al., 1993).

The formation of ferrous phosphate minerals (e.g., vivianite) has been proposed as an additional potential sink for reactive phosphate during early diagenesis. For example, Fe(II) phosphate has been implicated as a significant retention mechanism for P in Lake Ørn, Denmark (O'Connell et al., 2015) and Lake GroβGlienicke, Germany (Rothe et al., 2014). Both lakes are oxic, but the deeper sediment pore waters are characterised by

high concentrations of dissolved Fe^{2+}, and in these deep sediments the phosphate released from organic matter remineralization and Fe (oxyhydr)oxide reduction can re-precipitate as vivianite. Similarly, Fe(II) phosphate has been suggested as a prominent sink for P in a variety of coastal and deep-sea oxic water-column settings. Here, in sulfide-depleted sediments beneath the sulfate/methane transition zone (SMT; where porewater sulfate is depleted and methane concentrations increase), Fe (oxyhydr)oxide mineral reduction either via dissimilatory Fe reduction or via anaerobic oxidation of methane (AOM; using Fe (oxyhydr)oxides as the electron acceptor) and the availability of dissolved phosphate appears to promote vivianite formation (e.g., März et al., 2008a; Slomp et al., 2013; Hsu et al., 2014; Egger et al., 2015).

In addition, vivianite formation has been proposed to occur in a variety of anoxic water-column settings, including sediments of the Baltic Sea, in both the deeper euxinic basins (Jilbert and Slomp, 2013) and the intermittently anoxic Landsort Deep basin (Dijkstra et al., 2016), as well as in the seasonally anoxic Chesapeake Bay (Joshi et al., 2015) and in the euxinic Black Sea (Dijkstra et al., 2014). In all of these cases, vivianite has been suggested to form in microenvironments within shallow sulfidic sediments. However, Kraal et al. (2017) demonstrated that vivianite is rapidly dissolved via reaction with sulfide, and at least in the case of the euxinic Black Sea, the remobilised phosphate is more likely associated with carbonate minerals, rather than as vivianite. Thus the significance of vivianite formation as a longer-term trap for remobilised P in these modern sulfidic porewater environments is unclear.

Although active formation of vivianite has been demonstrated in a variety of settings, these environments are not particularly relevant analogues for the low-sulfate euxinic oceans of the Precambrian and Phanerozoic. In particular, while the limited availability of sulfate (and hence sulfide) during diagenesis in ancient low-sulfate euxinic settings could conceivably promote formation of vivianite, the importance of Fe(II) phosphate formation relative to the extent of P recycling remains unknown. In addition to the potential significance for the history of planetary oxygenation during the Precambrian, a detailed understanding of biogeochemical controls on P recycling under low-sulfate euxinic conditions is of key importance for evaluating productivity feedbacks during Phanerozoic episodes of euxinia (e.g., Mort et al., 2007; März et al., 2008b; Poulton et al., 2015).

Lake Cadagno, Switzerland, has been the focus of considerable research, largely due to its significance as a mid-Proterozoic euxinic ocean analogue (Canfield et al., 2010; Dahl

et al., 2010; Wirth et al., 2013). The lake represents an ideal location to study P cycling in relation to ancient euxinic settings as it is persistently euxinic at depth, with a relatively low sulfate content of 1.2 mM. In addition, the remote location of Lake Cadagno ensures insignificant anthropogenic phosphorus pollution, and phosphate concentrations in the water column (0.1-2 μM) tend to be lower than in other euxinic or seasonally euxinic settings, such as the Black Sea (2-7 μM) (Codispoti et al., 1991; Yakushev et al., 2008; Dellwig et al., 2010) and the Baltic Sea (3-5 μM) (Dellwig et al., 2010).

Here, we provide new water column and sediment data for Lake Cadagno, focusing on different parts of the basin, including the deeper euxinic waters, shallower oxic waters, and a site where the chemocline intersects the deposited sediments. We combine Fe and P speciation data with bulk geochemical analyses, to assess controls on P recycling under low-sulfate euxinic conditions. We specifically highlight the role of P recycling back to the water column, with a focus on the potential modulation of this flux by the diagenetic formation of Fe(II) phosphate minerals.

2.2 Sampling and methods

2.2.1 Sample location and geological setting

Lake Cadagno is a meromictic lake located at approximately 2000 m altitude in the central Alps of Swizerland (46º33’44’’N, 8º42’41’’E; Fig. 2.1). The bedrock includes felsic gneiss, dolomite and gypsum (Dahl et al., 2010). The basin is 0.26 km^2 with a maximum depth of 21 m (Krige, 1917). The water column is stratified, with oxic surface waters above the chemocline overlying euxinic deeper waters. This stratification has developed due to different densities of water flowing into the lake (Tonolla et al., 1998). Specifically, the oxic mixoliminion occurs at depths from 0 to 11 m and is fed by surface runoff. The euxinic bottom waters occur from 12 to 21 m depth, and these waters are supplied by deep sub-surface flow containing a high concentration of ions, including high dissolved sulfate concentrations in the range of 5 to 8 mM (Del Don et al., 1998; 2001). The oxic surface waters and deep sulfidic waters are separated by a chemocline of about 1 meter thickness (Tonolla et al., 1998; 1999). Above the chemocline, diatoms are one of the dominant phytoplankton (Camacho et al., 2001). Diatoms are microalgae with cell walls largely composed of silica which control the concentrations of silicate in the top of the water column, where concentrations from 0 to 5 m are stable at 0 mM, and increasing to 0.1 mM from 5 m to 12 m (Bossard et al.,

2001). Dissolved silicate may replace phosphate as the sorbed element onto iron precipitates, making phosphorus more available (Konhauser et al., 2007; Jones et al., 2015). The redox conditions of the lake are not seasonal, but the chemocline depth varies from 10.5 to 15 m (Tonolla et al., 2003; 2004). In the chemocline, the concentration of nitrate is approximately 1.2 mM, decreasing to 0 mM in the euxinic water column. At the same depths, the concentration of NH_4^+ increases from 0 to 0.06 mM from chemocline to euxinic water column (Tonolla et al., 2004). Alkalinity increases from 0.5 mM to 1.8 mM from chemocline to the euxinic water column (Tonolla et al., 1998), which may compete with phosphate to during iron (oyx)hydroxide precipitation (discussed in more detail below). The salinity increases from 0.16 psu to 0.45 psu from 7 m to 14 m, remaining stable to the bottom water (Halm et al., 2009) which has an influence on the diffusion coefficient of dissolved P. The sedimentation rates in the lake have occasionally been affected by landslides (Knoll-Heitz, 1991; Birch et al., 1996), which we consider in more detail below.

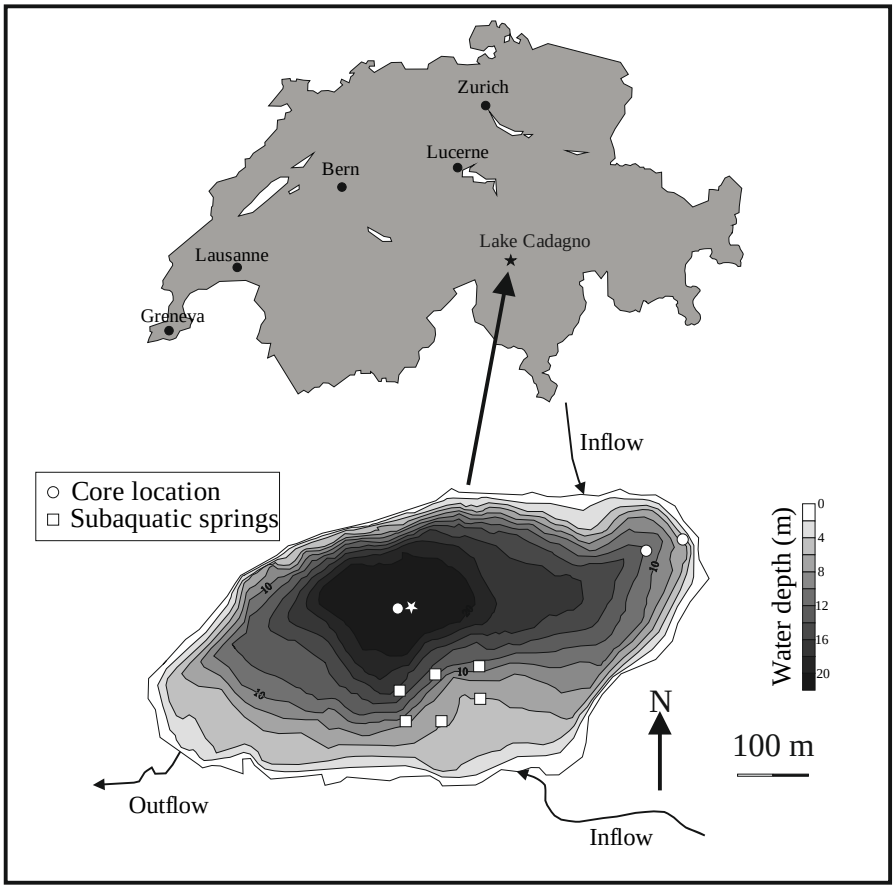

Figure 2.1 Geographical map and bathymetric map of Lake Cadagno, Switzerland (after Wirth et al., 2013; Tonolla et al., 1998). The star indicates the water samples location, the circles indicate the three sediment core locations, and the squares indicates the position of the subaquatic springs.

2.2.2 Water column, pore water and sediment sampling

The time for sampling was July 2014 in summer, and the whole sampling process took three days. Samples were collected through the oxic, chemocline and deeper euxinic waters by pumping from depth into expandable plastic containers, which were previously purged with N_2. Immediately after collection, water samples were filtered in a N_2 filled glove bag for immediate analysis of dissolved Fe(II) and phosphate, while dissolved sulfide was determined after fixing sulfide with 10 mM zinc acetate.

Short (up to 35 cm) gravity cores were taken from 3 different water depths: one representing deposition under euxinic conditions (20-21 m; euxinic core), another where the chemocline intersects the lake bottom (11-12 m; chemocline core), and a third in oxic waters (5-6 m; oxic core) (Fig. 2.1). After sampling, cores were stored upright and refrigerated at 4°C prior to processing (which occurred within 6 h). Sediment cores were sliced (generally in thicknesses of 1-2 cm) in the glove bag and placed in 50 mL centrifuge tubes. Pore water was extracted from each sample while still in the glove bag using rhizon ceramic filters (Rhizosphere research products). Immediately after opening the glove bag, sediment samples were frozen and pore waters were either analysed immediately (for dissolved Fe(II) and phosphate), or fixed with 10 mM zinc acetate (for later determination of dissolved sulfide). Sediment samples were freeze-dried, and stored frozen for further analysis.

2.2.3 Water content

To determine the water content with sediment depth, frozen cores sampled adjacent to the cores used for geochemical analysis were sliced with an electric saw (generally in thicknesses of 1-2 cm) and each slice was dried at 100°C overnight. The weight loss was then used to calculate water content (Birch et al., 1996).

2.2.4 Geochemical methods

2.2.4.1 Water column and pore water analysis

Immediately after filtration of both lake waters and pore waters, pH was measured with a calibrated pH meter (Mettler Toledo AG 8603). Dissolved Fe(II) concentrations were measured via the ferrozine method with a RSD of <2% (Stookey, 1970; Viollier et al., 2000). Dissolved P was measured via the molybdate blue method with a RSD of <3% (Koroleff, 1976; Ruttenberg, 1992). Dissolved sulfide was measured using the Cline method, with a RSD of <2% (Cline, 1969). For the measurement of dissolved sulfate,

2.5 mL of sample was treated with 100 µl of 10 mM zinc acetate to remove the sulfide by filtration, and then the filtrates were analysed by ion chromatography using a Dionex Ionpac^{TM} AS16 column with a RSD of <2%. Dissolved inorganic carbon (DIC) was measured using flow injection analysis (Hall, 1992) with a RSD of <1%.

2.2.4.2 Sediment analysis

Total carbon (TC), total organic carbon (TOC) and total sulphur (TS) were measured with a LECO C/S Analyzer. TOC samples were pre-treated with 10% HCl to remove carbonate phases. Replicate analyses of certified standards (Soil 502-309, Soil 502-062, Calcium carbonate 501-034 and Coal 502-671) gave RSDs of <2% for TC, <2% for TOC, and <4% for TS, with 100% recovery in all cases. Total inorganic carbon (TIC) was calculated as TIC = TC – TOC, and replicates of TIC analyses gave a RSD of <2%. Total Fe, Al, Ti and P were determined via a total digestion, whereby samples were initially ashed at 550°C, and then dissolved in HNO_3-HF-$HClO_4$ followed by evaporation to dryness. Boric acid was then added and evaporated to dryness overnight (to solubilise aluminium hexafluoride), and finally the sample was re-dissolved in hot HNO_3. Total Fe (Fe_T) was measured by AAS, while Al and Ti were measured by ICP-OES, and Total P (P_T) was measured by spectrophotometer using the molybdate blue method, as described above. Replicate analyses of a Lake Cadagno sediment sample gave RSDs of <2% for all four elements, and replicate analyses of international sediment standard PACS-2 gave recoveries of 98%, 96%, 93% and 100% for Fe, Al, Ti and P, respectively.

The Fe extraction methods were developed from Poulton and Canfield (2005) and Canfield et al. (1986). Together, the procedure targets six operationally-defined phases, with steps I-III performed sequentially (for extraction details see Table 2.1, which also reports target Fe phases and the precision of each extraction based on replicate extractions). In the step I, the extraction process was quickly finished to avoid the oxidization of Fe(II). $Fe(II)_{unsulf}$ (Table 2.1) was measured by spectrophotometer via the ferrozine method (Stookey, 1970), while the other unsulfidized Fe phases were measured by atomic absorption spectroscopy. Sulfide bound as acid-volatile sulfur (Fe_{AVS}) and pyrite (Fe_{py}) was extracted by the two-step acid Cr(II) method and trapped as Ag_2S, followed by stoichiometric conversion to Fe concentrations (Canfield et al., 1986; Fossing and Jorgensen, 1989). Replicate analyses of a Lake Cadagno sediment sample gave RSDs in each step.

Table 2.1 Fe extraction protocol.

Steps I-III are performed sequentially on a sub-sample, and steps IV and V are performed sequentially on a separate sub-sample.

Step	Extraction details	Target Fe phases	RSD (%)
I	5 mL 0.5 M HCl (shake for 1h)	**$Fe(II)_{unsulf}$**: Extraction targets reduced solid phase Fe, including AVS and Fe(II) phosphates. Subtraction of Fe_{AVS} (step IV) gives unsulfidized solid phase Fe(II) (including vivianite)	3
		Fe_{ox1}: Extraction also gives total Fe (i.e., Fe(II) + Fe(III)) solubilized by this technique. Subtraction of Fe(II) gives highly reducible ferric oxides such as ferrihydrite	11
II	10 mL sodium citrate/acetic acid/sodium dithionite solution (58.82 g/L sodium citrate, 20 mL/L acetic acid, 50 g/L sodium dithionite, shake for 2 h)	**Fe_{ox2}**: Reducible ferric oxides such as goethite and hematite	4
III	10 mL ammonium oxalate/oxalic acid (28.42g/L ammonium oxalate, 21.45 g/L oxalic acid, shake for 6h)	**Fe_{mag}**: Magnetite	5
IV	8 mL 50% HCl (boil for 1h)	**Fe_{AVS}**: Acid volatile sulfide	5
V	5 mL 1M chromous chloride dissolved in 50% HCl (boil for 1 h)	**Fe_{py}**: Pyrite	5

The pool of easily reducible ferric oxides such as ferrihydrite ($Fe(III)_{ox1}$) was calculated as the difference between the total Fe extracted by the 0.5 N HCl extraction (i.e., Fe(II) plus Fe(III)) and the Fe(II) measured in this extract (Goldberg et al., 2012; Zegeye et al., 2012). Because Fe_{AVS} is also extracted by the 0.5 N HCl extraction and measured as Fe(II) (Poulton and Canfield, 2005), the unsulfidized solid phase Fe(II) was calculated from the Fe(II) extracted by 0.5 N HCl after subtracting Fe_{AVS}. The total pool of Fe that is considered highly reactive (Fe_{HR}) to biotic and abiotic reduction in the euxinic water column and during early diagenesis (Canfield et al., 1992; Raiswell and Canfield, 1998; Poulton et al., 2004a) was calculated as:

$$Fe_{HR} = Fe(II)_{unsulf} + Fe(III)_{ox1} + Fe(III)_{ox2} + Fe_{mag} + Fe_{AVS} + Fe_{py} \quad (1)$$

The sequential extraction method (SEDEX) for different phosphorus phases was modified from Ruttenberg (1992). Five sedimentary P reservoirs were extracted by different reagents as detailed in Table 2.2. Fe-bound P (P_{Fe}) was determined via the molybdate blue method (Koroleff, 1976), after suitable dilution with matrix-matched standards, on a SEAL Analytical AA3 segmented flow analyser. All other P phases were determined via the molybdate blue method on a Thermo Genesys 6 spectrophotometer at 880 nm wavelength. Reactive P ($P_{reactive)}$ was calculated as:

$$P_{reactive} = P_{sorb} + P_{Fe} + P_{auth} + P_{org} \quad (2)$$

Table 2.2 Sequential SEDEX steps for different target P phases.

Step	Extractant	Target P phase	RSD (%)
I	5 mL 1 M $MgCl_2$ (pH 8, shake for 2h) × 2 5 mL MilliQ water (shake for 2h) × 2	$\mathbf{P_{sorb}}$: loosely sorbed P	5
II	10 mL sodium citrate/sodium bicarbonate/sodium dithionite solution (88.23 g/L sodium citrate, 84.01 g/L sodium bicarbonate, 24.38 g/L sodium dithionite, shake for 8 h) 5 mL 1 M $MgCl_2$ (pH 8, shake for 2 h) 5 mL MilliQ water (shake for 2 h)	$\mathbf{P_{Fe}}$: Fe-bound P (including vivianite)	2
III	10 mL, 1 M acetate sodium (pH 4, shake for 6h) 5 mL 1 M $MgCl_2$ (pH 8, shake for 2 h) × 2 5 mL MilliQ water (shake for 2 h)	$\mathbf{P_{auth}}$: Carbonate-associated P, authigenic apatite and biogenic apatite	3
IV	10 mL 10% HCl (shake for 16 h)	$\mathbf{P_{detr}}$: Detrital apatite and other inorganic P phases	2
V	Ash at 550 ℃ 10 mL 10% HCl (shake for 16 h)	$\mathbf{P_{org}}$: Organic phosphorus	3

Fe(II) phosphate (e.g., vivianite) was not part of the mineral suite tested during development of the SEDEX procedure (Ruttenberg, 1992). To address this we first synthesized vivianite by the method of Madsen and Hansen (2014), whereby 100 mL of 0.1 M NaH_2PO_4 was titrated into 250 mL of 0.025 M $(NH_4)_2Fe(SO_4)_2$, with the pH maintained at 7 using 0.5 M NaOH. The whole operation was completed under anoxic conditions and the product was subsequently characterised as vivianite by X-ray diffraction (XRD). Then we applied the first stages of the Fe and P sequential procedures and found that vivianite was completely dissolved by 0.5 M HCl in the Fe extractions (Table 2.1, Step I), and by citrate/dithionite/bicarbonate (CDB) in the P extractions (Table 2.2, Step II). Replicate analyses of a Lake Cadagno sediment sample gave RSDs in each step.

2.2.5 Geochemical modelling

The saturation indexes (SI) of porewater with respect to vivianite, siderite and pyrite were calculated using PHREEQC Interactive 3.3.7, utilising the databases of Laliberté (2009) and Appelo et al. (2014). The SI calculations were based on porewater data for the euxinic core, including pH and the concentrations of Fe^{2+}, HPO_4^{2-}, total sulfide, and DIC with depth. Calculations were performed at a temperature of 4°C (Dahl et al., 2010) and redox potential (Eh) of -300 mV, which correspond to values measured at the sediment-water interface (Gregersen et al., 2009; Dahl et al., 2010). Eh-pH mineral stability fields were calculated for a temperature of 4°C using Geochemist's Workbench 11.0. The input data was based on the euxinic core porewater data for Fe^{2+}, SO_4^{2-}, HPO_4^{2-} and HCO_3^- at 0-5 cm and 29.5-31.5 cm. The concentrations of HPO_4^{2-} and HCO_3^- were 25.74 μM and 3.75 mM in the surface sediments, and 24.83 μM and 5.11 mM in the deeper sediments, which were calculated from DIC and total dissolved P using PHREEQC.

2.3 Results

2.3.1 Water column

All geochemical data are presented in Appendix A. The water column is supersaturated with oxygen to a depth of ~7 m, below which the oxygen starts to decrease rapidly, with near-complete removal at ~11 m (Fig. 2.2a). Dissolved sulfate concentration increases with depth due to the input from subterranean springs (Fig. 2.1), with concentrations reaching 1.2 mM below the chemocline (Fig. 2.2b). Dissolved Fe^{2+} is low in concentration from the surface water to the chemocline (Fig. 2.2c). However, from 11 to

12 m, its concentration increases slightly to 1.1 μM just below the chemocline, with relatively constant concentrations below this depth. Dissolved sulfide increases in concentration below the chemocline, but remains relatively constant at 65 ± 5 μM below ~13 m depth. Dissolved phosphate concentration is low in surface waters, but progressively increases to ~2 μM with depth below the chemocline (Fig. 2.2d).

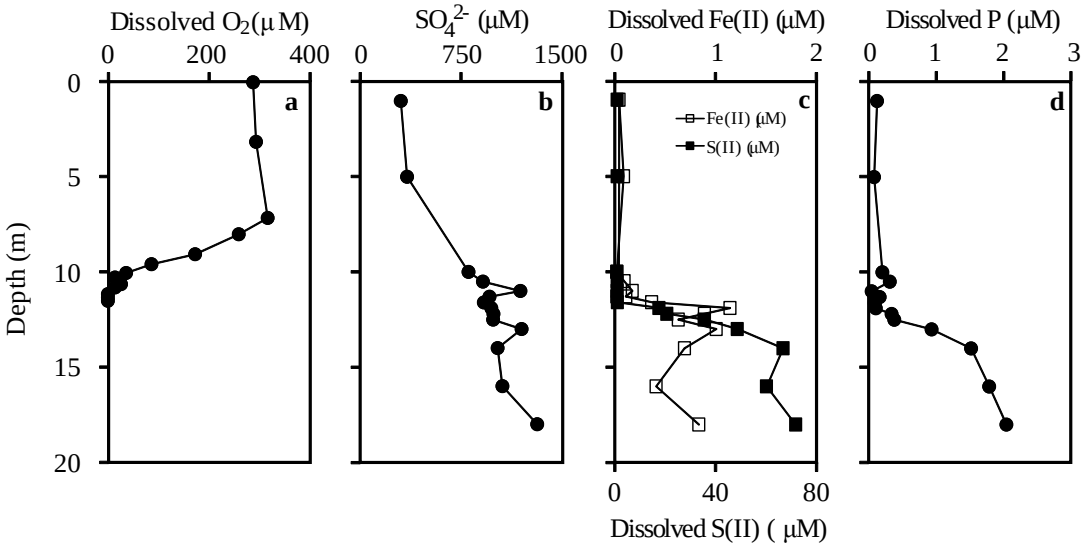

Figure 2.2 Vertical distribution of dissolved O_2, SO_4^{2-}, Fe^{2+}, sulfide, and PO_4^{3-} in the water column of Lake Cadagno. The O_2 profile is from Canfield et al. (2010).

2.3.2 Sediment water content

The water content of Lake Cadagno sediments was used to constrain the depth interval where normal sedimentation has been affected by landslides (Birch et al., 1996). During landslides, the sediments are compacted, thus less water is stored in the sediments. In the euxinic sediment core (Fig. 2.3a), the water content decreases with depth, but with a pronounced deviation to lower values between 12-18.5 cm. This corresponds well to the position of previously identified landslide layer (Birch et al., 1996) that occurred in 1951 (Knoll-Heitz, 1991). Birch et al. (1996) also found evidence for an older landslide starting about 4 cm below the first landslide interval and continuing for ~12 cm of sediment deposition. We see no evidence for this landslide based on the water content of the euxinic core between 18.5-23 cm, but unfortunately the core used to determine water content did not extend past 23 cm depth. However, based on a number of geochemical indicators (see below) we place the position of this earlier landslide from ~22.5 cm to the base of the core.

The chemocline core (Fig. 2.3b) shows a similar overall decrease in water content with depth, with a clear deviation to lower water content values between 12-26 cm, although

a return to slightly higher water content occurs at about 14-16.5 cm. This trend suggests that the interval from 12-26 cm captures the landslides outlined above. The oxic core was sampled from shallower water at the opposite side of the lake from where the landslides originated. The lack of any discrepancies in geochemical data trends (see below) confirms that this core is unlikely to have been affected by any of the landslides.

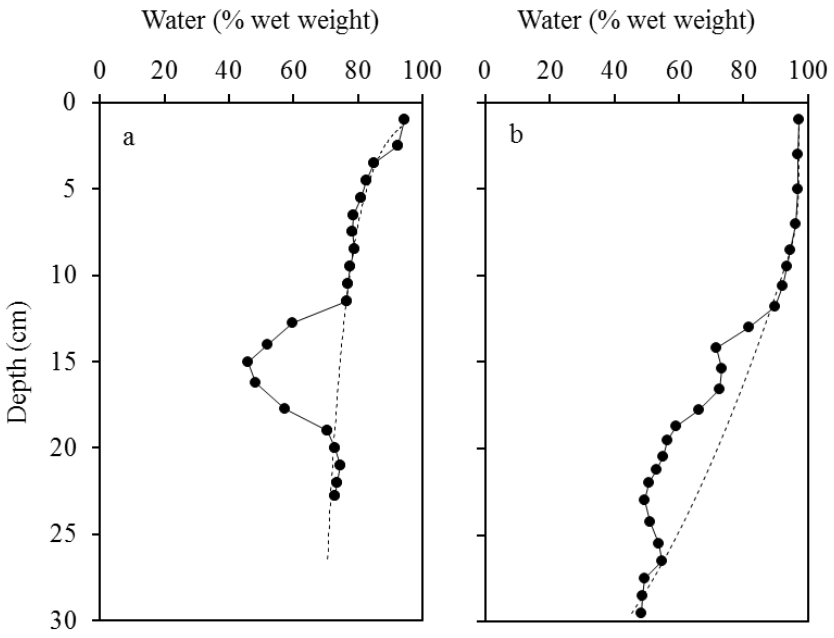

Figure 2.3 Water content profiles. a) euxinic core; b) chemocline core. Dashed lines indicate general depth trends.

2.3.3 Pore waters

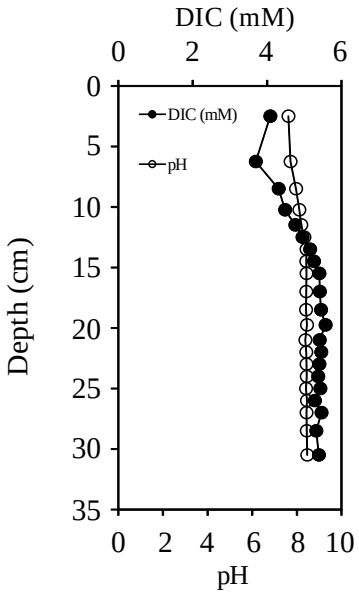

Figure 2.4 Dissolved inorganic carbon (DIC) and pH in the euxinic core porewaters.

DIC and pH were measured in the porewaters of the euxinic core in order to calculate mineral saturation indices. DIC shows an overall increase to a depth of ~15 cm, and then remains constant at 5.42 ± 0.15 mM (Fig. 2.4). The pH shows a similar depth profile to DIC with an increase to ~14 cm, below which values are relatively constant at 8.42 ± 0.04 (Fig. 2.4).

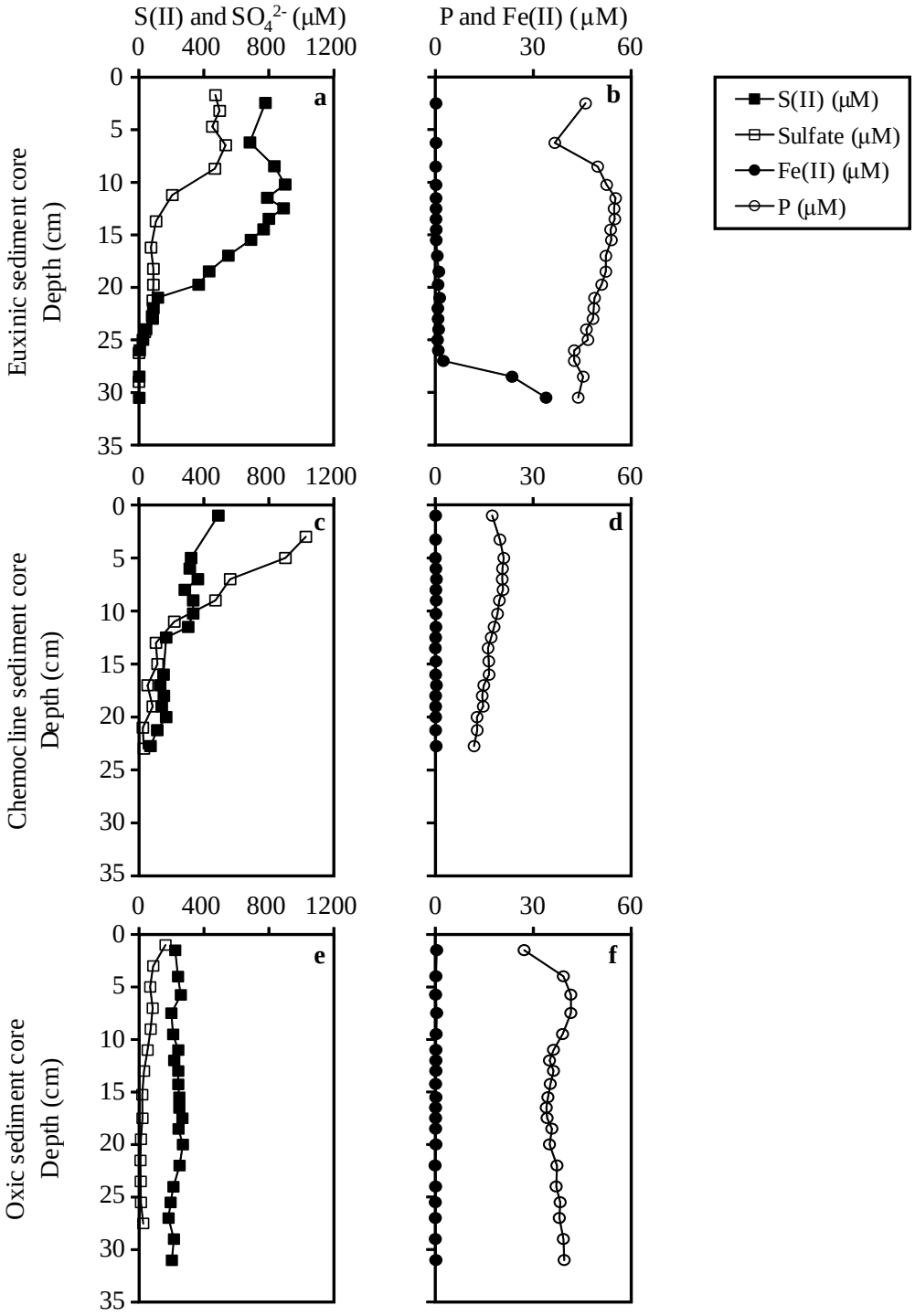

Figure 2.5 Porewater profiles for dissolved Fe^{2+}, PO_4^{3-}, sulfide and SO_4^{2-}. a) sulfide and SO_4^{2-} in the euxinic core; b) Fe^{2+} and PO_4^{3-} in the euxinic core; c) sulfide and SO_4^{2-} in the chemocline core; d) Fe^{2+} and PO_4^{3-} in the chemocline core; e) sulfide and SO_4^{2-} in the oxic core; f) Fe^{2+} and PO_4^{3-} in the oxic core.

In the porewaters of the euxinic sediment core (Fig. 2.5a), sulfate is relatively constant at 485 ± 5 μM to a depth of 9 cm, which is likely due to some mixing of poorly-consolidated organic-rich ooze which comprised the top few cm of the core. Below 9 cm depth, sulfate is depleted to close to zero at a depth of 26 cm. Dissolved sulfide is

significantly higher than in the overlying water column (Fig. 2.2c) and shows an overall increase over the top 13 cm, reaching ~900 μM. Sulfide then decreases to close to zero at 26 cm as sulfate is depleted. For both S(II) and sulfate, there are large differences in concentration between the deep water column and the top pore water samples, across the water-sediment interface. This difference is largely because the values in the deep water column are not representative of the real concentrations at the water-sediment interface, in addition, the top sediments are organic-rich oozes which are easily mixed, especially for the dissolved elements. From the S(II) and sulfate patterns in Dahl et al. (2010), the concentrations in the surface sediments are not affected by mixing, showing a general change from water column to the sediments, in addition, below 5 cm depth in the sediments, the patterns of S(II) and sulfate are consistent with our measurements. At 26 cm depth dissolved Fe^{2+} begins to accumulate, reaching 35 μM at 30 cm depth. Dissolved phosphate shows an overall increase to ~55 μM over the top 12 cm, followed by a gradual decrease through the lower part of the core, although concentrations remain above 40 μM at 30 cm depth. DIC in the surface sediments is lower than in the deeper sediments and shows an increase from 0 to 15 cm, followed by relatively constant concentrations of 5.42 ± 0.15 mM with depth (Fig. 2.4b). The pH shows a similar profile to DIC, with an increase from 0 to 14 cm, below which the value is relatively constant at 8.42 ± 0.04 (Fig. 2.4b).

In the porewaters of the chemocline core, sulfate concentrations decrease from >1 mM near the surface to much lower values below 20 cm, although concentrations do not reach zero (Fig. 2.5c). Sulfide steadily decreases in concentration from ~500 μM close to the sediment-water interface, but in contrast to the euxinic core, sulfide only decreases to ~70 μM at 23 cm depth. As a consequence, dissolved Fe^{2+} is present at low levels throughout the core (Fig. 2.5d). Dissolved phosphate shows a similar profile to the euxinic core, with a slight rise to ~21 μM at 8 cm, followed by a gradual decrease with depth. The surface sediments include more water and less solids than deep sediments, thus the depth resolution is varied with the whole depth.

In the oxic core, sulfate is relatively low throughout (<200 μM) and decreases with depth, although as with the chemocline core, values do not reach zero (Fig. 2.5e). Dissolved sulfide remains relatively constant at 230 ± 40 μM, and this buffers dissolved Fe^{2+}, which remains close to zero throughout the core (Fig. 2.5f). As with the euxinic and chemocline cores, dissolved phosphate initially increases slightly, to ~42 μM at 7.5 cm depth. However, after a slight decrease, dissolved phosphate then remains relatively

constant at 38 ± 2 μM, although there is some indication of a slight increase with depth. All of the porewater profiles show trends that are consistent with expected steady-state biogeochemical processes (Fig. 2.5). For example, dissolved sulfide decreases accompany the decrease of sulfate when sulfate reduction is the source of dissolved sulfide; Dissolved Fe(II) is controlled by dissolved sulfide and pyrite precipitation; Dissolved P decreases when dissolved Fe(II) starts to increase and dissolved sulfide is consumed. If landslides have affected the sediments, the dissolved species in the porewater may show unpredictable fluctuations or variations. This will be discussed in more detail below. As such, while some solid phase parameters have clearly been affected by the rapid deposition of landslide sediment (see below), there is no evidence for prolonged disturbance of porewater profiles. Instead, as expected, equilibrium with respect to diagenetic biogeochemical processes was likely rapidly re-attained after each landslide.

2.3.4 Sediment geochemistry

2.3.4.1 Bulk composition

The concentration of total inorganic C in the sediments generally decreases with depth in each core (Fig. 2.6), to values close to zero at ~19 cm in the euxinic core and ~16 cm in the chemocline core, although TIC remains somewhat higher throughout the oxic core. TOC concentrations in the sediments are high in the upper samples of all cores (Fig. 2.6), reaching more than 10 wt% in the euxinic and chemocline cores, and almost 20 wt% close to the sediment-water interface in the oxic core. The oxic core shows a steady down-core decrease in TOC due to microbial remineralization, whereas the more sudden decreases evident at depth in the euxinic and chemocline cores (Fig. 2.6) likely reflect additional dilution by landslide sediment. However, TOC concentrations at depth in the euxinic and chemocline cores generally remain above ~2 wt%. In the surface sediments of oxic core, TOC reaches to a high value at 20%, which may be caused by the algae assemblages or watershed plant cover (e.g. Meyers and Ishiwatari, 1993).

Total sulfur concentration fluctuates significantly in the sediments of the euxinic core, with transitions to lower values evident in the depth sections affected by landslides (Fig. 2.6). By contrast, TS shows a more stable profile in the chemocline and oxic cores, with an overall slight decrease with depth from ~2.5 wt% close to the sediment-water interface. Total Fe increases from ~3.6 wt% at the surface, to a peak of ~8.0 wt% at 21 cm in the euxinic core, followed by a subsequent decrease (Fig. 2.6). In the chemocline

and oxic cores, total Fe concentrations are lower and increase slightly with depth, but below ~20 cm in the chemocline core there is some suggestion of a slight decrease, similar to the euxinic core.

The detrital elements, Al and Ti show similar profiles (Fig. 2.6) with a downcore increase in all cores, but with pronounced increases associated with landslide-affected sediment in the euxinic and chemocline cores. Total P remains relatively constant in the euxinic (0.13 ± 0.03 wt%) and chemocline (0.12 ± 0.03 wt%) cores (Fig. 2.6). By contrast, total P concentrations are higher in the upper part of the oxic core and clearly decrease with depth.

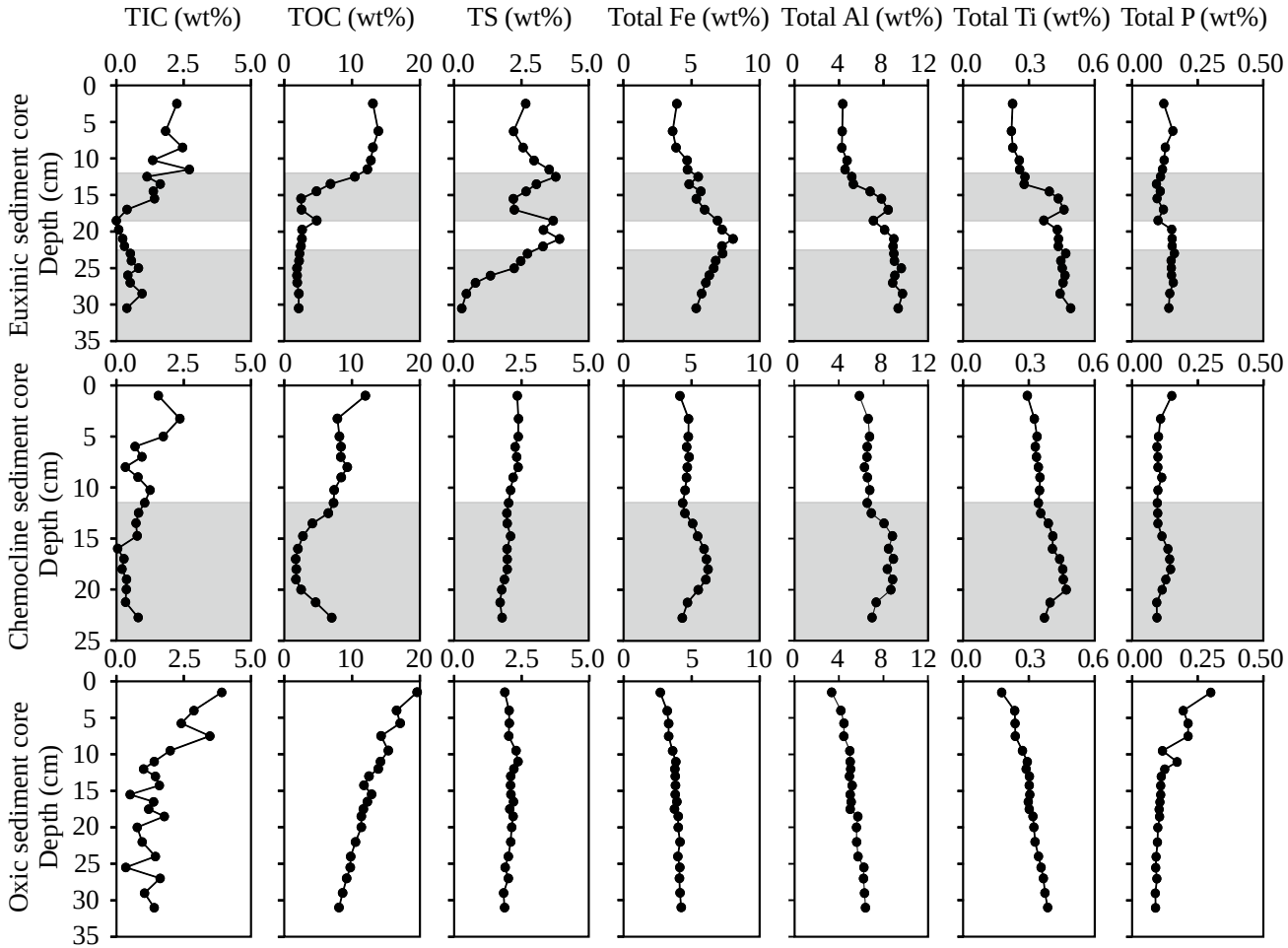

Figure 2.6 Profiles of TIC, TOC, TS, Fe, Al, Ti and P for the three sediment cores. Grey shading marks landslide intervals.

To evaluate potential changes in major element compositions due to the landslides, total Fe, Al, Ti, S and P profiles are plotted on a TIC (assuming TIC is present as $CaCO_3$) and TOC (assuming a formula CH_2O) free basis for the euxinic and chemocline cores in Fig. 2.7. The data show relatively limited variability in total Fe, Al and Ti for both cores, but in the euxinic core total Fe tends to be slightly lower in landslide-affected sediment, while Al and Ti tend to be slightly higher. These trends likely reflect minor differences in the bulk geochemistry of landslide sediment relative to the normal sediment input. By contrast, total S and P show significant variability on a TOC- and TIC-free basis (Fig. 2.7). This occurs partially due to dilution of the Fe-sulfides and organic-bound P that form in the water column, by the sediment deposited during landslides, but also reflects biogeochemical cycling during diagenesis, as discussed below.

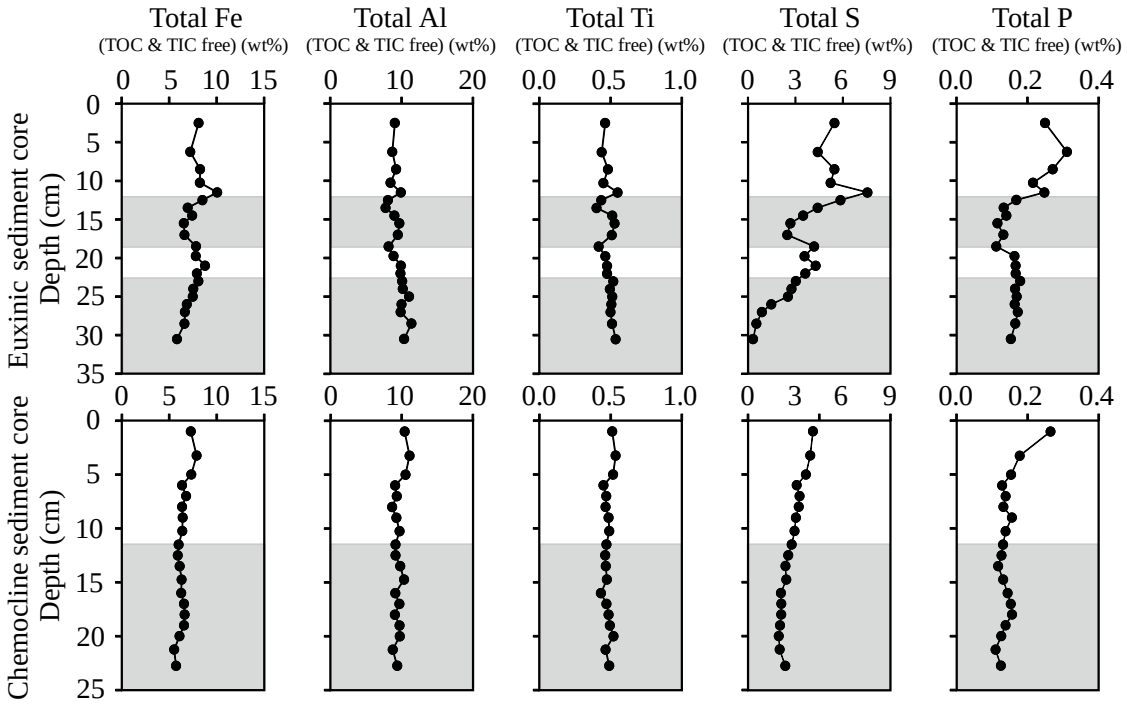

Figure 2.7 Profiles of total Fe, Al, Ti, S and P on a TOC-free and TIC-free basis for the euxinic and chemocline cores. Grey shading marks landslide intervals.

2.3.4.2 Iron speciation

In the euxinic core, abundant $Fe(II)_{unsulf}$ is present in the surface sediments (reaching almost 2 wt%), but the depth profile shows an overall decrease to ~15 cm, and then a subsequent increase below ~20 cm (Fig. 2.8). In the chemocline and oxic cores, $Fe(II)_{unsulf}$ is present at lower concentrations, with an overall slight decrease with depth. With the exception of two isolated samples in the euxinic core, the most reactive iron

oxide pool (Fe_{ox1}) is low in all cores (Fig. 2.8). In contrast, the more crystalline iron oxide pool (Fe_{ox2}) is more abundant and remains relatively constant with depth (Fig. 2.8). Fe_{mag} tends to be a minor constituent (Fig. 2.8), but concentrations are higher from 12.5-20 cm in the euxinic core.

Fe_{AVS} is present at relatively low concentrations in all cores, with a general decrease with depth (Fig. 2.8), presumably due to conversion to pyrite. Fe_{py} is relatively constant at ~1 wt% in the chemocline and oxic cores, although concentrations show a slight increase with depth over the top 12 cm of the oxic core (Fig. 2.8). In the euxinic core, Fe_{py} shows an overall increase to a depth of ~20 cm, but with a pronounced shift to lower concentrations in association with the most recent landslide. After reaching concentrations of almost 3 wt% below the most recent landslide, Fe_{py} progressively decreases to ~0.1 wt% through the earlier landslide interval (Fig. 2.8).

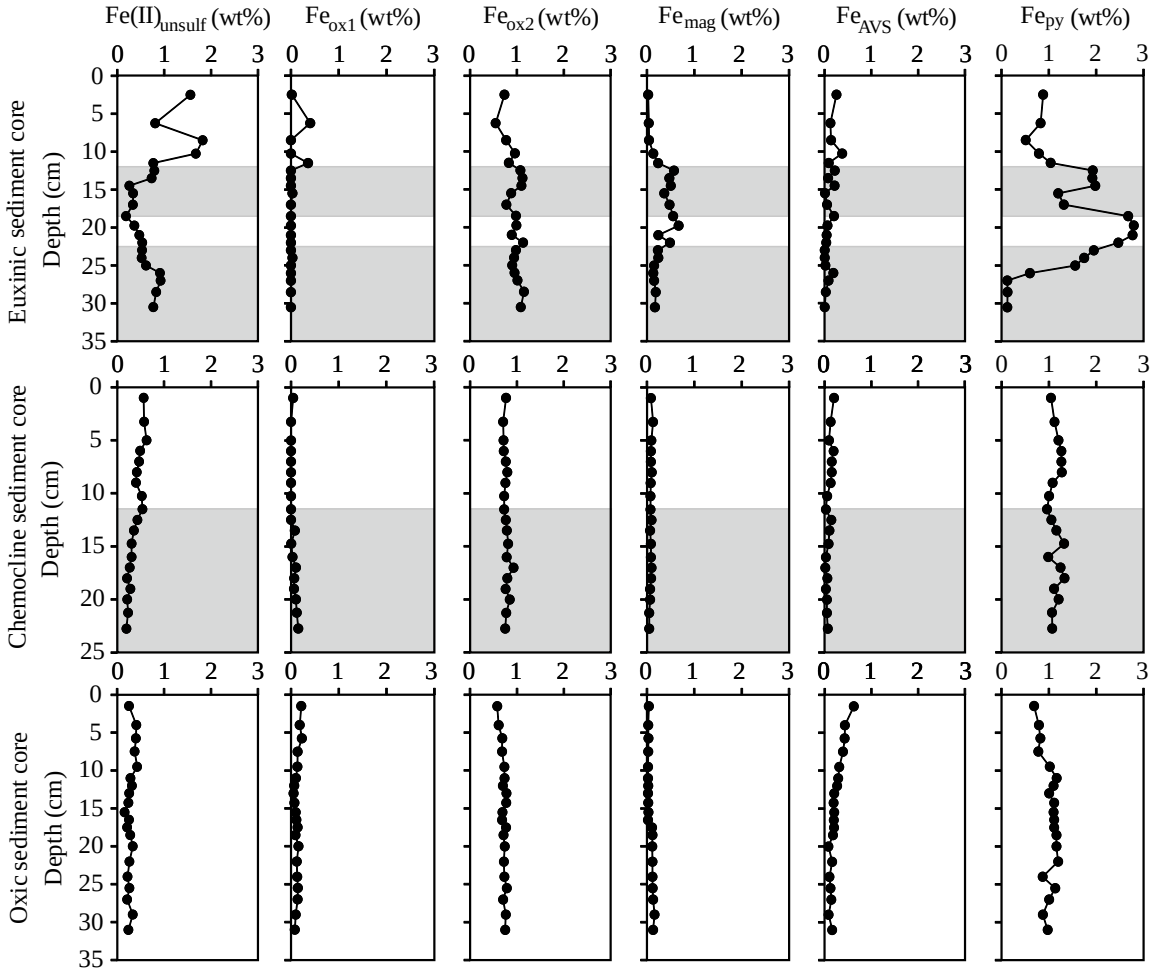

Figure 2.8 Iron speciation profiles in the three sediment cores. Grey shading marks landslide intervals.

2.3.4.3 Phosphorus speciation

Loosely-bound P (P_{sorb}) concentrations are very low in all three cores (Fig. 2.9). In the euxinic core, Fe-associated P (P_{Fe}) decreases to a depth of ~15 cm, but then progressively increases below ~18 cm. In the chemocline and oxic cores, P_{Fe} concentration generally decreases with depth, with a particularly strong decrease from relatively high surface concentrations in the oxic core (Fig. 2.9). P_{Fe} concentration also increases slightly from 15-22 cm depth in the chemocline core. Authigenic carbonate flourapatite (P_{auth}) is a minor component of all three cores and concentrations remain relatively constant with depth, although there is some suggestion of slightly lower values in landslide intervals (Fig. 2.9). Detrital P (P_{detr}) varies considerably, particularly across landslide intervals. In the euxinic core, the two landslide intervals are associated with excursions to much higher concentrations of P_{detr}. Higher concentrations of P_{detr} are also a feature of the landslide interval in the chemocline core (Fig. 2.9), which presumably reflects differences in the mineralogy of landslide sediment relative to the naturally sediment input to the lake. The oxic core displays much less variability in P_{detr}, but there is a clear gradual increase in concentration with depth. Organic-bound P (P_{org}) concentrations decrease with depth in each core, but with excursions to lower values in association with landslide intervals in the euxinic and chemocline cores (Fig. 2.9).

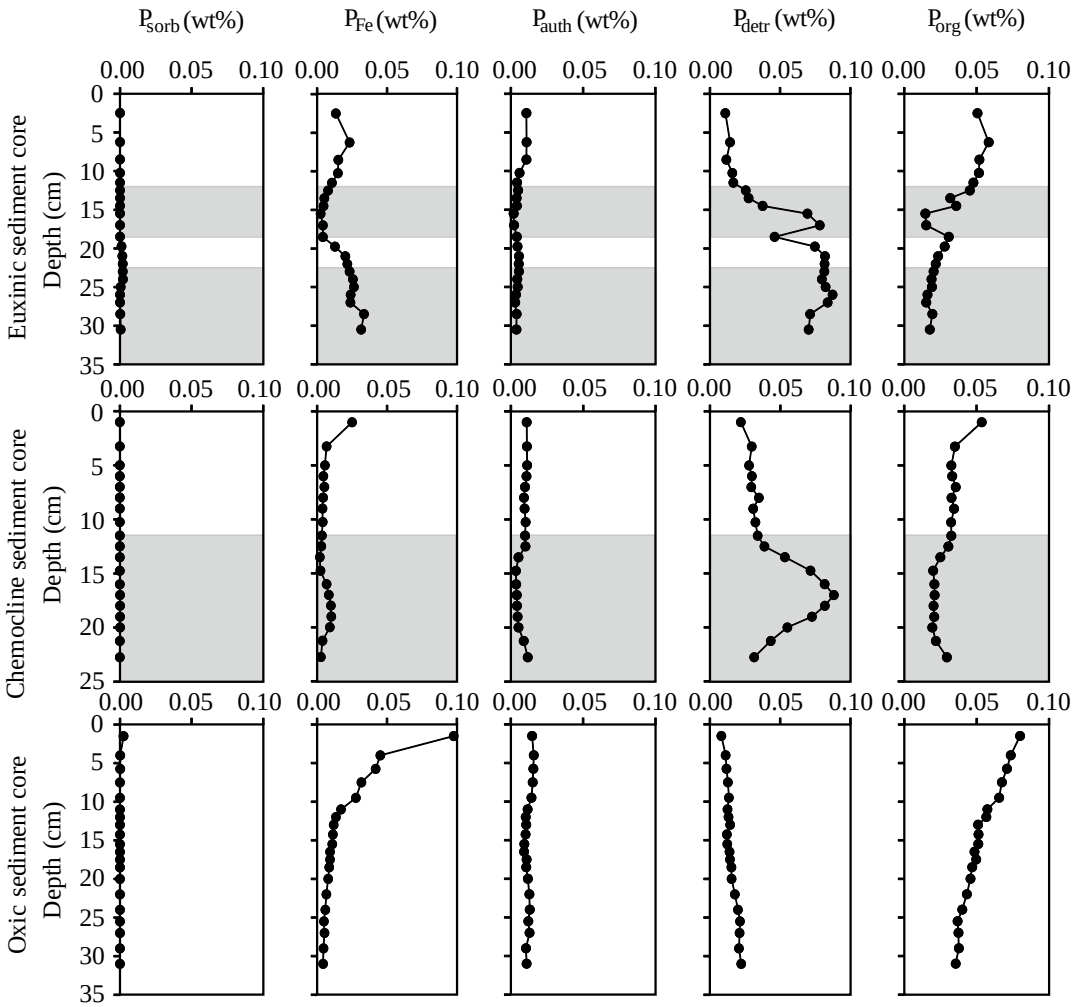

Figure 2.9 P speciation profiles for the three sediment cores. Grey shading marks landslide intervals.

2.4 Discussion

2.4.1 Water column chemistry

Water column data are broadly consistent with previous studies, demonstrating the persistent sulfidic nature of the basin below a depth of ~12 m (Fig. 2.2). In detail, however, our data compared to previous studies highlight temporal variability in the concentrations of different dissolved species. In particular, the concentration of dissolved sulfide at depth (65 ± 5 µM; Fig. 2.2) is lower than previous reports of 100-300 µM (Halm et al., 2009; Dahl et al., 2010; Canfield et al., 2010). This may be a consequence of lower rates of microbial sulfate reduction driven by a decrease in the flux of sulfate into the basin (see Boudreau and Westrich, 1984), since concentrations of up to 1.2 mM at depth in the present study (Fig. 2.2) are significantly lower than previous reports of 1.7-2 mM (Tonolla et al., 1998; Dahl et al., 2010; Canfield et al., 2010). Alternatively, the lower sulfide and sulfate concentrations in the present study may be due to more active mixing between the denser deep lake waters and the upper waters. Especially in summer, with the high season evaporation the cooler deep water is easily to mix with the upper water through upwelling caused by the wind stress (e.g. Verburg and Hecky 2003; Katsev et al., 2017). Similarly, relatively low concentrations of dissolved Fe(II) (~1 µM below the chemocline; Fig. 2.2) relative to previous reports of up to 3 µM (Tonolla et al., 1998; Halm et al., 2009) may be linked to enhanced water column mixing. At the pH of the water column, however, the range of dissolved Fe(II) and sulfide are in very good agreement with the solubility of FeS, suggesting that dissolved Fe(II) species are dominated by aqueous FeS clusters (Rickard, 2006), which exerts a primary control on the speciation of dissolved Fe(II) and sulfide.

A pertinent feature of the water column chemistry is the increase in phosphate with depth below the chemocline. Concentrations of up to 2 µM in deeper waters are consistent with previous studies (Tonolla et al., 1998), and the gradual increase observed with depth might be a consequence of release of phosphate from sinking organic matter during remineralisation via microbial sulfate reduction. Alternatively, the phosphate profile may also be generated from the release of phosphate from porewaters, which we consider in more detail below. In the surface water column (above 12 m), the concentrations of phosphate are low, which are inhibited by the adsorption to Fe (oxyhydr)oxides. Dissolved P in the chemocline is at the lowest concentrations in the water column because here P is controlled by the dissolution and precipitation of Fe(III) and F(II) phases. P mobilised from the decomposition of Fe (oxyhydr)oxides from the

oxic part of the water column is complexed by the reduced Fe(II), forming Fe(II) phosphate. Furthermore, at these depths, the dissolved P is inhibited by both Fe (oxyhydr)oxides and dissolved Fe(II).

2.4.2 Fe-S systematics in the sediment

The ratio of Fe_{HR}/Fe_T and Fe_{py}/Fe_{HR} are used to identify redox conditions in oceanic systems (Poulton and Raiswell, 2002), however, they do not work in this lake. In oceanic systems, Fe (oxyhydr)oxides are delivered to the shelf from terrestrial sources, then moved to open sea. After the fast precipitation in the shelf, Fe (oxyhydr)oxides are well reduced in the anoxic deep sea to form the stable redox conditions (Raiswell and Canfield, 2012). However, in the small and shallow Lake Cadagno, Fe (oxyhydr)oxides precipitate rapidly and although the water column is under euxinic conditions, a large amount of the Fe (oxyhydr)oxides are not reduced in the sediment. Therefore, the ratios in sediments cannot be used to identify the redox conditions in the water column of Lake Cadagno.

The Fe speciation data show several prominent features of pertinence to the present study. Firstly, discounting the landslide-affected sediment, there is an overall increase in Fe_{py} to a depth of ~20 cm (Fig. 2.8). This is consistent with diagenetic pyrite formation augmenting the flux of Fe-sulfide minerals from the water column. The reaction of dissolved sulfide with Fe (oxyhydr)oxide minerals produces mineral surface-associated Fe(II) (i.e., $Fe(II)_{unsulf}$), which subsequently dissolves slowly at the pH of most porewaters (Dos Santos Afonso and Stumm, 1992; Poulton et al., 2003). The most reactive Fe_{ox1} minerals are initially reduced via this process, and thus this phase is almost entirely consumed in all three cores, whereas the more crystalline Fe (oxyhydr)oxides comprising the Fe_{ox2} pool react more slowly (Canfield, 1989; Canfield et al., 1992; Poulton et al., 2004b) and persist with depth (Fig. 2.8). After dissolution, Fe(II) can react with dissolved sulfide to form Fe_{AVS} and ultimately pyrite. Thus, the associated decrease in $Fe(II)_{unsulf}$ over the top 15 cm of the euxinic core (and to a lesser extent in the other cores; Fig. 2.8) is consistent with the progressive formation of pyrite via this process. Fe_{mag} tends to be a minor constituent (Fig. 2.8), but concentrations are higher from 12.5-20 cm in the euxinic core. Since there is abundant dissolved sulfide at this depth in the euxinic core (Fig. 2.5), it is unlikely that this is magnetite formed by magnetotactic bacteria (e.g., Karlin et al., 1987), although we cannot rule out the possibility that the magnetite formed *in situ* before sulfidic conditions were re-established after the landslide. Alternatively, the increase in magnetite may be due to

increased magnetite concentrations in the landslide sediment, although this is not observed in the lower landslide interval.

By contrast, rapid sedimentation during landslides would dilute the flux of Fe-sulfide minerals forming in the water column, resulting in lower initial concentrations in the deposited sediment. In addition, rapid burial decreases the exposure time of reactive Fe minerals to the highest concentrations of dissolved sulfide, which occurs in the upper portion of sediment (Fig. 2.5). Dissolved sulfide concentration exerts a primary control on the rate of reductive dissolution of reactive Fe minerals (Canfield et al., 1992; Dos Santos Afonso and Stumm, 1992; Poulton et al., 2003), which would also contribute to the observed decrease in pyrite concentrations in landslide-affected sediment (Fig. 2.8).

A second prominent feature concerns the persistence of ferric (oxyhydr)oxide mineral phases with depth in all the three cores (dominantly Fe_{ox2}, with minor Fe_{ox1} in some cases). However, the relatively constant Fe_{ox2} depth trends (Fig. 2.8) are potentially misleading, as the profiles are affected by variable sediment dilution factors arising from the water column formation of TOC, carbonate minerals and pyrite, as well as the landslides. To evaluate whether Fe_{ox2} minerals, which are dominantly introduced to the basin in association with detrital phases, participate in biogeochemical reactions during diagenesis, we plot this phase normalised to Al (as a proxy for the detrital flux) in Fig. 2.10. These Fe_{ox2}/Al depth profiles demonstrate that the Fe_{ox2} pool is progressively dissolved in both the chemocline and oxic cores, but in particular, there is a major decrease below ~15 cm depth in the euxinic core. The reductive dissolution of Fe_{ox2} minerals at depth in the euxinic core would provide the dissolved Fe(II) required to precipitate the high concentrations of pyrite observed at this depth (Fig. 2.8), and would also source the increase in porewater Fe(II) concentrations observed lower in the core. In addition, the reduction of Fe_{ox2} minerals would account for the progressive increase in $Fe(II)_{unsulf}$ below ~15 cm (Fig. 2.8). Thus, although a proportion of the more crystalline Fe_{ox2} minerals persist with depth, these phases are biogeochemically reactive in all cores during diagenesis.

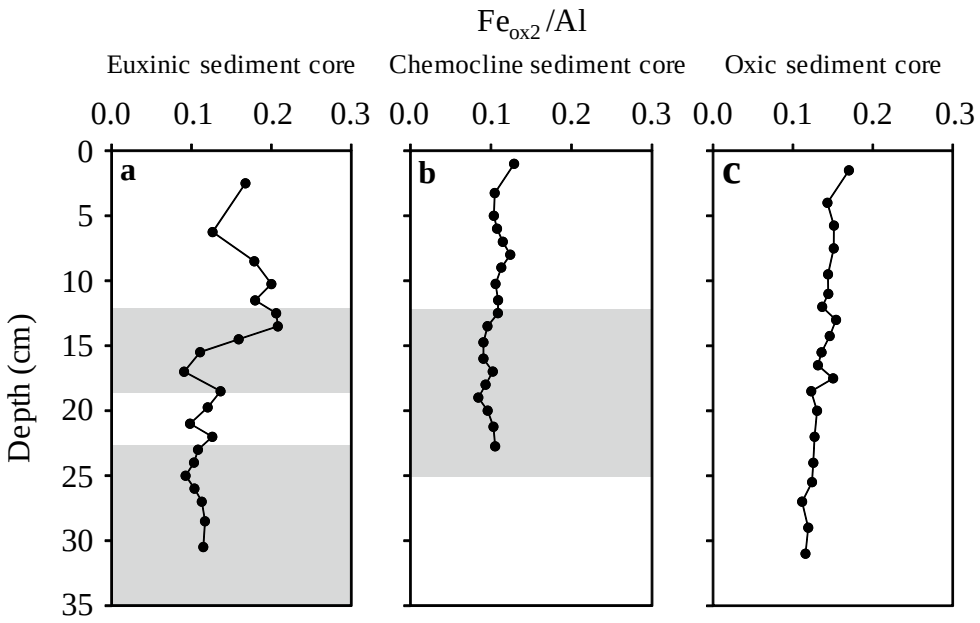

Figure 2.10 Fe_{ox2}/Al depth profiles for the three sediment cores. a) euxinic core; b) chemocline core; c) oxic core.

The reduction of crystalline ferric (oxyhydr)oxide minerals deeper in the euxinic core may occur via more than one pathway. Although methane was not measured in our study, anaerobic oxidation of methane has been demonstrated at depths of 16-20 cm in the euxinic sediments of Lake Cadagno (Schubert et al., 2011). Thus AOM using Fe(III) in (oxyhydr)oxide minerals may be responsible for the generation of dissolved Fe(II). In addition, however, it is also possible that Fe(II) is sourced from dissimilatory Fe reduction (e.g. Egger et al., 2015). The production of unsulfidized Fe(II) deeper in the euxinic sediment is a direct consequence of insufficient sulfate (and hence sulfide) to fully sulfidize the Fe_{HR} pool, and we consider the nature of this $Fe(II)_{unsulf}$ phase in more detail below.

2.4.3 Phosphorus cycling

2.4.3.1 Diagenetic recycling

The dissolved (Fig. 2.5) and solid phase (Fig. 2.9) P distributions clearly demonstrate active P cycling in each of the cores. The initial increase in dissolved phosphate observed over the top few cm of each core (Fig. 2.5), coupled with higher porewater concentrations than in the overlying water column (Fig. 2.2), likely reflects a balance between release of P from organic matter degradation and Fe (oxyhydr)oxide dissolution during early diagenesis, coupled with diffusive loss of dissolved P to the overlying water column. Although the P_{org} profiles in the euxinic and chemocline cores

have clearly been affected by the landslides (Fig. 2.9), molar TOC/P_{org} ratios (Fig. 2.11) provide strong evidence for extensive P mobilisation during organic matter degradation. In all cores at depths were the sediment has not been affected by landslides, molar TOC/P_{org} ratios are considerably higher (>600:1) than the Redfield Ratio of 106:1, which is entirely consistent with the preferential release of P from organic matter during microbial sulfate reduction (Ingall et al., 1993; Slomp et al., 2002, 2004; Jilbert et al., 2011). In landslide-affected intervals, organic matter is more rapidly buried beneath the depth at which porewater sulfate becomes depleted and hence there is less preferential release of P from organic matter degradation during sulfate reduction, although even in the most rapidly deposited sediment, TOC/P_{org} ratios are significantly higher than the Redfield Ratio.

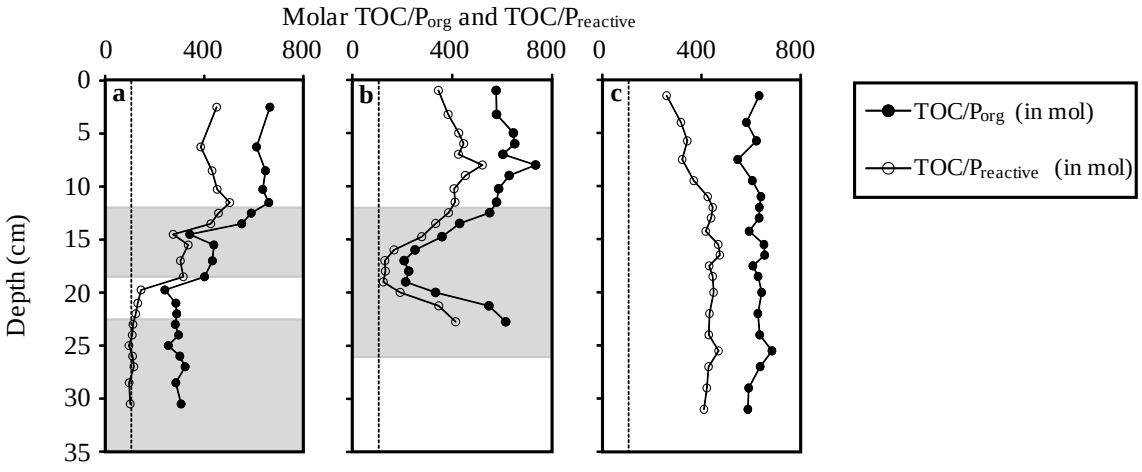

Figure 2.11 Molar TOC/P_{org} and $TOC/P_{reactive}$ for the three sediment cores. a) euxinic core; b) chemocline core; c) oxic core. Dashed lines represent the Redfield C/P ratio (106:1).

2.4.3.2 Controls on P recycling

The P released from Fe (oxyhydr)oxide reduction and organic matter degradation may either be retained in the sediment as secondary phases, or may be recycled back to the water column (e.g., Ruttenberg and Berner, 1993; Ingall and Jahnke, 1994, 1997; van Cappellen and Ingall, 1994; Slomp et al., 1996b, 2002, 2004). We evaluate these processes by first noting that molar $TOC/P_{reactive}$ ratios are considerably lower than TOC/P_{org} ratios (Fig. 2.11). These lower $TOC/P_{reactive}$ ratios suggest that Fe (oxyhydr)oxide minerals must contribute an additional source of P to the sediment, which is consistent with the higher concentrations of P_{Fe} observed in surface sediments (Fig. 2.9). Nevertheless, despite additional P drawdown in association with Fe

(oxyhydr)oxides, $TOC/P_{reactive}$ ratios remain well above the Redfield Ratio for sediment intervals not affected by landslides, demonstrating that a significant proportion of the P released during organic matter degradation and Fe (oxyhydr)oxide reduction is recycled back to the water column. This observation is further supported by the relatively low P_{auth} concentrations in all three cores (Fig. 2.9).

Since the actual fluxes of the different primary reactive P fractions to the sediment are not known, it is not possible to evaluate the relative extent of recycling of different P phases back to the water column. However, close to the sediment water interface, molar $TOC/P_{reactive}$ ratios increase from the oxic core (260:1), through the chemocline core (345:1), to the euxinic core (452:1), consistent with previous studies highlighting the role of water column anoxia, and particularly sulfidic conditions, in enhancing P recycling back to the water column (e.g., Ingall and Jahnke, 1994, 1997; van Cappellen and Ingall, 1994; Slomp et al., 2002, 2004). A significant flux of P from the sediments under euxinic conditions is supported by the increase in dissolved water column phosphate at depth (Fig. 2.2). The contrasting behaviour of the P cycle across intervals affected by landslides is also entirely as expected. The rapid burial of sediment would result in a greatly reduced flux of mobilised P back to the water column. Hence, $TOC/P_{reactive}$ ratios are considerably lower and close to 106 across all landslide intervals (Fig. 2.11a and b). Algeo and Ingall (2007) collect data from different aqueous systems and reported that beneath a well-oxygenated water column, the C_{org}/P ratio in sediments is below 50; in suboxic to anoxic systems (maybe nitrogenous to ferruginous conditions), the median value of C_{org}/P ratio is close to 106; and in sulfidic systems, the C_{org}/P ratio is much higher than 106. The redox proxy shows that C_{org}/P increases from oxic conditions to euxinic conditions, which is consistent with the $C_{org}/P_{reactive}$ in the Lake Cadagno sediments, in sediments unaffected by landslides. As the detrital P is not included in the $P_{reactive}$, the ratio of $C_{org}/P_{reactive}$ should be higher than C_{org}/P. The low ratio of C_{org}/P under oxic conditions is due to remineralized organic P trapped by adsorption and complexation reactions (Slomp et al., 1996a) or the biological sequestration of polyphosphates (Davelaar, 1993). However, in the sediments affected by landslides in Lake Cadagno, the low $C_{org}/P_{reactive}$ equalling closed to 106 is caused by the low remineralization rates of organic matter and Fe (oxyhydr)oxides, in addition, P is directly precipitated as primary minerals.

In terms of retention of dissolved P in the sediment, the carbonate-fluorapatite (P_{auth}) sink is relatively minor (Fig. 2.9), and much lower than proportions of the total P burial

flux typically found in marine sediments deposited beneath oxic bottom waters (~50%; Ruttenberg and Berner, 1993). The P_{detr} profiles in the euxinic and chemocline core have been strongly affected by the deposition of landslide sediment, but in the oxic core there is a minor increase in P_{detr} with depth. This could potentially be due to slight conversion of carbonate fluroapatite to more crystalline apatite, which would be extracted as P_{detr}. The sedimentary rate is 2 mm/y (Wirth et al., 2013), thus the sediments with the depth of 31.5 cm are deposited for about 160 years. Alternatively, this could be due to a gradual change in the mineralogy of the sediment entering the lake. In either case, this pool does not constitute a major sink for reactive P.

The gradual decrease in dissolved P with depth in the euxinic and chemocline cores does, however, imply the formation of a secondary P phase. In this context, the observed increase in P_{Fe} at depth in the euxinic core (Fig. 2.9) is particularly significant. The concentration of P_{Fe} begins to increase at a depth of ~20 cm, which is where sulfide concentrations rapidly decrease to low concentrations, and slightly below this depth, dissolved Fe(II) increases when dissolved sulfide is completely depleted (Fig. 2.5). There is no evidence for an increase in reactive Fe (oxyhydr)oxide minerals at this depth (and no evidence for re-adsorption of P; Figs. 8 and 9), and thus this increase in secondary P_{Fe} is unlikely to be due to uptake by ferric oxides (or carbonate minerals; c.f., Kraal et al., 2017). As discussed above, however, there is a clear concomitant increase in $Fe(II)_{unsulf}$ with the increase in P_{Fe}. Unlike some of the other solid phase parameters (such as Fe_{py}; Fig. 2.8), the increase in $Fe(II)_{unsulf}$ does not fluctuate in relation to the landslide-affected sediment. Instead, there is a gradual increase in $Fe(II)_{unsulf}$ below ~15 cm depth, indicating that the formation of this phase likely occurred after the re-establishment of steady state diagenetic conditions following the landslides.

Taken together, the porewater and solid phase geochemical profiles strongly imply the progressive formation of Fe(II) phosphate (vivianite) as porewater sulfate and sulfide become depleted (März et al., 2008a). High concentrations of vivianite are unlikely to occur higher in the core where significant sulfide is present (although vivianite could form in microenvironments, at least as a transient phase; Jilbert and Slomp, 2013), as its formation is suppressed by the formation of FeS (Manning et al., 1994; Reed et al., 2016).

The fine-grained, potentially poorly crystalline nature of vivianite makes direct mineralogical identification problematic at low concentrations in sediments (see Egger

et al., 2015). However, geochemical modelling provides support for the formation of vivianite. We initially consider the saturation index (SI) of vivianite and other key diagenetic minerals (pyrite and siderite). The SI of pyrite is high throughout the euxinic core (Fig. 2.12), but the very low level of sulfide at depth allows dissolved Fe(II) to accumulate in porewaters (Fig. 2.5). The increased availability of dissolved Fe(II) at depth increases the SI for both siderite and vivianite (Fig. 2.12), suggesting that both may potentially form. When additionally considered in terms of Eh-pH (Fig. 2.13), the stability field for pyrite decreases deeper in the sediment, and at the pH of the euxinic porewaters (~8; Fig. 2.4), the formation of vivianite is promoted over the formation of siderite.

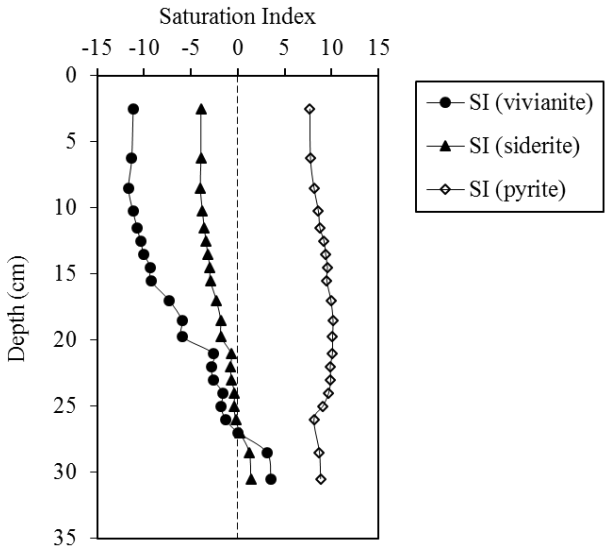

Figure 2.12 Saturation index for vivianite, siderite and pyrite in the euxinic core.

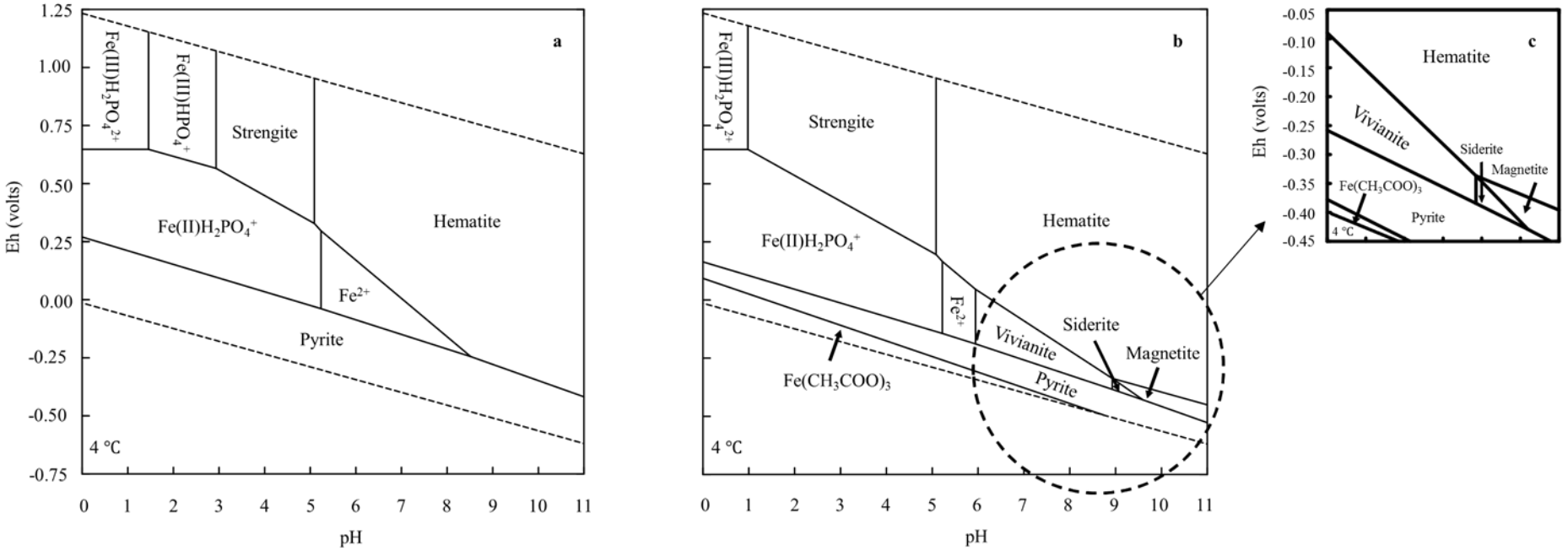

Figure 2.13 Eh-pH diagram showing stability fields for different iron minerals at different depths in the euxinic core (strengite is ferric phosphate mineral: $FePO_4 \cdot 2H_2O$). a) at 0-5 cm; b) at 29.5-31.5 cm; c) enlargement of highlighted area.

Our geochemical and modelling data thus support a growing body of evidence for the importance of vivianite as a significant sink for P during sediment diagenesis in a variety of aquatic environments (Rothe et al., 2014; Jilbert and Slomp, 2013; Slomp et al., 2013; Hsu et al., 2014; Egger et al., 2015; O'Connell et al., 2015; Dijkstra et al., 2014; 2016). Significantly, however, we provide the first evidence for this process as a major control on the permanent sequestration of P below the sulfate/methane transition in a low sulfate although CH_4 is not measured, euxinic water column setting. This is very different to other modern, high sulfate euxinic settings, where vivianite has been found (possibly as a transient phase; Kraal et al., 2017) forming in microenvironments within sediments that still contain significant dissolved sulfide (Jilbert and Slomp, 2013). Egger et al. (2015) found that vivianite formation accounts for 40-50% of total P burial below the sulfate/methane transition zone in sediments deposited beneath the oxic water column of the Bothnian Sea. The total burial flux of P in our euxinic core has been considerably affected by enhanced detrital P inputs from landslide sediment (Fig. 2.9). However, if we reasonably assume that the majority of P_{Fe} measured at depth in the euxinic core is present as vivianite, then this accounts for up to ~60% of the total reactive P burial flux (i.e., discounting P_{detr}) in euxinic Lake Cadagno sediments. Thus, even in euxinic water column settings, vivianite can be a major sink for remobilised phosphorus below a shallow sulfate/methane transition zone (SMTZ) when Fe_{ox} survives to pass into the euxinic water column and surface sediments. If the water is deep or the sedimentation rate is slow, causing all the reactive Fe_{ox} to be sulfidized, Fe is trapped as the more stable pyrite instead of vivianite (e.g. Lyons and Severmann, 2006).

2.5 Summary and implications

We provide the first detailed study of Fe and P cycling in a low sulfate, persistently euxinic setting. Phosphorus recycling to the water column is extensive throughout the basin, but is particularly enhanced beneath the deeper euxinic waters. This is entirely consistent with previous studies of P cycling in anoxic water column settings (e.g., Ingall and Jahnke, 1994, 1997; van Cappellen and Ingall, 1994; Slomp et al., 2002, 2004), but specifically extends this observation to the low sulfate, euxinic settings that were prevalent during Precambrian and Phanerozoic episodes of water column euxinia. Kipp and Stüeken (2017) also suggest that in Archean oceans the limited P is recycled back to water systems due to limited electron acceptors when TOC/P_{org} is close to 106. During this period, Fe(III) works as the main electron acceptor, but most of Fe(III) is

constrained by greenalite (Tosca et al., 2016). After the Proterozoic, a large amount of sulfate is delivered to ocean system while the electron acceptor is changed from Fe(III) to sulfate, the abundant organic matter is remineralized to release dissolved P when TOC/P_{org} is higher than 106 (Kipp and Stüeken, 2017). Phosphorus recycling significantly diminishes the overall P burial efficiency (Ingall and Jahnke, 1994; 1997), thus altering the total P content of the sediment, as well as TOC/P_{org} ratios, providing support for the suggestion (Poulton, 2017) that the total P content of ancient euxinic shales is unlikely to track water column P concentrations (c.f., Reinhard et al., 2017).

During the period of the first GOE (a short time scale), a high flux of sulfate is delivered to the marine system, which directly brings the recycling of P back to the water column in ancient euxinic settings. This consequence would promote a positive feedback in biological productivity, significantly enhancing organic carbon burial (Ingall and Jahnke, 1994; 1997; Van Cappellen and Ingall, 1994) and hence oxygen production. After the GOE during the whole Proterozoic period (long timescale) P recycling is inhibited slightly (Kipp and Stüeken, 2017), dampening the positive feedback in productivity, although euxinic conditions are still the main redox conditions. Our data also suggest that the flux of recycled P to the water column in ancient euxinic settings would have been modulated by the formation of authigenic Fe(II) phosphate minerals. In addition to requiring dissolved P, the formation of Fe(II) phosphate requires that unsulfidized Fe_{HR} minerals persist beneath the sulfate/methane transition zone. In this context, we note that studies of modern and ancient marine settings have demonstrated that 20-30% of the Fe_{HR} pool commonly remains unsulfidized under euxinic water column conditions (Anderson and Raiswell, 2004; März et al., 2008b). Thus, ancient euxinic settings commonly contained sufficient unsulfidized Fe_{HR} to promote vivianite formation beneath the sulfate/methane transition zone when Fe_{ox} passes through the euxinic water column and surface sediments.

The relative extent of water column P regeneration under euxinic conditions through Earth's history can be considered to be sulfate-dependent, since on a global scale, sulfate concentration will (at least partially) determine the depth in the sediment at which Fe(II) phosphate becomes a significant sink for remobilised P. In other words, on a global scale, low sulfate promotes vivianite formation closer to the sediment-water interface, due to the more rapid consumption of all of the dissolved sulfate and sulfide during early diagenesis. Enhanced vivianite formation closer to the sediment-water interface under low sulfate conditions would decrease the flux of P back to the water

column. Thus, as sulfate concentrations increased from the low micromolar range typical of the early Archean (Habicht et al., 2002; Crowe et al., 2014), through the low millimolar range of the later Proterozoic (Kah et al., 2004; Guilbaud et al., 2015), to the moderate millimolar range of many Phanerozoic euxinic episodes (e.g., Adams et al., 2010; Newton et al., 2011; Song et al., 2013; Poulton et al., 2015), the significance of the Fe(II) phosphate trap for remobilised P under euxinic conditions likely progressively diminished. As such, the formation of vivianite would be not be expected to exert such a strong control on P recycling under the higher sulfate concentrations typical of modern euxinic marine settings. As a natural extension of these observations, our data suggest that P recycling likely maintained mid-Proterozoic, shallow marine phosphate concentrations at moderate, rather than very low (c.f., Reinhard et al., 2017) levels, under the widespread euxinic conditions envisaged for such settings (e.g., Canfield, 1998; Scott et al., 2008; Poulton et al., 2010; Poulton and Canfield, 2011; Kendall et al., 2011), with significant implications for organic carbon production and burial, and hence the production of atmospheric oxygen.

After the first GOE, effective P recycling back to the water column likely maintains relatively high productivity, promoting organic carbon burial and hence net oxygen production. However, due to the low concentrations of sulfate envisaged for the mid-Proterozoic ocean, a significant proportion of the recycled P is ultimately trapped as iron phosphate, which would have helped to moderate productivity and hence maintain relatively low atmospheric oxygen levels, furthermore, the low PAL directly limits the eukaryotic evolution at this time. Thus, Fe(II) bound phosphate likely plays a significant, but currently under-appreciated, role in Earth's oxygenation history.

Chapter 3 Chemical controls on the formation of vivianite versus sulfate green rust

3.1 Introduction

Unlike the well oxygenated conditions of most of the modern ocean, anoxic conditions prevailed throughout much of Earth's history. Through the Precambrian, deeper water ferruginous conditions were widespread (e.g. Canfield et al., 2008; Poulton et al., 2010; Planavsky et al., 2011). However, from ~1.84 to 1.0 Ga, along productive continental margins and in epicontinental seas, euxinic conditions were also likely a widespread feature of mid-depth waters (e.g. Canfield et al., 1998; Poulton et al., 2004a; Scott et al., 2008; Poulton and Canfield, 2011). Through much of the Neoproterozoic, ferruginous conditions returned to dominance throughout most of the water column, beneath oxygenated surface waters (e.g. Canfield et al., 2008; Johnston et al., 2010; Guilbaud et al., 2015; Sperling et al., 2015), although in some environments euxinic conditions also occurred (e.g. Li et al., 2010; 2012; Sahoo et al., 2012; Och et al., 2016; Thomson, et al., 2015). During Phanerozoic ocean anoxic events (OAEs), euxinic and ferruginous conditions fluctuated across short time periods, which had a large impact on P cycling (Marz et al., 2008; Poulton et al., 2015).

Under global ferruginous water column conditions, bioavailable P is known as a limiting nutrient which, to a certain extent, is controlled by co-precipitation and adsorption onto Fe (oxyhydr)oxides (Bjerrum and Canfield, 2002; Jones et al., 2015; Reinhard et al., 2017). By contrast, under sulfidic conditions, bioavailable P may be more significantly released back to solution via the reductive dissolution of Fe (oxyhydr)oxides by hydrogen sulphide (Pyzik and Sommer, 1981; Dos Santos Afonso and Stumm, 1992; Peiffer et al., 1992; Poulton, 2003; Poulton et al., 2004b) and by release during organic matter degradation (Ingall et al., 1993; Dellwig et al., 2010). Therefore, redox controls on iron mineralogy play a substantial role in the cycling of phosphorus. In the absence of sulphide, Fe(II) produced by Fe(III) reduction may react and form a range of secondary minerals, whose nature depends on the provision of different oxyanions such as bicarbonate, sulphate and phosphate (Schwertmann and Taylor, 1972; Cornell et al., 1987; Fredrickson et al., 1998; Kukkadapu et al., 2004). For example, magnetite formation is favoured at high pH in the absence of phosphorus; at neutral pH and with high bicarbonate concentrations, Fe(II) may react to form siderite; under more acidic conditions, goethite or lepidocrocite become the dominant

Fe-bearing minerals during early diagenesis (Zachara et al., 2002). Furthermore, green rust (GR) has been suggested to be a prominent mineral forming under ferruginous water column conditions (Zegeye et al., 2012), which can adsorb large amounts of phosphate on surface sites (Bocher et al., 2004; Borch and Fendorf, 2008). Alternatively, in the presence of higher concentrations of phosphate, Fe(II) phosphates such as vivianite may form (Kukkadapu et al., 2004).

GR is a mixed Fe(II)/Fe(III) hydroxide, with brucite-like Fe(II)/Fe(III) tri-octahedral hydroxide layers alternated with interlayer anions (CO_3^{2-}, Cl^-, SO_4^{2-}) (Bernal et al., 1959), arranged in either hexagonal geometry for the sulphated species ($GRSO_4$), or rhombohedral geometry for the carbonated and chlorinated species ($GRCO_3$ and GRCl, respectively) (Simon et al., 2003). Because of the mixed valence of GR, its formation pathways involve the redox cycling of Fe. GR can form during partial Fe(II) oxidation by nitrate reducing bacteria or by photoferrotrophs (Kappler and Newman, 2004), or by the bioreduction of ferrihydrite under anoxic conditions (e.g. Fredrickson et al., 1998; Ona-Nguema et al., 2004). There are also a range of abiotic pathways accounting the formation of GR. For instance, GR can be directly formed by partial oxidation of $Fe(OH)_2$ (e.g., Schwertmann and Fechter, 1994; Refait et al., 1997, 1998; Randall et al., 2001), the partial reduction of ferrihydrite or lepidocrocite by non-sulphidic reducing agents (Hansen, 1989), or by the reaction between ferric (oxyhydr)oxides and Fe^{2+} (e.g. Usman et al., 2012). Because of their mixed Fe(II)/Fe(III) structure, GR particles can rapidly transform into magnetite (e.g. Guilbaud et al., 2013), and GR has been suggested to be a precursor of magnetite in banded iron formations (e.g. Li et al., 2017; Halevy et al., 2017). GR can accommodate large amounts of phosphate on the lateral {010} and {100} surface sites (Bocher et al., 2004), or P can co-precipitate with GR during the partial reduction of P-doped ferrihydrite (Borch and Fendorf, 2008). Importantly, when the P is sorped onto BIFs arguments, the presence of P stabilises GR minerals, diminishing the extent of potential oxidation or transformation into magnetite (Bocher et al., 2004).

Vivianite is a ferrous phosphate mineral, with the chemical formula $Fe_3(PO_4)_2{\cdot}8H2O$ (Nriagu, 1984). In the natural environment, vivianite may form as small monoclinic prismatic crystals (Mori and Ito, 1950). A body of natural examples suggest that vivianite occurs in shallow sulfidic sediments, at the interface where sulfide is consumed and Fe(II) diffusing from the reduction of ferrihydrite reacts with dissolved phosphate. In these environments, phosphate can derive from the reduction of organic

matter, or from P adsorbed to ferrihydite (e.g., März et al., 2008; Slomp et al., 2013; Hsu et al., 2014; Egger et al., 2015).

Although extensive vivianite formation has been observed in various sedimentary systems (e.g., Egger, 2015), the potential for vivianite to form in the water column of anoxic ferruginous environments is unclear (see Chapter 2). One of the important pathways of biogeochemical P cycling is the diffusion from sediments to the water column (e.g. Pyzik and Sommer, 1981; Dos Santos Afonso and Stumm, 1992; Peiffer et al., 1992; Poulton, 2003; 2017). When P is recycled back to the water column, it is assumed that it is eventually trapped again at the redoxcline, by co-precipitation or adsorption onto Fe and Mn oxide (e.g. Dellwig et al., 2010; Turnewitsch and Pohl, 2010; Dijikstra et al., 2016, 2018). Halevy et al. (2017) suggest that at the redoxcline, freshly formed GR particles may exert primary controls on P removal during adsorption. Due to GR stabilisation by P (Bocher et al., 2004), it is likely that green rust preferentially forms in the presence of phosphate, rather than magnetite (Kukkadapu, 2004). Furthermore, green rust has been reported in modern ferruginous lacustrine water columns (Zegeye et al., 2012). Therefore, when phosphorus is recycled back to the redoxcline, where both Fe(II) and Fe(III) may co-exist, GR minerals likely exert a major control on the cycling and the availability of phosphorus. Yet, there is experimental evidence suggesting that synthesised $GRSO_4$ can transform into vivianite upon P addition (Hansen and Poulsen, 1999), contrasting with the $GRCO_3$ species which tend to be more stable (Bocher et al., 2004; Barthélémy et al., 2012). However, little attention has been given to the P concentration limitations on vivianite versus GR formation (Hansen and Poulsen, 1999).

Here, I will provide new experimental insight into the effect of P concentration on the formation of GR versus vivianite. This study explores a range of Fe(II) to phosphate ratios in order to determine the threshold by which the Fe mineralogy changes, to ultimately provide constraints on controls on P cycling in modern and ancient ferruginous settings. Experiments were conducted in time series, in order to determine rates of reaction and the competition between different mineral phases and the cycling of P.

3.2 Methods

3.2.1 Reagents

Experiments were conducted under CO_2 and O_2-free conditions (<1 ppmv O_2), under a 98% N_2 and 2% H_2 atmosphere. H_2 was used to react with possible traces of O_2 on palladium catalysts. Solutions were made up using 18.2 MΩ cm deionised water (MQ), purged with O_2-free grade N_2 for 50 mins (Butler et al., 1994). Two kinds of reagent solution were prepared before the reaction. Solution 1 was the source of Fe(II), Fe(III) and sulfate, made by the dissolution of $NH_4Fe(III)(SO_4)_2 \cdot 12H_2O$ and $(NH_4)_2Fe(II)(SO_4)_2 \cdot 6H_2O$, to a final concentration of 6 mM Fe(III) and 12 mM Fe(II). The ratio between Fe(III) and Fe(II) was 1:2, according to the stoichiometry of $GRSO_4$ (Ruby et al., 2003). Solution 2 was the source of phosphorus and OH^-, and was made by the dissolution of NaH_2PO_4 and NaOH (36 mM). All the chemicals used here are the high purity salts. Several phosphorus concentrations were explored, as described in Table 3.1. The highest concentration was 8 mM, which corresponds to the stoichiometric ratio of Fe:P in vivianite ($Fe_3(PO_4)_2$).

Table 3.1 P concentrations in the different experimental groups.

	Group 1	**Group 2**	**Group 3**	**Group 4**	**Group 5**	**Group 6**
P concentrations (mM)	0 (no extra P added)	0.08	0.4	2.	4	8

3.2.2 Precipitation, ageing of mix solution, and sample preparation

In this study, the aim was to explore the mechanisms of P cycling operating during the formation of GR (eq. 1; Ruby et al., 2003), and the competition between GR and vivianite formation (eq. 2; Hansen and Poulsen, 1999):

$$4Fe^{2+} + 2Fe^{3+} + SO_4^{2-} + 12OH^- \rightleftharpoons Fe_4(II)Fe_2(III)(OH)_{12}SO_4 \qquad \text{(eq. 1)}$$

$$3Fe_4(II)Fe_2(III)(OH)_{12}SO_4 + 8H_2PO_4^- + 13NH_4^+ \rightleftharpoons 4Fe_3(PO_4)_2 + 6Fe(OH)_3 + 3SO_4^{2-} + 13NH_3 \cdot H_2O + 11H^+ + 5H_2O \qquad \text{(eq. 2)}$$

Six groups of experiments using different P concentrations, including one blank (Group 1) were conducted (Table 3.1). For each group, 25 ml of solution 2 was titrated into 25 ml of solution 1 in one serum bottle at a rate of 0.5 ml/s. This process was repeated 6 times for 6 different samples which were prepared in the 6 different serum bottles. In each group, the samples were prepared for time series experiments: sample 1 was analysed after 0.25 h, sample 2 was analysed after 1 h, sample 3 was analysed after 2 h, sample 4 was analysed after 4 h, sample 5 was analysed after 8 h and sample 6 was analysed after 24 h. When the two solutions were mixed together, a dark green precipitation appeared immediately. After sealing the serum bottles, samples were taken out of the chamber to shake at 100 r/min. After the required reaction time, the sample was moved back to the anoxic chamber for further preparation. The pH of the turbid liquid was measured by a HI 9024 pH meter (error = ± 0.01). During the reaction, 10 ml aliquots of the turbid liquid was withdrawn by 10 ml syringe, then filtered by PES filter (pore size = 0.2 μm) in order to collect the supernatant and analyse dissolved Fe(II), Fe(III) and P. Another 10 ml aliquot of the turbid liquid was vacuum filtered on a cellulose nitrate filter (pore size = 0.2 μm) to collect the solid phase. Collected solid samples were washed with MQ, $MgCl_2$ and a final MQ rinse to extract adsorbed P, Fe(II) and Fe(III) (Ruttenberg, 1992). The remaining 30 ml of the turbid liquid was also vacuum filtered in the same way. The final collected solid samples were washed with 0.1 M NaCl and MQ to decrease the conductivity (Rothe et al., 2014), then mixed with 100 μl glycerol to prevent oxidation during XRD analysis (Hansen, 1989; Guilbaud et al., 2013).

3.2.3 Analytical procedures

Dissolved Fe(II) and adsorbed Fe(II) were measured via the ferrozine method (Stookey, 1970; Viollier et al., 2000), with a RSD of <2%. Dissolved and adsorbed Fe(III) were reduced by 1.4 M hydroxylamine hydrochloride, and then measured via the same method. Dissolved and adsorbed P were measured via the molybdate blue method (Koroleff, 1976; Ruttenberg, 1992), with a RSD of <3%. Fe(II), Fe(III) and P in solid samples were calculated by subtracting the dissolved and adsorbed concentrations from total concentrations. The dissolved and adsorbed concentrations were measured as mentioned before, and the total concentrations were the original concentrations in the chemical reagents made in 3.2.1. P, Fe(II) and Fe(III) in solid species were not measured directly by dissolving the dry solid samples. This was because during drying, the Fe(II) minerals were especially sensitive to oxidation even in the anoxic chamber

where the concentration of oxygen was below 1 ppmv. Glycerol coated samples were smeared on a silicon plate in an anoxic dome, and analysed using a Bruker AXS D8 diffractometer (Cu-Kalpha, voltage = 40kV).Samples were analysed from 5 to 70^{o} 2θ, with a step size of 0.05^{o}-2θ and an integration time of 12 s.

3.3. Results

3.3.1. Dissolved species

For all 6 groups, pH values are relatively constant at 7.64, 7.66, 7.65, 7.71, 7.69 and 7.71, respectively, for the first 4 hours (Fig. 3.1). From 4 h to 8 h, the pH in group 1 increases slightly from 7.63 to 7.72 ± 0.03, and remains stable from 8 h to 24 h (Fig. 3.1a). The pH in group 2 shows a similar profile within the first 4 hours, but the increase becomes relatively low from 7.65 to 7.67 ± 0.03 (Fig. 3.1b). In groups 3, 4 and 5, the pH shows a similar trend, starting to decrease after 8 hours, but the extent of decrease grows significantly with the increase in initial P concentration (Fig. 3.1d, e and f). Specifically, the pH decreases from 7.66 to 7.63 ± 0.03 in group 3 between 8 and 24 h (Fig. 3.1d); in group 5, the variation of pH increases to 0.22 during the same time (Fig. 3.1e). In group 6, the pH starts to decrease after 4 h, reaching 7.39 after 24 hours of reaction (Fig. 3.1f).

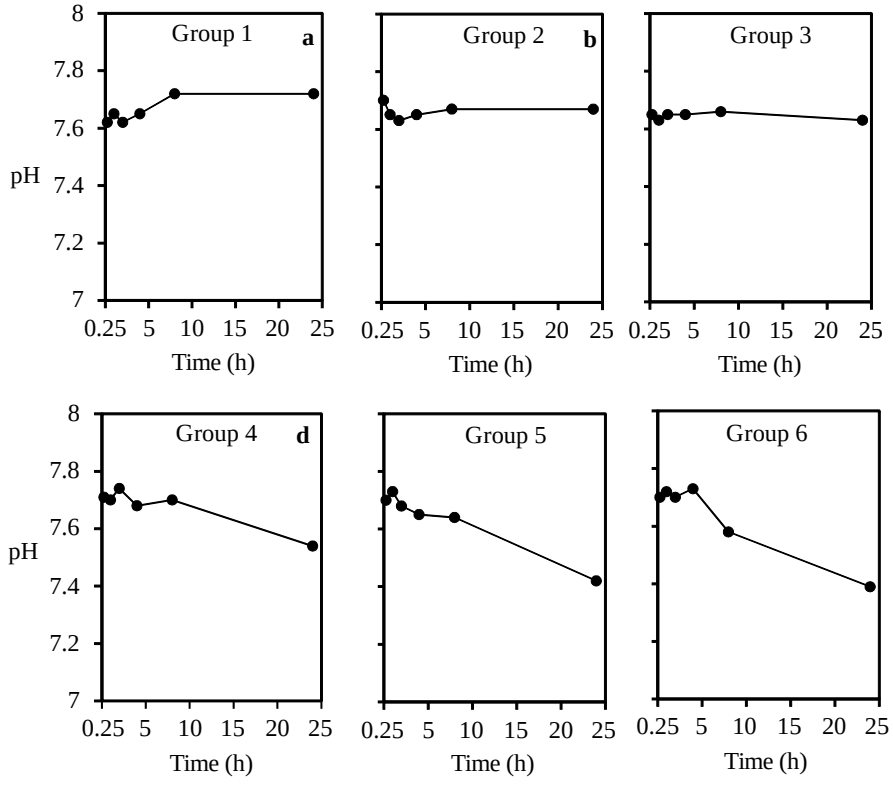

Figure 3.1 pH profiles. a) group 1; b) group 2; c) group 3; d) group 4; e) group 5; f) group 6.

The evolution of dissolved P through time in the experiments is illustrated in Fig. 3.2. For groups 2 and 3, the concentration of dissolved P increases dramatically in the first 4 h, from 0.74 μM to 1.43 μM and from 10.64 μM to 28.38 μM, respectively (Fig. 3.2a and b). After 4 h the rate of increase slows down, and from 8 h to 24 h, dissolved P concentrations stabilise (Fig. 3.2a and b). In the fourth and fifth groups, similar profiles of dissolved P are observed, whereby dissolved P increases in the first hour in both groups, and then decreases. After 8 h, the rate of [P] decrease is enhanced (Fig. 3.2c and d). In the last group, P concentrations keep decreasing throughout the experiment. More specifically, within the first hour, P rapidly decreases from 120.95 μM to 96.81 μM, but from 1 h to 4 h, the decrease slows down from 96.81 μM to 89.27 μM. During the 4 to 8 h period, the concentration of dissolved P decreases rapidly to 39.48 μM, followed by a slower decrease from 8 h to 24 h to 30.93 μM (Fig. 3.2e).

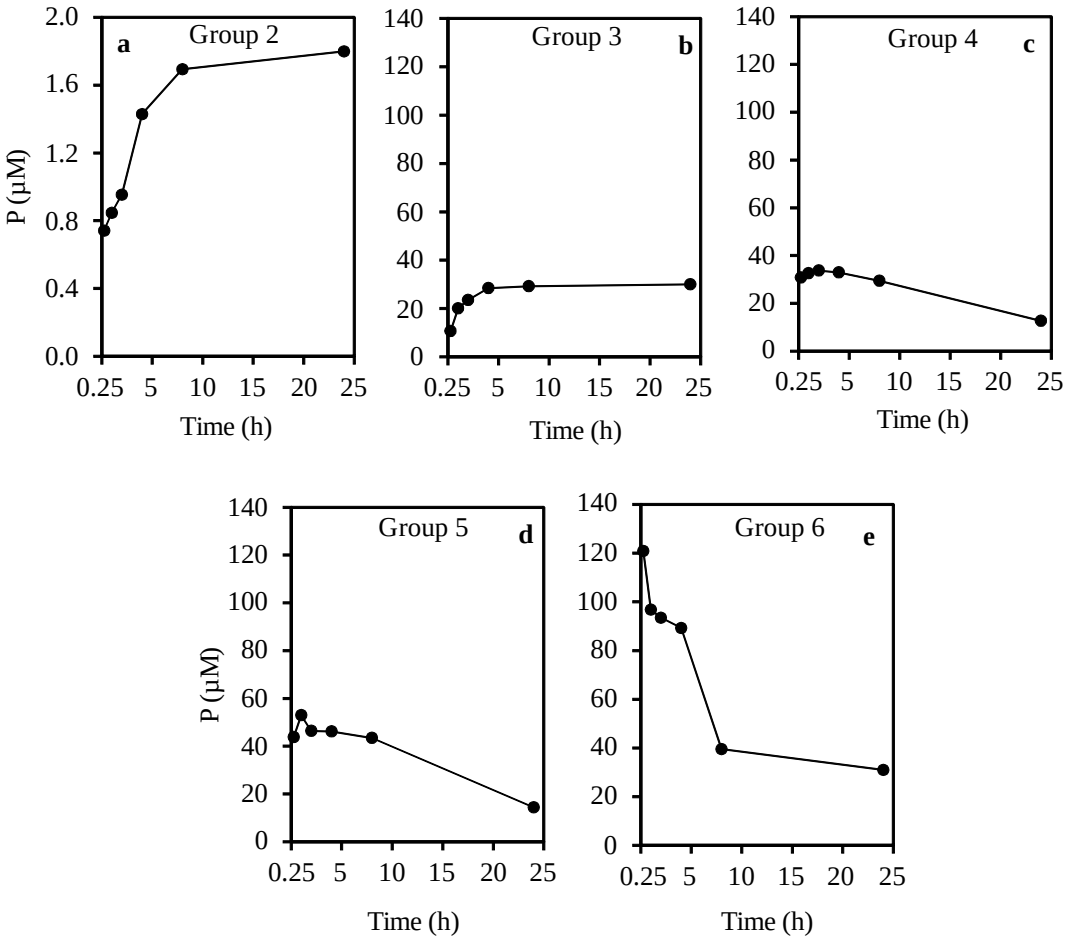

Figure 3.2 Evolution of dissolved P through time in the experiments. a) group 2; b) group 3; c) group 4; d) group 5; e) group 6.

Both dissolved Fe(II) and Fe(III) were measured in the 6 groups from 15 mins to 24 hours (Fig. 3.3). In all groups, no dissolved Fe(III) was detected. In group 1, the concentration of dissolved Fe(II) increases with time, from 0.77 mM to 1.2 mM (Fig. 3.3a). In the other 5 groups, Fe(II) concentrations all decrease with time (Fig. 3.3b, c, d, e and f). Groups 2 and 3 give similar dissolved Fe(II) profiles. In the first 4 h, there is an obvious decrease from 0.5 mM to 0.44 mM and from 0.64 mM to 0.46 mM, for group 2 and 3, respectively, followed by a gradual decrease from 4 h to 24 h (Fig. 3.3b and c). In groups 4 and 5, similar dissolved Fe(II) profiles are observed. The highest concentrations are found at the start of the experiment, with 0.885 ± 0.005 mM Fe(II), followed by a constant decrease from 15 mins to 8 h. Then, the concentrations decrease rapidly from 8 h to 24 h, to reach 0.37 mM and 0.30 mM, respectively (Fig. 3.3d and e). In the last group, Fe(II) concentrations decrease from 0.44 mM at 15 min to 0.16 mM for the 24 h reaction, although the concentrations remain stable at 0.38 ± 0.01 mM from 1 h to 4 h (Fig. 3.3f).

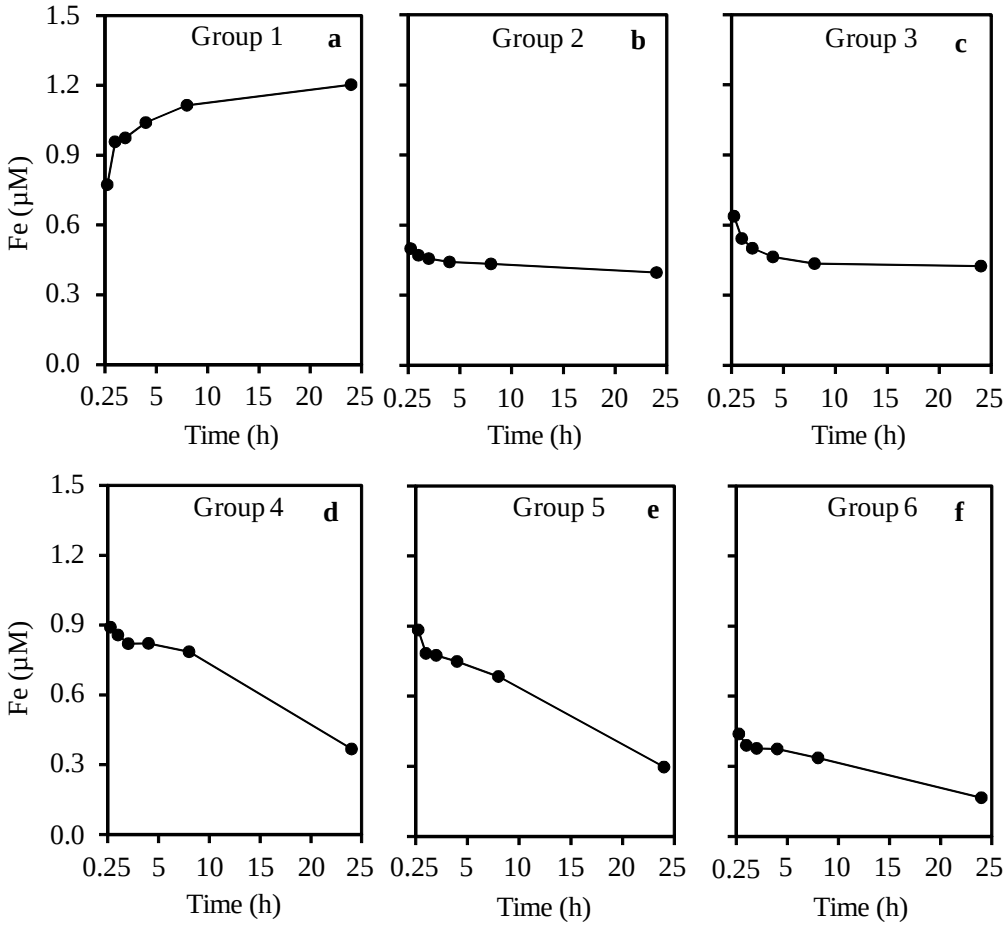

Figure 3.3 Evolution of dissolved Fe(II) through time. a) group 1; b) group 2; c) group 3; d) group 4; e) group 5; f) group 6.

3.3.2 P, Fe(II) and Fe(III) in adsorbed species

Adsorbed P was measured via the method of Ruttenberg (1992). For group 2, adsorbed P deceases from 0.033 μmol to 0.018 μmol in the first 8 h (Fig. 3.4a). From 8 h to 24 h, there is a slight increase from 0.018 μmol to 0.021 μmol from (Fig. 3.4a). For group 3 and group 4, there is a clear increase in adsorbed P in the first 4 h, from 0.85 μmol to 1.19 μmol, and 8.46 μmol to 9.37 μmol, respectively, followed by a strong decrease from 4 h to 8h (Fig. 3.4b and c). After 8 h, for group 3, adsorbed P remains constant at 0.954 μmol ± 0.002 μmol (Fig. 3.4b), however, for group 4, adsorbed P continues to decrease from 5.79 μmol to 3.73 μmol (Fig. 3.4c). For group 5, adsorbed P increases from 27.20 μmol to 30.78 μmol in the first 1 h (Fig. 3.4d). Then P rapidly decreases from 30.78 μmol to 6.76 μmol from 1 h to 24 h (Fig. 3.4d). For group 6, adsorbed P starts at the highest value of 42.37 μmol, decreasing dramatically from to 18.60 μmol from 15 mins to 24 h (Fig. 3.4e).

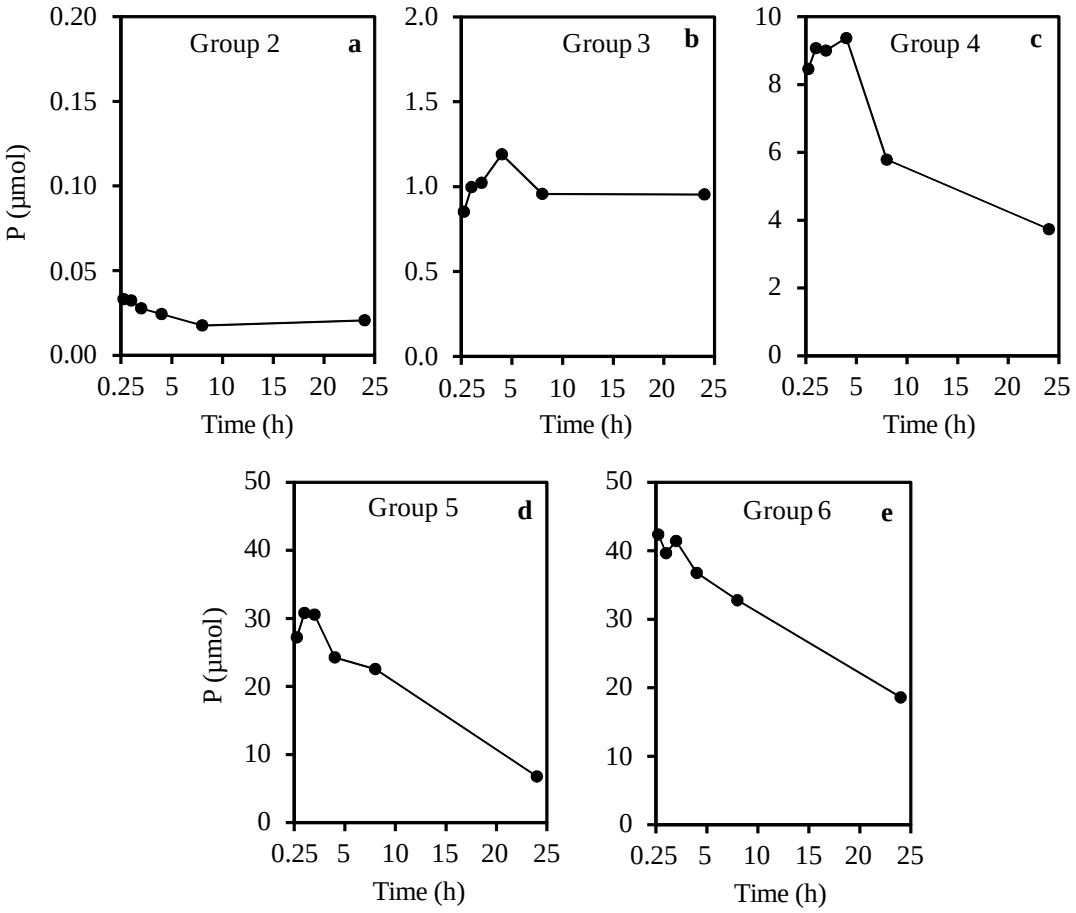

Figure 3.4 Evolution of adsorbed P through time. a) group 2; b) group 3; c) group 4; d) group 5; e) group 6.

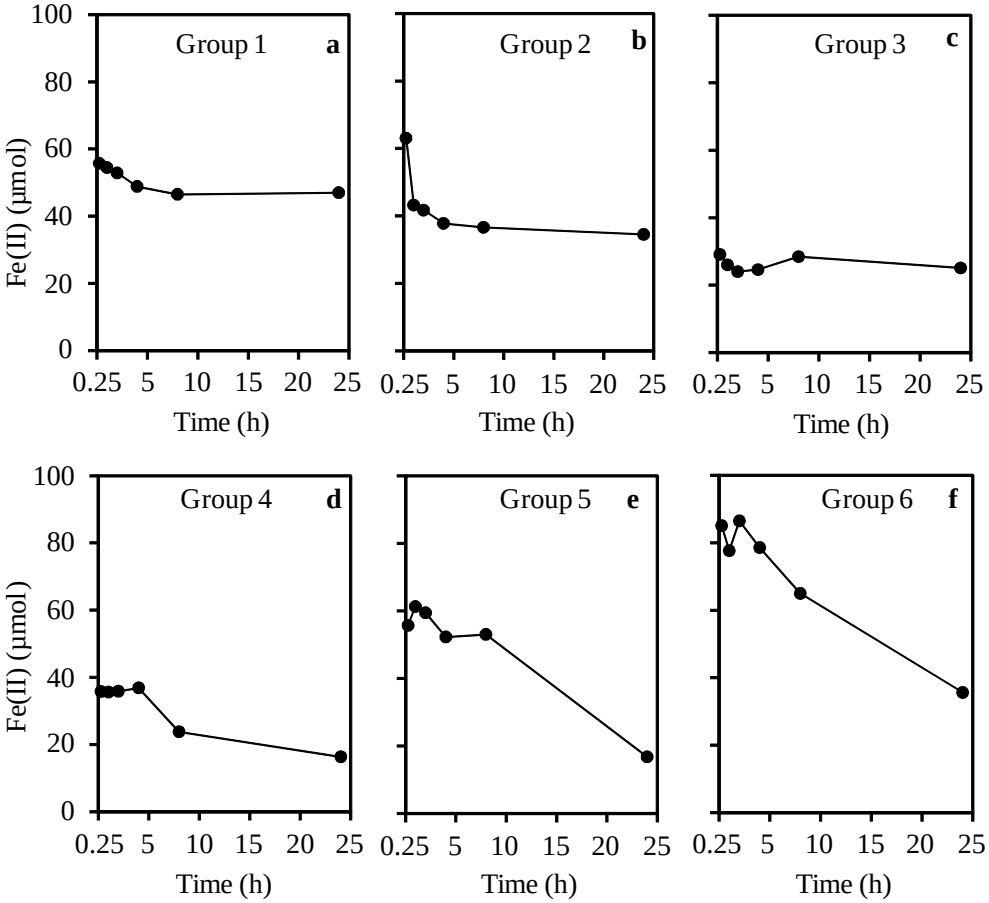

Figure 3.5 Evolution of adsorbed Fe(II) through time. a) group 1; b) group 2; c) group 3; d) group 4; e) group 5; f) group 6.

Both adsorbed Fe(II) and Fe(III) were measured in the 6 groups from 15 mins to 24 hours (Fig. 3.5). In all groups, no adsorbed Fe(III) was detected. In group 1, adsorbed Fe(II) decreases in the first 8 hours from 55.65 µmol to 46.45 µmol, then remains constant at 46.70 ± 0.25 µmol from 8 h to 24 h (Fig. 3.5a). For group 2, adsorbed Fe(II) decreases rapidly from 63.03 µmol to 37.80 µmol in the first 4 h, then the decrease slows down from 37.80 µmol to 34.56 µmol from 4 h to 24 h (Fig. 3.5b). For group 3, adsorbed Fe(II) decreases slightly from 29.14 µmol to 24. 05 µmol in the first 2 h, then increases slightly from 24.05 µmol to 28.46 µmol, followed a slight decrease from 28.46 to 25.12 µmol from 8 h to 24 h (Fig. 3.5c). For group 4, adsorbed Fe(II) stays constant at 35.99 ± 0.84 µmol in the first 4 h, followed by a rapid decrease from 36.83 to 16.26 µmol from 4 h to 24 h (Fig. 3.5d). For group 5 and 6, adsorbed Fe(II) remains relatively constant for the first 2 h at 58.78 ± 2.50 µmol and 83.06 ±3.50 µmol, respectively. However, from 2 h to 24 h, adsorbed Fe(II) decreases rapidly from 59.39 to 16.73 µmol and from 86.50 to 35.58 µmol, respectively (Fig. 3.5e and f).

3.3.3 P, Fe(II) and Fe(III) in solid species

Solid P, Fe(II) and Fe(III) were measured by subtraction of dissolved and adsorbed concentrations from total concentrations. In group 2, solid P decreases with time from 2.00 μmol to 1.96 μmol (Fig. 3.6a). In group 3, solid P decreases from 8.78 μmol to 7.56 μmol from 15 mins to 4 h, then increases slightly from 7.56 μmol to 7.75 μmol from 4 h to 8 h, subsequently remaining stable at 7.73 ± 0.02 μmol from 8 h to 24 h (Fig. 3.6b). In group 4, solid P remains constant from the beginning of the experiment to 4 h at 39.83 ± 0.60 μmol (Fig. 3.6c), followed by an increase from 39.42 μmol to 46.07 μmol from 4 h to 24 h. In group 5, solid P decreases during the first hour from 70.52 μmol to 66.48 μmol, but from 1 h to 24 h the solid P starts to increase from 66.48 μmol to 92.43 μmol (Fig. 3.6d). In the last group, solid P starts to increase at the beginning of the reaction from 152.35 μmol, peaking at 180.63 μmol after 24 hours of reaction (Fig 3.6e).

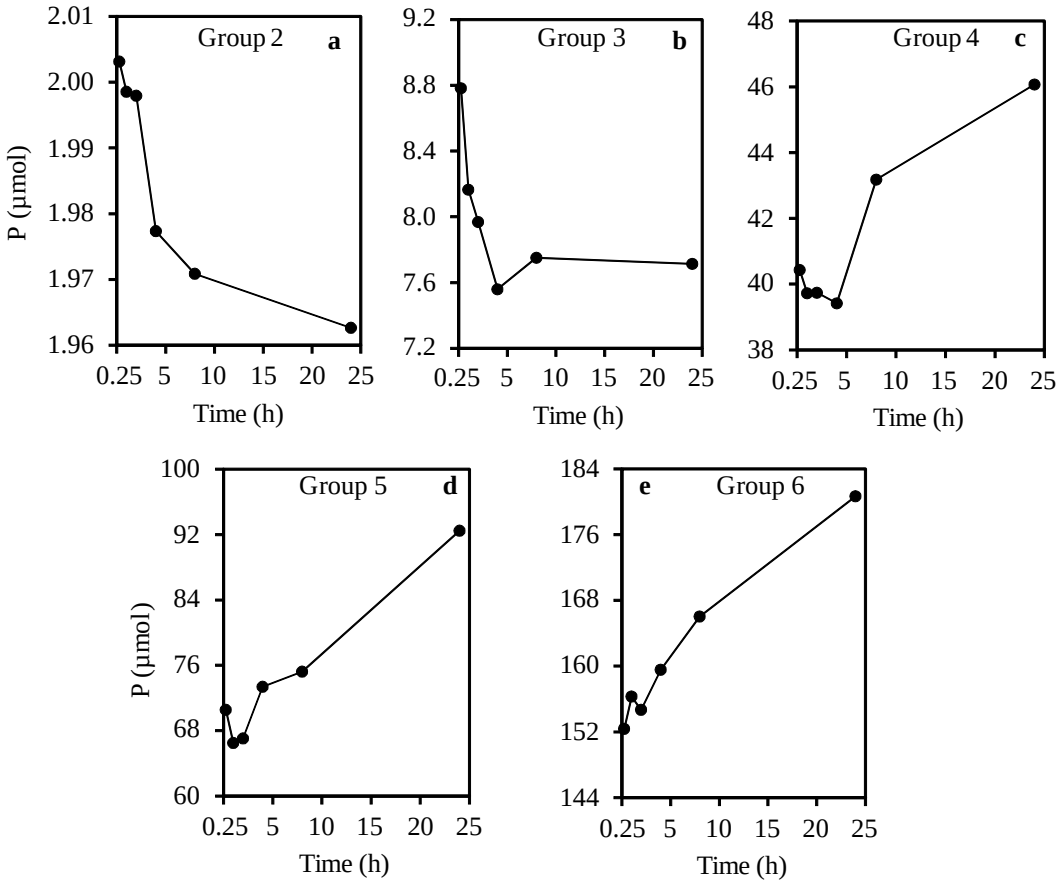

Figure 3.6 Evolution of solid-phase P through time. a) group 2; b) group 3; c) group 4; d) group 5; e) group 6.

Solid Fe(II) in group 1 decreases with time from 206.36 μmol to 193.53 μmol (Fig. 3.7a), but shows an overall increase in the other 5 groups. Groups 2 and 3 have similar

profiles: from 15 mins to 1 h, solid Fe(II) increases, followed by a constant increase from 232.89 µmol to 245.23 µmol and 246.50 µmol to 253.30 µmol, respectively (Fig. 3.7b and c). In groups 4 to 6, solid Fe(II) remains stable around 220.85 µmol ± 1.91 µmol, 203.96 µmol ± 7.31 µmol and 199.17 µmol ± 5.3 µmol, then increases fast from 4 h to 24 h to peak at 264.57 µmol, 269.42 µmol and 257.00 µmol, respectively (Fig. 3.7d, e and f). Since no adsorbed or dissolved Fe(III) were detected in any experimental groups, solid mineral Fe(III) is effectively accounts for 100 % of total Fe(III).

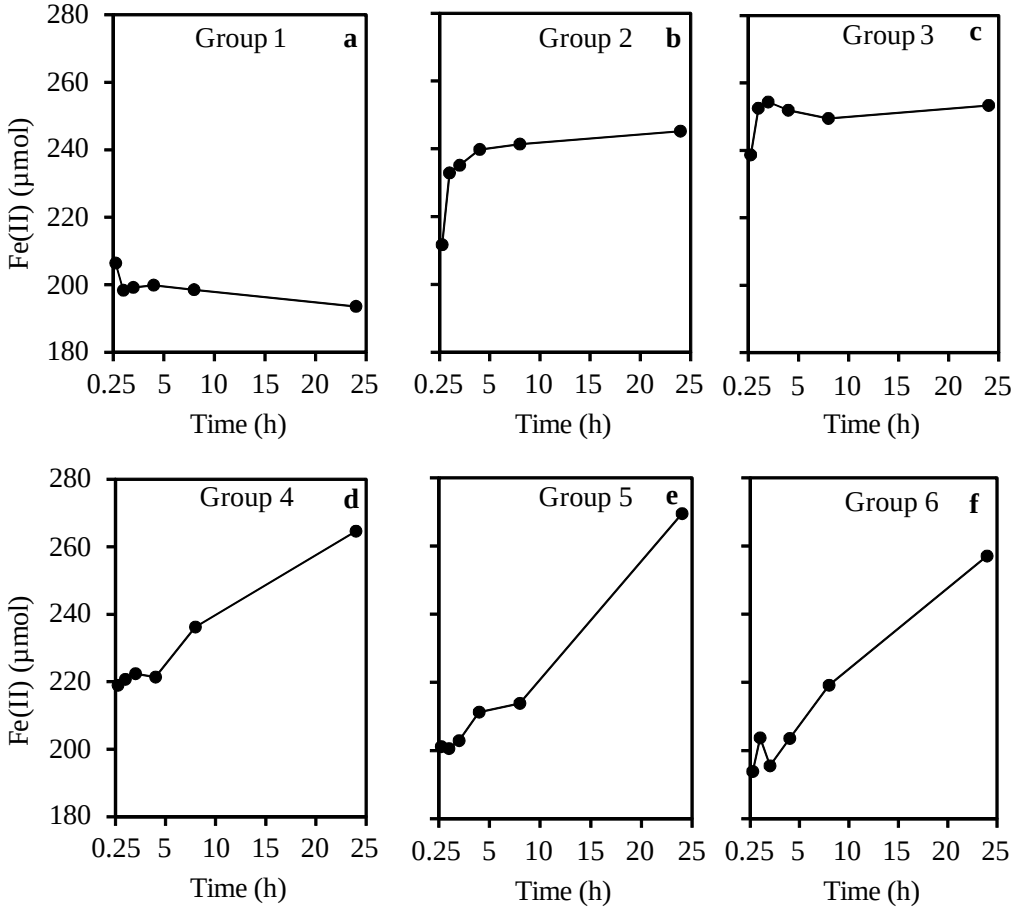

Figure 3.7 Evolution of solid Fe(II) through time. a) group 1; b) group 2; c) group 3; d) group 4; e) group 5; f) group 6.

3.3.4. Mineralogy of the solid phase

XRD was used to analyse the mineralogical evolution of the samples after 15 min, 4 h, 8 h and 24 h in the 6 different groups. In the first three groups (i.e., with zero or low P concentrations), GR is the only mineral identified throughout the entire experiment (Fig. 3.8a, b and c). Furthermore, peak intensities increase with time, indicating that GR particles became more and more crystalline. In group 4, the first 15 min of experiment are characterized by an absence of identifiable peaks, which start developing after 4 h (Fig. 3.8d). At 24 h, both GR and vivianite peaks are identified. In group 5, peak

inhibition is even more severe, with the first identifiable peaks restricted to the 24 h experiment (Fig. 3.8e). In group 6, peak inhibition also occur, but the 24 h experiment shows well developed vivianite peak patterns (Fig. 3.8f).

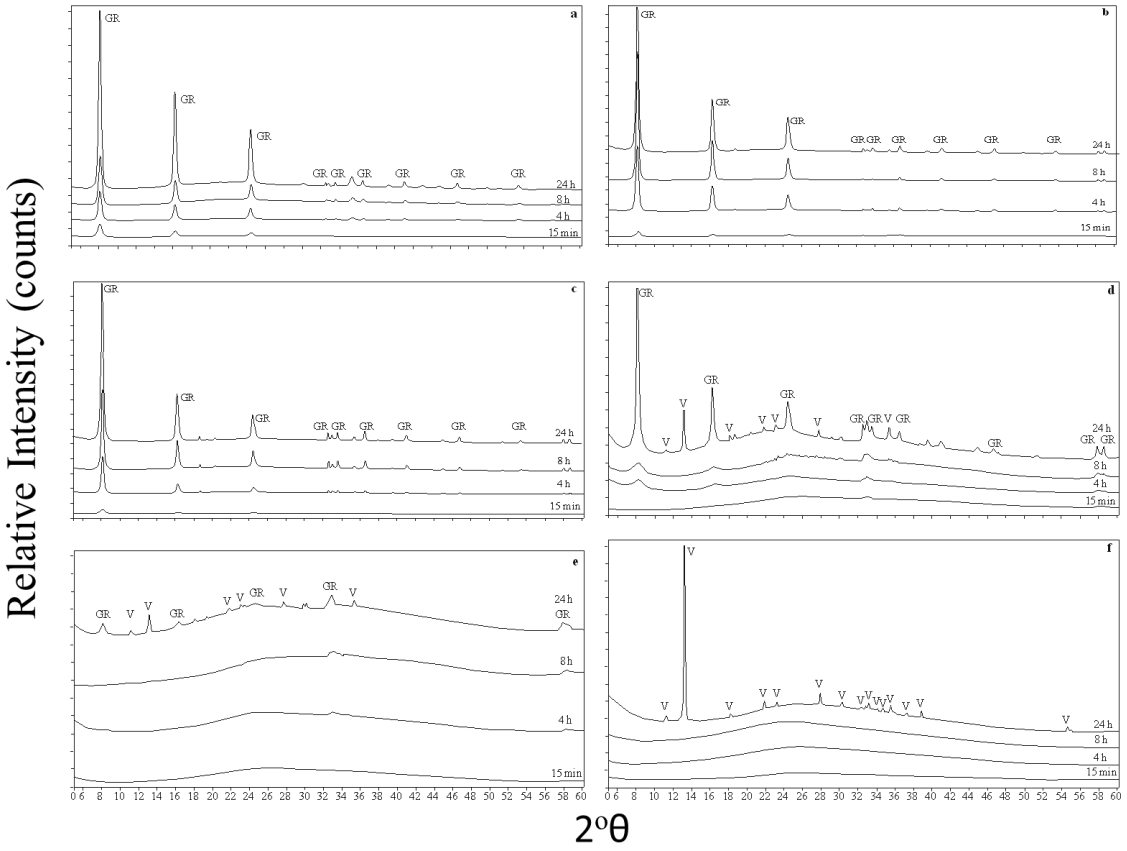

Figure 3.8 XRD spectra of the solid samples. a) group 1; b) group 2; c) group 3; d) group 4; e) group 5; f) group 6. GR stands for green rust and V for vivianite.

3.4. Discussion

The ratios of P and Fe(II) chosen in this experiment include the range of P/Fe(II) in the natural modern water column systems. For example, in group 5 the ratio of P and Fe(II) is 1:3 which is the same as the ratio in the water column of Lake Pavin (Busigny et al., 2014); The ratio of P and Fe(II) in the group 3 and group 4 (1:30 to 1:6) covers the ratio variations in the chemocline of Lake Cadagno (see Chapter 2) and the oligotrophic aqueous environments, such as Lake Matano (Crowe et al., 2008); The P/Fe(II) ratio in the group 2 equalling to 150 covers the ratio in Lake La Cruz (Thomson, 2018). The ratio of P and Fe(II) equalling to 1:1.5 in group 6 is the stoichiometric ratio of Fe:P in vivianite.

3.4.1 pH evolution and changes in reaction mechanisms

The pH profiles described above allow changes in the reactions involved during mineral precipitation and transformation to be tracked. As indicated by the blank (no added P) experiment, GR formation starts at pH = 7.64 ± 0.02, which is in agreement with previous studies (Ruby et al., 2003; Guilbaud et al., 2013). This also agrees with X-ray diffraction data where no peaks other than GR are present throughout group 1 experiments (Fig. 3.8a). When P is present in the experiment (groups 2 to 6), the pH values stay at 7.69 ± 0.05 during the `first 4 hours, which is close to the blank value, suggesting that during this time, the system may still be controlled by GR formation upon P addition. From 4 h to 8 h, the blank pH begins to increase and stays stable from 8 h to 24 h (Fig. 3.1a), suggesting that after 4 h, unstable $GRSO_4$ starts to transform into more stable phases such as lepidocrocite, $Fe(OH)_2$ or more likely magnetite (e.g. Schwertmann and Fechter, 1994; Guilbaud et al., 2013). GR transformation to magnetite releases OH^-, increasing the pH, which is also controlled by the presence of NH_4^+ ions. There is no mineralogical evidence for the formation of other crystalline phases (Fig. 3.8a; although their formation may be insufficient to register on the diffractograms), suggesting that GR is the dominant species. With increasing P levels, there is a heightened decrease in pH, which suggests the involvement of an alternative reaction. The formation of Fe(II) phosphate from GR (eq. 2) is accompanied by the release of protons, which would decrease the pH. This may suggest that the formation of Fe(II) phosphates such as vivianite may compete with GR in controlling P concentrations and pH under these conditions. Note that all experiments are within the pH window where both GR and vivianite can form. Specifically, GR begins to form at pH = 6.5, but to transform to magnetite when the pH value increases above 8 (Guilbaud et al., 2013). For vivianite precipitation, the best pH value equals between 7 and 8 (Madsen and Hansen, 2013).

3.4.2 P and Fe cycling at low P concentrations

At low P concentrations (groups 2 and 3), the synchronous increase in dissolved P and decrease in solid-phase P during the early stages of the experiment (Figs. 3.2a, 3.2b, 3.6a and 3.6b) suggest that dissolved P is sourced from the solid phase. As mentioned above, chemical and mineralogical data suggest that during the first hours of the experiment, GR is likely to be the only dominant Fe mineral, and the concentrations of P in both the solid and solution may be controlled by co-precipitation or adsorption onto GR surfaces. Bocher et al. (2004) suggest that GR-associated P is likely adsorbed to the

lateral faces of the particles, rather than incorporated into the interlayers of the mineral, implying that increased dissolved P concentrations cannot be sourced from interlayer phosphate anions. However, the geometry of $GRCO_3$ used in the Bocher et al. (2004) experiment differs from the $GRSO_4$ species used in this study, and phosphate may exchange with interlayer sulfate in $GRSO_4$ minerals (Dutta and Puri, 1989; Hansen and Poulsen, 1999). Therefore, the initial increase of P is released from adsorbed P and interlayer P when GR begins to transform. Furthermore, in the absence of P, increasing dissolved Fe(II) concentrations in the early stages of the reaction suggest that GR may dissolve and release Fe(II), implying that potential interlayer phosphate may also be released during this phase. Therefore, the increase in dissolved P likely reflects a combination of GR transformation (eq. 1) and P desorption from the positively charged GR surfaces at a pH below the point of zero charge for GR (Guilbaud et al., 2013). At low P concentrations, however, the observed decrease in dissolved Fe(II) (Fig. 3.3b and c), with concomitant increase in solid-phase Fe(II) (Fig. 3.7b and c), suggest that initial Fe(II) release from GR is rapidly compensated by the precipitation of a secondary Fe phase. However, the absence of peaks other than GR throughout these experiments (Fig. 3.8b, c, and d) suggests that this secondary phase is either amorphous Fe(II) phosphate, or in insufficient amount for detection by XRD.

3.4.3 P and Fe cycling at higher P concentration

At higher P concentrations (groups 4 and 5), the initial increase in dissolved P is rapidly compensated by a decrease in dissolved P concentrations after the first hour of the experiment (Fig. 3.2c and d). During this decrease, solid-phase P shows a concomitant increase (Fig. 3.6c and d) which can suggest partial removal of P from solution during re-adsorption, but more likely the precipitation of secondary P minerals. Indeed, the synchronous increase in solid-phase Fe(II) (Fig. 3.7d and e) supports the latter mechanism. XRD data also imply the precipitation of a secondary phase consisting of vivianite (Fig. 3.8d and e). It does appear, however, that the presence of phosphate hampers the development of crystalline phases in the early stages of the experiment, as reflected by the absence of diffraction peaks. In group 6, which is characterized by the highest P concentrations, there is no observable P increase during the initial stages and instead, dissolved P decreases from the start of the experiment (Fig. 3.2e), while solid-phase P increases rapidly (Fig. 3.6e). Therefore, it seems that dissolved P precipitates from amorphous Fe-P precursors, without the intervention of intermediate GR minerals. This is supported by the mineralogical data (Fig. 3.8f), which reveal that vivianite

constitutes the only measurable crystallites in the system. Of course, since Fe(II) precipitates as vivianite and dissolved Fe(III) was not detected throughout the experiment, it can be reasonably assumed that the total solid phase should also experience an increase in ferric Fe. The precipitation of amorphous $Fe(OH)_3$ is favoured between pH 7 and 8 (Christian, 2014), which would support the absence of ferric diffraction peaks in the XRD diffractograms. The presence of P may also explain the lack of crystallinity in the neoformed ferric species, as the development of crystalline ferric oxides such as hematite, goethite or lepidocrocite is slowed down by P (Gálvez et al., 1999). The solubility rate of GR is difficult to calculate because when GR releases dissolved Fe(II), it is also trapped by phosphate. However, the rate of Fe(II) phosphate formation in the groups with high P concentrations ([P] = 2mM, 4mM and 8mM) can be calculated. When the decomposition of GR is nearly complete, the formation of Fe(II) phosphate dominates the pathways of dissolved Fe(II) and dissolved P. The formation rates of Fe(II) phosphate can be calculated as 0.33 μmol/h, 1.12 μmol/h and 1.17 μmol/h, the data is used from Figure 3.6.

3.4.4 Mineralogical analysis

Dissolved Fe(II) concentrations for the 15 min experiments (the first data points) of each group were compared in order to understand the impact of P addition to the cycling of Fe(II) (Fig. 3.9). When P is present, initial dissolved Fe(II) concentrations decrease from 0.77 mM to 0.50 mM, implying that the early stages of the experiment promote the precipitation of an Fe-P phase, subsequent to the dissolution of GR. As opposed to $GRCO_3$, $GRSO_4$ is not inert (Bocher, et al., 2004; Barthélémy, et al., 2012), and phosphate is likely to exchange with sulfate anions and form amorphous Fe(II) phosphates. With increasing initial P concentrations, dissolved Fe(II) concentrations increase from 0.50 to 0.89, which suggests that increasing P concentration promotes the release of Fe(II) by GR dissolution. Therefore, when P concentrations increase, phosphorus-containing GR converts to amorphous Fe(II) phosphates, inhibiting the development of well crystalline GR (Hansen and Poulsen, 1999, Fig. 3.10a and b). However, as P reaches its highest initial concentration, dissolved Fe(II) decreases down to 0.44 mM (Fig. 3.9), implying that an alternative mineralization pathway operates under these conditions, with about half of dissolved Fe(II) (0.44:0.89) reacting directly with dissolved P to form amorphous iron phosphates.

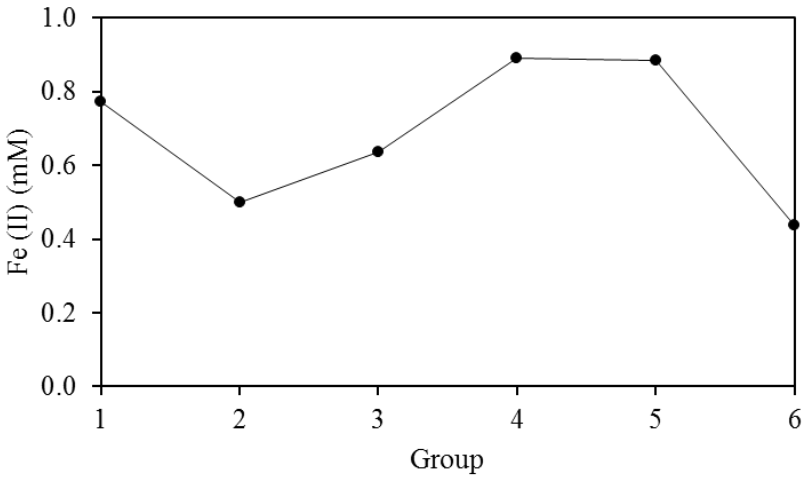

Figure 3.9 Dissolved Fe(II) concentrations in solution after 15 minutes of reaction in the 6 different groups**.**

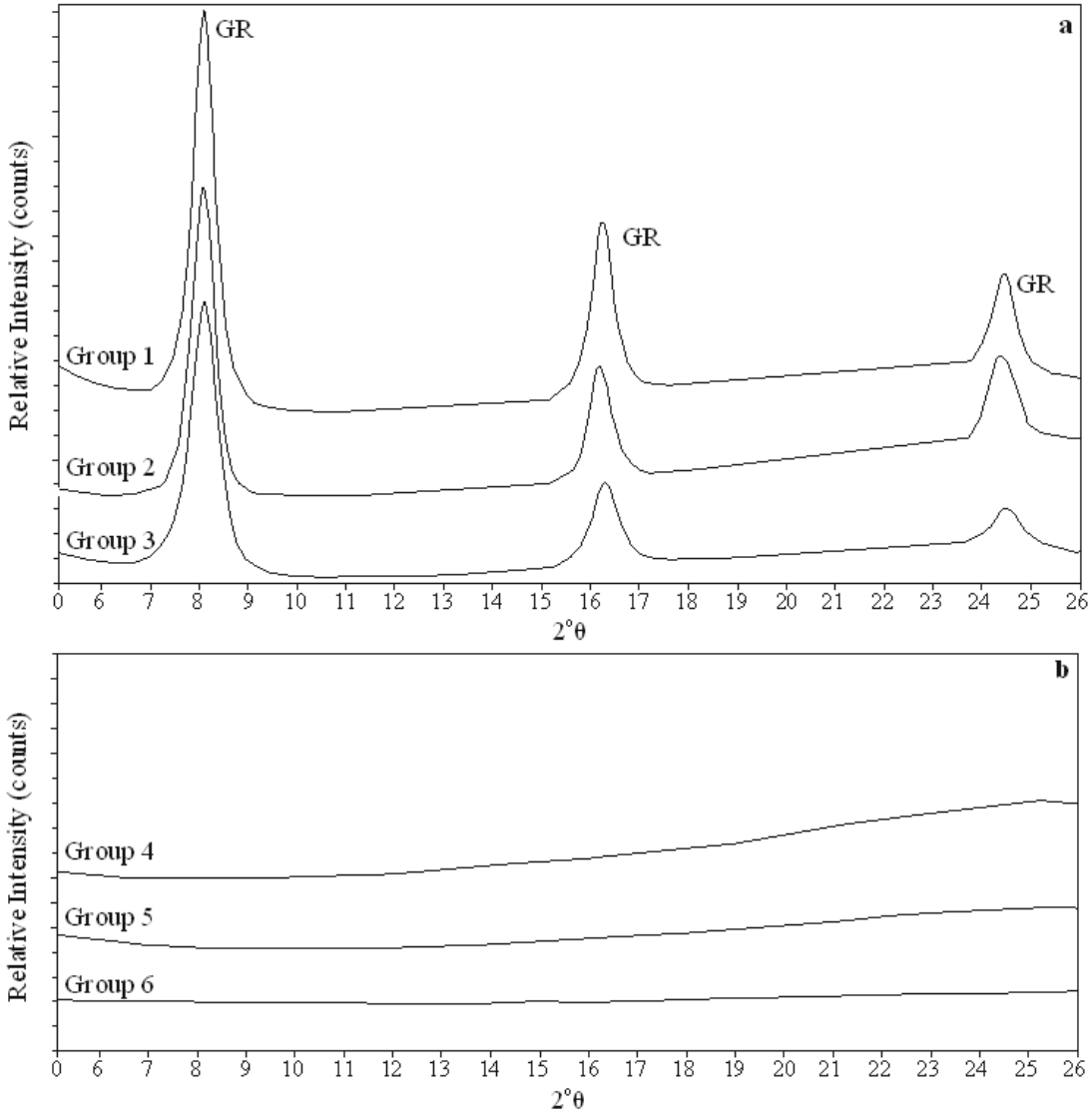

Figure 3.10 XRD spectra of solid samples for the 15 mins' reaction. a) group 1-3 b) group 4-6. GR stands for green rust.

As mentioned above, in the presence of low P, the development of crystalline GR requires a longer time, as indicated by the increase in peak intensity between the 15 min and the 24 h experiments (Figs. 3.10a and 3.11a), which agrees with previous studies (Hansen and Poulsen, 1999). For P concentrations >2 mM (groups 4 to 6), vivianite crystallises between 8 and 24 h (Figs. 3.10b and 3.11b). The lag time in vivianite crystallization is likely due to the formation of an amorphous intermediate phase during the conversion of interlayered-phosphate GR to vivianite (Hansen and Poulsen, 1999; Borch and Fendorf, 2008). Figure 3.12 shows the evolution of the molar Fe(II):P ratio throughout the group 6 series, in order to compare the stoichiometry of freshly precipitated Fe(II) phosphate to vivianite. From 15 min to 24 h, the ratio increases from 1.27 to 1.42, which is close to stoichiometric vivianite, and supports that a large part of precipitated P consists of amorphous Fe(II) precursors. Residual P solids transform gradually to Fe(II) phosphates, following the same pathway as for groups 4 and 5. Fe(II) phosphate precursors later convert to crystalline vivianite, the only measurable crystalline phase in the system.

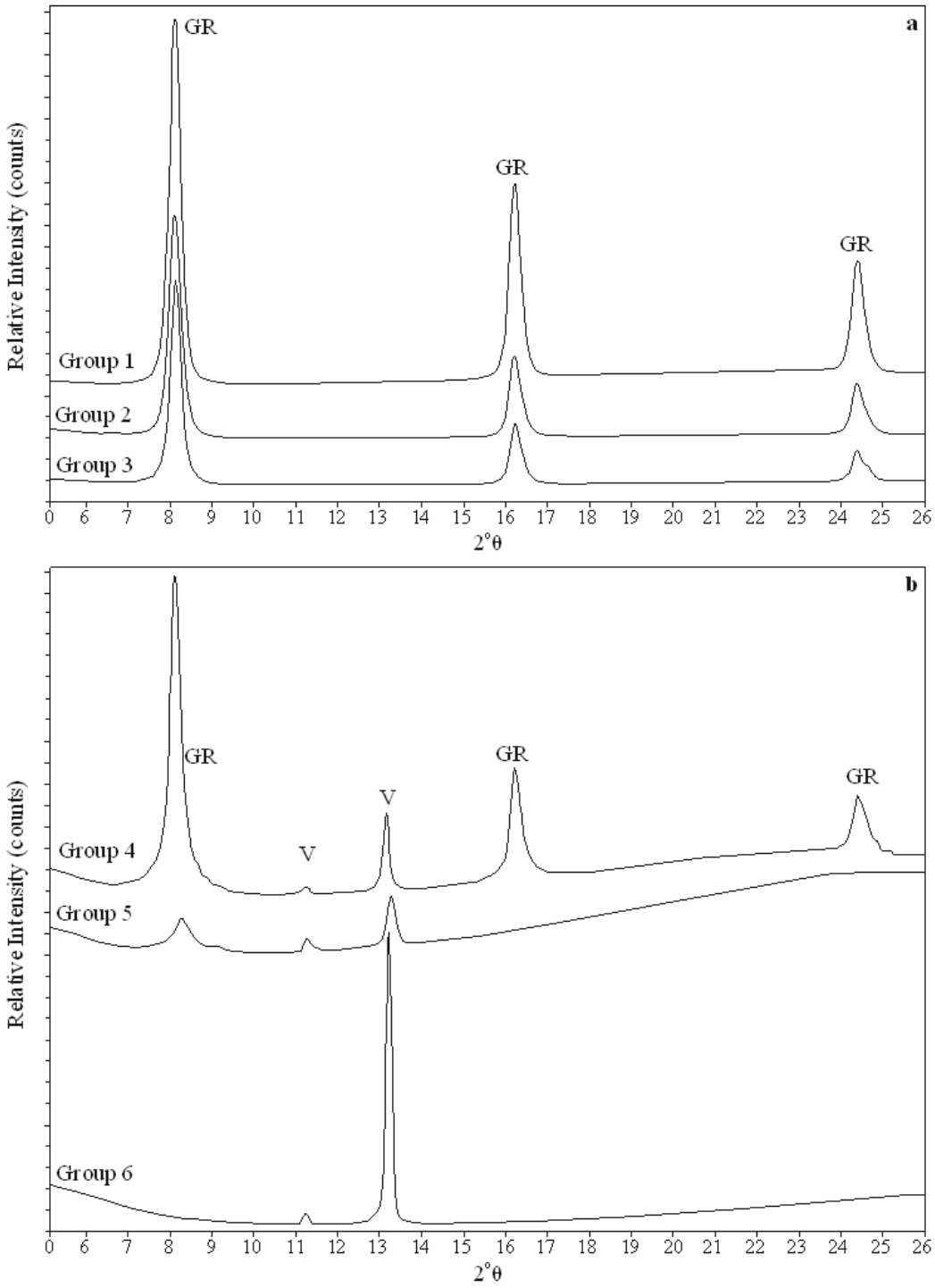

Figure 3.11 XRD spectra of solid samples for the 24 hours' reaction. a) group 1-3 b) group 4-6. GR stands for green rust and V for vivianite.

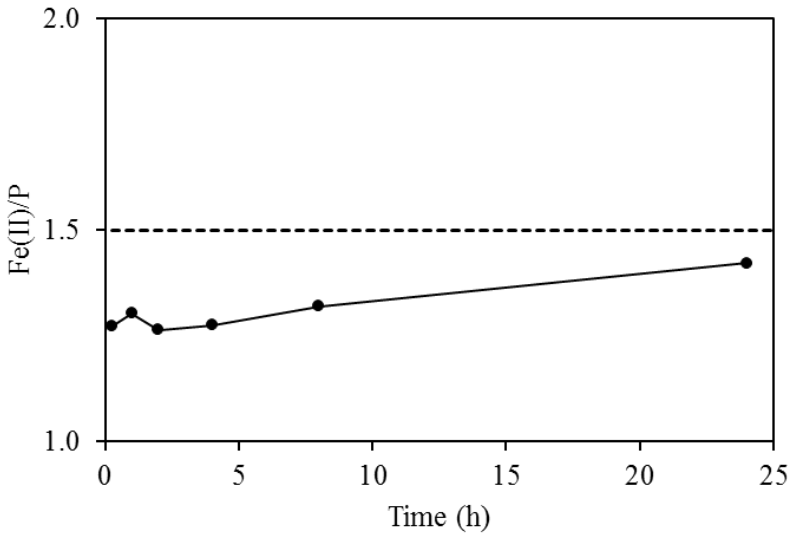

Figure 3.12 Molar Fe(II)/P ratio for group 6 experiment ([P] = 8mM) through time.

3.4.5 Fe(II)-P dynamics for different minerals formation

When Fe(II)/P is above 30:1 or no P is added, pure GR is the main mineral. With the increase of P (Fe(II)/P equalling between 6:1 and 3:1), the GR transforms into vivianite. When Fe(II)/P reaches to 1.5:1, only vivianite is formed. However, Derry (2015) suggest that vivianite begins to form when Fe(II)/P equals to 370 at pH = 7.5 and 160 at pH = 8 which are much higher than the results in this chapter. Their model does not consider Fe(III), instead only focuses on the saturation of vivianite. In other words, P adsorption to Fe minerals is not considered. Furthermore, Derry (2015) indicates that phosphorite formation is inhibited because P is trapped as vivianite. Kipp and Stüeken (2017) point out that phosphorite is inhibited because of limited P input to marine systems, which in turn indicates low levels of oxygen production. When more and more P is recycled back to water column producing a positive feedback of oxygen production, phosphorite begins to form as the dominant solid P phase. Combining with the results in this chapter, GR works as a buffered mineral to sustain solid P phase and avoid the formation of phosphorite. When more than one-third of Fe(II) is oxidized as Fe(III), the balance for phosphorite inhibition is broken. The dynamic of Fe(III)/P should be considered in phosphorite formation, in addition, based on the data from Derry (2015), Fe(III)/P > 123 at pH =7.5 and Fe(III)/P > 53 at pH = 8 contributes to phosphorite formation.

3.5. Conclusion and implications

Pure $GRSO_4$ forms in the absence of or at low P concentrations (< 0.4 mM). For P concentrations below 0.4 mM, P will indeed extensively adsorb at the surface of GR particles, and exchange with sulfate in the interlayers. This results in GR minerals of poorer crystallinity, but also likely more resistant to transform into magnetite. When the concentration of P increases to 2 mM, interlayer phosphate combines with Fe(II) to form intermediate amorphous Fe(II) phosphates. With time, amorphous phosphate converts into vivianite. When P and Fe(II) concentrations approach the molar ratio of stoichiometric vivianite, GR does not form as an intermediate phase and only crystalline vivianite is eventually synthesized. In the natural environment, GR is considered as a major mineral forming at the redoxcline of stratified ferruginous water columns (e.g. Zegeye et al., 2010; 2012; Halevy, et al., 2017), in addition, in the high concentration phosphate environment, Fe(II) phosphate is detected as the dominated mineral in the deeper anoxic water while in the chemocline, the dominated mineral is formed as Fe(II)-Fe(III)-phosphate phase (Cosmidis, et al., 2014).These studies show that P concentrations exert first order controls on the mineralogy of Fe minerals, with strong implications for the availability of dissolved P in the water column. For example, in a global ferruginous ocean where global productivity is low through continual removal of P in association with Fe minerals, GR formation would be expected to be the dominant mineral forming in the chemocline, hence continually removing P from solution and maintaining oligotrophic conditions. These environmental conditions were likely during intervals of the Archean, Paleoproterozoic, and early Neoproterozoic, when widespread ferruginous conditions are indicated by the formation of banded iron formations and via Fe speciation analyses (e.g., Canfield, 2005; Guilbuad et al., 2015). By contrast, during periods when sulphide was more dominant along productive continental margins, such as during the Neoarchean (e.g., Reinhard et al., 2009; Kendall et al., 2010; Zerkle et al., 2012), and the mid-Proterozoic (e.g., Shen et al., 2002; Poulton et al., 2004a; 2010; Scott et al., 2008), P cycling back to the water column was likely more intense (see Chapter 2). Under these conditions, GR was less likely to form. Instead, vivianite precipitation likely exerted a dominant mineralogical control on the bioavailability of P under these eutrophic conditions (e.g., Thomson, 2018). Sulfidic conditions are sustained by trapping re-dissolved P as vivianite which also limits the availability of some trace metals such as Mo, Cu, Zn and Cd (Lewis and Landing, 1992; Anbar and Knoll, 2002). Some work related to the adsorption of trace metals to iron minerals will

be mentioned in future work (Chapter 5.4). In the redoxcline, some studies also mention that Mn(IV)-Fe(III) is the important mineral for trapping dissolved P (Dellwig et al. 2010 and Dijkstra et al., 2018). When the Mn-Fe-P shuttle is active in the euxinic water column, P can be released back to water column, however, phosphorus is precipitated with this mineral in ferruginous conditions (Dellwig et al., 2010). From the behaviour of the P in these studies, Mn-Fe-P is stable in the redoxcline which is not affected by the P concentrations but affected by the redox conditions. If this mineral is combined in the experiment results, the ratio of P/Fe_{total} is changed for the formation of vivianite and GR. For vivianite precipitation, higher concentrations of P may be required.

Chapter 4 Modelling P cycling under different water column redox conditions

4.1 Introduction

Phosphorus, a limiting nutrient, has exerted an important control on primary productivity in the oceans through Earth's history. In oceanic systems, P is removed from the water column through burial in the sediments. This process is highly dependent on the redox condition of the oceanic system.

Under oxic bottom waters, dissolved P is released during the oxidation of organic matter, some of which may be adsorbed to Fe(III) (oxyhydr)oxide minerals (Einsele, 1936; Mortimer, 1941). Once in the sediments, dissolved P in the porewater may build up from the reduction of Fe(III) bound P and oxidation of organic P. This released P may diffuse back to water column, or may adsorb to Fe(III) (oxyhydr)oxides close to the sediment-water interface (Slomp and van Raaphorst, 1993; Slomp et al., 1996 a, b), or may precipitate as more stable carbonate fluorapatite (CFA) (Ruttenberg and Berner, 1993). In addition, the released P may directly precipitate as authigenic P minerals in the sediments, such as Fe(II) phosphate (e.g. März et al., 2008 a, b; Slomp et al., 2013; Hsu et al., 2014; Egger et al., 2015).

Under anoxic ferruginous bottom waters, P may also be buried in sediments in association with organic matter and Fe (oxyhydr)oxides, and P is released from organic matter and Fe (oxyhydr)oxides. However, there is a higher potential for P to recycle back from the sediment to the water column under ferruginous bottom waters than under oxic bottom waters. In a sulfidic water column, where Fe (oxyhydr)oxides are reduced by reaction with dissolved sulfide (e.g. Pyzik and Sommer, 1981; Dos Santos Afonso and Stumm, 1992; Peiffer et al., 1992; Poulton, 2003; Poulton et al., 2004b), much more P is likely recycled back to the water column during settling and from the sediments. In the sediments, released P may diffuse back to water column from the reduction of organic matter and Fe (oxyhydr)oxide (e.g., Ingall et al., 1993; Dellwig et al., 2010), and very little CFA may form (e.g. Mort et al., 2010). The formation of other authigenic P minerals such as vivianite is limited where dissolved sulfide is present. Instead, reduced Fe(II) is trapped as pyrite, to which P does not significantly adsorb (Krom and Berner, 1980; Anschutz et al., 1998). However, iron phosphate may occur when dissolved sulfide is absent (e.g. Mort et al., 2007; März et al., 2008b; Poulton et al., 2015).

Here, four key redox scenarios are considered and modeled, in order to investigate how redox conditions affect P dynamics, and how this may have varied in the past (see 1.4). Firstly, 1. oxic water column conditions with sulfidic porewaters are considered (an oxic setting in Lake Cadagno, Switzerland), which is representative of highly organic-rich sediments deposited under oxic conditions through Earth history. 2. Euxinic water column conditions are also considered for the deeper Lake Cadagno, as a mid-Proterozoic euxinic ocean analogue. 3. Eutrophic ferruginous water column conditions are represented by Lake La Cruz, Spain, represents anoxic conditions at times of organic-rich sedimentation, as might be expected when ferruginous conditions occur spatially adjacent to euxinic conditions (e.g., the 1.8 Ga Animikie Basin; Poulton et al., 2010). 4. Oligotrophic oxic water column conditions with Fe-rich sediments are represented by Golfo Dulce, Costa Rica, which we consider representative of Fe-rich sediments deposited alongside low concentrations of organic matter through Earth history, regardless of whether the water column was anoxic or oxic (e.g., during times of banded iron formation deposition, or under widespread oligotrophic ferruginous conditions).

Lake Cadagno is a meromictic lake and the geological details are described in Chapter 2.2.1.

Lake La Cruz is also a meromictic lake at approximately 1000 m altitude in the Iberian Range near Cuenca (Spain). The bedrock includes dolomite and marls (Santisteban, 1994). The diameter of the lake is 122 m and the maximum depth is 22 m in summer (Romero-Viana et al., 2009). The main source of water for this lake is from ground water located about 4-5 m above the bottom, and the system is closed with no connection to running water (Rodrigo et al., 2001). The stratification is due to the high density of deep water, where an increase of dissolved salts (mainly bicarbonate) maintains the density gradient (Rodrigo et al., 2001). From 0 to 11.5 m in Lake La Cruz, the oxic mixolimnion occurs, but from 11.5 m to the bottom, anoxic water occurs, with the chemocline being 3.5 m thick, from11.5 to 15 m. Reduced iron is detected below the oxic-anoxic boundary at a low concentration of ~15 μM, but an increase in deeper anoxic waters of up to ~1000 μM has been measured on several occasions (Rodrigo et al., 2001; Romero-Viana et al., 2009). Sedimentation in the lake is affected by annual summer ‘‘whiting", which is a short time of massive $CaCO_3$ precipitation (Rodrigo et al., 1993; Romero-Viana et al., 2008).

Golfo Dulce is a small embayment on the southern Pacific coast of Costa Rica. It has a fjord structure with a deep inner basin, the depth is more than 200 m and the bay is 50 km long. Golfo Dulce is separated from the open Pacific by a shallow sill at 60 m depth, with a width of 14 km. The sill limits the water circulation and causes stable anoxia in the deeper water column. From 40 to 55 m depth, the density of water increases rapidly to form a pycnocline (Dalsgaard et al., 2003). In the surface water and in the pycnocline, aerobic respiration dominates the decomposition of organic matter (Ferdelman et al., 2006). Across the pycnocline, the oxygen concentration steeply declines, to less than 1 μmol below 100 m, to form a stably anoxic deep water column (Ferdelman et al., 2006; Dalsgaard et al., 2003; Thamdrup et al., 1996). From 100 m to 180 m, nitrate reduction dominates water-column processes (e.g. Lipschultz et al., 1990; Bang et al., 2000; Deutsch et al., 2001). From 180 m to 200 m, sulfate reduction is the main biogeochemical reaction (e.g. Lewis and Landing, 1992), but the concentration of sulfide is not high (a maximum of 1 to 2 μM) (Dalsgaard et al., 2003), and sulfide also does not accumulate in the porewater (Ferdelman et al., 2006). Ferdelman et al. (2006) explain that the reason for the low concentration of sulfide is due to the frequent input of oxygenated water from the Pacific, causing S-oxidation. Thamdrup et al. (1996) also point out that a high sedimentation rate of reactive iron phases may constrain sulfide at low concentrations. Sedimentation in the anoxic sediments for this system has been affected by turbidites, especially between 1989 and 1992 (Ferdelman et al., 2006). Different from Lake Cadagno and Lake La Cruz, the organic carbon content of Golfo Dulce stays at a much lower value of about 2% wt (Nichols-Driscoll, 1976; Thamdrup et al., 1996). The sediment core for this study was from an oxic part of the basin, sampled at a water depth of 16 m.

Here, I report P speciation, TIC (total inorganic carbon) and TOC (total organic carbon) data for the sediments, combined with dissolved porewater species, for the different redox conditions in Lake Cadagno, Lake La Cruz and Golfo Dulce. I combine all the geochemical data to make mass balance models to quantify the cycling and burial of P, to determine how much P is fixed in the sediment and how much is recycled back to water column under different redox conditions, analogous to those which were prevalent at various time in Earth history.

4.2. Method

4.2.1 Water column, sediment and porewater sampling

The details of water column sampling of Lake Cadagno were described in chapter 2.2.2. The same method for water column sampling is adapted from Lake La Cruz, and the samples were collected through the oxic, chemocline and deeper ferruginous waters from 4 m to 19 m (Thomson, 2018). No water samples were collected in Golfo Dulce, but the details of dissolved species have previously been reported (Córdoba and Vargas, 1996; Thamdrup et al., 1996; Dalsgaard et al., 2003; Ramsing and Wawer, 2006). Sediment samples were collected by short (up to 35 cm) gravity cores in the different water environments. In the Lake Cadagno, the deposited environments represented were under euxinic conditions (20-21 m) and oxic conditions (5-6 m). In the Lake La Cruz, the sediment core was collected under ferruginous conditions (21-22 m). In the Golfo Dulce, the sediment core was collected under oxic conditions (17-18 m). The details of sediment and porewater sampling in Lake Cadagno were described in chapter 2.2.2. The same methods for the sediment and porewater samples were adopted for Lake La Cruz and Golfo Dulce. The sediment and porewater samples were collected from 0 to 35 cm in summer in 2014 in Lake La Cruz (Thomson, 2018) and were collected from 0 to 28 cm in March in 2008 in Golfo Dulce (Guilbaud, unpublished data).

4.2.2 Physical sediment parameters

Sediment water content (wc) for all environments including these four cores was determined with sediment depth through the method in chapter 2.2.3. Solid phase density was measured with depth in the sediments which were treated by homogenizing freeze-dry. Specifically, the ground freeze-dry sediment was added into a 10 ml weighed cylinder which was filled with 8 ml water, then use the volume displacement and mass change to calculate the solid phase density (van de Velde et al., 2016). Sediment porosity was defined as the ratio of the volume of interconnected water to the volume of total sediment (Burdige, 2006). The formula was showed below:

$$\varphi = \frac{wc(\%)/\rho 1}{(\frac{wc(\%)}{\rho 1} + \frac{1-wc(\%)}{\rho 2})}$$

where φ is sediment porosity, wc (%) was water content, ρ1 was the water density and ρ2 was the solid phase density.

4.2.3 Porewater and sediment analysis

Dissolved Fe(II), P, S(II) and sulfate were measured in the porewaters for all the environments including these four cores. The detailed processes were described in chapter 2.2.4.1.TOC, TIC and P speciation were measured in the solid sediment phases for all the environments including these four cores. The detailed processes were mentioned in chapter 2.2.4.2.

4.2.4 Reactive transport model

4.2.4.1 General description

The reactions included in the sediments for this model were developed from the benthic-pelagic reactive transport model (Reed et al., 2011). The reactions were used to describe the mass balance of dissolved and particulate P in different sediment cores with depth. With different depths, different reactions and transport processes are subject to the P cycling. The dissolved P was transported in the model by diffusion biochemical reductions. The solid P was transported by sedimentation and secondary diagenesis. The model contains two groups of reactions, group 1 (first 4) is for the sources of dissolved P, which include the degradation of organic matter and degradation of Fe(III)-bound P or Fe(III) adsorbed P (Table 4.1). The orders for the organic matter mineralization were followed the standard Gibbs free energy yield (high to low) (Canfield and Thamdrup, 2009). Group 2 (last 3) is for the sources of solid P, which include the secondary diagenesis of the authigenic apatite and Fe(II) phosphate formation (Table 4.1). The reactions were secondary and taken from Dalsgaard et al. (2003), Canfield and Thamdrup (2009) and Kraal et al. (2012):

Table 4.1 Primary and secondary redox reaction equations.

Chemical reactions included in the model (not balanced)
$OM + NO_3^- \rightarrow NH_4^+ + NO_2^- + N_2 + CO_2 + PO_4^{3-}$ (nitrate reduction)
$OM + Fe(III) \rightarrow Fe(II) + CO_2 + PO_4^{3-}$ (Fe reduction)
$OM + SO_4^{2-} \rightarrow S(II) + CO_2 + PO_4^{3-}$ (sulfate reduction)
$Fe(III)O(OH)\cdot P + S(II)\ (OM) \rightarrow Fe(II) + S^0 + (CO_2) + PO_4^{3-}$
$PO_4^{3-} \rightarrow P_{auth}$ (secondary diagenesis)
$PO_4^{3-} + Fe(II) \rightarrow Fe(II)_3(PO4)_2$ (secondary diagenesis)
$PO_4^{3-} + Fe(III)O(OH) \rightarrow Fe(III)O(OH)\cdot PO_4^{3-}$ (secondary diagenesis)

OM in this table means organic matters.

4.2.4.2 Flux analysis and rate estimation

The flux of dissolved P to water column and porewater were calculated from the profile of P in the porewater, using Fick's first law:

$$J = \varphi \cdot \frac{D_0(S,T)}{\theta^2} \cdot \frac{\partial C}{\partial x} \qquad (1)$$

where J was the flux of P, C was the P concentration in the porewater, x was the depth of sediment, φ was the average porosity of sediments, θ^2 was the correction factor for sediment tortuosity, which was calculated as $1 - 2In\varphi$ (Boudreau and Meyman, 2006), D_0 was the diffusion coefficient, which was calculated by salinity and temperature using the R package CRAN: marelac (Soetaert et al., 2010), which was based on the constitutive relations presented in Boudreau (1997). $\frac{\partial C}{\partial x}$ meant the linear slope which was calculated from concentrations profile of P in the porewater.

Production and consumption rates of dissolved species could also be calculated through the same formula (Berg et al., 1998; van de Velde et al., 2016). By specifically using the ionic drift in the specific biogeochemical reaction in the restricted redox conditions, the rate of organic mineralization was estimated.

4.2.4.3 Burial rate estimation

Burial rates of loosely sorbed P, Fe-bound P and organic P were calculated from the extraction step I, II and V of the SEDEX P extraction procedure (Table 2.2), using the formula:

$$R = (1-\varphi)\cdot V\cdot C\cdot \rho \qquad (2)$$

where R was the burial rate, φ was the porosity of sediments, V was the average sedimentation rate which was determined from the logarithmic regression of ^{210}Pb in previous research, C was the P concentration with the deepest depth in these four cores, ρ was the average dry sediment density (van de Velde et al., 2016).

4.2.4.4 Rate estimation of released P and re-precipitated P

The rate of released P from organic matter mineralization and Fe(III) reduction was calculated from the extraction step V, I and II of the SEDEX P extraction procedure (see table 2.1), using the formula:

$$R = (1-\varphi)\cdot V\cdot \rho\cdot (C_1 - C_2) \qquad (3)$$

where R was the released P rate, φ was the average porosity of sediments, V was the average sedimentation rate which was determined from the logarithmic regression of ^{210}Pb in previous research, ρ was the average dry sediment density, C_1 was the concentrations of P as the start value before biogeochemical reactions, and C_2 was the concentration of P as the terminal value after biogeochemical reactions (van de Velde et al., 2016).

This calculation was also used to determine the re-precipitated P rate including P re-adsorption and P secondary diagenesis, using the data from the extraction step I, II and III of the SEDEX P extraction procedure (Table 2.2). The C_1 was the concentration of P as the terminal value after biogeochemical reactions, and the C_2 was the concentrations of P as the start value before biogeochemical reactions (van de Velde et al., 2016).

4.3 Results

4.3.1 Lake Cadagno

4.3.1.1 Water column

The water column profiles of dissolved P, Fe(II), S(II) and sulfate for Lake Cadagno are described in chapter 2.3.1.

4.3.1.2 Euxinic setting

In the sediments of euxinic setting in Lake Cadagno, the basic parameters are showed in Fig 4.1. The details of water content have been described in chapter 2.3.2. The profile of density increases slightly from 1.51 to 1.80 g/cm^3 from surface to 9.5 cm, and remain stable at 1.86 ± 0.07 g/ml from 9.5 to 13 cm (Fig. 4.1a). From 13 to 18 cm, the density increases rapidly from 1.79 to 2.79 g/cm^3, remaining constant at 2.81 ± 0.02 g/cm^3 with depth (Fig. 4.1a). The rapid increase is caused by landslides which is discussed before. The profile of porosity is calculated from the water content and density, but the core for measuring the water column is not as long as the core for measuring density. Here, the profile of porosity from 23.5 to 31.5 cm is calculated depending on the water content data in Birch et al. (1996). Specifically, the porosity decreases slightly from 0.95 to 0.85 from surface to 11 cm depth, then drop fast from 0.85 to 0.66 from 11 to 14 cm (Fig. 4.1b). However, from 14 to 20.5 cm, the values of porosity increase fast to 0.89, remaining stable at 0.89 ± 0.01 from 20.5 to 23.5 cm (Fig. 4.1b). From 23.5 to 24.5 cm, the values of porosity decrease rapidly in a second time from 0.88 to 0.76, remaining constant at 0.75 from 24.5 to 29.5 cm (Fig. 4.1b). From 29.5 to 31.5 cm, the values of

porosity increase back to 0.9 again from 29.5 to 31.5 cm (Fig. 4.1b). The sedimentary rate is 2 mm/y with the surface depth from 0 to 14 cm (Wirth et al., 2013), the deep sedimentary rate is seriously affected by the landslide which is consistent with the profile of density. The degrees of temperature and the values of salinity are estimated from the interface between water column and sediments, equaling to 4 ℃ and 0.46, respectively (Wirth et al., 2013; Tonolla et al., 2004).

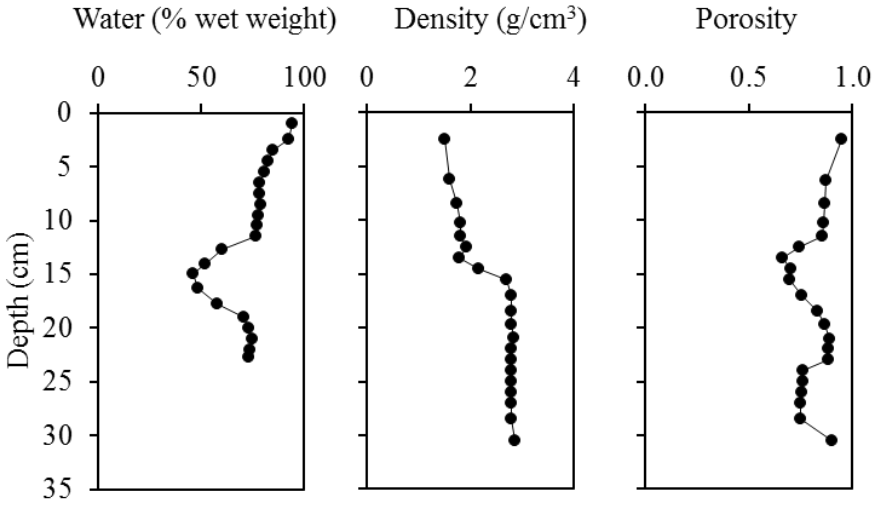

Figure 4.1 Basic parameters profiles in the sulfidic sediments beneath the sulfidic water column in Lake Cadagno. a) dry sediment density profile; b) porosity profile; c) pH of porewater profile.

In the euxinic sediments, the geochemical data including TOC, TIC and P speciation in the sediments has been described in chapter 2.3.4.1 and 2.3.4.3. The concentrations of dissolved species including sulfate, S(II), P and Fe(II) in the porewater have been described in chapter 2.3.3.

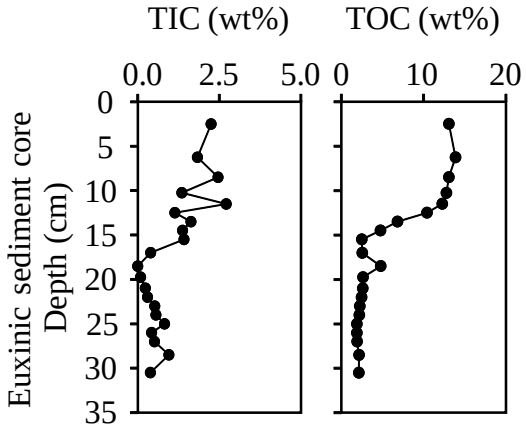

Figure 4.2 Profiles of TOC and TIC in the ferruginous sediments in the euxinic sediment core of Lake Cadagno.

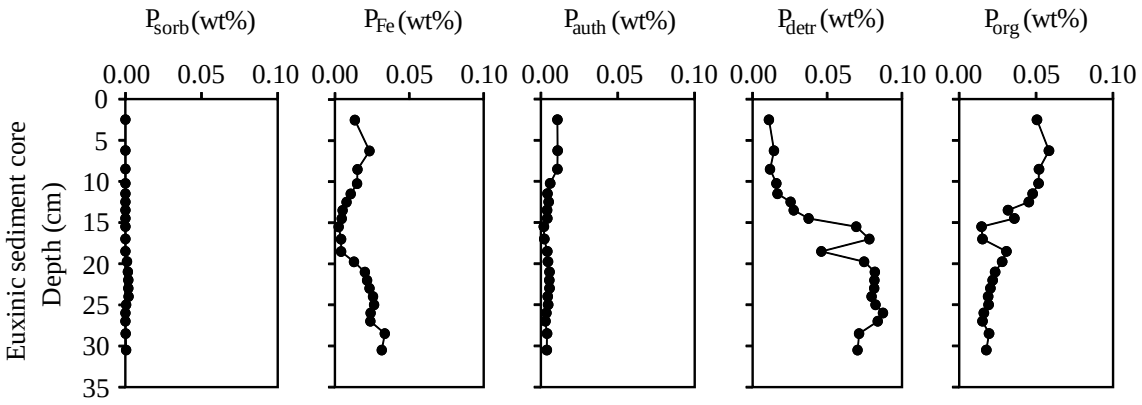

Figure 4.3 P speciation profiles for the euxinic sediment core in Lake Cadagno.

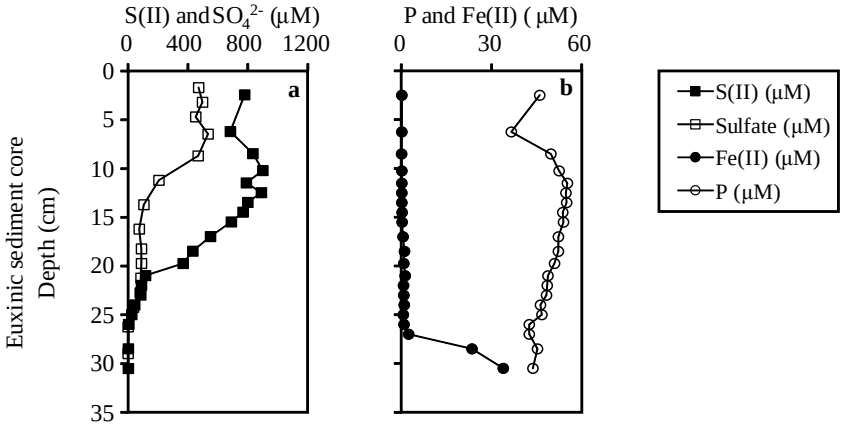

Figure 4.4 Porewater profiles for dissolved sulfate, sulfide, P and Fe(II) in the euxinic sediments core in Lake Cadagno.

4.3.1.3 Oxic setting

In the sediments of oxic setting, the basic parameters are provided in Figure 4.5. With depth, water content decreases slowly from 96.87% to 72.77% (Fig. 4.5a). The values of densities remain constant at 1.69 ± 0.01 g/ml from 0 to 23 cm, then increase to 1.85 g/ml from 23 to 25 cm, remaining constant at 1.85 g/ml from 25 to 32 cm (Fig. 4.5b). The profile of porosity shows a general decrease trend from 0.98 to 0.83 with depth (Fig. 4.5c). The sedimentary rate is 2 mm/y with the whole depth (Wirth et al., 2013). The degrees of temperature and the values of salinity are estimated from the interface between water column and sediments, equaling to 11.7 ℃ and 0.19, respectively (Wirth et al., 2013; Tonolla et al., 2004).

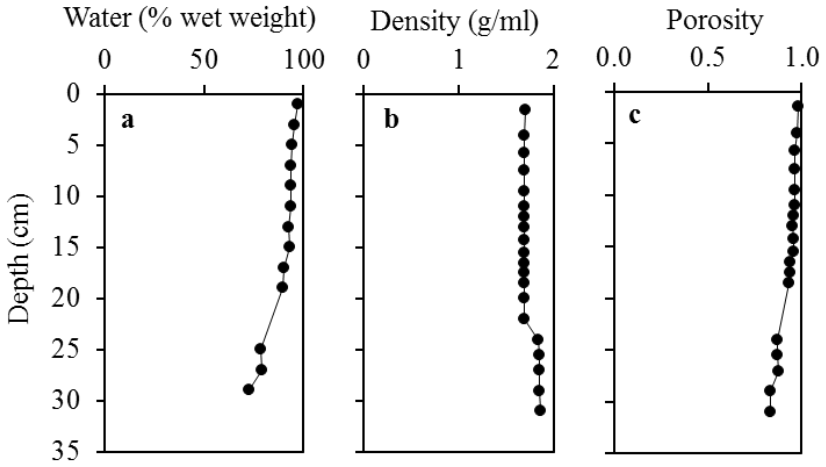

Figure 4.5 Basic parameters profiles in the sulfidic sediments beneath the oxic water column in Lake Cadagno. a) water content profiles; b) dry sediment density profile; c) porosity profile.

In the sediments of oxic setting, the geochemical data including TOC, TIC and P speciation in the sediments has been described in chapter 2.3.4.1 and 2.3.4.3. The concentrations of dissolved species including sulfate, S(II), P and Fe(II) in the porewater have been described in chapter 2.3.3.

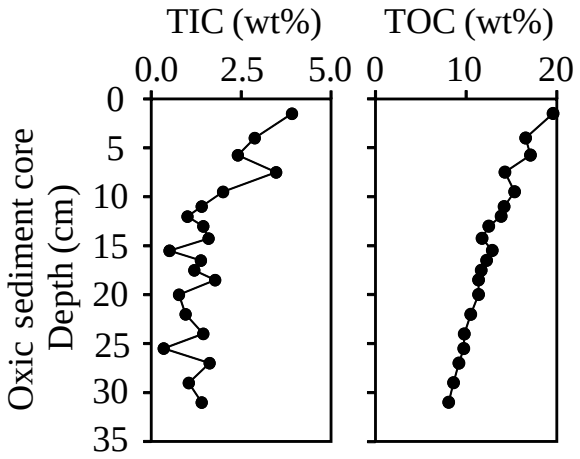

Figure 4.6 Profiles of TOC and TIC in the ferruginous sediments in the oxic sediment core of Lake Cadagno.

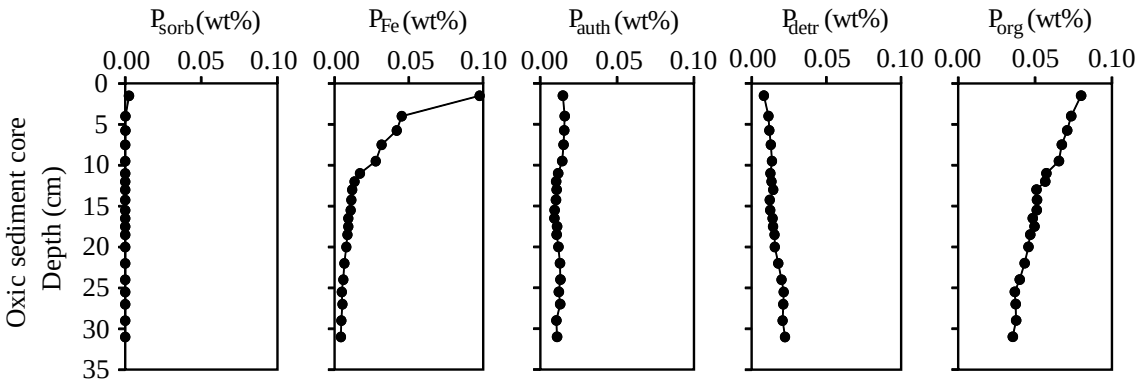

Figure 4.7 P speciation profiles for the oxic sediment core in Lake Cadagno.

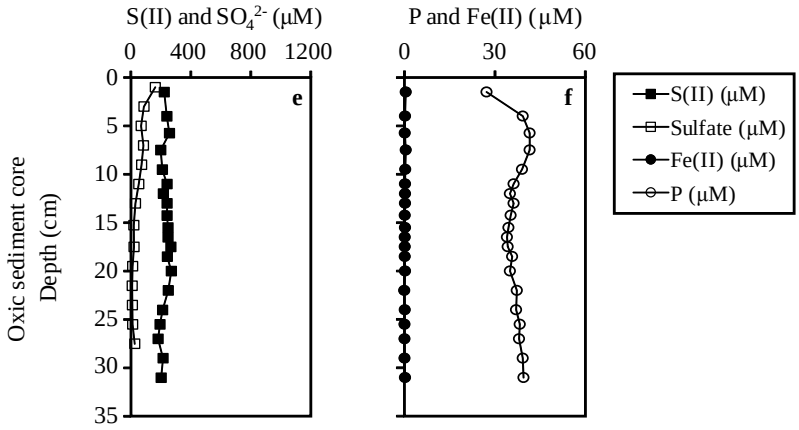

Figure 4.8 Porewater profiles for dissolved sulfate, sulfide, P and Fe(II) in the oxic sediments core in Lake Cadagno.

4.3.2 Lake La Cruz

The data of the Lake La Cruz is from Thomson (2018).

4.3.2.1 Water column

The profiles of dissolved species in the water column include P, Fe(II), sulfide and sulfate (Fig. 4.9). Dissolved P is present until 17.5 m, increasing fast from 0.036 to 2.5 µM with the depth of 17.5 to 19 m (Fig. 4.9a). The concentrations of dissolved Fe(II) stay at less than 1 µM from 0 to 13.5 m, but increase rapidly from 1.2 to 252.3 µM with the depth of 14 to 19 m (Fig. 4.9b). The concentrations of dissolved sulfide stay at less than 1µM from surface to 16 m, and increase rapidly from 0.18 to 3.68 µM, but still stay at a low level (Fig 4.9c). The concentrations of sulfate decrease from 31.44 to 2.45 µM with the depth of 4 to 16 m, and remain at low concentrations of 4.41 ± 2.45 µM from 16 to 19 m (Fig. 4.9d). However, in the previous research, the concentration of sulfate in the bottom water is about 20 µM (Rodrigo et al., 2001).

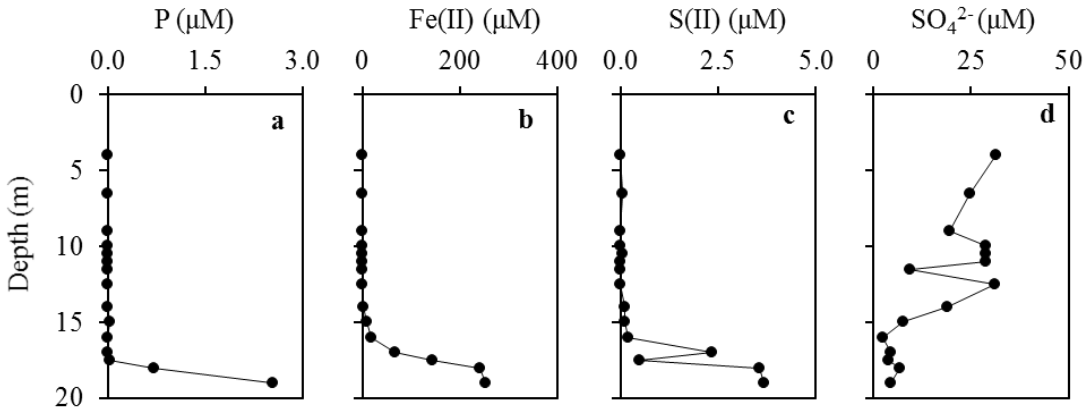

Figure 4.9 Vertical distribution of dissolved P, Fe(II), sulfide and sulfate in water column of Lake La Cruz (Thomson, 2018).

4.3.2.2 Sediments

The basic parameters of the sediments are showed in Fig 4.4. From 0.75 to 5.9 cm in the surface sediments, water contents decrease from 95.27% to 77.73%, remaining relatively constant at 79.68 ± 2.54% with the depth from 5.9 to 34.5 cm (Fig. 4.10a). The values of densities increase from 2.21 to 2.58 g/ml at the depth from 0.75 to 4.25 cm, remaining relatively constant at 2.55 ± 0.06 from 4.25 to 22.25 cm (Fig 4.10b). In addition, from 22.25 to 25.25 cm, the values of densities decrease slightly from 2.49 to 2.33 g/ml, remaining constant at 2.29 ± 0.04 g/ml from 25.25 to 34.5 cm (Fig. 4.10b). The values of porosities decrease from 0.98 to 0.90 at the depth from 0.75 to 5.75 cm, remaining constant at 0.91 ± 0.01 g/ml (Fig. 4.10c). The sedimentary rates are not constant with depth in this sediments due to the high influx of littoral material (Romero-Viana et al., 2009). Specifically, from 0.75 to 10.25 cm, sedimentary rates stay at 5 mm/y, but from 10.25 to 16.25 cm, the sedimentary rates decrease to 1.5 mm/y, in the deep sediments from 16.25 to 34.5 cm, the sedimentary rate has a further decrease to 1 mm/y. The degrees of temperature and the values of salinity are estimated from the interface between water column and sediments, equaling to 6.5 ℃ and 0.41, respectively (Rodrigo et al., 2001; Romero-Viana et al., 2009).

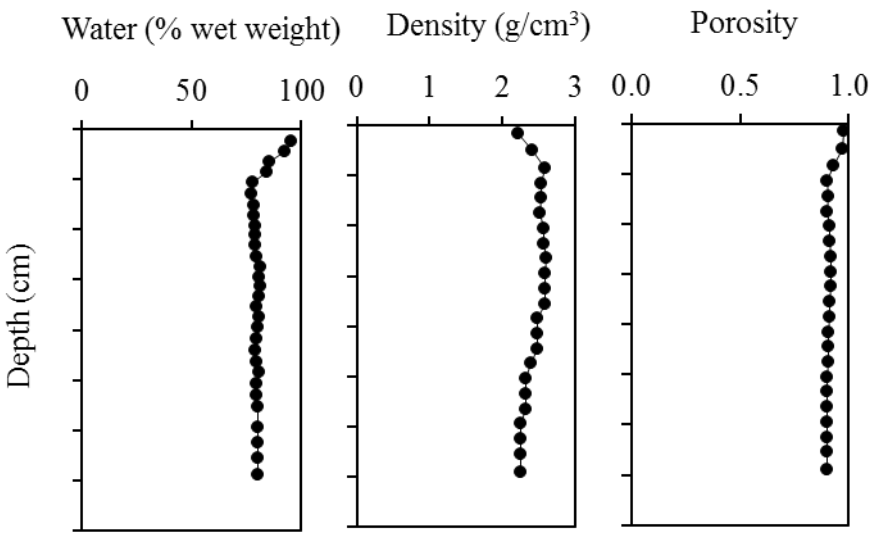

Figure 4.10 Basic parameters profiles in the ferruginous sediments in Lake La Cruz. a) water content profiles; b) dry sediment density profile; c) porosity profile; d) sedimentary rate (Thomson, 2018).

The profiles of TOC and TIC are showed in Fig 4.5. In the surface sediments from 0.75 to 5.75 cm, the concentrations of TOC decrease from 7.43 to 3.65 wt%, in addition, from 5.75 to 34.5 cm, the profile of TOC shows a general increase trend from 3.65 to 8.91 although there is a fluctuation with the depth of 16.25 and 26.75 cm (Fig. 4.11a). From 0.75 to 34.5 cm, the concentrations of TIC remain relatively constant at 9.67 ± 2.11 wt% (Fig. 4.11b).

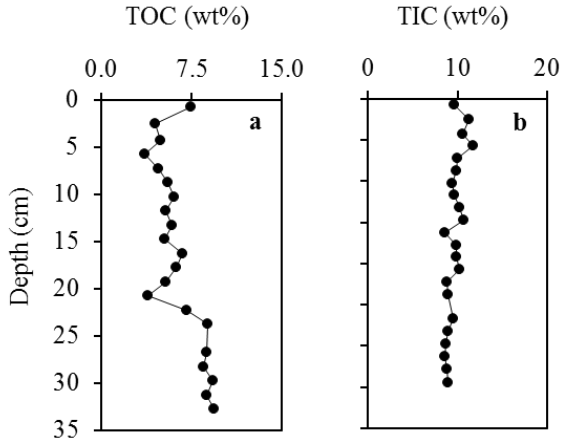

Figure 4.11 Profiles of TOC and TIC in the ferruginous sediments in Lake La Cruz (Thomson, 2018).

The profiles of P speciation are showed in Fig. 4.12. The concentrations of P_{sorb} decrease from 0.0018 to 0.0009 wt% in the surface sediments from 0.75 to 13.25 cm

(Fig. 4.12a), then the profile of P_{sorb} from 13.25 to 34.5 cm shows a general increase trend from 0.0009 to 0.0014 wt% (Fig. 4.12a). The profile of P_{Fe} shows a similar profile as P_{sorb}, specifically, the concentrations of P_{Fe} decrease from 0.017 to 0.01 wt% in the surface sediments from 0.75 to 4.25 cm and show a general increase trend from 0.01 to 0.024 with the depth from 4.25 to 34.5 cm (Fig. 4.12b). The concentrations of P_{auth} decrease from 0.008 to 0.006 wt% in the surface sediments from 0.75 to 4.25 cm (Fig. 4.12c), and there is a general increase from 0.006 to 0.010 wt% with the depth from 4.25 to 34.5 cm (Fig. 4.12c). Although there is a fluctuation in the profile of P_{org} from 0.75 to 28.25 cm (Fig. 4.12d), the whole profile of P_{org} has a general increase trend from 0.009 to 0.018 wt% with the depth from 0.75 to 34.5 cm (Fig. 4.12d). For $P_{detr,}$ in the surface sediments from 0.75 to 22.25 cm, the concentrations fluctuated, but remain relatively constant at 0.0028 ± 0.003 from 23.75 to 34.5 cm (Fig. 4.12e). These profiles of TOC and P_{org} are not expected to be see with increasing depth. It is possible that detrital phosphorus is controlling these the concentration of TOC and P_{org} in the water column. From the profile of P_{detr} and P_{org}, the trends are exactly opposite from 15 cm to 35 cm which shows that P_{detr} determines the profile of P_{org}.

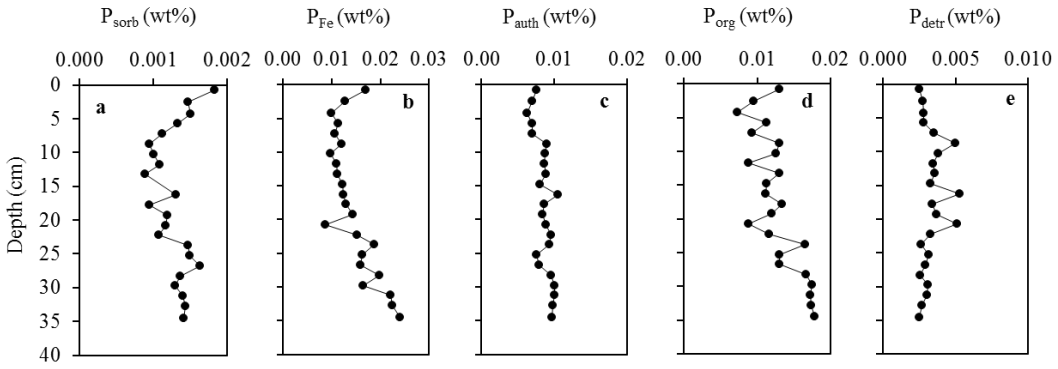

Figure 4.12 P speciation profiles for the ferruginous sediments in Lake La Cruz (Thomson, 2018).

4.3.2.3 Porewater

The profiles of dissolved species including sulfate, S(II), P and Fe(II) are showed in Fig. 4.13. In the surface sediments from 0.75 to 5.75 cm, the concentrations of sulfate decrease rapidly from 8.9 to 1.21 μM, then remain relatively constant at 1.36 ± 0.82 μM (Fig. 4.13a). The concentration of sulfate in the surface sediments is approximately 9 μM, which is twice as high as the sulfate concentration in bottom waters, but lower than the previous record (20 μM; Rodrigo et al. 2001). Furthermore, the uncertainty of measured sulfate concentrations in bottom water should not be ignored, which is used to

recalculate the sulfate concentrations in bottom water at 2 to 7 μM. Here, the maximum value, 7 μM, is close to 9 μM in the bottom waters. The concentrations of sulfide stay at a low concentration (less than 3.13 μM) with the whole depth (Fig. 4.13b). The concentrations of dissolved P increases from 5.8 to 27.31 μM with depth from 0.75 to 14.75 cm (Fig.4.13c), after 3 cm fluctuation, the profile of the dissolved P shows a general decrease trend from 27.46 to 17.18 μM with the depth from 17.75 to 32.75 cm (Fig. 4.13c). The concentrations of dissolved Fe(II) increase from 5.8 to 507.76 ± 22.02 μM with the whole depth (Fig. 4.13d). In the sediments, respiration is controlled by Fe(III). Because Fe(III) is more active than sulfate as the electron acceptor for respiration process (Canfield and Thamdrup, 2009), all of sulfate could not be consumed when Fe(III) remains the electron acceptor.

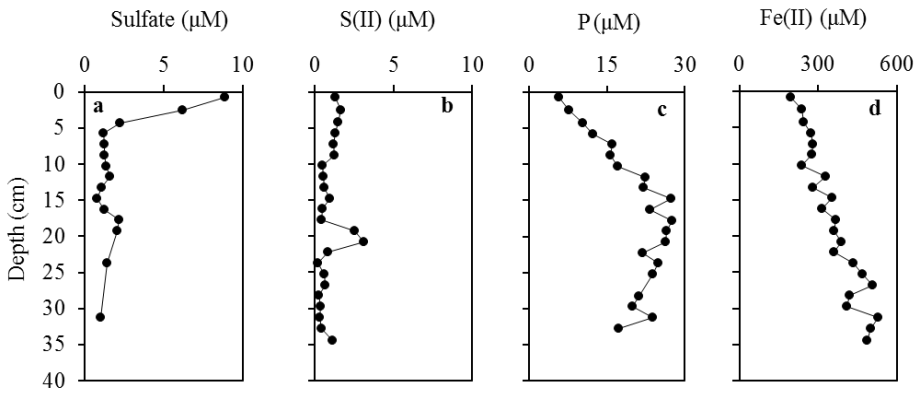

Figure 4.13 Porewater profiles for dissolved sulfate, sulfide, P and Fe(II) in the ferruginous sediments in Lake La Cruz (Thomson, 2018).

4.3.3 Golfo Dulce

The data of the Golfo Dulce is from Romain Guilbaud (unpublished).

4.3.3.1 Water column

The water column data is not measured in this environment. The data is collected from the Thamdrup et al. (1996) and Dalsgaard et al. (2003). From 0 to 17 m, the dissolved sulfide and Fe(II) are not measured. The concentrations of dissolved P increase from 0.5 to 0.7μM with the depth from 0 to 17 m. The concentrations of NH_4^+ increase from 0.67 to 0.84 μM.

4.3.3.2 Sediments

The profiles of the basic parameters are showed in Fig 4.8. From 0 to 4 cm, the water contents decrease from 75.82 to 52.52%, remaining relatively constant at 51.95 ± 7% from 0 to 28 cm (Fig. 4.14a). The density stays constant at 2.04 ± 0.13 g/ml with the whole depth (Fig. 4.14b). The porosity decreases from 0.87 to 0.70 with the depth from 0 to 4 cm, remaining relatively constant at 0.69 ± 0.07 (Fig. 4.14c). In the shallow basin the sediments are not affected by the turbidite, thus the sedimentary rate is estimated as 1 mm/y with the whole depth for this core (Ferdelman et al., 2006). The degrees of temperature and the values of salinity are estimated from the interface between water column and sediments, equaling to 28.3 ℃ and 0.032, respectively (Córdoba and Vargas, 1996; Thamdrup et al., 1996).

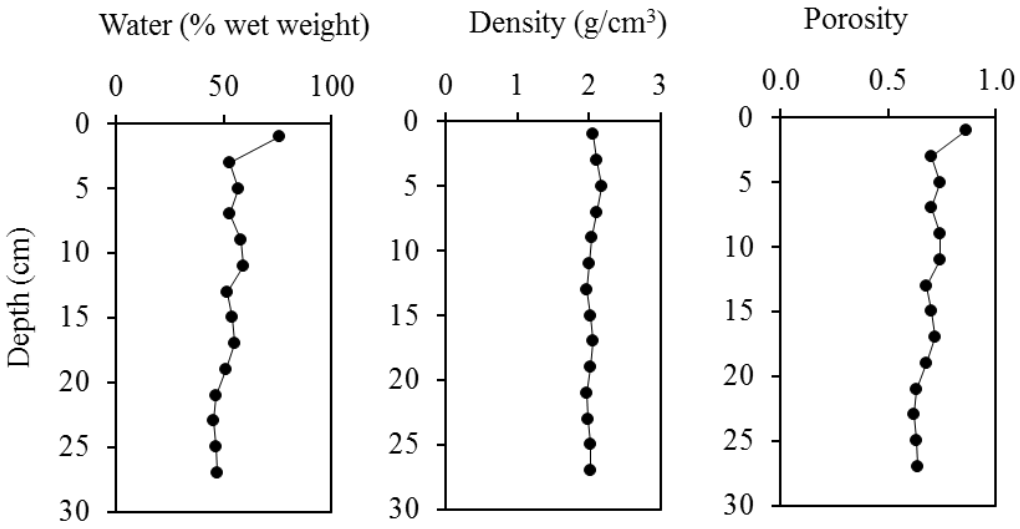

Figure 4.14 Basic parameters profiles in the ferruginous sediments in Golfo Dulce. a) water content profiles; b) dry sediment density profile; c) porosity profile; d) sedimentary rate (Guilbaud, unpublished data).

The profiles of TOC and TIC are showed in Fig. 4.15. From 0 to 8 cm, the concentrations of TOC remain relatively constant at 0.97 ± 0.05 wt%, then fluctuate between 0.81 and 1.52 wt% from 8 to 28 cm (Fig. 4.15a). From 0 to 4 cm, the concentrations of TIC decrease from 0.74 to 0.46 wt%, then increase to 0.58 wt% from 2 to 6 cm, remaining constant at 0.55 ± 0.06 wt% from 6 to 18 cm (Fig. 4.15b). From 16 to 20 cm, the concentrations of TIC decrease from 0.61 to 0.46 wt%, then have a small fluctuation between 0.47 and 0.34 wt% to the bottom (Fig. 4.15b).

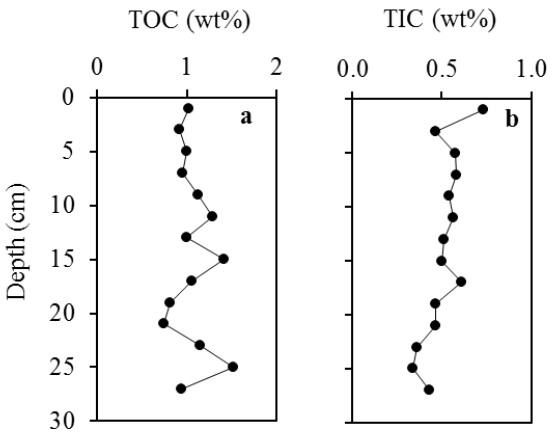

Figure 4.15 Profiles of TOC and TIC in the ferruginous sediments in Golfo Dulce (Guilbaud, unpublished data).

The profiles of P speciation are showed in Fig. 4.16. The concentrations of P_{sorb} fluctuate with the whole depth from 0 to 28 cm, however, the general profile shows an increasing trend from 0.0008 to 0.0022 wt% (Fig 4.10a). The profile of P_{Fe} shows a similar profile as P_{sorb}, specifically, it shows a general increase trend from 0.011 to 0.017 wt% with the whole depth, but with this depth, the concentrations of P_{Fe} have a fluctuation (Fig. 4.16b). The concentrations of P_{auth} increase from 0.015 to 0.023 wt% with the depth from 0 to 16 cm, then decrease to 0.013 wt% at 20 cm, remaining constant at 0.014 ± 0.001 from 20 to 28 cm (Fig. 4.16c). The concentrations of P_{org} remain constant at 0.011 wt% in the surface sediments from 0 to 8 cm, then increase to 0.014 wt% at 10 cm (Fig. 4.16d). From 10 to 28 cm, the concentrations of P_{org} fluctuate, but show a general decrease trend from 0.14 to 0.009 wt% (Fig. 4.16d). For $P_{detr,}$ the concentrations decrease from 0 to 6 cm, remaining relatively constant at 0.03 wt% from 6 to 10 cm, then continue to decrease to the lowest concentration at 0.025 wt% at 16 cm (Fig. 4.16e). From 16 to 22 cm, the concentrations of P_{detr} increase back to 0.035, and remain constant at 0.033 ± 0.002 wt% (Fig. 4.16e).

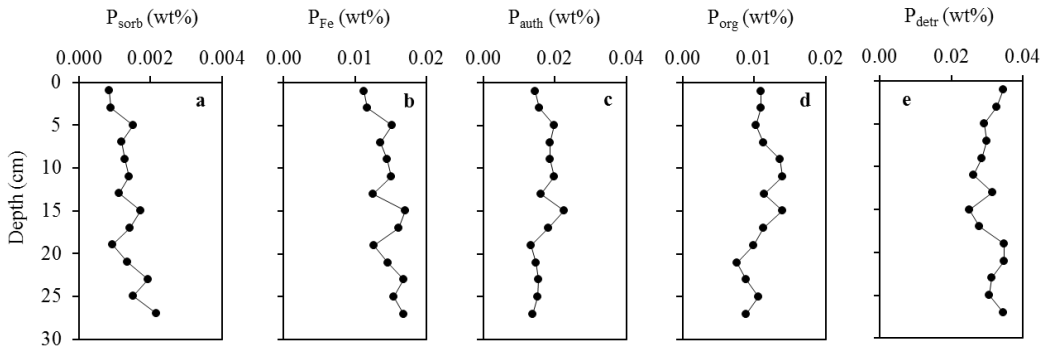

Figure 4.16 P speciation profiles for the ferruginous sediments in Golfo Dulce (Guilbaud, unpublished data).

4.3.3.3 Porewater

The profiles of dissolved species including P, Fe(II), S(II) and NH_4^+ are showed in Fig. 4.17. The concentrations of dissolved P increase from 1.38 to 7.87 μM with the depth of 0 to 10 cm, then the increased speed is accelerated, and the concentrations of dissolved P peak at 26.06 μM at 20 cm (Fig. 4.17a). The concentrations of dissolved Fe(II) increases fast from 65.12 to 216.08 μM with the depth from 0 to 8 cm, then the increased speed is slowed down, and the concentration of dissolved P peak at 262.70 μM at 26 cm (Fig. 4.17b). No sulfide is measured in the porewater (Fig. 4.17c). The concentrations of NH_4^+ increase fast from 55.07 to 155.16 μM with the depth of 0 to 4 cm, then the increased speed is slow down slightly, and the concentrations of NH_4^+ increase to 262.24 μM at 10 cm, remaining relatively constant at 250.61 ± 14.6 μM from 10 to 20 cm (Fig. 4.17d). In this environment, nitrate reduction plays a much more important role in organic matter respiration than sulfate (Thamdrup et al., 1996), thus the profile of sulfate is not shown here, instead, the profile of NH_4^+ is provided.

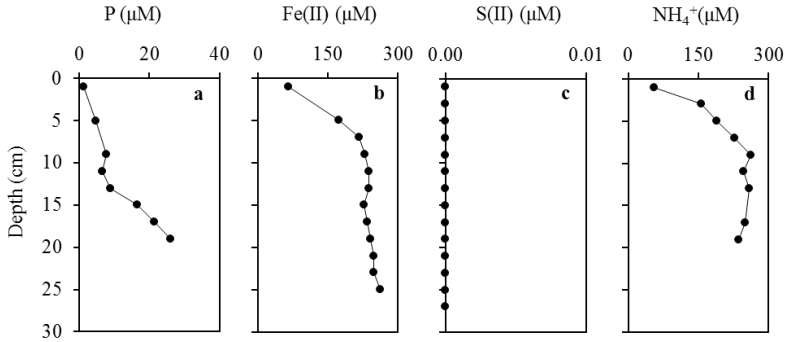

Figure 4.17 Porewater profiles for dissolved P, Fe(II), sulfide and NH_4^+ in the ferruginous sediments in Golfo Dulce (Guilbaud, unpublished data).

4.4 Discussion

4.4.1 Lake Cadagno

4.4.1.1 Box model in the euxinic setting

Based on the discussion of P cycling in chapter 2.4.3, the main sources of released P in the sediments are from Fe (oxyhydr)oxide reduction and organic matter degradation. The released P is proved to recycle back to water column and re-trapped as the process of secondary diagenesis, forming the Fe(II) phosphate (see chapter 2.4.3). The carbonate-fluorapatite (P_{auth}) sink is relatively minor, staying at a low concentrations from 9.5 cm (Fig. 2.9), but in the surface sediments from 0 to 9.5 cm, the P_{auth} is not negligible (Fig. 2.9) which may be defined as a switched sink from the recycled released P (e.g., Dijkstra et al., 2014). Therefore, the box model of P cycling in the sediments of euxinic setting (Fig. 4.18) can be made below:

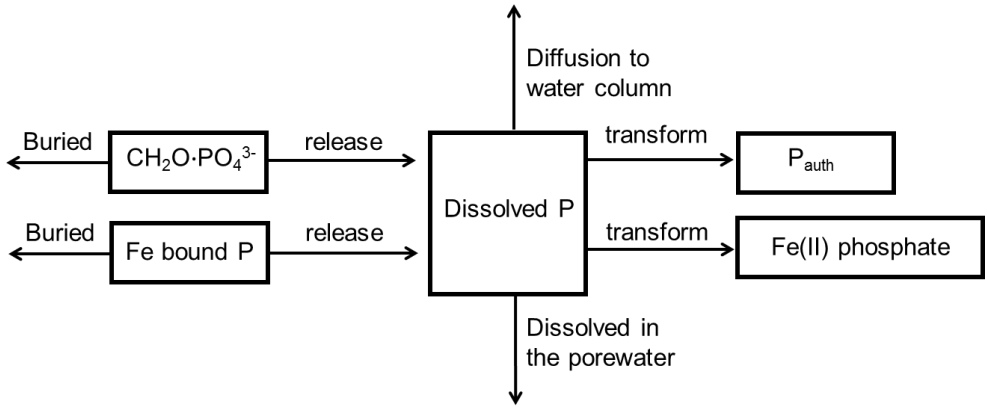

Figure 4.18 Box model of P cycling in the sediments of euxinic setting in the Lake Cadagno.

4.4.1.2 Released P rate from organic matter mineralization in the euxinic setting

The organic matter mineralization is the dominant pathway for the early diagenetic transformations (Burdige, 2006; Aller, 2014). During the processes, released organic P is the important source for the released P in the sediments. The increase of the released P co-responds to decrease of P_{org}. From the P_{org} profile, there is a general decline trend from the surface sediments to the deep sediments except the depth from 0 to 7.5 cm and the depth from 12 cm to 15 cm (Fig. 2.9). In the surface sediments, oozes are the main deposits which are easily mixed to disturb the results, thus the surface data of P_{org} from 0 to 5 cm is not used for the calculation. From 12 cm to 15 cm, the sudden decrease is caused by the landslide, thus the lowest data of P_{org} is not used for the calculation of the

consumption. Formula (3) in 4.2.4.4 is used. The average porosity with the whole depth is 0.81, the sedimentary rate is 2 mm/y, and the average density of the whole depth is 2.41 g/cm^3. The concentration of P_{org} in the surface sediments from 5 to 7.5 cm is 0.058 wt% and the concentration of P_{org} in the deep sediments from 29.5 to 31.5 cm is 0.018 wt%. The rate of P_{org} consumption (R_{min}) is calculated as 32.95 μmol/(m^2·d). However, the deep sediment is also affected by the landslide which causes the concentration of the P_{org} in the deep sediments lower than the real value. Therefore the real rate should be lower than 32.95 μmol/(m^2·d).

4.4.1.3 Released P rate from the reduction of Fe(III) (oxyhydr)oxide in the euxinic setting

The reduction of Fe(oxyhydr)oxide is another important source of released P. Furthermore, two major processes contribute to the production of the released P: one is from P adsorption ($P_{sorb)}$, and the other one is from the P complexation P_{Fe}. In this system, no P_{sorb} is measured (Fig. 2.9), but large amounts of released P is from the reduction of P_{Fe}. From 0 to 16 cm, there is an obvious decrease trend of P_{Fe} which means that in the surface sediments large amounts of Fe(oxyhydr)oxide is reduced (see chapter 2.4.2), however from 16 cm to the deep sediments, the P_{Fe} increases which means a new mineral formation which has been discussed in chapter 2.4.3. In the surface sediments, because of the ooze mix, there is a fluctuation from 0 to 7.5 cm (Fig. 2.9). For the modelling calculation, the first value from 0 to 5 cm is not used, and the first surface value for the P_{Fe} is 0.0232 wt% at the depth of 5 to 7.5 cm (Fig. 2.9). At the depth of 15 to 16 cm, the concentration of P_{Fe} decreases to the lowest value at 0.0025 wt%, however the sediment at this depth is affected by the landslide, thus for the modelling calculation, the sediments from 18 to 19 cm affected by a slight landslide is used for the P terminal point from Fe(III) (oxyhydr)oxide reduction at 0.0042 wt%. For the calculation, the average porosity from 0 to 18 cm is 0.80, the same sedimentary rate is 2 mm/y, and the average density from 0 to 18 cm is 2.06 g/cm^3. The rate of released P from Fe(oxyhydr)oxide reduction (R_{red}) is calculated as 13.84 μmol/(m^2·d).

4.4.1.4 Organic phosphorus and Fe(III) bound P burial rate in the euxinic setting

One of the fate for the P removed from water column is the burial as the organic matter. During the geochemical reaction in the sediments, some of the organic P is highly reactive to be oxidized as the released dissolved P, but some of them is not reactive which is directly buried in the sediments. The P_{org} burial rate is calculated from the formula 2. The same values of average porosity, sedimentary rate and density are used

as those in 4.4.1.2. The concentrations of P_{org} (0.0177 wt%) in the deepest depth from 29.5 to 31.5 cm is used for the calculation to ensure that most highly reactive organic phosphorus is oxidized. The organic phosphorus burial rate (R_{orgb}) is calculated as 14.33 μmol/(m^2·d). However the landslide in the deep sediments dilutes the concentration of P_{org}, thus the real burial rate of P_{org} should be higher than 14.33 μmol/(m^2·d).

The same thesis is used to calculate the burial rate of Fe(oxyhydr)oxide·P (R_{Feb}) while not all the Fe(III) bound P is released from the reduction in 4.4.1.3. For the calculation, the average porosity from 0 to 18 cm is 0.80, the same sedimentary rate is used at 2 mm/y, and the average density from 0 to 18 cm is 2.06 g/cm^3.The burial rate for the Fe(III) bound P is 3 μmol/(m^2·d).

4.4.1.5 Rate of secondary diagenesis as P_{Fe} in the euxinic setting

With time, the released P has the secondary diagenesis which is formed as P_{Fe} (Fe(II) phosphate; see chapter 2.4.3). In this system, the secondary diagenesis starts at 15.5 cm depth where the trend turns to increase, but in order to avoid the affection of landslide, the concentration of P_{Fe} equaling to 0.0042 wt% at 18 to 19 cm depth is used as the start point for the modeling calculation (Fig. 2.9). The terminal point for the P_{Fe} is 0.032 wt% at 29.5 to 31.5 cm depth (Fig. 2.9). The average porosity from 18 to 31.5 cm is 0.81, the sedimentary rate is 2mm/y, and the average density from 18 to 31.5 cm is 2.8 g/cm^3. Formula 3 is used for the calculation. The rate of secondary diagenesis as P_{Fe} (R_{Fe}) is calculated at 26.14 μmol/(m^2·d), however, the terminal point of the P_{Fe} is affected by the landslide which makes the value lower than the real value. The real rate should be higher than 26.14 μmol/(m^2·d).

4.4.1.6 Rate of secondary diagenesis as P_{auth} in the euxinic setting

As mentioned in the 2.4.3, the P_{auth} is inhabited in this system, thus the rate of secondary diagenesis as P_{auth} is 0. However, in the surface sediments from 0 to 12 cm, the concentrations of P_{auth} have a slight decrease which is not affected by the landslide (Fig. 2.9). Because the P_{auth} is stable as one of the terminal fate of P in the natural environment (Anderson et al., 2001), the unusual increase from deep sediments to surface sediments may be caused by the dissolved P diffusing (e.g. Dijkstra et al., 2014). The secondary diagenesis as P_{auth} in the surface sediments is calculated through the formula 3. The average porosity from 0 to 12 cm is 0.88, the sedimentary rate is 2 mm/y, and the average density from 0 to 18 cm is 1.69 g/cm^3. To avoid the ooze mix,

the value from 0 to 5 cm is not used for the calculation. The rate of the secondary diagenesis as P_{auth} (R_{auth}) is 2.3 μmol/(m^2·d).

4.4.1.7 Flux of dissolved P to water column and porewater in the euxinic setting

Fick's first law (formula 1) is used to calculate the flux of the dissolved P to porewater. The profile of dissolved P in the porewater is generally divided into two parts by the slopes. From 0 to 14cm, the concentrations of dissolved P increases with depth, but from 14 to 31.5 cm they decrease with depth (Fig. 2.5). In the deep sediments, the profile of dissolved P is controlled by the different biogeochemical reactions, but in the surface sediments, the profile of dissolved P is controlled by the exchange of dissolved P between water column and sediments. Therefore, the dissolved P in the surface sediments is used to calculate how much dissolved P is recycled back to the water column, and the dissolved P in the deep sediments is used to calculate how much dissolved P is reserved in the porewater. The best fit line for the points is important to calculate the slope. In this environment, the dissolved P concentration in the water-sediment interface is not measured, thus all the possible fluxes should be estimated.

For the calculation of the dissolved P flux to water column, two possible results are calculated because of the fluctuation of dissolved P from 0 to 7 cm (Fig. 2.5). In the first situation, the value from 5 to 7.5 cm is not used and the slope is calculated as 0.97 (Fig 4.13a). In the second situation, the value from 0 to 5 cm is not used and the slope is calculated as 0.26 (Fig 4.13b). In both calculations, the average porosity from 0 to 14 cm is 0.88. D_0 of P is 2.756×10^{-5} m^2/d when the temperature is 4 ℃ and salinity is 0.46. The flux of the dissolved P to water column in the first situation is 1.99 μmol/(m^2·d). The flux of the dissolved P to water column in the second situation is 7.35 μmol/(m^2·d). Therefore, the possible flux of the P diffusion to water column (F_{diff}) is 1.99 to 7.35 μmol/(m^2·d).

For the calculation of the dissolved P flux to porewater, the average porosity from 14 to 31.5 cm is 0.79, the same D_0 is used as the calculation for the flux of dissolved P to water column, and the slope from 14 to 31.5 cm is 1.19 (Fig. 4.19c) The flux of the dissolved P to porewater (F_{pw}) is calculated as 1.24 μmol/(m^2·d).

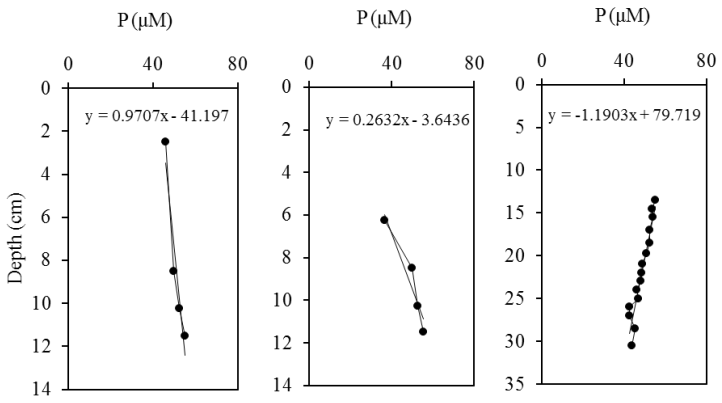

Figure 4.19 Linear slope of the best fit line for the vertical depth profile of P in the porewater in the sulfidic sediments beneath sulfidic water column in Lake Cadagno.

4.4.1.8 Mass balance of the model in the euxinic setting

In this system, the original precipitation phases of P in the sediment are organic P and P bound to Fe(III) minerals. With time, the original phosphorus phases are consumed to release dissolved P, then the dissolved P may be re-trapped through secondary diagenesis, recycled back to the water column or remain dissolved in the porewaters. Therefore, for the consumption of P, it includes released P from the mineralization of organic matter and reduction of Fe (oxyhydr)oxide which is calculated as $R_{min} + R_{red} <$ 46.79 µmol/(m^2·d). The new production of P includes secondary P diagenesis, P diffusion to water column and dissolved P in the porewater which is calculated as $R_{Fe} + R_{auth} + F_{diff} + F_{pw} >$ 31.67 to 37.03 µmol/(m^2·d). The recovery rate is calculated as > 67.69% to 78.93%. From the recovery rate, when the diffusion flux is 7.35 µmol/(m^2·d), the results are more accurate. The only 78.93% recovery rate is possibly caused by the landslide, specifically, which increases the consumption rate and decreases the production rate. The second reason is possibly caused by the surface ooze mix, which seriously affects the dissolved P concentrations in the surface sediments, then cause the diffusion flux lower than the real value. Therefore, the concentration of dissolved P at the lowest depth (interface between water column and sediments) is combined with the porewater to avoid the surface ooze mix. In this sediments, the concentration of P in the interface equals to 2.9 µM (Tonolla et al., 1998). The new slope is calculated as 0.18 (Fig. 4.20), then using the Fick's law, the flux of the P diffusion to water column is 10.61 µmol/(m^2·d) which increase the recovery to > 86.11%.

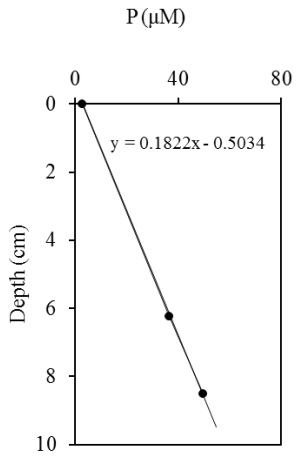

Figure 4.20 Linear slope of the best fit line for the vertical depth profile of P in the porewater and sediment-water interface in the sulfidic sediments beneath the sulfidic water column in Lake Cadagno.

Total P in this model is calculated by the sum of the P consumption rate and the burial rate (calculated in 4.4.1.1.4) as $R_{min} + R_{red} + R_{orgb} + R_{Feb} = 64.12$ μmol/(m^2·d). In addition, the percentages of different P phases are calculated in Table 4.2.

Table 4.2 The percent of different P phases in the modelling of the eutrophic euxinic water column with sulfidic porewaters in Lake Cadagno.

P phases	Percent (%)
P_{org} precipitate	> 22.35 ± 0.67
$P_{Fe(III)}$ precipitate	4.68 ± 0.09
P_{auth} precipitate	3.59 ± 0.11
$P_{Fe(II)}$ precipitate	> 40.78 ± 0.82
Diffused P to water column	16.55
Dissolved P in the porewater	1.93

4.4.1.9 Box model in the oxic setting

Based on the discussion of P cycling in chapter 2.4.3 and results in P speciation in oxic sediments (Fig. 2.9), the main sources of released P in the sediments are from Fe (oxyhydr)oxide reduction and organic matter degradation. Different from the sediments of the euxinic setting in Lake Cadagno, P released from the Fe (oxyhydr)oxide

reduction includes two processes: one is from P adsorption ($P_{sorb)}$, and the other one is from the P complexation (P_{Fe}), in addition, the concentrations of P_{sorb} decrease in the surface sediments (0 to 8.5 cm, Fig 2.9). Based on the concentrations of P in the porewater (Fig. 2.5), the released P is diffused to the water column and re-dissolved in the porewater, however, the released P is not formed as the new Fe(II) phosphate where the concentrations of P_{Fe} decrease with depth (Fig. 2.9), furthermore, the concentrations of P_{auth} increase slightly from 0.009 to 0.015 ± 0.001 μM from 17 to 0 cm as a switched sink from the recycled released P (e.g., Dijkstra et al., 2014) and increase slightly from 0.009 to 0.012 ± 0.001 from 17 to 32 cm as a sink switch from the re-dissolved P (Van Cappellen and Berner, 1988; Ruttenberg and Berner, 1993). Therefore, the box model of P cycling in the sediments of oxic setting can be made below:

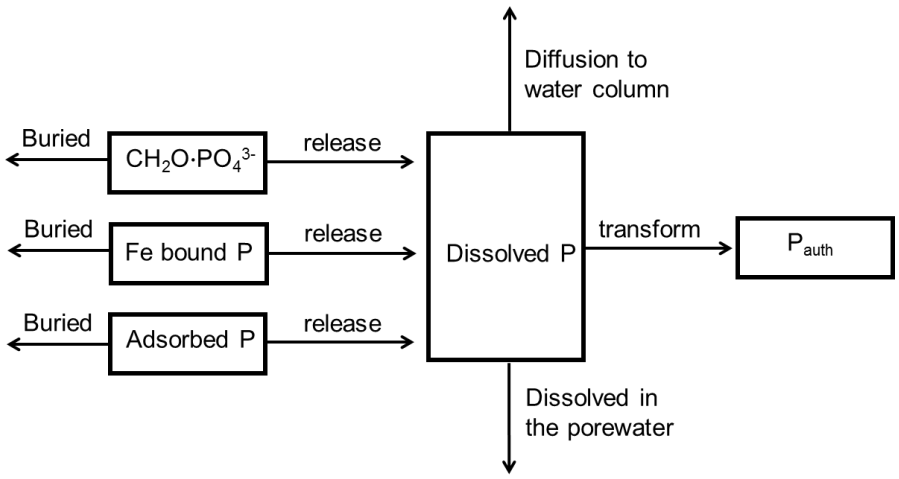

Figure 4.21 Box model of P cycling in the sediments of oxic setting in the Lake Cadagno.

4.4.1.10 Released P rate from organic matter mineralization in the oxic setting

The same theory in 4.4.1.2 is used to calculate the released P rate from organic matter mineralization in the oxic setting. The rate of is calculated from the profile of P_{org} (Fig. 2.9). Specifically, the concentrations of P_{org} decrease from 0.080 wt% to 0.035 wt% with the whole depth (Fig. 2.9). For this calculation, the average density from 0 to 32 cm is 1.73 g/ml, the sedimentary rate is 2 mm/y and the average porosity from 0 to 32 cm is 0.93. R_{min} is calculated as 9.63 μmol/(m^2·d).

4.4.1.11 Released P rate from the reduction of Fe(III) (oxyhydr)oxide in the oxic setting

Two kinds of P are released from the Fe (oxyhydr)oxide reduction in this system. One is the adsorbed P and the other one is complexed P. For P_{sorb}, most of P is released in the surface sediments from 0 to 8.5 cm while the concentrations of P_{sorb} decrease from 0.0026 wt% to 0.0001wt% (Fig. 2.9). In the deep sediments from 8.5 to 32cm, the concentration of P_{sorb} remains constant at 0.0001 wt% (Fig. 2.9) which points that in the deep sediments, the reduction is stopped. For the calculation, the average density from 0 to 8.5 cm is 1.7 g/ml, the sedimentary rate is 2 mm/y and the average porosity from 0 to 8.5 cm is 0.97. R_{red1} = 0.23 μmol/(m^2·d). For $P_{Fe,}$ the reduction of Fe(III) releases the P with the whole depth while the concentration of P_{Fe} decreases from 0.098 wt% to 0.004 wt% (Fig. 2.9). For this calculation, the average density from 0 to 32 cm is 1.73 g/ml, the sedimentary rate is 2 mm/y and the average porosity from 0 to 32 cm is 0.93. R_{red2} is calculated as 20.12 μmol/(m^2·d).

4.4.1.12 Organic phosphorus, adsorbed P and Fe(III) bound P burial rate in the oxic setting

The same theory in 4.4.1.4 is used to calculate the burial rate of Organic phosphorus, adsorbed P and Fe(III) bound P. The concentrations of P in the deepest depth at 30 to 32 cm (P_{org} = 0.035 wt%; P_{sorb} = 0.0001 wt%; P_{Fe} = 0.004 wt%) is used for the burial rate calculation because this value is defined as the terminal point for the mineralization and reduction finished in this environments. For the calculations, the average density from 0 to 32 cm is 1.73 g/ml, the sedimentary rate is 2 mm/y and the average porosity from 0 to 32 cm is 0.93. R_{orgb} is calculated as 7.49 μmol/(m^2·d), the burial rate of adsorbed P (R_{sorbb}) is calculated as 0.01 μmol/(m^2·d), and R_{Feb} is calculated as 0.86 μmol/(m^2·d).

4.4.1.13 Rate of secondary diagenesis as P_{auth} in the oxic setting

As mentioned in 4.4.1.6, secondary diagenesis of P_{auth} may be formed in both surface sediments and deep sediments from 17 to 0 cm and 17 to 32 cm. However, in the deep sediments, from 25 to 32 cm, the concentrations of P_{auth} decrease slightly from 0.0013 to 0.0011 (Fig. 2.9). Because the P_{auth} is stable as the terminal fate of P which could not be transformed through the geochemical reactions (Anderson et al., 2001), with this depth from 25 to 32 cm, landslide may slightly affect the profile of P_{auth}. Furthermore, combining the slight decrease of water content (Fig. 4.5a) and the slight increase of dry sediments density (Fig. 4.5b) at the same depth, a slight landslide is proved in this

depth. As the landslide is slight and the concentrations of P_{detr} are quite low through the whole depth, the rate of P_{auth} formation may be not affected. For the calculation of secondary diagenesis rate as P_{auth} in the surface sediment (R_{auth1}), the average density from 0 to 17 cm is 1.69 g/ml, the sedimentary rate is 2 mm/y and the average porosity from 0 to 17 cm is 0.96. R_{auth1} is calculated as 0.72 μmol/(m^2·d). For the calculation of secondary diagenesis rate as P_{auth} in the deep sediment (R_{auth2}), the average density from 17 to 32 cm is 1.78g/ml, the sedimentary rate is 2 mm/y and the average porosity from 17 to 32 cm is 0.88. R_{auth2} is estimated as 1.51 μmol/(m^2·d).

4.4.1.14 Flux of dissolved P to water column and porewater in the oxic setting

The same method is used to calculate the flux of dissolved P to water column and porewater as that in 4.4.1.7. The profile of dissolved P in porewater is also generally divided into 2 parts by slopes. In the surface sediments from 0 to 6.5 cm, the slope equalling to 0.27 (Fig. 4.22a) is used to calculate the flux of dissolved P to water column. In the deep sediments from 16 cm to 32 cm, the slope equalling to 2.44 (Fig. 4.22b) is used to calculate the flux of dissolved P to porewater. From 6.5 cm to 16 cm, the slopes fluctuate which do not give a stable P flux. D_0 of P is 3.71×10^{-5} m^2/d when the temperature is 11.7℃ and salinity is 0.19. For the calculation of F_{diff}, the average porosity from 0 to 6.5 cm is 0.97. F_{diff} is calculated as 12.58 μmol/(m^2·d). For the calculation of F_{pw}, the average porosity from 16 to 32 cm is 0.89. F_{pw} is calculated as 1.1 μmol/(m^2·d).

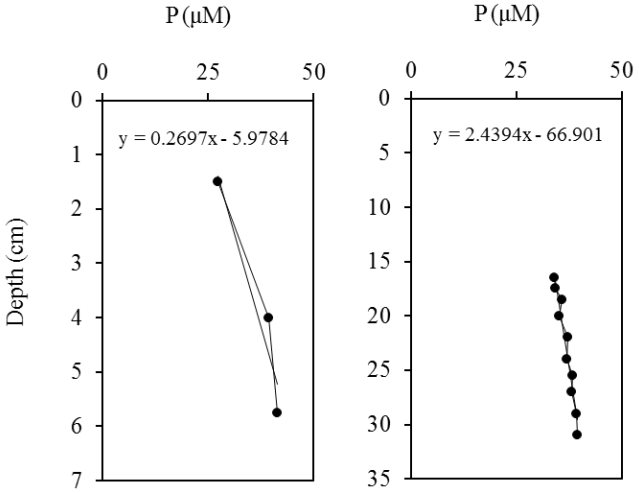

Figure 4.22 Linear slope of the best fit line for the vertical depth profile of P in the porewater in the sulfidic sediments beneath oxic water column in Lake Cadagno.

4.4.1.15 Mass balance of the model in the oxic setting

The consumption rate of P is calculated as $R_{min} + R_{red1} + R_{red2} = 29.98$ μmol/(m^2·d). The production rate of P is calculated as $R_{auth1} + R_{auth2} + F_{diff} + F_{pw} = 15.91$ μmol/(m^2·d). Therefore, the recovery rate is calculated at 53.07%. The mass balance is poor as 47.93% less in the production rate. The same way in 4.4.1.8 is used to complement the model. Here, the concentration of P in the water column at the depth 5 m equalling to 0.04 μM (Fig, 2.2d) is used as the dissolved P concentration in the interface between water column and sediments. To combine the P concentration in the interface and surface sediments, the new slope is calculated as 0.12 (Fig. 4.23), and the F_{diff} is re-calculated as 27.87 μmol/(m^2·d). Therefore the production rate of P is calculated as 31.2 μmol/(m^2·d) which increase the recovery to 104.07%. The production rate is 4.07% higher than the consumption rate. The possible reason is that the diffusion rate is not accurate. In the surface samples, oozes are the main deposits in the sediments which mix the porewater P concentrations.

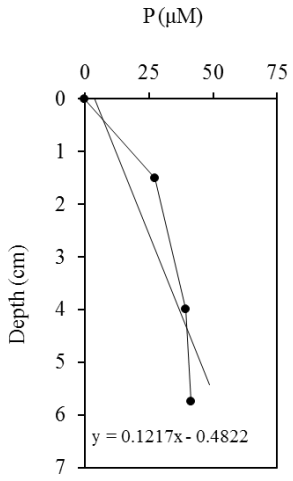

Figure 4.23 Linear slope of the best fit line for the vertical depth profile of P in the porewater and sediment-water interface in the sulfidic sediments beneath the oxic water column in Lake Cadagno.

Total P in this model is calculated by the sum of the P consumption rate and the burial rate (calculated in 4.4.1.12) as $R_{min} + R_{red1} + R_{red2} + R_{sorbb} + R_{orgb} + R_{Feb} = 38.34$ μmol/(m^2·d). In addition, the percentages of different P phases are calculated in Table 4.3.

Table 4.3 The percent of different P phases in the modelling of the eutrophic oxic water column with sulfidic porewaters in Lake Cadagno.

P phases	Percent (%)
P_{org} precipitate	19.54 ± 0.59
$P_{Fe(III)}$ precipitate	2.24 ± 0.04
P_{sorb} precipitate	0.03 ± 0.02
P_{auth} precipitate	2.35 ± 0.07
Diffused P to water column	72.69
Dissolved P in the porewater	2.87

4.4.2 Lake La Cruz

4.4.2.1. Box model

From 16 m, the water column turns to anoxic (Rodrigo et al., 2001; Romero-Viana et al., 2009), and dissolved Fe(II) starts to increase fast to form a ferruginous water column in the deep depth from 16 m to 20 m (Fig. 4.9b). In the deep sediments at 20 m, the concentrations of P_{sorb} and P_{Fe} both decrease in the surface sediment (Fig. 4.12a,b) which shows that P_{sorb} and P_{Fe} are reduced as the source for the released P. In addition, not as the last two environments, the profiles of P_{org} shows an increasing trend with depth (Fig. 4.12d) which points out that the mineralization of organic matter is not the source for the released P. However, in the anoxic ferruginous conditions, organic P is normally oxidized by Fe(III) to release dissolved Fe(II) (e.g. Slomp et al., 1996b; Anschutz., 1998). Furthermore, in this sediments, the concentrations of sulfate decrease rapidly (Fig. 4.13a) and the concentrations of Fe(II) increase with the whole depth (Fig. 4.13d) which both prove that the organic matter is reduced with depth (e.g. Canfield 1989; Canfield et al., 1993a, b). Therefore, organic matter is also an important source for the released P in this system. From profile of dissolved P in the porewater, the dissolved P increase to about 30 μM (Fig. 4.13c) which means that in this model, the diffused P to water column and re-dissolved P to porewater should be considered for the consummation of released P. From the profiles of P_{sorb}, P_{Fe} and P_{auth} in the sediments from 8.75 cm, 4.25 cm and 4.25 cm, all of three show an increase trend which means that there are the re-adsorption P and the secondary diagenesis of P including the

formation of Fe(II) phosphate and P_{auth} (Fig. 4.12a,b,c). For P_{auth}, the increasing profile shows another source of secondary diagenesis of P_{auth} by the diffused P (Fig. 4.12c). Therefore the box model of P cycling in the ferruginous sediments (Fig. 4.24) can be made below:

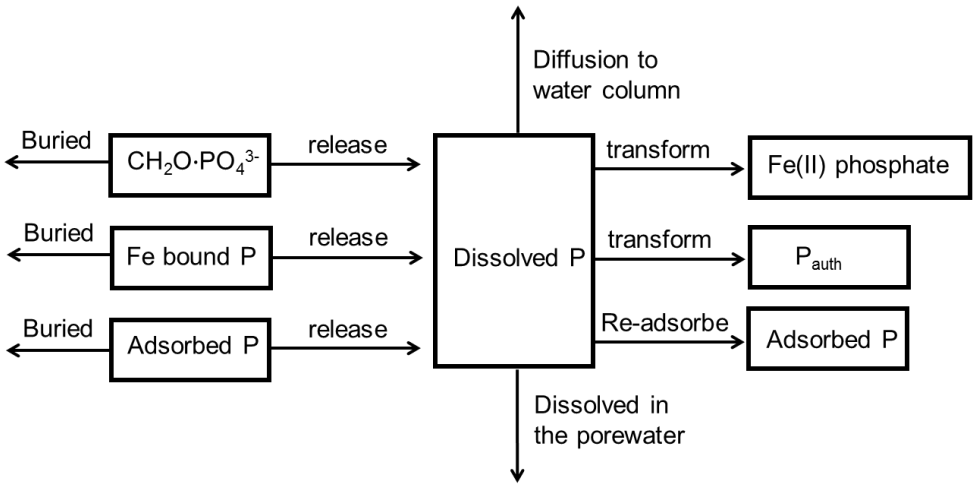

Figure 4.24 Box model of P cycling in the ferruginous sediments in the Lake La Cruz.

4.4.2.2 Released P rate from organic matter mineralization

In the Lake Cadagno's sediments, the released P from organic matter mineralization rate is directly calculated by the profile of $P_{org.}$ However, in this La Cruz lake, the profile of P_{org} is weird, showing an unexpected increase profile. Therefore, new ways of calculation are considered. The organic matter is oxidized accompanied with sulfate reduction and Fe(III) reduction which are worked as the electron donor (Canfield and Thamdrup, 2009). Therefore, the mineralization rate can be determined based on the profiles of dissolved sulfate and Fe(II) in the porewater. From the reactions of sulfate reduction, 1 mole of sulfate oxidizes 2 mols of carbon, therefore, the rate of the released P_{org} from organic matter mineralization is estimated as $R_{min} = P/C \cdot 2R_{sulfate}$ (rate of sulfate consumption) (van de Velde et al., 2016). Fick's first law is used for the calculation of $R_{sulfate}$. From the profile of dissolved sulfate in porewater, sulfate is reduced in the surface sediments from 0.75 to 4.25 (Fig. 4.13a). The slope is calculated as 0.6 (Fig. 4.25a), the average porosity is 0.94 from 0.75 to 5.75 cm, the average of C/P in mol with the whole depth is 1219.51 and the D_0 of sulfate at temperature equalling to 6.5 ℃ and salinity equalling to 0.41 is 5.51×10^{-5} m^2/d (Soetaert et al., 2010). The rate of mineralization is calculated as 0.013 μmol/(m^2·d). Similar calculation way is used for the calculation of Fe(III) reduction. Here, all the dissolved Fe(II) is hypothesized to be released by the Fe(III) reduction. From the reaction, 1 mole of Fe(II) production needs

to consume 0.25 mole of carbon, therefore the rate of the released P_{org} from organic matter mineralization is estimated as $R_{min} = P/C \cdot 0.25 R_{Fe}$ (rate of Fe(II) production) (van de Velde et al., 2016). The slope is calculated as 0.099 (Fig. 4.25b), the average porosity is 0.91, the same average of C/P in mol is used and the D_0 of dissolved Fe(II) at temperature equalling to 6.5 ℃ and salinity equalling to 0.41 is 3.70×10^{-5} m^2/d (Soetaert et al., 2010). The rate of mineralization is calculated as 0.006 μmol/(m^2·d). To combine the two results, the total rate of released P from organic matter mineralization is 0.019 μmol/(m^2·d).

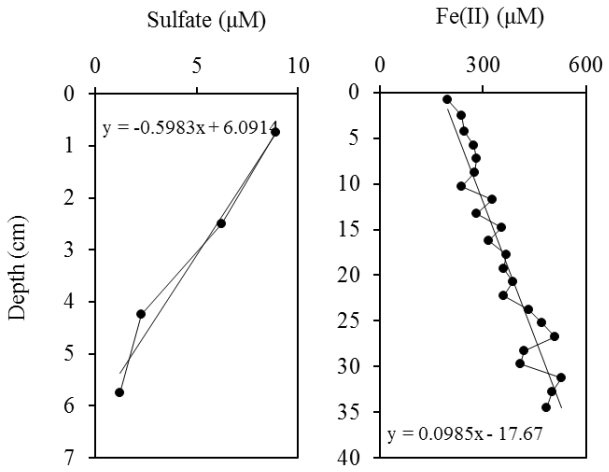

Figure 4.25 Linear slope of the best fit line for the vertical depth profile of sulfate and Fe(II) in the porewater in the ferruginous sediments in Lake La Cruz.

4.4.2.3 Released P rate from the reduction of Fe(III) (oxyhydr)oxide

In this sediments, the released P from Fe(oxyhydr)oxide reduction also include two pathways, one is the reduction of P adsorbed Fe(III) (oxyhydr)oxides, and the other one is the reduction of Fe(III) (oxyhydr)oxides bound P. The reduction rate is calculated from the surface profile of P_{sorb} from 0.75 to 8.75 cm where the P_{sorb} decreases from 0.0018 to 0.0009 wt% (Fig. 4.12a), showing that the reduction of Fe(III) released the adsorbed P. In addition, from 0.75 to 13.25 cm, the average porosity is calculated as 0.93, the average sedimentary rate is 4.22 mm/y and the average density is 2.49 g/ml. By the same theory in 4.4.1.3, R_{red1} = 0.59 μmol/(m^2·d). For calculation of the released P rate from P_{Fe}, the surface profile from 0.75 to 4.25 cm shows a decreasing trend from 0.017 to 0.010 wt% (Fig. 4.12b) which is the profile of the reduction of Fe(III) (oxyhydr)oxides bound P. In addition, from 0.75 to 4.25 cm, the average of porosity is

calculated as 0.96, the average of sedimentary rate is 5 mm/y and the average density is 2.39 g/ml. By the same theory in 4.4.1.3, R_{red2} = 3 μmol/(m^2·d).

4.4.2.4 Organic phosphorus, adsorbed P and Fe(III) bound P burial rate

The burial rate of organic P is calculated by the concentration of P_{org} at 0.018 wt% with the deepest depth at 34.5 cm (Fig. 4.12d) as the terminal point of mineralization of organic matter. In addition, with the whole depth, the average porosity is calculated as 0.93, the average of sedimentary rate is 4.22 mm/y and the average density is 2.49 g/ml. By the same theory in 4.4.1.4, R_{orgb} = 7.96 μmol/(m^2·d). The burial rates of adsorbed P and Fe(III) bound P are calculated by the concentrations of P_{sorb} equalling to 0.0009 wt% at 8.75 cm (Fig. 4.12a) and P_{Fe} equalling to 0.01 wt% at 4.25 cm (Fig. 4.12b), using the same calculation method in 4.4.1.4. The reason why not use the value in the deepest depth is that the profile of P_{sorb} and P_{Fe} in the deep sediments shows an opposite trend of the surface profile, which shows the secondary diagenesis reactions, thus new formation of P_{sorb} and P_{Fe} is not the right value for the calculation of the target burial. In addition, for the calculation of P_{sorb} burial rate, from 0.75 to 13.25 cm, the average porosity is calculated as 0.93, the average sedimentary rate is 4.22 mm/y and the average density is 2.49 g/ml. R_{sorb} = 0.59 μmol/(m^2·d). For the calculation of P_{Fe} burial rate, from 0.75 to 4.25 cm, the average of porosity is calculated as 0.96, the average sedimentary rate is 5 mm/y and the average density is 2.39 g/ml. By the same theory in 4.4.1.3, R_{Feb} = 4.22 μmol/(m^2·d). This result is almost negligible, much lower than that in Lake Cadagno because the sulfate reduction is not the dominant reaction in ferruginous sediments, and the dissolved Fe(II) is controlled by dissolved sulfide and phosphate. Therefore, the organic matter mineralization should be much higher than this result.

4.4.2.5 Rate of re-adsorbed P and secondary diagenesis as P_{Fe}

From 8.75 to 34.5 cm, the trend of P_{sorb} profile changes to increase from 0.0009 to 0.0018 wt% although there are some fluctuations from 8.75 to 28.25 cm (Fig. 4.12a). As large amounts of Fe(III) is precipitated from water column, the released P is easy to be re-trapped by the Fe(III) (oxyhydr)oxides in the second time (e.g. Slomp and van Raaphorst, 1993; Slomp et al., 1996 a, b). In addition, from 8.75 to 34.5 cm, the average porosity is calculated as 0.91, the average sedimentary rate is 1.1 mm/y and the average density is 2.41 g/ml. By the same calculation theory of the calculation in P_{Fe} in 4.4.1.5, the rate of re-adsorbed P (R_{sorb}) = 0.11μmol/(m^2·d). From 4.25 to 34.5 cm, the trend of P_{Fe} profile changes to increase from 0.01 to 0.24 wt% points out that new P_{Fe} formation,

and this new mineral is formed in the anoxic sediments which is the possible Fe(II) phosphate formation. In addition, from 4.25 to 34.5 cm, the average of porosity is calculated as 0.91, the average sedimentary rate is 2 mm/y and the average density is 2.44 g/ml. By the same calculation theory in 4.4.1.5, R_{Fe} = 5.43 μmol/(m^2·d).

4.4.2.6 Rate of secondary diagenesis as P_{auth}

As mentioned in 4.4.1.2.1, secondary diagenesis of P_{auth} may be formed in both surface sediments and deep sediments, here are from 4.25 to 0.75 cm and 4.25 to 34.5 cm. In the surface sediments, the concentrations of P_{auth} increase from 0.006 to 0.008 wt%, and the average porosity is calculated as 0.96, the average of sedimentary rate is 5 mm/y and the average density is 2.39 g/ml, thus the R_{auth1} = 0.84 μmol/(m^2·d). Furthermore, in the deeper sediments, the concentrations of P_{auth} increase from 0.006 to 0.01 wt%, and the average of porosity is calculated as 0.91, the average of sedimentary rate is 2.3 mm/y and the average density is 2.43 g/ml, thus the R_{auth2} = 1.77 μmol/(m^2·d). However, during this depth from 7.25 to 28.25 cm, there are some fluctuations of P_{auth} which will be discussed in mass balance of the model in 4.4.2.8.

4.4.2.7 Flux of dissolved P to water column and porewater

The same method is used to calculate the flux of dissolved P to water column and porewater as that in 4.4.1.7. The profile of dissolved P in porewater is also divided into 2 parts by slopes. In the surface sediments from 0 to 14.75 cm, the slope equalling to 0.67 (Fig. 4.26a) is used to calculate the flux of dissolved P to water column. In the deep sediments from 17.75 cm to 32.75 cm, the slope equalling to 1.34 (Fig. 4.26b) is used to calculate the flux of dissolved P to porewater. From 14.75 cm to 17.75 cm, the slopes fluctuate which do not give a stable P flux. D_0 of P is 3.06 × 10^{-5} m^2/d when the temperature is 6.5 ℃ and salinity is 0.41. For the calculation of F_{diff}, the average porosity from 0 to 14.75 cm is 0.93. F_{diff} is calculated as 3.71 μmol/(m^2·d). For the calculation of F_{pw}, the average porosity from 17.75 to 32.75 cm is 0.9. F_{pw} is calculated as 1.7 μmol/(m^2·d). For the flux of diffusion, if the interface concentration of dissolved P equalling to 2.54 μM is combined, the F_{diff} is nearly not changed which will not be discussed in 4.4.2.8.

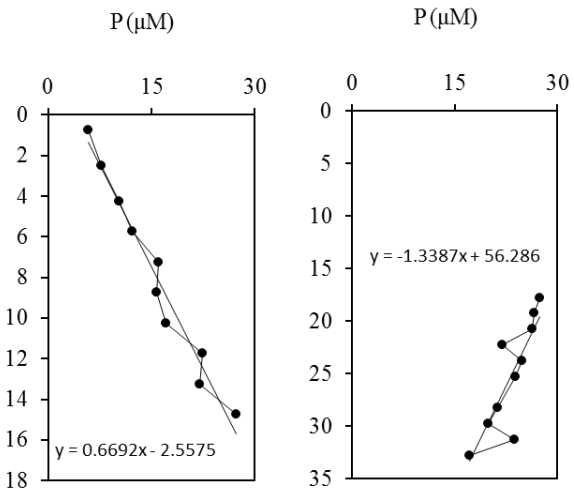

Figure 4.26 Linear slope of the best fit line for the vertical depth profile of P in the porewater in the ferruginous sediments in Lake La Cruz.

4.4.2.8 Mass balance of the model

The consumption rate of P is calculated as $R_{min} + R_{red1} + R_{red2} = 3.6$ μmol/(m^2·d). The production rate of P is calculated as $R_{sorb} + R_{Fe} + R_{auth1} + R_{auth2} + F_{diff} + F_{pw} = 13.56$ μmol/(m^2·d). The rate of production is much higher than the rate of consumption. Therefore, the values of each P phases are discussed below. For the production rate, the rates of R_{sorb}, R_{Fe}, R_{auth1} and R_{auth2} are not accurate. During the calculation, there are serious fluctuations in P_{sorb}, P_{Fe} and P_{auth} which are affected by detrital. However, the concentrations of P_{detr} is stable at 0.0028 wt% in both surface sediments from 0.75 to 5.75 cm and deep sediments from 23.75 to 34.5 cm, and fluctuate to high concentrations from 5.75 to 23.75 cm, thus the start value and the terminal value for the calculation of secondary P diagenesis are correct. For the calculation of consumption rate, the R_{red1} and R_{red2} are calculated from the profile of P_{sorb} and P_{Fe} from surface sediments, thus the calculation of rates is not affected by detrital. The only problem for the unbalanced mass is R_{min} which is calculated from the respiratory pathways of sulfate and Fe(II). However, the sulfate reduction is not the dominated reaction in the ferruginous sediments, and the dissolved Fe(II) is controlled by the dissolved sulfide and phosphate for the secondary diagenesis. The R_{min} should be much lower than the real value. If the production rate, R_{red1} and R_{red2} are accurate enough, the real R_{min} can be estimated as $13.56 – (R_{red1} + R_{red2}) = 9.98$ μmol/(m^2·d).

Total P in this model is calculated by the sum of the P consumption rate and the burial rate (calculated in 4.4.2.4) as $R_{min} + R_{red1} + R_{red2} + R_{sorbb} + R_{orgb} + R_{Feb} = 26.33$

μmol/(m^2·d). In addition, the percentages of different P phases are calculated in Table 4.4.

Table 4.4 The percent of different P phases in the modelling of the eutrophic ferruginous water column with ferruginous porewaters in Lake La Cruz.

P phases	Percent (%)
P_{org} precipitate	30.23 ± 1.1
$P_{Fe(III)}$ precipitate	16.03 ± 0.32
P_{sorb} precipitate	2.66 ± 0.13
P_{auth} precipitate	9.91 ± 0.30
$P_{Fe(II)}$ precipitate	20.62 ± 0.41
Diffused P to water column	14.09
Dissolved P in the porewater	6.46

4.4.3 Golfo Dulce

4.4.3.1. Box model

In the surface water column from 0 to 17 m, the system stays under the oxic conditions (Thamdrup et al., 1996; Dalsgaard et al., 2003). In the sediments, the dissolved Fe(II) in the porewater starts to increase to a high concentration (more than 200 μM) and the concentrations of sulfide are detection limited (Fig. 4.17a,b), thus the redox conditions in the sediments stay under the ferruginous conditions. In the sediments, the profile of P_{sorb} and P_{Fe} both show a general increase profile (Fig) which means that the released P is not from the P_{sorb} and P_{Fe} by the reduction of Fe(III) (oxyhydr)oxide reduction, instead, the increased profile shows that large amounts of released P re-adsorbed to Fe(III) (oxyhydr)oxide and have a secondary diagenesis, forming Fe(II) phosphate. The concentrations of P_{auth} increase from 0 to 16 cm which may show a secondary diagenesis of P_{auth} formation (Fig. 4.16c). For the profile of P_{org}, no obvious decrease trend is observed (Fig. 4.16d), however, under ferruginous conditions, the profile of dissolved Fe(II) increase in the porewater (Fig. 4.17b) is normally due to the respiratory pathway (Fe reduction), in addition, the profile of NH_4^+ increase in the porewater (Fig. 4.17d) also proves that the organic matter is consumed during the respiratory pathway (Denitrification). Therefore, the mineralization of organic matter is

an important source for the released P from P_{org}. From the profile of dissolved P in the porewater, the dissolved P increase to 26.06 μM (Fig. 4.17a) which means that the diffused P to water column and re-dissolved P to porewater should be considered for the consummation of released P. Therefore the box model of P cycling in the ferruginous sediments (Fig. 4.27) can be made below:

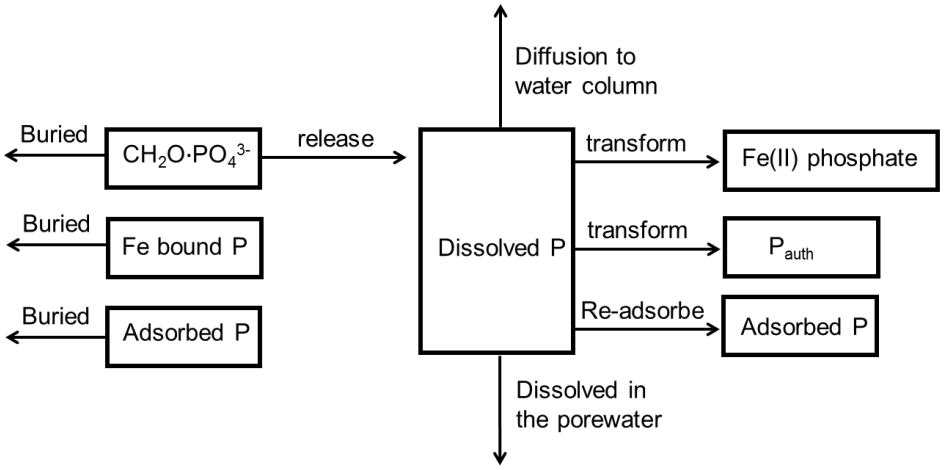

Figure 4.27 Box model of P cycling in the ferruginous sediments in the Golfo Dulce.

4.4.3.2 Released P rate from organic matter mineralization

In this sediments, the organic matter mineralization rate is difficult to calculate from the profile of P_{org} due to the opposite trend in the surface sediments (Fig. 4.16a). As the organic matter is oxidized accompanied with Fe(III) and NO_3^- reduction which are worked as the electron donor (Dalsgaard et al., 2003; Canfield and Thamdrup, 2009), the mineralization rate can be determined based on the profiles of dissolved Fe(II) and NH_4^+ in the porewater. The same theory in 4.4.2.2 is used to calculate the consumption rate of organic matter through the profile of dissolved Fe(II), then using the ratio of organic C/P in mole to calculate the rate of released P from P_{org}. Here, the slope is calculated as 0.039 (Fig. 4.28a), the average porosity is 0.78 from 0 to 6 cm, the average of C/P in mol with the whole depth is 250 and the D_0 of Fe (II) at temperature equalling to 28.3 ℃ and salinity equalling to 0.032 is 6.52×10^{-5} m^2/d (Soetaert et al., 2010). The rate of released P from organic matter mineralization is calculated as 0.087 μmol/(m^2·d). From the denitrification, 1 mole of NH_4^+ formation requires 6.625 mols of carbon consumption, therefore, the rate of the released P_{org} from organic matter mineralization is estimated as $R_{min} = P/C{\cdot}6.625R_{NH4}$ (rate of NH_4^+ production) (van de Velde et al., 2016). Fick's first law is used for the calculation of R_{NH4}. As the increased speed is slowed down (Fig. 4.17d) due to the anammox reaction (Dalsgaard et al.,

2003). The slope is calculated as 0.02 (Fig. 4.28b), the average porosity is 0.78 from 0 to 4 cm, the average of C/P in mol with the whole depth is 250 and the D_0 of NH_4^+ at temperature equalling to 28.3 ℃ and salinity equalling to 0.032 is 1.83×10^{-4} m^2/d. The rate of released P from P_{org} is calculated as 12.63 μmol/(m^2·d). To combine the concentration in the interface, the results are nearly not changed. In sum, the rate of the released P_{org} is calculated as R_{min} = 0.087 + 12.63 = 12.72 μmol/(m^2·d).

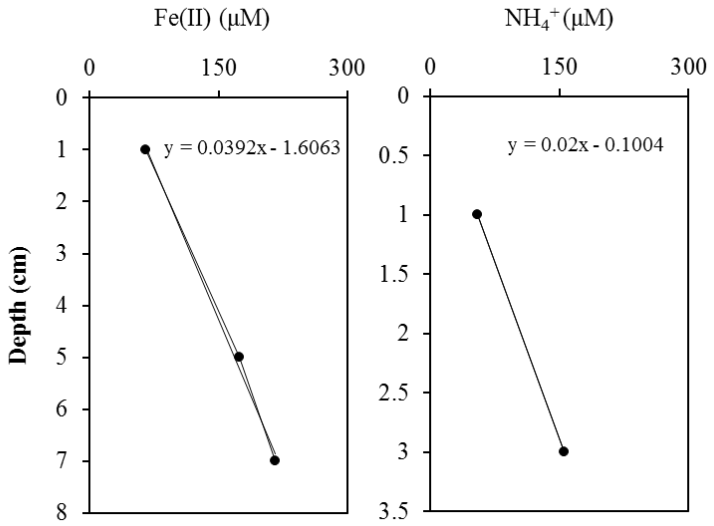

Figure 4.28 Linear slope of the best fit line for the vertical depth profile of Fe(II) and NH_4^+ in the porewater in the ferruginous sediments in Golfo Dulce.

4.4.3.3 Organic phosphorus, adsorbed P and Fe(III) bound P burial rate

The burial rate of organic P is calculated by the concentration of P_{org} at 0.009 wt% with the deepest depth at 28 cm (Fig. 4.16d) as the terminal point of mineralization of organic matter. In addition, with the whole depth, the average of porosity is calculated as 0.70, the average sedimentary rate is 1 mm/y and the average density is 2.04 g/ml. By the same theory in 4.4.1.4, R_{orgb} = 4.87 μmol/(m^2·d). The burial rates of adsorbed P and Fe(III) bound P are calculated by the concentrations of P_{sorb} equalling to 0.0008 wt% and P_{Fe} equalling to 0.011 wt% at 0 cm (Fig. 4.16a,b), using the same calculation method in 4.4.1.4. From 0 cm depth, new P_{sorb} and P_{Fe} start to form during the secondary mineral diagenesis, thus the concentrations of P_{sorb} and P_{Fe} with the deepest depth are not the right values for the calculation of the burial rate. In addition, for the calculation of P_{sorb} and P_{Fe} burial rates, at 0 cm depth, the porosity is 0.87, the sedimentary rate is 1 mm/y and the density is 2.06 g/ml. R_{sorbb} = 0.19 μmol/(m^2·d) and R_{Feb} = 2.6 μmol/(m^2·d).

4.4.3.4 Rate of re-adsorbed P and secondary diagenesis as P_{Fe}

Although the concentrations of P_{sorb} and P_{Fe} fluctuate with the whole depth, both of the profiles show the general increase which is pointed out that the released P is re-trapped through the re-adsorbed Fe(III) (oxyhydr)oxide and the secondary diagenesis formation as P_{Fe}. For the rates calculation of re-adsorbed P and secondary diagenesis, with the whole depth, the average of porosity is calculated as 0.7, the sedimentary rate is 1 mm/y and the average density is 2.04 g/ml. By the same calculation theory in 4.4.2.5, R_{sorb} = 0.75 μmol/(m^2·d) and R_{Fe} = 3.25 μmol/(m^2·d).

4.4.3.5 Rate of secondary diagenesis as P_{auth}

From the profile of P_{auth}, the secondary diagenesis processes from 0 to 16 cm while the concentrations increase from 0.015 to 0.023 wt% (Fig. 4.16c). The rate is calculated by the same theory in 4.4.2.6, in addition, with the depth from 0 to 16 cm, the average of porosity is calculated as 0.73, the sedimentary rate is 1 mm/y and the average density is 2.07 g/ml. R_{auth} is calculated as 3.95μmol/(m^2·d). However, from 16 to 28 cm, the concentrations of P_{auth} decrease to 0.014 wt% (Fig. 4.16c). As the P_{auth} is a stable precipitation of P which does not decrease through geochemical reactions (Anderson et al., 2001), the concentrations with this deep depth should be diluted which will be discussed in mass balance of the model (4.4.3.7).

4.4.3.6 Flux of dissolved P to water column and porewater

The same method is used to calculate the flux of dissolved P to water column and porewater as that in 4.4.1.1.7. The profile of dissolved P in porewater is also generally divided into 2 parts by slopes. In the surface sediments from 0 to 10 cm, the slope equalling to 1.23 (Fig. 4.29a) is used to calculate the flux of dissolved P to water column. In the deep sediments from 14 cm to 20 cm, the slope equalling to 0.42 (Fig. 4.29b) is used to calculate the flux of dissolved P to porewater. From 10 cm to 14 cm, the slopes fluctuate which do not give a stable P flux. D_0 of P is 5.75×10^{-5} m^2/d when the temperature is 28.3 ℃ and salinity is 0.032 (Soetaert et al., 2010). For the calculation of F_{diff}, the average porosity from 0 to 10 cm is 0.75. F_{diff} is calculated as 2.24 μmol/(m^2·d). For the calculation of F_{pw}, the average porosity from 14 to 20 cm is 0.7. F_{pw} is calculated as 5.56 μmol/(m^2·d). For the flux of diffusion, if the interface concentration of dissolved P equalling to 0.7 μM is combined (Thamdrup et al., 1996), the F_{diff} is nearly not changed.

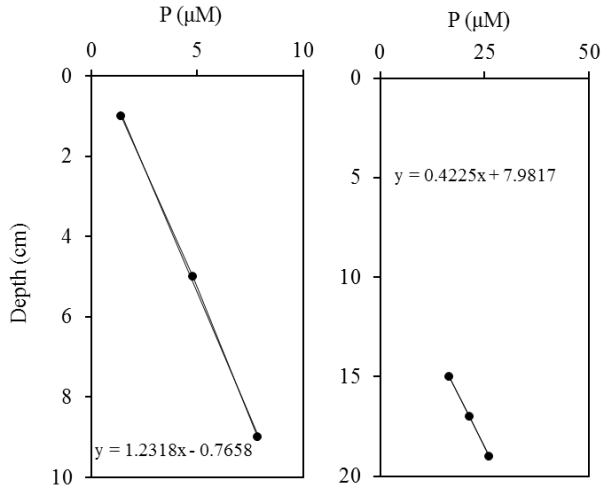

Figure 4.29 Linear slope of the best fit line for the vertical depth profile of P in the porewater in the ferruginous sediments in Golfo Dulce.

4.4.3.7 Mass balance of the model

The consumption rate of P is calculated as R_{min} = 12.72 μmol/(m^2·d). The production rate of P is calculated as $R_{sorb} + R_{Fe} + R_{auth} + F_{diff} + F_{pw}$ = 15.75 μmol/(m^2·d). The recovery rate is calculated at 124.7. Here, the production rate is 24.7 % higher than the consumption rate. Not like the calculation as the sediments in Lake Cadagno, the R_{min} is calculated from the respiratory pathways which means that the calculations may be limited to calculate all the possible reactions. For example, based on the energy required for the reactions, Mn reduction is not considered between the denitrification and Fe reduction because of the data limitation (e.g. Froelich et al., 1979; Luther et al., 1998; Schippers et al., 2005). Another possible reason for the unbalanced mass may be due to detrital affection. From the profile of $P_{detr,}$ in the surface (0 to 6 cm) and deep (20 to 28 cm) sediments, the concentrations are relatively high than those between 6 and 20 cm (Fig. 4.16e) which means that the surface and the deep sediments may be diluted by the detrital. Therefore, the real concentrations of P_{auth} from 16 to 28 cm are higher than those in Fig. 4.16c which may explain the impossible profile of P_{auth} described in 4.4.3.5. Furthermore, the fluctuation of P_{detr} with the depth is absolutely opposite to the fluctuation of P_{sorb}, P_{Fe}, P_{auth} and P_{org} (Fig. 4.16). Therefore, the profile of P_{sorb} and P_{Fe} may show a decreasing trend from 0 to 6 cm which directly supplies the new sources of released P from the reduction of Fe(III) to satisfy the recovery rate. Furthermore, the average concentrations of P_{detr} from 0 to 6 cm and 20 to 28 cm are 0.32 wt% and 0.33 wt%, respectively (Fig. 4.16e) which are nearly the same, thus the rates of P re-

absorption and Fe(II) phosphate diagenesis may not be affected due to the same increased level of the start point and the terminal point. In addition, as the terminal point increase, the burial rate of $P_{Fe(III)}$ and P_{sorb} are obviously higher than the calculated values. For P_{auth}, the profile in the surface sediments may show a new diagenesis due to the recycled P the same as Lake La Cruz, thus the P_{auth} should be higher than the calculated value. This is also pointed out that the real P_{org} in the surface sediments should be higher than that in Fig 4.10d. If the surface concentrations of P_{org} are re-corrected, the decreasing trend of P_{org} is formed which also prove that the organic matter mineralization plays an important role for the released P.

Because the results of the consumption rate is not accurate, here, the total P in this model is estimated by the sum of the P production rate and the burial rate (calculated in 4.4.2.4) as $R_{sorb} + R_{Fe} + R_{auth} + F_{diff} + F_{pw} + R_{sorbb} + R_{orgb} + R_{Feb} = 23.41$ μmol/(m^2·d). In addition, the percentages of different P phases are calculated in Table 4.5.

Table 4.5 The percent of different P phases in the modelling of the oligotrophic oxic water column with ferruginous porewaters in Golfo Dulce.

P phases	Percent (%)
P_{org} precipitate	20.80 ± 0.73
$P_{Fe(III)}$ precipitate	> 11.11 ± 0.22
P_{sorb} precipitate	> 4.02 ± 0.20
P_{auth} precipitate	> 16.87 ± 0.51
$P_{Fe(II)}$ precipitate	13.88 ± 0.28
Diffused P to water column	9.57
Dissolved P in the porewater	23.75

4.4.4 P cycling under different redox conditions

In all the four different systems, P_{org} is an important sink for the P preserved in the sediments. Even for the oligotrophic system, P_{org} accounts for 20.8% of the total P (Table 4.5). P trapped by Fe(III) (oxyhydr)oxides includes both co-precipitated and adsorbed P. In both of the sediments dominated by sulfidic porewaters (the euxinic and oxic settings in Lake Cadagno), less than 5% of the P is trapped by Fe(III) (oxyhydr)oxides (table 4.2 and 4.3), which shows the effectiveness of Fe reduction by

sulfide in releasing P back to solution. However, in the case of the ferruginous sediments (Lake La Cruz and Golfo Dulce), the P trapped by Fe(III) (oxyhydr)oxides accounts for more than 15% (Table 4.4 and 4.5) which shows that a significant proportion of dissolved P is retained in association with Fe (oxyhydr)oxides (e.g. Slomp and van Raaphorst, 1993; Slomp et al., 1996 a, b). Furthermore, this also suggests that under ancient episodes of ferruginous conditions a significant proportion of P may be retained in association with Fe (oxyhydr)oxide minerals.

In both of the sulfidic sediments (oxic and euxinic Lake Cadagno), P_{auth} accounts for less than 4% of total P (Table 4.2 and 4.3), but in the ferruginous sediments beneath a ferruginous water column (Lake La Cruz), the percentage of P_{auth} increases to almost 10% (Table 4.4). In addition, in the ferruginous sediments deposited beneath an oxic water column (Golfo Dulce), the percentage of P_{auth} is more than 15% (Table 4.5). Therefore, sulfidic porewater conditions limit the formation of P_{auth}, which has also been found in sulfidic sediments of the Baltic Sea (Mort et al., 2010). By contrast, P_{auth} formation is promoted under ferruginous conditions.

Fe(II) phosphate formation ($P_{Fe(II)}$) occurs below the zone of sulfidic porewaters in sediments deposited beneath the euxinic water column of Lake Cadagno, and in both of the ferruginous sediments. By contrast, no $P_{Fe(II)}$ is formed in the sulfidic sediments deposited under oxic conditions in Lake Cadagno. Specifically, in the euxinic Lake Cadagno, Fe(II) phosphate is ultimately the main sink for P (Table 4.2). In the oxic Lake Cadagno, more than 70% of the total P flux is recycled back to the water column (Table 4.3). This highlights the significance of Fe phosphate formation in constraining the flux of P back to the water column under low sulfate euxinic settings (see Chapter 2), and highlights that during past episodes of widespread, low sulfate euxinia, such as during the mid-Proterozoic and during Phanerozoic episodes of euxinia, the positive primary productivity feedback would have been constrained by this process. Although the diffusion of P is lower in the euxinic Lake Cadagno setting compared to the oxic water column setting, the percentage is still higher than the 14.09% modeled for the ferruginous lake La Cruz and 9.57% for the ferruginous sediments of Golfo Dulce. This suggests that ferruginous settings in the past likely had lower fluxes of recycled P back to the water column than under euxinic conditions, due to both re-uptake by Fe (oxyhydr)oxides, and the formation of Fe phosphate minerals.

It is also interesting to consider the very high diffusive flux of P from the oxic Lake Cadagno sediments. This setting has by far the highest flux of P back to the water

column. This occurs because all of the biogeochemistry of this core is poised at a condition which promotes P recycling. Sulfidic porewater conditions promote P release from both organic matter and Fe (oxyhydr)oxides, and also, this setting has an extremely high organic matter content close to the sediment-water interface. Thus, very high concentrations of P are released to the solution from organic matter degradation. Precipitation of P_{auth} is limited by dissolved sulfide, which also limits the formation of Fe phosphate minerals, and hence there is no efficient trap for the high concentration of P released, which thus fluxes back to the water column. This highlights that it is not only water column redox that controls the recycling of P. The nature of the porewaters close to the sediment-water interface (i.e., sulfidic versus ferruginous), plus the flux of organic matter to the sediment also play major roles. This contrasts somewhat with the widely held view that under oxic conditions, dissolved P is extensively fixed by uptake to Fe(oxyhydr)oxide minerals at the sediment-water interface – clearly the prevalence of this process depends on the additional factors outlined here. In another word, the P trap rate by Fe (oxyhydr)oxides in the surface sediments is much lower than the P release rate from the decomposition of Fe (oxyhydr)oxides.

4.5. Conclusion and implications

Four key redox scenarios in the three different water systems are considered to investigate how redox conditions affect P dynamics. They are eutrophic oxic water column conditions with sulfidic porewaters in Lake Cadagno, eutrophic euxinic water column conditions with sulfidic porewaters in Lake Cadagno, eutrophic ferruginous water column conditions with ferruginous porewaters in Lake La Cruz and oligotrophic oxic water column conditions with ferruginous porewaters. Depended on the geochemical data from the water column, sediments and porewaters, the box models of P cycling including the chemical reaction pathways are made for each scenario. Based on the box model, the percent of different P phases involved P_{org} precipitate, $P_{Fe(III)}$ precipitate, P_{sorb} precipitate, P_{auth} precipitate, $P_{Fe(II)}$ precipitate, diffused P to water column and dissolved P in the porewater are quantified.

From our results, P_{org} is the important sink under all the redox conditions, accounting for about 20% of the total P. In the eutrophic ferruginous system, the concentrations of P_{org} even reach to about 30%. A significant proportion of dissolved P is trapped by Fe(III) (oxyhydr)oxides (more than 15%) in the ferruginous conditions, however, in the sulfidic sediments, less than 5% of the P is retained in association with Fe(III) (oxyhydr)oxides. P_{auth} is inhibited in the sulfidic sediments, accounting for 4% of the

total P, by contrast, P_{auth} formation is promoted under ferruginous conditions. Fe(II) phosphate in the sulfidic sediments beneath the sulfidic water column plays the key role for the retention of dissolved P, accounting for more than 40%, and in both ferruginous sediments, Fe(II) phosphate also account for a high proportion, at 20.62% and 13.88%. However, in the sulfidic sediments beneath the oxic water column, no Fe(II) phosphate is formed, instead, more than 70% of the total P flux is recycled back to the water column.

Considering the results analogous to those which were prevalent at various time in Earth history, under ancient episodes of ferruginous conditions, the low flux of recycled P back to water column is controlled by both P re-uptake by Fe(III) (oxyhydr)oxide and the formation of Fe(II) phosphate. During the mid-Proterozoic and during Phanerozoic, under low sulfate euxinia, the flux of recycled P is constrained by Fe(II) phosphate formation. Therefore, This study provides supporting evidence to the suggestion that the positive primary productivity feedback is constrained by these processes.

Finally, based on the result of the high flux of P back to the water column, it highlights the nature of the porewaters close to the sediment-water interface, plus the flux of organic matter to the sediment also play key roles of P recycling, rather than water column redox conditions.

Chapter 5 Summary and suggestions for future research

This project is to investigate mineralogical controls on P cycling under different redox conditions. To reach the aim, new geochemical data is reported in Lake Cadagno, new experiments are designed for mineralogical control and mass balance models are utilized under different redox conditions. The main findings of this work are summarised here, and suggestions for possible future research directions are presented.

5.1 Phosphorus cycling in Lake Cadagno, Switzerland: A low sulfate euxinic ocean analogue

New water column and sediment data for Lake Cadagno are provided, focusing on different parts of the basin, including the deeper euxinic waters, shallower oxic waters, and a site where the chemocline intersects the deposited sediments. To combine Fe and P speciation data with bulk geochemical analyses, P cycling under low-sulfate euxinic conditions is investigated.

- Phosphorus recycling to the water column is particularly enhanced beneath the deeper euxinic waters by the mineralization of organic matter and reduction of Fe (oxyhydr)oxide minerals, promoting the high concentrations of water column phosphorus.
- Not all the dissolved P is recycled back to water column due to the formation of authigenic Fe(II) phosphate minerals. The minerals are formed below the sulfate/methane transition zone.
- The formation of Fe(II) phosphate minerals is sulfate-dependent. Low sulfate promotes vivianite formation due to the more rapid consumption of all of the dissolved sulfate and sulfide during early diagenesis. Under high concentration of euxinic marine sulfate, Fe(II) is trapped to form pyrite not as vivianite.
- Low sulfate, euxinic water column conditions were a common feature of many Precambrian and Phanerozoic periods of ocean anoxia. The modulation of P recycling due to the Fe(II) production under the low sulfate euxinic conditions highlights that during Precambrian and Phanerozoic periods, the primary productivity including organic carbon and oxygen production is constrained.

In summary, this chapter uses the data from the analogue lake to give details of P cycling after the first GOE during the Proterozoic. These results sit in contrast to the

recent study of Reinhard et al. (2017), but consistent with the results of Kipp and Stüeken (2017). Specifically, during the GOE, high levels of dissolved P are recycled back to the water column, increasing biological oxygen production, which increases terrestrial sulphide weathering, resulting in the increase of sulfate input to seawater. After the GOE in the Proterozoic, P concentrations remain at higher levels but much lower than that in the GOE. Reinhard et al. (2017) suggest that dissolved P is trapped by Fe(III) oxide minerals to explain the lower levels of dissolved P, but they ignore the widespread euxinic conditions present during this period. Here I give the explanation of why P decreases after the GOE. The recycled P is partly re-trapped by Fe(II) to form Fe(II) phosphate (vivianite). Furthermore, it also explains that oxygen remains higher than that in the Archean but lower than that in the GOE.

5.2 Chemical controls on the formation of vivianite versus sulfate green rust

New experimental insight into the effect of P concentration on the formation of GR versus vivianite is provided. This study explores a range of Fe(II) to phosphate ratios in order to determine the threshold by which the Fe mineralogy changes, to ultimately provide constraints on controls on P cycling in modern and ancient ferruginous settings.

- With the increase of P concentration, the formation of $GRSO_4$ is affected. In the absence or at low P concentrations, pure $GRSO_4$ is observed. When the concentrations of P increases, a significant proportion of P is adsorbed at the surface of GR particles to exchange with sulfate. This process directly causes a poorer crystallinity of GR mineral. When the concentrations of P continue to increase, the GR is transformed to amorphous Fe(II) phosphate. With time, amorphous phosphate converts into vivianite.
- When P and Fe(II) concentrations approach the molar ratio of stoichiometric vivianite, GR does not form as an intermediate phase, only crystalline vivianite is synthesized.

During the early Archean, the remineralization of organic matter is constrained due to lack of electron acceptors (Tosca et al., 2016). In the mid-Archean, the Fe(III) works as the electron acceptor, but dissolved P is still low. In the previous work, Fe(III) oxide minerals have been considered the main agent for trapping dissolved P, resulting in low levels of phosphorus (Bjerrum and Canfield, 2002; Jones et al., 2015), here GR is considered as the major mineral forming at the redoxcline to remove dissolved P.

Phosphorus is adsorbed to GR maintaining low P concentrations in the water column, causing a negative feedback of primary productivity and oxygen production. After the GOE, during the period of the mid-Proterozoic, Fe(III) oxide is defined as the major mineral to trap the dissolved P (Reinhard et al., 2017). Here, I present a new idea suggesting that green rust traps a large portion of recycled P in the redoxcline, transforming to vivianite as the new P precipitate phase to maintain low levels of primary production and oxygen production.

5.3 Modelling P cycling under different water column redox conditions

All the geochemical data is combined to make mass balance models to quantify the cycling and burial of P, to see how much P is fixed in the sediment and how much is recycled back to water column under different redox conditions, analogous to those which were prevalent at various time in Earth history.

- P_{org} is the important sink under all the redox conditions. A significant proportion of dissolved P is trapped by Fe(III) (oxyhydr)oxides in the ferruginous conditions, however, in the sulfidic sediments, nearly no P is retained in association with Fe(III) (oxyhydr)oxides. P_{auth} is inhibited in the sulfidic sediments, by contrast, P_{auth} formation is promoted under ferruginous conditions. Fe(II) phosphate in the sulfidic sediments beneath the sulfidic water column plays the key role for the retention of dissolved P, and in both ferruginous sediments, Fe(II) phosphate also account for a high proportion. However, in the sulfidic sediments beneath the oxic water column, no Fe(II) phosphate is formed.

- Under ancient episodes of ferruginous conditions, the low flux of recycled P back to water column is controlled by both P re-uptake by Fe(III) (oxyhydr)oxide and the formation of Fe(II) phosphate. During the mid-Proterozoic and during Phanerozoic, under low sulfate euxinia, the flux of recycled P is constrained by Fe(II) phosphate formation. This study provides supporting evidence to the suggestion that oxygenation of the earth systems is constrained by these processes.

- Based on the result of the high flux of P back to the water column, it highlights the nature of the porewaters close to the sediment-water interface, plus the flux of organic matter to the sediment also play key roles of P recycling, rather than water column redox conditions. However, this result contrasts the widely

accepted view that dissolved P is fixed by Fe(oxyhydr)oxide minerals at the interface between sediments and water column.

In summary, 4 analogue lakes were investigated in this chapter. Firstly, two Proterozoic analogue lakes, Lake Cadagno with a euxinic sediment core, and Lake La Cruz a with ferruginous sediment core. In both cores, most of the P is trapped as $P_{Fe(II)}$ precipitate, especially for Lake Cadagno euxinic core (about 40%). The value is higher than the P trapped as $P_{Fe(III)}$, which is directly opposite to the results of Reinhard et al. (2017). In their opinions, most of P is scavenged by Fe(III) oxide minerals during the period of the Proterozoic.

Secondly, the oxic water column and euxinic sediment core in Lake Cadagno shows a high value of diffused P (~ 72%). This system may show the features during the first GOE. When most of Fe(III) is still inhibited by greenalite (Tosca et al., 2016), and high concentration of sulfate is input into ocean system to form euxinic conditions (Poulton and Canfield, 2011). The P diffusion flux becomes much higher than the rate of P trapped by Fe(III) which is consistent with the positive feedback of primary productivity and oxygen. The results are also consistent with the model of Kipp and Stüeken (2017), in the first GOE high levels of P are recycled back to water systems.

Thirdly, the oligotrophic oxic water column with ferruginous pore waters in Golfo Dulce show that P_{auth} and $P_{Fe(III)}$ become the important precipitate. P_{auth} formation is accompanied with oxygen increases and high P recycling back to water column (Derry 2015; Reinhard et al., 2017), however, in this environment, the nutrient (P) is limited. Thus, this environment could be treated as the analogue of the environment after the second GOE when the growth of dissolved P in ocean system is maintained by Fe(III) oxide minerals, then transforming to P_{auth} with time. In addition, the results are consistent with the model in Reinhard et al. (2017), which show that the oxygen stays at a low level prior to 800 million years ago after the second GOE. In Reinhard et al.'s model, only shale samples are considered which brings a direct bias in the P cycling during the period of the Proterozoic, when the P cycling is affected by the formation of Fe(II) phosphate, however, for P cycling dominated by the $P_{auth,}$ the shale samples seem working well.

No Archean analogue lakes were considered in this chapter, though this model is ready for data from an appropriate analogue lake which we will work on in the future.

5.4 Suggestions for future research

Understanding the input and recycling of major nutrients (e.g. P, N), bioessential trace metals (e.g. Fe, Ni, Cu, Mo) in the oceans has major implications for the regulation of primary productivity, organic carbon burial and oxygen production in both modern and ancient environments. One of the main geochemical processes that affects the bioavailability of these elements is uptake by reactive Fe minerals. Subsequently, the behaviour of Fe minerals and associated elements during early diagenesis exerts the dominant control on whether nutrients and bioessential trace metals are either sequestered in the sediment or released back into the water column. Clearly, the fixation of elements in the deposited sediment effectively limits their bioavailability, and thus it is crucial to understand the behaviour of nutrients during uptake by minerals under different redox conditions and during early diagenesis in order to evaluate implications for primary production and ultimately the rise of oxygen early in Earth's history.

The modern ocean is largely characterized by an abundance of dissolved oxygen, and as a result, Fe oxides are the major group of Fe minerals that have been widely examined in terms of their uptake capacity for major and trace metal nutrients. However recent research suggest that, considering the entirety of Earth history, the dominate behaviors of Fe are dissolved Fe (ferruginous) and pyrite (euxinic(sulfidic)). Development of these anoxic conditions in the water column is also a major concern with regard to the future impact of modern climate change on oxygen levels in the ocean. There is growing evidence that iron phosphate (vivianite) or green rust is major initial Fe precipitates, dependent on the precise chemistry of the anoxic waters. However, controls on the formation of these minerals, and on the behaviour of phosphorus and bioessential trace metals during their formation and transformation is poorly understood, particularly in terms of processes likely to operate under redox oceanic conditions and during early diagenesis in anoxic porewaters.

The future work will focus on the uptake of phosphorus, trace metal nutrients (Fe, Ni, Cu and Mo) and part of the trace metal isotope fractionation (Fe, Mo) to minerals formed under different redox conditions such as oxic, nitrogenous, ferruginous and euxinic conditions, and will investigate the subsequent potential for these elements to be fixed in the sediment or released to water column during early diagenesis, finally will make a mass balance model to quantize the behaviours of these elements in the recycling. The ultimate goal will be to build an understanding of the role of Fe minerals in the biogeochemical cycling of elements such as Ni, Cu and Mo under different redox

conditions. This, in turn, will provide a greater understanding of the potential for these elements to limit key biogeochemical processes, with a key aim to consider implications for the production of oxygen in Earth's history.

The initial experimental phases will examine nutrient, trace metal and their isotope fractionation uptake during the synthesis of green rust. Controlled experiments will examine nutrient and trace metal and their isotope fractionation uptake during the transformation (oxidization) of green rust to different phases such as hematite or magnetite. All of these experiments will be conducted in different media (with or without dissolved silica and in MQ water or sea water), and will be compared to the results of separate adsorption experiments to pre-formed green rust. The final experimental phases will be aimed at investigating the release and/or fixation of adsorbed elements during conditions encountered during early diagenesis.

The field-based phase of the future work will involve sampling and characterizing particulate and dissolved species in the different lake systems (Banyoles, Montcortés, Lake La Cruz, EI Tobar). These lakes are good analogue lakes through the Earth history. Geochemical extraction techniques (e.g. Fe and P speciation) will be combined with the isotope fractionation analysis at Cardiff and a range of mineralogical techniques available at Leeds (e.g. XRD, TEM). With the potential for further characterization of minerals at the Diamond Light Source Facility.

The modelling phase of the future work will make a mass balance model to quantize the formation or decomposition rates of different behaviours of these elements based on the data from the field-based phase.

List of References

Adams D. D., Hurtgen M. T. and Sageman B. B. (2010) Volcanic triggering of a biogeochemical cascade during Oceanic Anoxic Event 2. *Nat. Geosci*. **3**, 201-204.

Algeo T. J. and Ingall E. (2007) Sedimentary Corg:P ratios, paleocean ventilation and Phanerozoic atmospheric pO2. Palaeogeog. *Palaeoclim. Palaeoeco.* **256**, 130-155.

Aller R. C. (2014) Sedimentary diagenesis, depositional environments, and benthic fluxes. In *Treatise on Geochemistry*, second ed. Springer, pp. 293-334.

Anbar A. D. and Knoll A. H. (2002) Proterozoic ocean chemistry and evolution: A bioinorganic bridge? *Science* **297**, 1137-1142.

Anbar A. D., Duan Y., Lyons T. W., Arnold G. L. and Kendall B. (2007) A whiff of oxygen before the Great Oxidation Event? *Science*, **317**, 1903-1906.

Anderson L. D., Delaney M. L. and Faul K. L. (2001) Carbon to phosphorus ratios in sediments: implications for nutrient cycling. *Global Biogeochem. Cyc*. **15**, 65-79.

Anderson T. F. and Raiswell R. (2004) Sources and mechanisms for the enrichment of highly reactive iron in euxinic Black Sea sediments. *Am. J. Sci.* **304**, 203-233.

Anschutz P., Zhong S., Sundby B., Mucci A. and Gobeil C. (1998) Burial efficiency of phosphorus and the geochemistry of iron in continental margin sediments. *Limnol. Oceanogr.* **43**, 53–64.

Appelo C. A. J., Parkhurst D. L. and Post V. E. A. (2014) Equations for calculating hydrogeochemical reactions of minerals and gases such as CO_2 at high pressures and temperatures. *Geochim. Cosmochim. Acta* **125**, 49-67.

Bange H. W., Rixen A. M., Siefert R. L., Ramesh R., Ittekkot V., Hoffmann M. R. and Andreae M. O. (2000) A revised nitrogen budget for the Arabian Sea. *Global Biogeochem. Cycles* **14**, 1283-1297.

Barthélémy K., Naille S., Despas C., Ruby C. and Mallet M. (2012) Carbonated ferric green rust as a new material for efficient phosphate removal. *J. Interface Sci.* **384**, 121-127.

Berg P., Risgaard-Petersen N. and Rysgaard S. (1998) Interpretation of measured concentration profiles in the sediment pore water. *Limnol. Oceanogr*. **43**, 1500-1510.

Bernal J. D., Dasgupta D. T. and Mackay A. L. (1959) The oxides and hydroxides of iron and their structural inter-relationships. *Clay Mineral. Bull.* **4**, 15-30.

Berner R. A. (1986) *Early Diagenesis: A Theoretical .Approach*. Princeton, 241 p.

Berner R. A. and Canfield D. E. (1989) A new model for atmospheric oxygen over Phanerozoic time. Am. J. *Sci.* **289**, 333-361.

Berner R. A. and Rao J.-L. (1994) Phosphorus in sediments of the Amazon River and estuary: implications for the global flux of phosphorus to the sea. *Geochim. Cosmochim. Acta* **58**, 2333-2339.

Bieleski R. L. and Ferguson I. B. (1983) Physiology and metabolism of phosphate and its compounds. In *Inorganic Plant Nutrition, Encyclopedia of Plant Physiology, New Series; v. 15* (eds. A. Länchli and R. L. Bieleski). Springer, Berlin, pp. 422-449.

Birch L., Hanselmann K. W. and Bachofen R. (1996) Heavy metal conservation in Lake Cadagno sediments: Historical records of anthropogenic emissions in a meromictic alpine lake. *Water Res.* **30**, 679-687.

Bjerrum C. J. and Canfield D. E. (2002) Ocean productivity before about 1.9 Gyr ago limited by phosphorus adsorption onto iron oxides. *Nature* **417**, 159-162.

Bocher F., Géhin A., Ruby C., Ghanbaja J., Abdelmoula M. and Génin J.-M. R. (2004) Coprecipitation of Fe(II–III) hydroxycarbonate green rust stabilised by phosphate adsorption. *Solid State Sciences* **6**, 117-124.

Borch T. and Fendorf S. (2008) Phosphate interactions with Iron (hydroxides): mineralization pathways and phosphorus retention upon bioreduction. In *Adsorption of Metals by Geomedia*, vol. 7 (eds. Barnett M. and Kent D.). Elsevier, pp. 325-353.

Bossard, P., Gammeter, S., Lehmann, C., Schanz, F., Bachofen, R., Burgi, H.R., Steiner, D. and Zimmermann, U. (2001) Limnological description of the Lakes Zurich, Lucerne, and Cadagno. *Aquat. Sci.* **63**, 225-249.

Boudreau B. P. (1997) *Diagenetic Models and Their Implementation*. Springer.

Boudreau B. P. and Westrich J. T. (1984) The dependence of bacterial sulfate reduction on sulfate concentration in marine sediments. *Geochim. Cosmochim. Acta* **48**, 2503-2516.

Boudreau B. P. and Meysman F. J. R. (2006) Predicted tortuosity of muds. *Geology* **34**, 693-696.

Boyle E. A. (1990) Quaternary deepwater paleoceanography. *Science* **249**, 863-870.

Broecker W. S. (1982) Ocean chemistry during glacial time. *Geochim. Cosmochim. Acta* **46**, 1689-1705.

Burdige D. J. (2006) *Geochemistry of Marine Sediments*. Princeton University Press.

Busigny V., Planavsky N. J., Jézéquel D., Crowe S., Louvat P., Moureau J., Viollier E. and Lyons T. W. (2014) Iron isotopes in an Archean ocean analogue. *Geochim. Cosmochim. Acta* **133**, 443-462.

Butler I. B., SchoonenM. A. A. and Rickard D. T. (1994) Removal of dissolved oxygen from water: a comparison of four common techniques. *Talanta* **41**, 211-215.

Camacho A., Erez J., Chicote A., Florin M., Squires M. M., Lehmann C. and Bachofen R. (2001) Microbial microstratification, inorganic carbon photoassimilation and dark carbon fixation at the chemocline of the meromictic Lake Cadagno (Switzerland) and its relevance to the food web. *Aquat. Sci.* **63**, 91-106.

Canfield D. E. (1989) Reactive iron in marine sediments. *Geochim. Cosmochim. Acta* **53**, 619– 632.

Canfield D. E. (1998) A new model for Proterozoic ocean chemistry. *Nature* **396**, 450-453.

Canfield D. E. (2005) The early history of atmospheric oxygen: Homage to Robert M. Garrels. *Annu. Rev. of Earth Planet. Sci.* **33**, 1-36.

Canfield D. E., Jørgensen B. B., Fossing h., Glud R., Gundersen J., Ramsing N. B., Thamdrup B., Hansen J. W., Nielsen L. P., and Hall P. O. J. (1993a) Pathways of organic carbon oxidation in three coastal sediments. *Mar. Geol*. **113**, 27-40.

Canfield D. E., Thamdrup, B. and Hansen J. W. (1993b) The anaerobic degradation of organic matter in Danish coastal sediments: Fe reduction, Mn reduction and sulfate reduction. *Geochim. Cosmochim. Acta* **57**, 3867-3883.

Canfield D. E., Raiswell R., Westrich J. T., Reaves C. M. and Berner R. A. (1986) The use of chromium reduction in the analysis of reduced inorganic sulfur in sediments and shales. *Chem. Geol.* **54**, 149-155.

Canfield D. E., Raiswell R. and Bottrell S. (1992) The reactivity of sedimentary iron minerals towards sulfide. *Amer. J. Sci.* **292**, 659-683.

Canfield D. E., Rösing M. T. and Bjerrum C. (2006) Early anaerobic metabolisms. *Phil. Trans. Roy. Soc. B* **361**, 1819-1836.

Canfield, D. E., Poulton S. W. and Narbonne G. M. (2007) Late-Neoproterozoic deep-ocean oxygenation and the rise of animal life. *Science*, **315**, 92-95.

Canfield D. E., Poulton S. W., Knoll A. H., Narbonne G. M., Ross G., Goldberg T. and Strauss H. (2008) Ferruginous conditions dominated Later Neoproterozoic deep-water chemistry. *Science* **321**, 949-952.

Canfield D. E. and Thamdrup B. (2009) Towards a consistent classification scheme for geochemical environments, or, why we wish the term 'suboxic' would go away. *Geobiology* **7**, 385-392.

Canfield D. E., Farquhar J. and Zerkle A. L. (2010) High isotope fractionations during sulfate reduction in a low-sulfate euxinic ocean analog. *Geology* **38**, 415-418.

Caraco, N. F., Cole, J. J. and Likens, G. E. (1989) Evidence for sulfatecontrolled phosphorus release from sediments of aquatic systems. Nature **341**, 316-318.

Christian G. D. (2014) *Analytical chemistry* (eds. Christian G. D. et al.). Hoboken, NJ: John Wiley and Sons, Inc.

Cline J. D. (1969) Spectrophotometric determination of hydrogen sulfide in natural waters. *Limnol. Oceanogr.* **14,** 454-458.

Cembella A. D., Antia N. J. and Harrison P. J. (1984a) The utilization of inorganic and organic phosphorus compounds as nutrients by eukaryotic microalgae: a multidisciplinary perspective. Part 1. *CRC Crit. Rev. Microbiol.* **10**, 317-391.

Cembella A. D., Antia N. J. and Harrison P. J. (1984b) The utilization of inorganic and organic phosphorus compounds as nutrients by eukaryotic microalgae: a multidisciplinary perspective. Part 2. *CRC Crit. Rev. Microbiol.* **11**, 13-81.

Córdoba R. and Vargas J. A. (1996). Temperature, salinity, oxygen, and nutrient profiles at a 200 m deep station in Golfo Dulce, Pacific coast of Costa Rica. *Rev. Biol. Trop*. **44**, 233-236.

Codispoti L. A., Friederich G. E., Murray J. W. and Sakamoto C. M. (1991) Chemical variability in the Black Sea: implications of continuous vertical profiles that penetrated the oxic/anoxic interface. *Deep-Sea Res.* **38**, 691-710.

Colman A. S., Holland H. D. and Mackenzie F. T. (1997) Redox stabilization of the atmosphere and oceans by phosphorus limited marine productivity: discussion and reply. *Science* **276**, 406-408.

Cornell, R. M., Giovanoli, R. and Schindler, P. W. (1987) Effect of silicate species on the transformation of ferrihydrite into goethite and hematite in alkaline media. *Clays Clay Miner.* **35**, 21-28.

Cosgrove D. J. (1977) Microbial transformations in the phosphorus cycle. *Adv. Microb. Ecol.* **1**, 95-135.

Cosmidis J., Benzerara K., Morin G., Busigny V., Lebeau O., Jézéquel D., Noël V., Dublet G. and Othmane G. (2014) Biomineralization of mixed valence iron-phosphates in the anoxic water column of Lake Pavin (Massif Central, France). *Geochim. Cosmochim. Acta* **126**, 78–96.

Crowe S. A., O'Neill A. H., Katsev S., Hehanussa P., Haffner G. D., Sundby B., Mucci A. and Fowle D. A. (2008) The biogeochemistry of tropical lakes: a case study from Lake Matano, Indonesia. *Limnol. Oceanogr*. **53**, 319-331.

Crowe S. A., Døssing L. N., Beukes N. J., Bau M., Kruger S. J., Frei R. and Canfield D. E. (2013) Atmospheric oxygenation three billion years ago. *Nature* **501**, 535-538.

Crowe S. A., Paris G., Katsev S., Jones C., Kim S., Zerkle A. L., Nomosatryo S., Fowle D. A., Adkins J. F., Sessions A. L., Farquhar J. and Canfield D. E. (2014) Sulfate was a trace constituent of Archean. *Science* **346**, 735-739.

Dahl T. W., Anbar A. D., Gordon G. W., Rosing M. T., Frei R. and Canfield D. E. (2010) The behavior of molybdenum and its isotopes across the chemocline and in the sediments of sulfidic Lake Cadagno, Switzerland. *Geochim. Cosmochim. Acta* **74**, 144-163.

Dalsgaard T., Canfield D. E., Petersen J., Thamdrup B., and Acuna-González J. (2003) N2 production by the anammox reaction in the anoxic water column of Golfo Dulce, Costa Rica. *Nature* **422**, 606-608.

Daines S. J., Mills B. J. W. and Lenton T. M. (2016) Atmospheric oxygen regulation at low Proterozoic levels by incomplete oxidative weathering of sedimentary organic carbon. *Nat. Commun.* **8**, 1-11.

Davelaar, D. (1993) Ecological significance of bacterial polyphosphate metabolism in sediments. *Hydrobiol.* **253**:179-192.

Delaney M. L. (1998) Phosphorus accumulation in marine sediments and the oceanic phosphorus cycle. *Global Biogeochem. Cycles* **12**, 563-672.

Del Don C., Hanselmann K. W., Peduzzi R. and Bachofen R. (1998) Orographical and geochemical description of the meromictic Alpine Lake Cadagno. *Documenta Ist. Ital. Idrobiol.* **63**, 5-9.

Del Don C., Hanselmann K. W., Peduzzi R. and Bachofen R. (2001) The meromictic alpine Lake Cadagno: orographical and biogeochemical description. *Aquat. Sci.* **63**, 70-90.

Dellwig O., Leipe T., März C., Glockzin M., Pollehne F., Schnetger B., Yakushev E. V., Boettcher M. E. and Brumsack H. (2010) A new particulate Mn-Fe-P-shuttle at the redoxcline of anoxic basins. Geochim. Cosmochim. Acta **74**, 7100-7115.

Derry L.A. (2015) Causes and consequences of mid-Proterozoic anoxia. *Geophys. Res. Lett.* **42**, 8538-8546.

Deutsch C., Gruber N., Key R. M., Sarmiento J. L. and Ganachaud A. (2001) Denitrification and N2 fixation in the Pacific Ocean. *Glob. Biogeochem. Cycles* **15**, 483-506.

Dijkstra N., Kraal P., Kuypers M. M. M., Schnetger B. and Slomp C. P. (2014) Are iron-phosphate minerals a sink for phosphorus in anoxic Black Sea sediments? *PLoS ONE* **9**, e101139.

Dijkstra N., Slomp C. P., Behrends T. and Expedition 347 Scientists (2016) Vivianite is a key sink for phosphorus in sediments of the Landsort Deep, an intermittently anoxic deep basin in the Baltic Sea. *Chem. Geol.* **438**, 58-72.

Dijkstra N., Kraal P., Séguret M. J. M., Flores M. R., Gonzalez S., Rijkenberg M.J.A., Slomp, C. P. (2018) Phosphorus dynamics in and below the redoxcline in the Black Seaand implications for phosphorus burial. *Geochim. Cosmochim. Acta* **222**, 685-703.

Dos Santos Afonso M. and Stumm W. (1992) Reductive dissolution of iron (III) (hydr)oxides by hydrogen sulfide. *Langmuir* **8**, 1671-1675.

Dutta R. K. and Puri M. (1989) Anion exchange in lithium aluminate hydroxides. *Journal of Physical Chemistry* **96**, 376-381.

Egger M., Jilbert T., Behrends T., Rivard C. and Slomp C. P. (2015) Vivianite is a major sink for phosphorus in methanogenic coastal surface sediments. *Geochim. Cosmochim. Acta* **169**, 217-235.

Farquhar J., Bao H., and Thiemens M. H. (2000) Atmospheric influence of Earth's earliest sulfur cycle. *Science* **289**, 756–759.

Fennel K., Follows M. and Falkowski P. G. (2005) The coevolution of the nitrogen, carbon and oxygen cycles in the Proterozoic ocean. *Am. J. Sci.* **305**, 526-545.

Ferdelman T. G., Thamdrup B., Canfield D. E., Glud R. N., Kuever J., Lillebaek R., Ramsing N. B. and Wawer C. (2006) Biogeochemical controls on the oxygen, nitrogen and sulfur distributions in the water column of Golfo Dulce. An anoxic basin on the Pacific coast of Costa Rica revisited. *Rev. Biol. Trop*. **54**, 171-191.

Filippelli G. M. (1997a) Controls on phosphorus concentration and accumulation in marine sediments. *Mar. Geol.* **139**, 231-240.

Filippelli G. M. (1997b) Intensification of the Asian monsoon and a chemical weathering event in the late Miocene-early Pliocene: implications for late Neogene climate change. *Geology* **25**, 27-30.

Fogg G. E. (1973) Phosphorus in primary aquatic plants. *Water Res.* **7**, 77-91.

Fossing H. and Jørgensen B. B. (1989) Measurement of bacterial sulfate reduction in sediments: Evaluation of a single-step chromium reduction method. *Biogeochemistry* **8**, 205-222.

Fredrickson J. K., Zachara J. M., Kennedy D. W., Dong H., Onstott T. C., Hinman N. W. and Li S.-M. (1998) Biogenic iron mineralization accompanying the dissimilatory reduction of hydrous ferric oxide by a groundwater bacterium. *Geochim. Cosmochim. Acta* **62**, 3239-3257.

Froelich P.N., Klinkhammer G.P., Bender M.L., Luedtke N.A., Heath G.R., Cullen D., Dauphin P., Hammond D., Hartman B. and Maynard V. (1979) Early oxidation of organic matter in pelagic sedimentsof the eastern equatorial Atlantic: suboxic diagenesis. *Geochim. Cosmochim. Acta* **43**, 1075-1090.

Froelich P. N., Arthur M. A., Burnett W. C., Deakin M., Hensley V., Jahnke R., Kaul L., Kim K.-H., Roe K., Soutar A. and Vathakanon C. (1988) Early diagenesis of organic

matter in Peru continental margin sediments: phosphorite precipitation. *Mar. Geol.* **80**, 309-343.

Gálvez N., Barrón V. and Torrent J. (1999) Effect of phosphate on the crystallization of hematite, goethite, and lepidocrocite from ferrihydrite. *Clays Clay Miner* **47**, 304-311.

Ganeshram R. S., Pedersen T. F., Calvert S. E. and Francois R. (2002) Reduced nitrogen fixation in the glacial ocean inferred from changes in marine nitrogen and phosphorus inventories. *Nature* **415**, 156-159.

Gill B. C., Lyons T. W., Young S. A., Kump L. R., Knoll A. H. and Saltzman M. R. (2011) Geochemical evidence for widespread euxinia in the Later Cambrian ocean. *Nature* **469**, 80-83.

Godfrey L. V., Poulton S. W., Bebout G. E. and Fralick P. W. (2013) Stability of the nitrogen cycle during development of sulfidic water in the redox-stratified late Paleoproterozoic ocean. *Geology* **41**, 655-658.

Goldberg T., Archer C., Vance D., Thamdrup B., McAnena A. and Poulton S. W. (2012) Controls on Mo isotope fractionations in a Mn-rich anoxic marine sediment, Gullmar Fjord, Sweden. *Chem. Geol.* **296-297**, 73-82.

Guidry M. W. and Mackenzie F. T. (2000) Apatite weathering and the Phanerozoic phosphorus cycle. *Geology* **28**, 631-634.

Guilbaud R., White M. and Poulton S. W. (2013) Surface charge and growth of sulphate and carbonate green rust in aqueous media. *Geochim. Cosmochim. Acta* **108**, 141-153.

Guilbaud R., Poulton S. W., Butterfield N. J., Zhu M. and Shields-Zhou G. A. (2015) A global transition to ferruginous conditions in the early Neoproterozoic oceans. *Nat. Geosci.* **8**, 466-470.

Gregersen L. H., Habicht K. S., Peduzzi S., Tonolla M., Canfield D. E., Miller M., Cox R. P. and Frigaard N.-U. (2009) Dominance of a clonal green sulfur bacterial population in a stratified lake. *FEMS Microbiol. Ecol.* **70**, 30-41.

Habicht K. S., Gade M., Thamdrup B., Berg P. and Canfield D. E. (2002) Calibration of Sulfate Levels in the Archean Ocean. *Science* **298**, 2372-2374.

Halevy I., Alesker M., Schuster E. M., Popovitz-Biro R. and Feldman Y. (2017) A key role for green rust in the Precambrian oceans and the genesis of iron formations. *Nature Geosci.* **10**, 135-139.

Hall P. O. J. and Aller R. C. (1992) Rapid, small-volume flow injection analysis for CO_2 and NH_4^+ in marine and freshwaters. *Limnol.Oceanogr.* **37**, 1113-1119.

Halm H., Musat N., Lam P., Langlois R., Musat F., Peduzzi S., Lavik G., Schubert C. J., Sinha B., LaRoche J. and Kuypers M. M. (2009) Co-occurrence of denitrification and nitrogen fixation in a meromictic lake, Lake Cadagno (Switzerland), *Environ. Microbiol.* **11**, 1945-1958.

Hammarlund E. U., Dahl T. W., Harper D. A. T., Bond D. P. G., Nielsen A. T., Bjerrum C. J., Schovsbo N. H., Schönlaub H., Zalasiewicz J. A. and Canfield D. E. (2012) A sulfidic driver for the end-Ordovician mass extinction. *Earth Planet. Sci. Lett.* **331-332**, 128-139.

Hansen H. C. B. (1989) Composition, stabilization, and light adsorption of Fe(II)Fe(III) hydroxycarbonate (green rust). *Clay Minerals* **24**, 663-669.

Hansen H. C. B. and Poulsen I. F. (1999) Interaction of synthetic sulphate "green rust" with phosphate and the crystallization of vivianite. *Clays Clay Miner.* **47**, 312–318.

Hecky R. E. and Kilham P. (1988) Nutrient limitation of phytoplankton in freshwater and marine environments: a review of recent evidence on the effects of enrichment. *Limnol. Oceanogr.* **33**, 796-822.

Howarth R. (1988) Nutrient limitation of net primary production in marine ecosystems. *Ann. Rev. Ecol.* **19**, 89-110.

Holland H. D. (1984) *The Chemical Evolution of the Atmosphere and Oceans*. Princeton University Press.

Holland H. D. (2006) The oxygenation of the atmosphere and oceans. *Phil. Trans. Roy. Soc. B* **361**, 903-915.

Howarth R. (1988) Nutrient limitation of net primary production in marine ecosystems. *Ann. Rev. Ecol.* **19**, 89-110.

Howarth R. W., Jensen H. S., Marino R. and Postma H. (1995) Transport to and processing of P in near-shore and oceanic waters. In *Phosphorus in the Global Environment. SCOPE 54, chap. 19* (ed. H. Tiessen). Wiley, Chichester, pp. 323–345,

Hsu T., Jiang W. and Wang Y. (2014) Authigenesis of vivianite as influenced by methane-induced sulfidization in cold- seep sediments off southwestern Taiwan. *J. Asian Earth Sci.* **89**, 88-97.

Ingall E. D. and Jahnke R. (1994) Evidence for enhanced phosphorus regeneration from marine sediments overlain by oxygen depleted waters. *Geochim. Cosmochim. Acta* **58**, 2571-2575.

Ingall E. D. and Jahnke R. (1997) Influence of water-column anoxia on the elemental fractionation of carbon and phosphorus during sediment diagenesis. *Mar. Geol.* **139**, 219-229.

Ingall E. D., Bustin R. M. and van Cappellen P. (1993) Influence of water column anoxia on the burial and preservation of carbon and phosphorus in marine shales. *Geochim. Cosmochim. Acta* **57**, 303-316.

Ingall, E. D., Kolowith, L., Lyons, T. W. and Hurtgen, M. T. (2005) Sediment carbon, nitrogen and phosphorus cycling in an anoxic fjord, Effingham Inlet, British Columbia. *Am. J. Sci.* **305**, 240-258.

Iversen N. and Jørgensen B. B. (1985) Anaerobic methane oxidation rates at the sulfate-methane transition in marine sediments from Kattegat and Skaggerak (Denmark). *Limnol. Oceanogr.* **30**,944-955.

Jahnke R. A. (1992) The phosphorus cycle. In *Global Geochemical Cycles. chap. 14* (eds. S. S. Butcher, R. J. Charlson, G. H. Orians, and G. V. Wolff). Academic, San Diego, pp. 301-315.

Jarvis I., Burnett W. C., Nathan Y., Almbaydin F. S. M., Attia A. K. M., Castro L. N., Flicoteaux R., Ezzeldim Hilmy M., Husain V., Qutawnah A. A., Serjani A. and Zanin Y. N. (1994) Phosphorite geochemistry: State-of-the-art and environmental concerns. *Eclogae geologicae Helvetiae.* **87**, 643-700.

Jenkyns H. C. (2010) Geochemistry of oceanic anoxic events. *Geochem. Geophys. Geosyst.* **11**, doi: 10.1029/2009GC002788.

Jilbert T. and Slomp C. P. (2013) Iron and manganese shuttles control the formation of authigenic phosphorus minerals in the euxinic basins of the Baltic Sea. *Geochim. Cosmochim. Acta* **107**, 155-169.

Jilbert T., Slomp C. P., Gustafsson B. G. and Boer W. (2011) Beyond the Fe-P-redox connection: preferential regeneration of phosphorus from organic matter as a key control on Baltic Sea nutrient cycles. *Biogeosciences* **8**, 1699-1720.

Johnston D. T., Wolfe-Simon F., Pearson A. and Knoll A. H. (2009) Proterozoic Ocean Chemistry and Evolution: A Bioinorganic Bridge? *Proc. Natl. Acad. Sci. U.S.A.* **106**, 16925-16929.

Johnston D. T., Poulton S. W., Dehler C., Porter S., Husson J., Canfield D. E. and Knoll A. H. (2010) An emerging picture of Neoproterozoic ocean chemistry: Insights from the Chuar Group, Grand Canyon, USA. *Earth Planet. Sci. Lett.* **290**, 64-73.

Jones C., Nomosatryo S., Crowe S. A., Bjerrum C. J. and Canfield D. E. (2015) Iron oxides, divalent cations, silica, and the early earth phosphorus crisis. *Geology* **43**, 135-138.

Joshi, S. R., Kukkadapu, R. K., Burdige, D., Bowden, M., Sparks, D. L. and Jaisi, D. P. (2015) Organic matter remineralization predominates phosphorus cycling in the mid-Bay sediment in the Chesapeake Bay. *Environ. Sci. Technol.* **49**, 5887-5896.

Kah L. C., Lyons T. W. and Frank T. D. (2004) Low marine sulphate and protracted oxygenation of the Proterozoic biosphere. *Nature* **431**, 834-838.

Kappler A. and Newman D. K. (2004) Formation of Fe(III)-minerals by Fe(II)-oxidizing photoautotrophic bacteria. *Geochimica et Cosmochimica Acta* **68**, 1217–1226.

Kappler A., Pasquero C., Konhauser K. O. and Newman D. K. (2005) Deposition of banded iron formations by anoxygenic phototrophic Fe(II)-oxidizing bacteria. *Geology* **33**(11), 865-868.

Karlin R., Lyle M. and Heath C. R. (1987) Authigenic magnetite formation in suboxic marine sediments. *Nature* **326**, 490-493.

Katsev S., Verburg P., Llirós M., and Minor E. (2017). Chemical setting and tropical meromictic lakes: specifics of meromixis and case studies of Lakes Tanganyika, Malawi, and Matano, in *Ecology of Meromictic Lakes*, eds E. S. Zadereev, R. D. Gulati, and A. G. Degermendzhy (Amsterdam: Elsevier).

Kendall B., Reinhard C. T., Lyons T. W., Kaufman A. J., Poulton S. W. and Anbar A. D. (2010) Pervasive oxygenation along late Archaean ocean margins. *Nat. Geosci.* **3**, 647-652.

Kipp M. A. and Stüeken E. E. (2017) Biomass recycling and Earth's early phosphorus cycle. *Sci. Adv.* **3**, 1-6.

Knoll-Heitz F. (1991) Piora-Konzept für die Erhaltung einer Landschaft (Piora-a concept for the preservation of a landscape). WWF Sezione Svizzera Italiana, St Gallen, Switzerland.

Koehler M. C., Stüeken E. E., Kipp M. A., Buick R. and Knoll A. H. (2017) Spatial and temporal trends in Precambrian nitrogen cycling: a Mesoproterozoic offshore nitrate minimum. *Geochim. Cosmochim. Acta* **198**, 315-337.

Konhauser K. O., Lalonde S. V., Amskold L. and Holland H. D. (2007) Was there really an Archean phosphate crisis? *Science* **315**, 1234.

Koroleff F. (1976) Determination of phosphorus. In *Methods of seawater analysis, 2nd ed*. (eds. K. Grasshoff et al.). Verlag Chemie, Weinheim, pp. 117-156.

Kraal P., Slomp C. P., Reed D. C., Reichart G. J. and Poulton S. W. (2012) Sedimentary phosphorus and iron cycling in and below the oxygen minimum zone of the Northern Arabian Sea. *Biogeosci. Discuss*. **9**, 3829-3880.

Kraal P., Dijkstra N., Behrends T. and Slomp C. P. (2017) Phosphorus burial in sediments of the sulfidic deep Black Sea: Key roles for adsorption by calcium carbonate and apatite authigenesis. *Geochim. Cosmochim. Acta* **204**, 140-158.

Krige L. J. (1917) Petrographische Untersuchungen im Val Piora und Umgebung. *Eclogae Geol. Helv*. **14**, 519-654.

Krom M. D. and Berner R. A. (1980) Adsorption of phosphate in anoxic marine sediments. *Limnol. Oceanogr.* **25**, 797-806.

Krom M. D. and Berner R. A. (1981) The diagenesis of phosphorus in a nearshore marine sediment. *Geochim. Cosmochim. Acta* **45**, 207-216.

Kukkadapu R. K., Zachara J. M., Fredrickson J. K. and Kennedy D. W. (2004) Biotransformation of two-line silica-ferrihydrite by a dissimilatory Fe(III)-reducing bacterium: formation of carbonate green rust in the presence of phosphate. *Geochim. Cosmochim. Acta* **68**, 2799-2814.

Kump L. (1988) Terrestrial feedback in atmospheric oxygen regulation by fire and phosphorus. *Nature* **335**, 152-154.

Kump, L. R. (2008) The rise of atmospheric oxygen. *Nature*, **451**, 277-278.

Lajtha K. and Harrison A. F. (1995) Strategies of phosphorus acquisition and conservation by plant species and communities. In *Phosphorus in the Global Environment. SCOPE 54, chap. 8* (ed. H. Tiessen). Wiley, New York, pp. 139-147.

Laliberté M. (2009) A model for calculating the heat capacity of aqueous solutions, with updated density and viscosity data. *J. Chem. Eng. Data.* **54**, 1725-1760.

Lam P., Jensen M. M., Lavik G., McGinnis D. F., Muller B., Schubert C. J., Amann R.,

Lebo M. (1991) Particle-bound phosphorus along an urbanized coastal plain estuary. *Mar. Chem*. **34**, 225-246.

Lenton T. M., Boyle R. A., Poulton S. W., Shields-Zhou G. A. and Butterfield N. J. (2014) Co-evolution of eukaryotes and ocean oxygenation in the Neoproterozoic Era. *Nat. Geosci*. **7**, 257-265.

Lerman A., Mackenzie F. T. and Garrels R. M. (1975) Modeling of geochemical cycles: phosphorus as an example. Geol. Soc. *Am. Memoirs*. **142**, 205-217.

Lewis, B.L. and Landing, W. M. (1992) The investigation of dissolved and suspended-particulate trace metal fractionation in the Black Sea. *Deep Sea Res.* **38** (Suppl.), S773-S803.

Li C., Love G. D., Lyons T. W., Fike D. A., Sessions A. L. and Chu X. (2010) A Stratified Redox Model for the Ediacaran Ocean. *Science* **328**, 80-83.

Li C., Love G. D., Lyons T. W., Scott C. T., Feng L., Huang J., Chang H., Zhang Q. and Chu X. (2012) Evidence for a redox stratified Cryogenian marine basin, Datangpo Formation, South China. *Earth Planet. Sci. Lett.* **331-332**, 246-256.

Likens G. E., Bormann F. H., Pierce R. S., Eaton J. S. and Johnson N. M. (1977) *Biogeochemistry of a Forested Ecosystem*. Springer, New York.

Lipschultz F., Wofsy S. C., Ward B. B., Codispoti L. A., Friederich G. and Elkins J. W. (1990) Bacterial transformations of inorganic nitrogen in the oxygen-deficient waters of the eastern tropical South Pacific Ocean. *Deep-Sea Res*. **37**, 1513-1541.

Lucotte M. and D'Anglejan B. (1983) Forms of phosphorus and phosphorus–iron relationships in the suspended matter of the St. Lawrence Estuary. *Can. J. Earth Sci.* **20**, 1880-1890.

Luther G. W., Brendel P. J., Lewis B. L., Sundby B., Lefrancois L., Silverberg N. and Nuzzio D. B. (1998) Simultaneous measurement of O2, Mn, Fe, I, and S2 in marine

pore waters with a solid-state voltammetric microelectrode. *Limnol. Oceanogr*. **43**, 325-333.

Lyons T. W. and Severmann S. (2006) A critical look at iron paleoredox proxies: new insights from modern euxinic marine basins. *Geochim. Cosmochim. Acta* **70**, 5698-5722.

Lyons T. W., Reinhard C. T. and Planavsky N. J. (2014) The rise of oxygen in Earth's early ocean and atmosphere. *Nature* **506**, 307-315.

März C., Hoffmann J., Bleil U., de Lange G. J. and Kasten S. (2008a) Diagenetic changes of magnetic and geochemical signals by anaerobic methane oxidation in sediments of the Zambezi deep-sea fan (SW Indian Ocean). *Mar. Geol.* **255**, 118-130.

März C., Poulton S. W., Beckmann B., Küster K., Wagner T. and Kasten S. (2008b) Redox sensitivity of P cycling during marine black shale formation: Dynamics of sulfidic and anoxic, non-sulfidic bottom waters. *Geochim. Cosmochim. Acta* **72**, 3703-3717.

Mackenzie F. T., Ver L. M., Sabine C., Lane M. and Lerman A. (1993) C, N, P, S Global biogeochemical cycles and modeling of global change. In *Interactions of C, N, P and S Biogeochemical Cycles and Global Change. NATO ASI Series 1, vol. 4* (eds. R. Wollast, F. T. Mackenzie, and L. Chou). Springer, Berlin, pp. 1-61.

Madsen H. E. L. and Hansen H. C. B. (2014) Kinetics of crystal growth of vivianite, $Fe_3(PO_4)_2{\cdot}8H_2O$, from solution at 25, 35 and 45℃. *J. Cryst. Growth* **401**, 82-86.

Manning P. G., Murphy T. P. and Prepas E. E. (1994) Forms of iron and the bioavailability of phosphorus in eutrophic Amisk Lake, Alberta. *Can. Mineral.* **32**, 459-468.

McConnell, D. (1973). *Apatite, its crystal chemistry, mineralogy, utilization, and geologic and biologic occurrences.* New York: Springer.

Melack J. M. (1995) Transport and transformations of P in fluvial and lacustrine ecosystems. In *Phosphorus in the Global Environment. SCOPE, chap. 15* (ed. H. Tiessen). Wiley, pp. 245-254.

Meybeck M. (1982) Carbon, nitrogen, and phosphorus transport by world rivers. *Am. J. Sci.* **282**, 401-450.

Meyers P. A. and Ishiwatari R. (1993) Lacustrine organic geochemistry-an overview of indicators of organic matter sources and diagenesis in lake sediments. *Org. Geochem.* **20**(7), 867-900.

Michiels C. C., Darchambeau F., Roland F. A. E., Morana C., Llirós M., García-Armisen T., Thamdrup B., Borges A. V., Canfield D. E., Servais P., Descy J. and Crowe S. A. (2017) Iron-dependent nitrogen cycling in a ferruginous lake and the nutrient status of Proterozic oceans. *Nat. Geosci.* **10**, 217-221.

Mori H. and Ito T. (1950) The structure of vivianite and symplesite. *Acta Crystallographica*. **3**, 1-6.

Mort H. P., Adatte T., Föllmi K., Keller G., Steinmann P., Matera V., Berner Z. and Stüben D. (2007) Phosphorus and the roles of productivity and nutrient recycling during oceanic anoxic event 2. *Geology* **35**, 483-486.

Mort H. P., Slomp C. P., Gustafsson B. G. and Andersen T. J. (2010) Phosphorus recycling and burial in Baltic Sea sediments with contrasting redox conditions. *Geochim. Cosmochim. Acta* **74**, 1350-1362.

Mortimer C. H. (1941) The exchange of dissolved substances between mud and water in lakes: I and II. *J. Ecol*. **29**, 280-329.

Murray J. W., Jannasch H. W., Honjo S., Anderson R. F., Reeburgh W. S., Top Z., Friederich G. E., Codispoti L. A. and Izdar E. (1989) Unex-pected changes in the oxic／anoxic interface in the Black Sea. *Nature* **338**, 411-413.

Murray J. W., Codispoti L. A., and Friederich G. E. (1995) Oxidation-reduction environments: The suboxic zone of the Black Sea. In *Aquatic Chemistry: lnterfacial and Interspecies Processes vol. 244.* (eds. C. P. Huang et al.). American, Chemical Society, pp. 157-176.

Newton R. J., Reeves E. P., Kafousia N., Wignall P. B., Bottrell S. and Sha J. (2011) Low marine sulfate concentrations and the isolation of the European epicontinental sea during the Early Jurassic. *Geology* **39**, 7-10.

Nichols-Driscoll, J. (1976) Benthic invertebrate communities in Golfo Dulce, Costa Rica, an anoxic basin. *Rev. Biol. Trop*. **24**, 281-297.

Nriagu J. O. (1984). Phosphate Minerals: Their properties and General Modes of Occurrence. In *Phosphate minerals* (eds. Nriagu, J. O. and Moore P. B.). Springer, Berlin, pp. 126

O'Connell D. W., Jensen M. M., Jakobsen R., Thamdrup B., Andersen T. J., Kovacs A. and Hansen H. C. B. (2015) Vivianite formation and its role in phosphorus retention in Lake Ørn, Denmark. *Chem. Geol.* **409**, 42-53.

Och L. M. and Shields-Zhou G. A. (2012) The Neoproterozoic oxygenation event: environmental perturbations and biogeochemical cycling. *Earth-Sci. Rev.* **110**, 26-57.

Och L. M., Cremonese L., Shields-Zhou G. A., Poulton S. W., Struck U., Ling H., Li D., Chen X., Manning C., Thirlwall M., Strauss H. and Zhu M. (2016) Palaeoceanographic controls on spatial redox distribution over the Yangtze Platform during the Ediacaran–Cambrian transition. *Sedimentology* **63**, 378-410.

Ona-Nguema G., Carteret C., Benali O., Abdelmoula M., Genin J. M. and Jorand F. (2004) Competitive formation of hydroxycarbonate green rust 1 versus hydroxysulphate green rust 2 in Shewanella putrefaciens cultures. *Geomicrobiol. J.* **21**, 79-90.

Pavlov, A. A. and Kasting, J. F. (2002) Mass-independent fractionation of sulfur isotopes in Archean sediments: strong evidence for an anoxic Archean atmosphere. *Astrobiology* **2**, 27-41.

Peiffer S., Dos Santos Afonso M., Wehrli B. and Gaechter R. (1992) Kinetics and mechanism of the reaction of H_2S with lepidocrocite. *Environ. Sci. Technol.* **26**, 2408-2413.

Petsch S. T. and Berner R. A. (1998) Coupling the geochemical cycles of C, P, Fe and S: the effect on atmospheric O2 and the isotopic records of carbon and sulfur. *Am J. Sci.* **298**, 246-262.

Planavsky N. J., Rouxel O. J., Bekker A., Lalonde S. V., Konhauser K. O., Reinhard C. T. and Lyons T. W. (2010) The evolution of the marine phosphate reservoir. *Nature* **467**, 1088-1090.

Planavsky, N. J., McGoldrick, P., Scott, C. T., Li, C., Reinhard, C. T., Kelly, A. E., Chu, X., Bekker, A., Love, G. D., and Lyons, T. W. (2011) Widespread iron-rich conditions in the mid-Proterozoic ocean. *Nature* **477**, 448-451.

Planavsky N. J., Reinhard C. T., Wang X., Thomson D., McGoldrick P., Rainbird R. H., Johnson T., Fischer W. W. and Lyons T. W. (2014) Low Mid-Proterozoic atmospheric oxygen levels and the delayed rise of animals. *Science* **346**, 635-638.

Poulton S. W. (2003) Sulfide oxidation and iron dissolution kinetics during the reaction of dissolved sulfide with ferrihydrite. *Chem. Geol.* **202**, 79-94.

Poulton S. W. (2017) Early phosphorus redigested. *Nat. Geosci.* **10**, 75-76.

Poulton S. W. and Canfield D. E. (2005) Development of a sequential extraction procedure for iron: implications for iron partitioning in continentally derived particulates. *Chem. Geol.* **214**, 209-221.

Poulton S. W. and Raiswell R. (2002) The low-temperature geochemical cycle of iron: From continental fluxes to marine sediment deposition. *Am. J. Sci.* **302**, 774-805.

Poulton S. W. and Canfield D. E. (2011) Ferruginous conditions: A dominant feature of the ocean through Earth's history. *Elements* **7**, 107-112.

Poulton S. W., Krom M. D., van Rijn J., Raiswell R., and Bows R. (2003) Detection and removal of dissolved hydrogen sulphide in flow-through systems via the sulphidation of hydrous iron (III) oxides. *Environ. Technol.* **24**, 217-229.

Poulton S. W., Fralick P. W. and Canfield D. E. (2004a) The transition to a sulphidic ocean ~ 1.84 billion years ago. *Nature* **431**, 173-177.

Poulton S. W., Krom M. D. and Raiswell R. (2004b) A revised scheme for the reactivity of iron (oxyhydr)oxide minerals towards dissolved sulfide. *Geochim. Cosmochim. Acta* **68**, 3703-3715.

Poulton S. W., Fralick P. W. and Canfield D. E. (2010) Spatial variability in oceanic redox structure 1.8 billion years ago. *Nat. Geosci.* **3**, 486-490.

Poulton S. W., Henkel S., März C., Urquhart H., Flögel S., Kasten S., Sinninghe Damsté J. S. and Wagner T. (2015) A continental-weathering control on orbitally driven redox-nutrient cycling during Cretaceous Oceanic Anoxic Event 2. *Geology* **43**, 963-966.

Pyzik A. J. and Sommer S. E. (1981) Sedimentary iron monosulfides: Kinetics and mechanism of formation. *Geochim. Cosmochim. Acta* **45**, 687-698.

Randall S. R., Sherman D. M. and Ragnarsdottir K. V. (2001) Sorption of As(V) on green rust ($Fe_4(II)Fe_2(III)(OH)_{12}SO_4 \cdot 3H_2O$) and lepidocrocite (c-FeOOH): surface complexes from EXAFS spectroscopy. *Geochimica et Cosmochimica Acta* **65**, 1015-1023.

Raiswell R. and Canfield D. E. (1998) Sources of iron for pyrite formation in marine sediments. *Am. J. Sci.* **298**, 219-245.

Raiswell R. and Canfield D. E. (2012) The iron biogeochemical cycle past and present. *Geochem. Perspect.* **1**, 1-214.

Reed D. C., Slomp C. P. and Gustafsson B. G. (2011) Sedimentary phosphorus dynamics and the evolution of bottom-water hypoxia: a coupled benthic-pelagic model of a coastal system. *Limnol. Oceanogr*. **56**, 1075-1092.

Reed D. C., Gustafsson B. G. and Slomp C. P. (2016) Shelf-to-basin iron shuttling enhances vivianite formation in deep Baltic Sea sediments. *Earth Planet. Sci. Lett.* **434**, 241-251.

Redfield A. C., Ketchum B. H., and Richards F. A. (1963) The influence of organisms on the composition of sea water. In *The Sea (ed. M. N. Hill), vol. 2*. Interscience, New York, pp. 26-77.

Refait P., Drissi S. H., Pytkiewicz J. and Génin J.-M. R. (1997) The anionic species competition in iron aqueous corrosion: role of various green rust compounds. *Corrosion Science* **39**, 1699-1710.

Refait P., Abdelmoula M. and GÉnin J.-M. R. (1998) Mechanisms of formation and structure of green rust one in aqueous corrosion of iron in the presence of chloride ions. *Corrosion Science* **40**, 1547–1560.

Reinhard C. T., Raiswell R., Scott C., Anbar A. D. and Lyons T. W. (2009) A Late Archean sulfidic sea stimulated by early oxidative weathering of the continents. *Science* **326**, 713-716.

Reinhard C. T., Planavsky N. J., Gill B. C., Ozaki K., Robbins L. J., Lyons T. W., Fischer W. W., Wang C., Cole D. B. and Konhauser K. O. (2017) Evolution of the global phosphorus cycle. *Nature* **541**, 386-401.

Richey J. E. (1983) The phosphorus cycle. In *The Major Biogeochemical Cycles and Their Interactions. SCOPE 21* (eds. B. Bolin and R. B. Cook). Wiley, Chichester, pp. 51-56.

Rickard D. (2006) The solubility of FeS. *Geochim. Cosmochim. Acta* **70**, 5779-5789.
Rodrigo M. A., Vicente E. and Miracle M. R. (1993) Short-term calcite precipitation in the karstic meromictic Lake La Cruz. *Verh. Internat. Verein. Limnol.* **25**: 711-719.

Rodrigo M. A., Miracle M. R. and Vicente E. (2001) The meromictic Lake La Cruz (Central Spain). Patterns of stratification. *Aquat. sci.* **63**, 406-416.

Romero-Viana L., Julià R., Camacho A., Vicente E. and Miracle M. R. (2008) Climate signal in varve thickness; Lake La Cruz (Spain), a case study. J. *Paleolimnol*. **40**, 703-714.

Romero-Viana L., Keely B. J., Camacho A., Vicente E. and Miracle M. R. (2009). Primary production in Lake La Cruz (Spain) over the last four centuries: reconstruction based on sedimentary signal of photosynthetic pigments. *J. Paleolimnol*. **43**, 771-786.

Roscoe S. M. (1969) *Huronian rocks and uraniferous conglomerates.* Department of Energy, Mines and Resources, Ottwa.

Rothe M., Frederichs T., Eder M., Kleeberg A. and Hupfer M. (2014) Evidence for vivianite formation and its contribution to long-term phosphorus retention in a recent lake sediment: a novel analytical approach. *Biogeosciences* **11**, 5169-5180.

Ruby C., Géhin A., Abdelmoula M., Génin J.-M. R. and Jolivet J.-P. (2003) Coprecipitation of Fe(II) and Fe(III) cations in sulphated aqueous medium and formation of hydroxysulphate green rust. *Solid State Sciences* **5**, 1055-1062.

Ruttenberg, K. C. (1992) Development of a sequential extraction method for different form of phosphorus in marine sediments. *Limnol. Oceanogr.* **37**, 1460-1482.

Ruttenberg K. C. and Berner R. (1993) Authigenic apatite formation and burial in sediments from non-upwelling, continental margin environments. *Geochim. Cosmochim. Acta* **57**, 991-1007.

Ruttenberg, K. C. (2003) The Global Phosphorus Cycle. In: *Treatise on Geochemistry, vol. 8* (eds. K.K. Turekian and H.D. Holland). Elsevier, Amsterdam; London, pp. 585-643.

Sahoo S. K., Planavsky N. J., Kendall B., Wang X., Shi X., Scott C., Anbar A. D., Lyons T. W. and Jiang G. (2012) Ocean oxygenation in the wake of the Marinoan glaciation. *Nature* **489**, 546-549.

Sannigrahi, P. and Ingall, E. D. (2005). Polyphosphates as a source of enhanced P fluxes in marine sediments overlain by anoxic waters: evidence from ^{31}P NMR. *Geochem. Trans.* **6**, 52-59.

Santisteban, C. (1994) Control estructural del sistema cárstico de la zona de los lagos de Cañada del Hoyo (Cuenca). *Simposium sobre los ecosistemas acuáticos de Castilla-La Mancha*. Book of abstracts, pp: 45.

Schenau S. J., Slomp C. P. and de Lange G. J. (2000) Phosphogenesis and active phosphorite formation in sediments from the Arabian Sea oxygen minimum zone. *Mar. Geol.* **169**, 1-20.

Schindler D. W. (1970) Evolution of phosphorus limitation in lakes. *Science* **195**, 260-262.

Schippers A., Neretin L. N., Lavik G., Leipe T. and Pollehne F. (2005) Manganese (II) oxidation driven bilateral oxygen intrusions in the western Black Sea. *Geochim. Cosmochim. Acta* **69**, 2241-2252.

Schubert C. J., Vazquez F., Losekann-Behrens T., Knittel K., Tonolla M. and Boetius A. (2011) Evidence for anaerobic oxidation of methane in sediments of a freshwater system (Lago di Cadagno). *FEMS Microbiol. Ecol.* **76**, 26-38.

Schulz H. N. and Schulz H. D. (2005) Large sulfur bacteria and the formation of phosphorite. *Science* **307**, 416-418.

Schwertmann, U. and Taylor, R. M. (1972) Influence of silicate on transformation of lepidocrocite to goethite and hematite crystallization under alkaline conditions and in the presence of phosphate. *Am. Mineral*. **90**, 1852-1860.

Schwertmann U. and Fechter H. (1994) The formation of green rust and its transformation to lepidocrocite. *Clay Minerals* **29**, 87-92.

Scott C.T., Lyons T. W., Bekker A., Shen Y., Poulton S. W., Chu X. and Anbar A. D. (2008) Tracing the stepwise oxygenation of the Proterozoic ocean. *Nature* **452**, 456-459.

Scott C. T., Bekker A., Reinhard C. T., Schnetger B., Krapež B., Rumble III D. and Lyons T. W. (2011) Late Archean euxinic conditions before the rise of atmospheric oxygen. *Geology* **39**, 119-122.

Shen Y., Canfield D. E. and Knoll A. H. (2002) Middle Proterozoic ocean chemistry: evidence from the McArthur Basin, northern Australia. *Am. J. Sci.* **302**, 81-109.

Simon L., François M., Refait P., Renaudin G., Lelaurain M. and Génin J.-M. R. (2003) Structure of the Fe(II–III) layered double hydroxysulphate green rust two from Rietveld analysis. *Solid State Sciences* **5**, 327–334.

Slomp C. P. and van Raaphorst W. (1993) Phosphate adsorption in oxidized marine sediments. *Chem. Geol.* **107**, 477-480.

Slomp C. P., Epping E. H. G., Helder W. and van Raaphorst W. (1996a) A key role for iron-bound phosphorus in authigenic apatite formation in North Atlantic continental platform sediments. *J. Mar. Res.* **54**, 1179-1205.

Slomp C. P., Van der Gaast S. J. and van Raaphorst W. (1996b) Phosphorus binding by poorly crystalline iron oxides in North Sea sediments. *Mar. Chem.* **52**, 55-73.

Slomp C. P., Thompson J. and de Lange G. J. (2002) Enhanced regeneration of phosphorus during formation of the most recent eastern Mediterranean sapropel (S1). *Geochim. Cosmochim. Acta* **66**, 1171-1184.

Slomp C. P., Thomson J. and de Lange G. J. (2004) Controls on phosphorus regeneration and burial during formation of eastern Mediterranean sapropels. *Mar. Geol.* **203**, 141-159.

Slomp C. P., Mort H. P., Jilbert T., Reed D. C., Gustafsson B. G. and Wolthers M. (2013) Coupled dynamics of iron and phosphorus in sediments of an oligotrophic coastal basin and the impact of anaerobic oxidation of methane. *PLoS ONE* **8**, e62386.

Soetaert K., Petzoldt, T. and Meysman F. (2010) marelac: Tools for Aquatic Sciences. R Package Version 2.1. http://CRAN.Rproject.org/package=marelac.

Song H., Tong J., Algeo T. J., Song H., Qiu H., Zhu Y., Tian L., Bates S., Lyons T. W., Luo G. and Kump L. R. (2013) Early Triassic seawater sulfate drawdown. *Geochim. Cosmochim. Acta* **128**, 95-113.

Spear, N., Holland, H. D., Garcia-Veígas, J., Lowenstein, T. K., Giegengack, R. & Peters, H. 2013. Analyses of fluid inclusions in Neoproterozoic marine halite provide odlest measurement of seawater chemistry. *Geology*, **42**, 103-106.

Spear N., Holland H. D., Garcia-Veígas J., Lowenstein T. K., Giegengack R. and Peters, H. (2013) Analyses of fluid inclusions in Neoproterozoic marine halite provide odlest measurement of seawater chemistry. *Geology*, **42**, 103-106.

Sperling E. A., Wolock C. J., Morgan A. S., Gill B. C., Kunzmann M., Halverson G. P., Macdonald F. A., Knoll A. H. and Johnston D. T. (2015) Statistical analysis of iron geochemical data suggests limited late Proterozoic oxygenation. *Nature* **523**, 451-454.

Stookey L. L. (1970) Ferrozine-A new spectrophotometric reagent for iron. *Anal. Chem.* **42**, 779-781.

Stumm W. and Morgan J. J. (1981) *Aquufic Chemistry*, 2nd edn. J. Wiley & Sons, 780p.

Stüeken E. E. (2013) A test of the nitrogen-limitation hypothesis for retarded eukaryote radiation: nitrogen isotopes across a Mesoproterozoic basinal profile. *Geochim. Cosmochim. Acta* **120**, 121-139.

Tamburini F., Fo¨llmi K. B., Adatte T., Bernasconi S. M. and Steinmann P. (2003) Sedimentary phosphorus record from the Oman margin: new evidence of high productivity during glacial periods. *Paleoceanography* **18**, 1015 doi:10.1029/2000PA000616.

Tarapchak S. J. and Nawelajko C. (1986) Synopsis: phosphorus- plankton dynamics symposium. *Can. J. Fish. Aquat. Sci.* **43**, 416-419.

Thamdrup B. and Kuypers M. M. M. (2007) Linking crenarchaeal and bacterial nitrification to

anammox in the Black Sea. *Proc. Natl. Acad. Sci. U.S.A.* **104**, 7104-7109.

Thamdrup B., Canfield D. E., Ferdelman T. G., Glud R. N. and Gundersen J. K. (1996) A biogeochemical survey of the anoxic basin Golfo Dulce, Costa Rica. *Rev. Biol. Trop*. **44**, 19-33.

Thomson D., Rainbird R. H., Planavsky N., Lyons T. W. and Bekker A. (2015) Chemostratigraphy of the Shaler Supergroup, Victoria Island, NW Canada: A record of ocean composition prior to the Cryogenian glaciations. *Precambr. Res*. **263**, 232-245.

Thomson J. (2018) *Iron and Phosphorus Cycling under Ferruginous Conditions*. University of Leeds.

Tonolla M., Demarta A. and Peduzzi R. (1998) The chemistry of Lake Cadagno. In *Lake Cadagno: A meromictic alpine lake*. (eds. Peduzzi R. et al.). Consiglio nazionale delle ricerche, Istituto italiano di idrobiologia, Verbania Pallanza, pp. 11-17.

Tonolla M., Demarta A., Peduzzi R. and Hahn D. (1999) *In situ* analysis of phototrophic sulfur bacteria in the chemocline of meromictic Lake Cadagno (Switzerland). *Appl. Environ. Microbiol.* **65**, 1325-1330.

Tonolla M., Peduzzi S., Hahn D. and Peduzzi R. (2003) Spatiotemporal distribution of phototrophic sulfur bacteria in the chemocline of meromictic Lake Cadagno (Switzerland). *Fems Microbiol. Ecol.* **43**, 89-98.

Tonolla M., Peduzzi S., Demarta A., Peduzzi R. and Hahn,D. (2004) Phototropic sulfur and sulfate-reducing bacteria in the chemocline of meromictic Lake Cadagno, Switzerland. *J. Limnol.* **63**: 161-170.

Turnewitsch R. and Pohl C. (2010) An estimate of the efficiency of the iron- and manganese-driven dissolved inorganic phosphorus trap at an oxic/euxinic water column redoxcline. *Global Biogeochem. Cycles* **24**, GB4025. http://dx.doi.org/10.1029/2010GB003820.

Tosca N. J., Guggenheim S. and Pufahl P. K. (2015) An authigenic origin for Precambrian greenalite: Implications for iron formation and the chemistry of ancient seawater. *Geol. Soc. Am. Bull.*

Tyrrell T. (1999) The relative influences of nitrogen and phosphorus on oceanic primary production. *Nature* **400**, 525-531.

Usman M., Abdelmoula M., Hanna K., Gre´goire B., Faure P. and Ruby C. (2012) Fe^{II} induced mineralogical transformations of ferric oxyhydroxides into magnetite of variable stoichiometry and morphology. J. *Solid State Chem.* **194**, 328-335.

Van Cappellen P. and Berner R. A. (1988) A mathematical model for the early diagenesis of phosphorus and fluorine in marine sediments; apatite precipitation. *Am. J. Sci.* **288**, 289-333.

Van Cappellen P. and Ingall E. D. (1994a) Benthic phosphorus regeneration, net primary production, and ocean anoxia: A model of the coupled marine biogeochemical cycles of carbon and phosphorus. *Paleoceanography* **9**, 677-692.

Van Cappellen P. and Ingall E. D. (1994b) Redox stabilization of the atmosphere by phosphorus-limited marine productivity. *Science* **271**, 493-496.

van de Velde S., Lesven L., Burdorf L. D., Hidalgo-Martinez S., Geelhoed J. S., Van Rijswijk P. Gao Y. and Meysman F. J. R. (2016). The impact of electrogenic sulfur oxidation on the biogeochemistry of coastal sediments: a field study. *Geochim. Cosmochim. Acta* **194**, 211-232.

Verburg P. and Hecky R. E. (2003) Wind patterns, evaporation and related physical variables in Lake Tanganyika. *East Afr J Great Lakes Res* **29**(Suppl 2):48-61.

Viollier E., Hunter K., Roychoudhury A. N. and van Cappellen P. (2000) The ferrozine method revisited: Fe(II)/Fe(III) determination in natural waters. *Appl. Geochem.* **15**, 785-790.

Walker T. W. and Syers J. K. (1976) The fate of phosphorus during pedogenesis. *Geoderma* **15**, 1-19.

Westheimer F. H. (1987) Why nature chose phosphate. *Science* **235**, 1173-1178.

Wheat C. G., Feely R. A. and Mottl M. J. (1996) Phosphate removal by oceanic hydrothermal processes: an update of the phosphorus budget of the oceans. *Geochim. Cosmochim. Acta* **60**, 3593-3608.

Wignall P. B. and Twitchett R. J. (1996) Oceanic anoxia and the End Permian mass extinction. *Science* **272**, 1155-1158.

Wignall P. B., Bond D. P. G., Kuwahara K., Kakuwa Y., Newton R. J. and Poulton S. W. (2010) An 80 million year oceanic redox history from Permian to Jurassic pelagic sediments of the Mino-Tamba terrane, SW Japan, and the origin of four mass extinctions. *Glob. Planet. Chang*. **71**, 109-123.

Wirth S. B., Gilli A., Niemann H., Dahl T. W., Ravasi D., Sax N., Hamann Y., Peduzzi R., Peduzzi S., Tonolla, M., Lehmann, M. F. and Anselmetti F. S. (2013) Combining sedimentological, trace metal (Mn, Mo) and molecular evidence for reconstructing past water-column redox conditions: The example of meromictic Lake Cadagno (Swiss Alps). *Geochim. Cosmochim. Acta* **120**, 220-238.

Yakushev E. V., Chasovnikov V. K., Murray J. W., Pakhomova S. V., Podymov O. I. and Stunzhas P. A. (2008) Vertical hydrochemical Structure of the Black Sea. *Handbook Environ. Chem.* **5**, 277-307.

Zachara J. M., Kukkadapu R. K., Fredrickson J. K., Gorby Y. A., and Smith S. C. (2002) Biomineralization of poorly crystalline Fe(III) oxides by dissimilatory metal reducing bacteria (DMRB). *Geomicrobiol. J.* **19**, 179-207.

Zegeye A., Mustin C. and Jorand F. (2010) Bacterial and iron oxide aggregates mediate secondary iron mineral formation: green rust versus magnetite. *Geobiology* **8**, 209-222.

Zegeye A., Bonneville S., Benning L. G., Sturm A., Fowle D. A., Jones C., Canfield D. E., Ruby C., MacLean L. C., Nomosatryo S., Crowe S. A. and Poulton S. W. (2012) Green rust formation controls nutrient availability in a ferruginous water column. *Geology* **40**, 599-602.

Zerkle A. L., House C., Cox R. and Canfield D. (2006) Metal limitation of cyanobacterial N_2 fixation and implications for the Precambrian nitrogen cycle. *Geobiology* **4**, 285-297.

Zerkle A. L., Claire M., Domagal-Goldman S. D., Farquhar J. and Poulton S. W. (2012) A bistable organic-rich atmosphere on the Neoarchaean Earth. Nat. *Geosci.* **5**, 359-363.

Zhang Y., Jacob D. J., Horowitz H., M., Chen L., Amos H. M., Krabbenhoft D. P., Slemr F., St. Louis V. L. and Sunderland E. M. (2016) Observed decrease in atmospheric mercury explained by global decline in anthropogenic emissions. *Proc. Natl. Acad. Sci. U.S.A.* **113**, 526-531.

Appendix A

A.1 Lake Cadagno

In the euxinic sediment core (Fig. S1a), organic S slightly increases in the shallow sediment from 0 cm to 12 cm to a peak at 2.28%, followed by a sudden decrease from 12 cm to 15 cm, and finally shows a constant decrease with depth to 0.14%. In the chemocline sediment core (Fig. S2a), organic S gradually decreases from 1.03% to 0.52%. Only in the oxic sediment core, the value remains relatively stable at the value <1%. When the organic S is combined with TOC (Fig S2), it shows organic S is varied with the variation of TOC in the euxinic and chemocline cores, however, in the oxic core, the organic S keeps constant. Therefore, organic matter in the oxic conditions is not formed in the presence of dissolved sulfide (porewater), instead, forming in the oxic water column and in the chemocline and euxinic core, the organic S is formed in the euxinic water column.

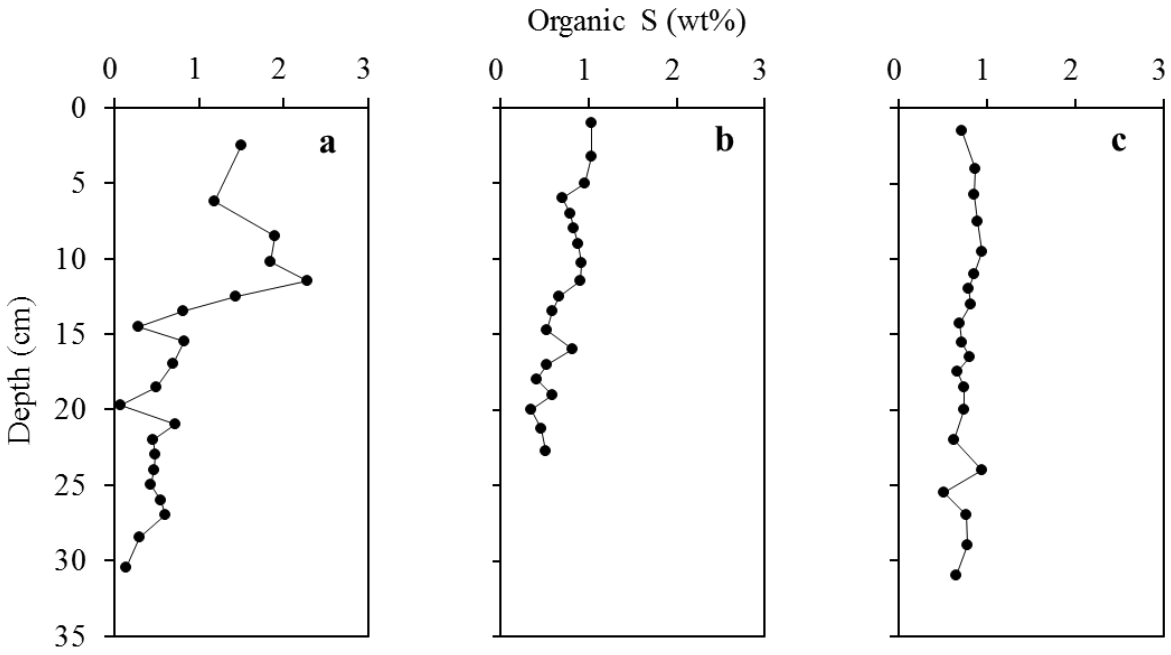

Figure S1.1. Organic S depth profiles for the three sediment cores; a) euxinic core; b) chemocline core; c) oxic core.

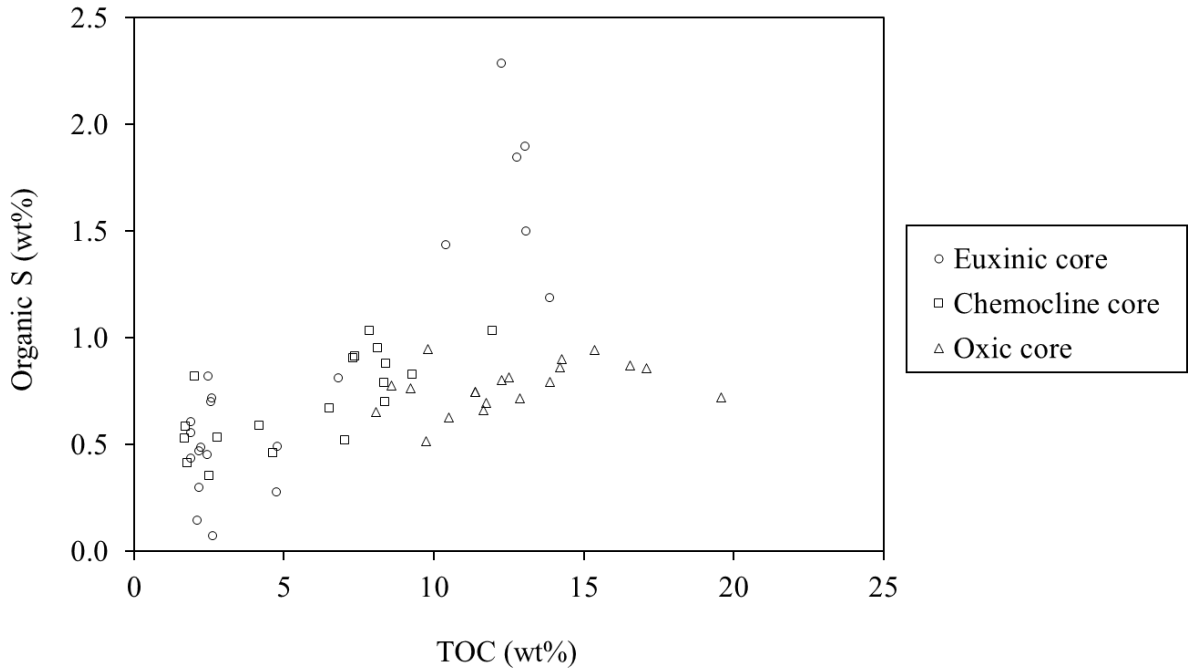

Figure S1.2. The scatter graph of organic S vs TOC in the three different cores.

Table S1.1 Water column dissolved species data.

Water Column					
Sample i.d.	Depth (m)	SO_4^{2-} (μM)	Fe(II) (μM)	S(II) (μM)	P (μM)
WC-A	1	297.37	0.02	0.07	0.09
WC-B	5	343.59	0.07	0.07	0.04
WC-C	10	794.96	0.00	0.00	0.16
WC-D	10.5	901.54	0.07	0.15	0.28
WC-E	11	1177.00	0.15	0.07	0.01
WC-F	11.3	950.49	0.09	0.00	0.12
WC-G	11.6	908.22	0.34	0.22	0.05
WC-H	11.9	962.42	1.11	16.51	0.07
WC-I	12.2	977.24	0.86	19.59	0.30
WC-J	12.5	975.57	0.60	34.28	0.34
WC-K	13	1184.09	0.97	47.33	0.89
WC-L	14	1008.52	0.66	65.29	1.48
WC-M	16	1043.90	0.39	58.76	1.75
WC-N	18	1298.96	0.81	70.18	2.01

Table S1.2 Water content data in the porewater.

Euxinic Core		
Sample i.d.	Depth (cm)	Water content (% wet weight)
1	0-2	94.24
2	2-3	92.42
3	3-4	85.04
4	4-5	82.66
5	5-6	80.78
6	6-7	78.50
7	7-8	78.14
8	8-9	78.95
9	9-10	77.57
10	10-11	76.97
11	11-12	76.59
12	12-13.5	59.82
13	13.5-14.5	51.96
14	14.5-15.5	46.03
15	15.5-17	48.27
16	17-18.5	57.45
17	18.5-19.5	70.55
18	19.5-20.5	72.73
19	20.5-21.5	74.50
20	21.5-22.5	73.68
21	22.5-23	72.99
Chemocline Core		
Sample i.d.	Depth (cm)	Water content (% wet weight)
1	0-2	97.01

2	2-4	96.98
3	4-6	96.89
4	6-8	96.07
5	8-9	94.31
6	9-10	93.44
7	10-11.2	92.21
8	11.2-12.4	89.71
9	12.4-13.6	81.77
10	13.6-14.8	71.59
11	14.8-16	73.30
12	16-17.2	72.53
13	17.2-18.4	66.27
14	18.4-19	59.01
15	19-20	56.36
16	20-21	55.19
17	21-21.5	52.98
18	21.5-22.5	50.72
19	22.5-23.5	49.50
20	23.5-25	51.17
21	25-26	53.60
22	26-27	54.67
23	27-28	49.44
24	28-29	48.68
25	29-30	48.29

Table S1.3 Sulfate data in the porewater.

Euxinic Core		
Sample i.d.	Depth (cm)	SO_4^{2-} (μM)
1	1-2.5	471.55
2	2.5-4	496.86
3	4-5.5	451.01
4	5.5-7.5	534.37
5	7.5-10	467.22
6	10-12.5	205.97
7	12.5-15	105.59
8	15-17.5	75.20
9	17.5-19	90.01
10	19-20.5	88.88
11	20.5-22	85.99
12	22-23.5	81.74
13	23.5-25	36.39
14	25-27.5	0.00
15	27.5-30.5	0.00
Chemocline Core		
Sample i.d.	Depth (cm)	SO_4^{2-} (μM)
1	2-4	1026.88
2	4-6	900.73
3	6-8	560.30
4	8-10	470.34
5	10-12	217.74
6	12-14	103.51
7	14-16	114.65
8	16-18	53.30
9	18-20	85.63

10	20-22	24.21
11	22-24	29.58

Oxic Core

Sample i.d.	Depth (cm)	SO_4^{2-} (μM)
1	0-2	164.57
2	2-4	88.42
3	4-6	70.71
4	6-8	85.53
5	8-10	73.18
6	10-12	54.41
7	12-14	31.58
8	14-16.5	20.72
9	16.5-18.5	23.29
10	18.5-20.5	13.77
11	20.5-22.5	9.92
12	22.5-24.5	11.24
13	24.5-26.5	12.42
14	26.5-28.5	27.51

Table S1.4 Porewater data for the different dissolved species. ND = not determined.

Euxinic Core						
Sample i.d.	Depth (cm)	pH	DIC (mM)	S(II) (μM)	Fe(II) (μM)	P (μM)
1	0-5	7.62	4.09	778.54	0.13	46.03
2	5-7.5	7.72	3.69	682.24	0.09	36.57
3	7.5-9.5	7.96	4.31	832.40	0.08	49.76
4	9.5-11	8.11	4.49	899.32	0.11	52.49
5	11-12	8.2	4.76	789.96	0.10	55.23
6	12-13	8.34	4.95	889.52	0.15	54.73
7	13-14	8.43	5.15	799.76	0.15	54.98
8	14-15	8.42	5.26	767.11	0.24	53.74
9	15-16	8.43	5.41	688.77	0.20	53.99
10	16-18	8.42	5.42	550.04	0.57	52.25
11	18-19	8.41	5.45	432.52	0.99	52.25
12	19-20.5	8.45	5.57	367.23	0.73	51.00
13	20.5-21.5	8.38	5.41	117.52	1.22	48.76
14	21.5-22.5	8.42	5.46	89.77	0.70	48.51
15	22.5-23.5	8.43	5.41	84.87	0.77	48.27
16	23.5-24.5	8.44	5.37	44.07	0.93	46.27
17	24.5-25.5	8.41	5.43	24.48	0.65	46.77
18	25.5-26.5	8.45	5.28	6.15	0.83	42.54
19	26.5-27.5	8.43	5.46	ND	2.41	42.54
20	27.5-29.5	8.44	5.32	2.33	23.50	45.28
21	29.5-31.5	8.46	5.39	2.18	33.88	43.79
Chemocline Core						
Sample i.d.	Depth (cm)	pH	DIC (mM)	S(II) (μM)	Fe(II) (μM)	P (μM)
1	0-2	ND	ND	488.01	0.17	17.52

2	2-4.5	ND	ND	ND	0.18	19.83
3	4.5-5.5	ND	ND	319.90	0.10	21.02
4	5.5-6.5	ND	ND	311.74	0.26	20.66
5	6.5-7.5	ND	ND	362.34	0.44	20.55
6	7.5-8.5	ND	ND	282.36	0.21	20.76
7	8.5-9.5	ND	ND	332.96	0.32	19.68
8	9.5-11	ND	ND	332.96	0.28	19.11
9	11-12	ND	ND	301.95	0.24	18.04
10	12-13	ND	ND	167.09	0.14	17.16
11	13-14	ND	ND	ND	0.11	16.19
12	14-15.5	ND	ND	ND	0.26	16.44
13	15.5-16.5	ND	ND	150.46	0.16	16.55
14	16.5-17.5	ND	ND	130.56	0.38	14.93
15	17.5-18.5	ND	ND	153.35	0.17	14.44
16	18.5-19.5	ND	ND	139.24	0.13	14.75
17	19.5-20.5	ND	ND	167.09	0.19	12.79
18	20.5-22	ND	ND	111.76	0.15	12.90
19	22-23.5	ND	ND	70.16	0.33	11.92

Oxic Core

Sample i.d.	Depth (cm)	pH	DIC (mM)	S(II) (μM)	Fe(II) (μM)	P (μM)
1	0-3	ND	ND	224.24	0.65	27.37
2	3-5	ND	ND	242.68	0.46	39.31
3	5-6.5	ND	ND	260.04	0.38	41.55
4	6.5-8.5	ND	ND	201.81	0.67	41.55
5	8.5-10.5	ND	ND	212.30	0.48	39.06
6	10.5-11.5	ND	ND	243.40	0.44	36.32
7	11.5-12.5	ND	ND	219.17	0.45	35.08
8	12.5-13.5	ND	ND	243.77	0.39	36.32
9	13.5-15	ND	ND	244.49	0.38	35.33

10	15-16	ND	ND	249.55	0.45	34.58
11	16-17	ND	ND	249.55	0.35	34.08
12	17-18	ND	ND	268.36	0.33	34.33
13	18-19	ND	ND	244.85	0.35	35.83
14	19-21	ND	ND	273.06	0.41	35.08
15	21-23	ND	ND	252.08	0.21	37.32
16	23-25	ND	ND	213.75	0.33	37.07
17	25-26	ND	ND	196.75	0.24	38.31
18	26-28	ND	ND	183.73	0.28	38.06
19	28-30	ND	ND	216.28	0.23	39.31
20	30-32	ND	ND	203.98	0.41	39.56

Table S1.5 Bulk element data in the sediments.

Euxinic Core								
Sample i.d.	Depth (cm)	TIC (wt%)	TOC (wt%)	TS (wt%)	Total Fe (wt%)	Total Al (wt%)	Total Ti (wt%)	Total P (wt%)
1	0-5	2.25	13.08	2.65	3.94	4.40	0.22	0.121
2	5-7.5	1.83	13.88	2.21	3.62	4.35	0.22	0.155
3	7.5-9.5	2.46	13.06	2.56	3.87	4.32	0.23	0.127
4	9.5-11	1.35	12.78	2.96	4.68	4.81	0.26	0.122
5	11-12	2.71	12.27	3.53	4.71	4.62	0.26	0.115
6	12-13	1.14	10.40	3.77	5.50	5.23	0.28	0.108
7	13-14	1.63	6.81	3.05	4.83	5.37	0.28	0.092
8	14-15	1.38	4.77	2.67	5.69	6.90	0.39	0.107
9	15-16	1.42	2.48	2.20	5.37	7.94	0.43	0.094
10	16-18	0.40	2.56	2.24	5.97	8.55	0.46	0.119
11	18-19	0.00	4.79	3.67	6.91	7.20	0.37	0.098
12	19-20.5	0.09	2.62	3.31	7.26	8.24	0.43	0.151
13	20.5-21.5	0.24	2.60	3.91	8.04	9.07	0.43	0.152
14	21.5-22.5	0.30	2.45	3.30	7.24	9.00	0.43	0.152
15	22.5-23.5	0.52	2.24	2.72	7.28	9.07	0.47	0.161
16	23.5-24.5	0.56	2.17	2.47	6.78	9.13	0.45	0.148
17	24.5-25.5	0.82	1.90	2.23	6.64	9.76	0.45	0.150
18	25.5-26.5	0.43	1.89	1.35	6.30	9.16	0.46	0.150
19	26.5-27.5	0.52	1.91	0.80	6.05	8.96	0.46	0.157

20	27.5-29.5	0.96	2.16	0.46	5.74	9.85	0.44	0.143
21	29.5-31.5	0.39	2.11	0.29	5.34	9.46	0.49	0.140

Chemocline Core

Sample i.d.	Depth (cm)	TIC (wt%)	TOC (wt%)	TS (wt%)	Total Fe (wt%)	Total Al (wt%)	Total Ti (wt%)	Total P (wt%)
1	0-2	1.56	11.96	2.34	4.15	5.94	0.29	0.151
2	2-4.5	2.36	7.85	2.39	4.78	6.73	0.32	0.108
3	4.5-5.5	1.74	8.14	2.38	4.77	6.86	0.34	0.100
4	5.5-6.5	0.69	8.37	2.26	4.65	6.65	0.33	0.094
5	6.5-7.5	0.95	8.34	2.32	4.83	6.63	0.33	0.098
6	7.5-8.5	0.33	9.29	2.37	4.70	6.40	0.34	0.098
7	8.5-9.5	0.80	8.41	2.19	4.64	6.67	0.35	0.112
8	9.5-11	1.25	7.37	2.10	4.54	6.89	0.35	0.098
9	11-12	1.05	7.30	2.02	4.36	6.65	0.34	0.096
10	12-13	0.82	6.51	1.95	4.52	7.02	0.35	0.097
11	13-14	0.73	4.17	1.97	5.09	8.17	0.39	0.098
12	14-15.5	0.77	2.78	2.09	5.46	8.94	0.41	0.113
13	15.5-16.5	0.04	2.03	1.96	5.92	8.59	0.41	0.136
14	16.5-17.5	0.28	1.70	1.97	6.11	9.04	0.44	0.143
15	17.5-18.5	0.20	1.78	1.97	6.21	8.47	0.45	0.146
16	18.5-19.5	0.37	1.73	1.87	6.06	8.97	0.46	0.128
17	19.5-20.5	0.37	2.52	1.76	5.51	8.80	0.47	0.114
18	20.5-22	0.34	4.65	1.71	4.71	7.48	0.40	0.094

19	22-23.5	0.81	7.03	1.78	4.32	7.09	0.37	0.094

Oxic Core

Sample i.d.	Depth (cm)	TIC (wt%)	TOC (wt%)	TS (wt%)	Total Fe (wt%)	Total Al (wt%)	Total Ti (wt%)	Total P (wt%)
1	0-3	3.91	19.59	1.87	2.69	3.41	0.18	0.300
2	3-5	2.88	16.56	2.03	3.20	4.24	0.23	0.195
3	5-6.5	2.41	17.09	2.04	3.30	4.53	0.24	0.214
4	6.5-8.5	3.47	14.27	2.02	3.30	4.51	0.24	0.214
5	8.5-10.5	2.00	15.36	2.29	3.60	5.07	0.27	0.116
6	10.5-11.5	1.40	14.21	2.36	3.83	5.09	0.29	0.171
7	11.5-12.5	1.00	13.87	2.20	3.76	5.13	0.29	0.125
8	12.5-13.5	1.44	12.49	2.09	3.78	5.03	0.30	0.112
9	13.5-15	1.59	11.74	2.08	3.81	5.28	0.30	0.109
10	15-16	0.51	12.89	2.09	3.79	5.09	0.30	0.109
11	16-17	1.38	12.27	2.19	3.91	5.19	0.30	0.107
12	17-18	1.20	11.66	2.05	3.74	5.09	0.30	0.104
13	18-19	1.78	11.38	2.17	4.01	5.79	0.32	0.105
14	19-21	0.77	11.37	2.12	4.01	5.66	0.32	0.099
15	21-23	0.95	10.51	2.09	4.13	5.68	0.33	0.097
16	23-25	1.45	9.81	2.00	3.98	5.81	0.34	0.092
17	25-26	0.34	9.75	1.88	4.13	6.34	0.36	0.090
18	26-28	1.62	9.22	2.00	4.10	6.31	0.37	0.095
19	28-30	1.04	8.60	1.82	4.15	6.39	0.37	0.089
20	30-32	1.40	8.07	1.86	4.23	6.48	0.39	0.090

Table S1.6 Fe speciation data in the sediments.

Euxinic Core							
Sample i.d.	Depth (cm)	$Fe(II)_{unsulf}$ (wt%)	Fe_{ox1} (wt%)	Fe_{ox2} (wt%)	Fe_{mag} (wt%)	Fe_{AVS} (wt%)	Fe_{py} (wt%)
1	0-5	1.560	0.020	0.738	0.023	0.257	0.880
2	5-7.5	0.811	0.403	0.549	0.037	0.128	0.826
3	7.5-9.5	1.824	0.000	0.773	0.041	0.138	0.511
4	9.5-11	1.677	0.000	0.961	0.130	0.379	0.789
5	11-12	0.770	0.360	0.830	0.234	0.088	1.041
6	12-13	0.791	0.000	1.077	0.570	0.220	1.928
7	13-14	0.734	0.000	1.119	0.471	0.076	1.918
8	14-15	0.259	0.000	1.098	0.502	0.214	1.979
9	15-16	0.340	0.032	0.880	0.364	0.010	1.198
10	16-18	0.336	0.000	0.776	0.477	0.053	1.318
11	18-19	0.187	0.000	0.981	0.554	0.201	2.677
12	19-20.5	0.367	0.000	0.990	0.668	0.064	2.797
13	20.5-21.5	0.471	0.000	0.891	0.239	0.044	2.767
14	21.5-22.5	0.535	0.000	1.135	0.486	0.038	2.470
15	22.5-23.5	0.530	0.000	0.981	0.233	0.007	1.949
16	23.5-24.5	0.523	0.034	0.942	0.238	0.007	1.746
17	24.5-25.5	0.613	0.000	0.903	0.152	0.018	1.557
18	25.5-26.5	0.912	0.000	0.949	0.133	0.188	0.602
19	26.5-27.5	0.924	0.000	1.013	0.151	0.087	0.121
20	27.5-29.5	0.831	0.000	1.151	0.187	0.026	0.126

21	29.5-31.5	0.771	0.000	1.086	0.167	0.006	0.122

Chemocline Core

Sample i.d.	Depth (cm)	$Fe(II)_{unsulf}$ (wt%)	Fe_{ox1} (wt%)	Fe_{ox2} (wt%)	Fe_{mag} (wt%)	Fe_{AVS} (wt%)	Fe_{py} (wt%)
1	0-2	0.565	0.043	0.767	0.085	0.197	1.043
2	2-4.5	0.573	0.000	0.706	0.129	0.127	1.120
3	4.5-5.5	0.624	0.000	0.713	0.096	0.092	1.201
4	5.5-6.5	0.486	0.000	0.717	0.087	0.188	1.266
5	6.5-7.5	0.465	0.000	0.763	0.084	0.148	1.266
6	7.5-8.5	0.415	0.000	0.795	0.102	0.148	1.271
7	8.5-9.5	0.400	0.000	0.755	0.082	0.127	1.078
8	9.5-11	0.525	0.000	0.730	0.079	0.054	1.005
9	11-12	0.535	0.000	0.727	0.075	0.026	0.959
10	12-13	0.432	0.000	0.765	0.098	0.139	1.051
11	13-14	0.355	0.078	0.785	0.068	0.100	1.156
12	14-15.5	0.306	0.003	0.812	0.087	0.081	1.323
13	15.5-16.5	0.307	0.033	0.780	0.086	0.024	0.987
14	16.5-17.5	0.264	0.103	0.927	0.099	0.011	1.248
15	17.5-18.5	0.206	0.067	0.794	0.091	0.057	1.328
16	18.5-19.5	0.281	0.063	0.760	0.070	0.024	1.108
17	19.5-20.5	0.212	0.101	0.847	0.068	0.047	1.206
18	20.5-22	0.228	0.121	0.772	0.051	0.045	1.067
19	22-23.5	0.193	0.150	0.748	0.049	0.064	1.068

Oxic Core

Sample i.d.	Depth (cm)	$Fe(II)_{unsulf}$ (wt%)	Fe_{ox1} (wt%)	Fe_{ox2} (wt%)	Fe_{mag} (wt%)	Fe_{AVS} (wt%)	Fe_{py} (wt%)
1	0-3	0.254	0.216	0.579	0.041	0.624	0.689
2	3-5	0.410	0.182	0.608	0.027	0.436	0.791
3	5-6.5	0.402	0.227	0.684	0.031	0.430	0.818
4	6.5-8.5	0.375	0.138	0.682	0.026	0.393	0.777
5	8.5-10.5	0.426	0.133	0.730	0.022	0.314	1.019
6	10.5-11.5	0.286	0.103	0.734	0.022	0.290	1.164
7	11.5-12.5	0.315	0.069	0.700	0.026	0.269	1.098
8	12.5-13.5	0.258	0.055	0.774	0.024	0.208	1.004
9	13.5-15	0.242	0.073	0.771	0.026	0.194	1.112
10	15-16	0.160	0.099	0.691	0.032	0.206	1.097
11	16-17	0.254	0.114	0.681	0.024	0.196	1.111
12	17-18	0.213	0.141	0.765	0.106	0.204	1.113
13	18-19	0.281	0.093	0.711	0.115	0.178	1.158
14	19-21	0.334	0.158	0.737	0.111	0.082	1.161
15	21-23	0.263	0.122	0.721	0.114	0.160	1.196
16	23-25	0.222	0.129	0.729	0.116	0.105	0.870
17	25-26	0.264	0.142	0.785	0.119	0.126	1.131
18	26-28	0.217	0.140	0.704	0.128	0.146	1.004
19	28-30	0.335	0.099	0.761	0.161	0.085	0.872
20	30-32	0.240	0.083	0.749	0.131	0.162	0.975

Table S1.7 P speciation data in the sediments.

Euxinic Core						
Sample i.d.	Depth (cm)	P_{sorb} (wt%)	P_{Fe} (wt%)	P_{auth} (wt%)	P_{detr} (wt%)	P_{org} (wt%)
1	0-5	0.0000	0.0135	0.0107	0.0111	0.0506
2	5-7.5	0.0000	0.0232	0.0108	0.0144	0.0584
3	7.5-9.5	0.0000	0.0152	0.0107	0.0118	0.0519
4	9.5-11	0.0000	0.0149	0.0060	0.0160	0.0517
5	11-12	0.0001	0.0106	0.0043	0.0168	0.0478
6	12-13	0.0001	0.0079	0.0051	0.0256	0.0454
7	13-14	0.0001	0.0053	0.0040	0.0277	0.0318
8	14-15	0.0001	0.0046	0.0041	0.0377	0.0359
9	15-16	0.0001	0.0025	0.0019	0.0695	0.0145
10	16-18	0.0001	0.0042	0.0022	0.0783	0.0152
11	18-19	0.0001	0.0042	0.0041	0.0461	0.0307
12	19-20.5	0.0011	0.0129	0.0046	0.0748	0.0280
13	20.5-21.5	0.0017	0.0202	0.0055	0.0820	0.0234
14	21.5-22.5	0.0020	0.0217	0.0055	0.0816	0.0218
15	22.5-23.5	0.0019	0.0233	0.0055	0.0816	0.0203
16	23.5-24.5	0.0021	0.0257	0.0044	0.0798	0.0188
17	24.5-25.5	0.0004	0.0264	0.0047	0.0825	0.0191
18	25.5-26.5	0.0000	0.0240	0.0036	0.0875	0.0161
19	26.5-27.5	0.0001	0.0240	0.0030	0.0840	0.0152
20	27.5-29.5	0.0002	0.0336	0.0040	0.0713	0.0195
21	29.5-31.5	0.0004	0.0315	0.0039	0.0704	0.0177
Chemocline Core						
Sample i.d.	Depth (cm)	P_{sorb} (wt%)	P_{Fe} (wt%)	P_{auth} (wt%)	P_{detr} (wt%)	P_{org} (wt%)
1	0-2	0.0001	0.0250	0.0110	0.0220	0.0536

2	2-4.5	0.0000	0.0066	0.0110	0.0297	0.0351
3	4.5-5.5	0.0000	0.0054	0.0112	0.0277	0.0325
4	5.5-6.5	0.0000	0.0044	0.0109	0.0298	0.0332
5	6.5-7.5	0.0000	0.0051	0.0098	0.0294	0.0357
6	7.5-8.5	0.0000	0.0042	0.0090	0.0347	0.0327
7	8.5-9.5	0.0000	0.0038	0.0095	0.0306	0.0345
8	9.5-11	0.0000	0.0039	0.0103	0.0322	0.0324
9	11-12	0.0000	0.0033	0.0098	0.0338	0.0326
10	12-13	0.0000	0.0028	0.0102	0.0388	0.0306
11	13-14	0.0000	0.0019	0.0053	0.0533	0.0250
12	14-15.5	0.0000	0.0022	0.0035	0.0715	0.0200
13	15.5-16.5	0.0001	0.0067	0.0037	0.0816	0.0209
14	16.5-17.5	0.0002	0.0083	0.0041	0.0881	0.0211
15	17.5-18.5	0.0002	0.0097	0.0043	0.0816	0.0203
16	18.5-19.5	0.0003	0.0100	0.0047	0.0726	0.0208
17	19.5-20.5	0.0002	0.0090	0.0052	0.0550	0.0195
18	20.5-22	0.0001	0.0037	0.0089	0.0432	0.0219
19	22-23.5	0.0000	0.0026	0.0117	0.0314	0.0295

Oxic Core

Sample i.d.	Depth (cm)	P_{sorb} (wt%)	P_{Fe} (wt%)	P_{auth} (wt%)	P_{detr} (wt%)	P_{org} (wt%)
1	0-3	0.0026	0.0978	0.0147	0.0081	0.0799
2	3-5	0.0002	0.0452	0.0159	0.0112	0.0735
3	5-6.5	0.0002	0.0419	0.0156	0.0118	0.0708
4	6.5-8.5	0.0001	0.0317	0.0152	0.0129	0.0674
5	8.5-10.5	0.0001	0.0276	0.0142	0.0135	0.0655
6	10.5-11.5	0.0001	0.0171	0.0117	0.0125	0.0573
7	11.5-12.5	0.0001	0.0134	0.0103	0.0132	0.0565
8	12.5-13.5	0.0001	0.0118	0.0106	0.0143	0.0509
9	13.5-15	0.0001	0.0112	0.0102	0.0121	0.0511

10	15-16	0.0000	0.0108	0.0092	0.0124	0.0510
11	16-17	0.0001	0.0092	0.0092	0.0140	0.0483
12	17-18	0.0001	0.0092	0.0110	0.0143	0.0495
13	18-19	0.0001	0.0085	0.0106	0.0153	0.0467
14	19-21	0.0001	0.0078	0.0119	0.0154	0.0456
15	21-23	0.0001	0.0066	0.0129	0.0177	0.0432
16	23-25	0.0001	0.0058	0.0132	0.0200	0.0399
17	25-26	0.0001	0.0048	0.0121	0.0214	0.0367
18	26-28	0.0001	0.0052	0.0129	0.0211	0.0373
19	28-30	0.0000	0.0045	0.0105	0.0206	0.0376
20	30-32	0.0001	0.0043	0.0110	0.0222	0.0354

A.2 Lake La Cruz

Table S2.1 Water column dissolved species data.

Sample i.d.	Depth (m)	SO_4^{2-} (μM)	Fe(II) (μM)	S(II) (μM)	P (μM)
WC 1	4	31.44	0	0	0
WC 2	6.5	24.83	0.13	0.06	0
WC 3	9	19.63	0	0	0
WC 4	10	28.94	0.06	0	0
WC 5	10.5	28.73	0..06	0.06	0
WC 6	11	28.68	0.06	0	0
WC 7	11.5	9.42	0	0	0
WC 8	12.5	31.27	0.06	0	0
WC 9	14	19.09	1.2	0.12	0
WC 10	15	7.59	9.12	0.12	0.04
WC 11	16	2.45	19.38	0.18	0
WC 12	17	4.53	67.95	2.33	0
WC 13	17.5	3.83	144.08	0.49	0.04
WC 14	18	6.86	241.61	3.56	0.72
WC 15	19	4.40	252.3	3.68	2.54

Table S2.2 Water content data in the porewater

Sample i.d.	Depth (cm)	Water content (% wet weight)
1	1.2	95.27
2	2.2	92.82
3	3.2	85.76
4	4.25	84.14
5	5.35	77.73
6	6.5	77.14
7	7.6	78.72
8	8.6	78.25
9	9.6	78.92
10	10.6	78.92
11	11.6	78.92
12	12.7	79.58
13	13.7	81.27
14	14.7	80.96
15	15.7	81.21
16	16.7	80.86
17	17.7	79.81
18	18.7	80.75
19	19.8	80.20
20	20.95	79.45
21	22.05	79.08
22	23.15	79.54
23	24.25	80.61
24	25.4	79.65
25	26.55	79.92
26	27.65	80.02
27	29.75	80.02

28	31.25	80.02
29	32.75	80.02
30	34.5	80.02

Table S2.3 Basic parameter of sediments

Sample i.d.	Depth (m)	Density （g/ml）	Porosity	Sedimentary rate (mm/y)
1	0.75	2.21	0.98	5
2	2.5	2.40	0.97	5
3	4.25	2.58	0.93	5
4	5.75	2.54	0.90	5
5	7.25	2.54	0.90	5
6	8.75	2.52	0.90	5
7	10.25	2.56	0.91	5
8	11.75	2.56	0.91	1.5
9	13.25	2.60	0.92	1.5
10	14.75	2.59	0.92	1.5
11	16.25	2.59	0.92	1.5
12	17.75	2.59	0.91	1
13	19.25	2.49	0.91	1
14	20.75	2.49	0.91	1
15	22.25	2.49	0.90	1
16	23.75	2.40	0.91	1
17	25.25	2.33	0.90	1
18	26.75	2.33	0.90	1
19	28.25	2.33	0.90	1
20	29.75	2.25	0.90	1
21	31.25	2.25	0.90	1
22	32.75	2.25	0.90	1
23	34.5	2.25	0.90	1

Table S2.4 Porewater data for the different dissolved species. ND = not determined.

Sample i.d.	Depth (cm)	Sulfate (μM)	S(II) (μM)	P (μM)	Fe(II) (μM)
1	0.75	8.90	1.29	5.80	197.57
2	2.5	6.22	1.66	7.77	237.83
3	4.25	2.25	1.47	10.35	245.38
4	5.75	1.21	1.29	12.28	271.81
5	7.25	1.24	1.17	15.97	281.88
6	8.75	1.27	1.23	15.71	276.84
7	10.25	1.38	0.49	17.11	237.83
8	11.75	1.57	0.55	22.37	328.44
9	13.25	1.05	0.61	21.98	280.62
10	14.75	0.78	0.92	27.31	353.60
11	16.25	1.23	0.49	23.30	315.85
12	17.75	2.18	0.43	27.46	367.45
13	19.25	2.03	2.52	26.56	359.90
14	20.75	ND	3.13	26.31	387.58
15	22.25	ND	0.80	21.91	359.90
16	23.75	1.43	0.18	24.84	432.88
17	25.25	ND	0.61	23.84	470.63
18	26.75	ND	0.67	ND	509.64
19	28.25	ND	0.25	21.23	419.04
20	29.75	ND	0.37	19.90	410.23
21	31.25	1.00	0.31	23.73	529.78
22	32.75	ND	0.43	17.18	502.09
23	34.5	ND	1.10	ND	485.73

Table S2.5 TOC and TIC in the sediments.

Sample i.d.	Depth (cm)	TOC (wt%)	TIC (wt%)
1	0.75	7.43	9.64
2	2.5	4.49	11.22
3	4.25	4.94	10.53
4	5.75	3.65	11.78
5	7.25	4.74	9.99
6	8.75	5.52	9.85
7	10.25	6.04	9.36
8	11.75	5.37	9.60
9	13.25	5.85	10.21
10	14.75	5.30	10.68
11	16.25	6.74	8.59
12	17.75	6.22	9.88
13	19.25	5.36	9.91
14	20.75	3.90	10.22
15	22.25	7.12	8.87
16	23.75	8.86	8.90
17	25.25	ND	ND
18	26.75	ND	9.50
19	28.25	8.73	8.93
20	29.75	8.50	8.74
21	31.25	9.25	8.55
22	32.75	8.73	8.80
23	34.5	9.34	8.91

Table S2.6 P speciation data in the sediments. ND = not determined.

Sample i.d.	Depth (cm)	P_{sorb} (wt%)	P_{Fe} (wt%)	P_{auth} (wt%)	P_{detr} (wt%)	P_{org} (wt%)
1	0.75	0.0018	0.017	0.008	0.0025	0.013
2	2.5	0.0015	0.013	0.007	0.0028	0.009
3	4.25	0.0015	0.010	0.006	0.0028	0.007
4	5.75	0.0013	0.011	0.007	0.0028	0.011
5	7.25	0.0011	0.011	0.007	0.0035	0.009
6	8.75	0.0009	0.012	0.009	0.0050	0.013
7	10.25	0.0010	0.010	0.009	0.0038	0.013
8	11.75	0.0011	0.011	0.009	0.0034	0.009
9	13.25	0.0009	0.011	0.009	0.0036	0.013
10	14.75	ND	0.012	0.008	0.0033	0.011
11	16.25	0.0013	0.012	0.011	0.0053	0.011
12	17.75	0.0010	0.013	0.009	0.0034	0.013
13	19.25	0.0012	0.014	0.008	0.0037	0.012
14	20.75	0.0012	0.009	0.009	0.0051	0.009
15	22.25	0.0011	0.015	0.010	0.0033	0.012
16	23.75	0.0015	0.019	0.009	0.0027	0.017
17	25.25	0.0015	0.016	0.008	0.0031	0.013
18	26.75	0.0016	0.016	0.008	0.0030	0.013
19	28.25	0.0014	0.020	0.010	0.0026	0.017
20	29.75	0.0013	0.016	0.010	0.0031	0.017
21	31.25	0.0014	0.022	0.010	0.0030	0.017
22	32.75	0.0014	0.022	0.010	0.0027	0.017
23	34.5	0.0014	0.024	0.010	0.0025	0.018

A.3 Golfo Dulce

Table S3.1 Porewater data for the different dissolved species. ND = not determined.

Sample i.d.	Depth (m)	NH_4^+ (μM)	Fe(II) (μM)	S(II) (μM)	P (μM)
1	0-2	55.07	65.12	0.00	1.38
2	2-4	155.16	ND	0.00	ND
3	4-6	188.81	173.90	0.00	4.79
4	6-8	226.84	216.08	0.00	ND
5	8-10	262.24	229.40	0.00	7.87
6	10-12	246.50	238.28	0.00	6.49
7	12-14	257.87	238.28	0.00	8.83
8	14-16	ND	226.44	0.00	16.60
9	16-18	250.44	233.47	0.00	21.38
10	18-20	236.01	240.50	0.00	26.06
11	20-22	ND	247.90	0.00	ND
12	22-24	ND	247.90	0.00	ND
13	24-26	ND	262.70	0.00	ND
14	26-28	ND	ND	0.00	ND

Table S3.2 Water content data in the porewater

Sample i.d.	Depth (cm)	Water content (% wet weight)
1	0-2	75.82
2	2-4	52.52
3	4-6	56.80
4	6-8	52.70
5	8-10	58.10
6	10-12	58.98
7	12-14	51.68
8	14-16	53.64
9	16-18	55.06
10	18-20	51.09
11	20-22	46.61
12	22-24	45.18
13	24-26	46.21
14	26-28	46.82

Table S3.3 Basic parameter of sediments

Sample i.d.	Depth (cm)	Density (g/ml）	Porosity
1	0-2	2.06	0.87
2	2-4	2.12	0.70
3	4-6	2.17	0.74
4	6-8	2.11	0.70
5	8-10	2.05	0.74
6	10-12	2.02	0.74
7	12-14	1.98	0.68
8	14-16	2.02	0.70
9	16-18	2.06	0.72
10	18-20	2.02	0.68
11	20-22	1.97	0.63
12	22-24	2.00	0.62
13	24-26	2.02	0.63
14	26-28	2.02	0.64

Table S3.4 TOC and TIC in the sediments.

Sample i.d.	Depth (cm)	TOC (wt%)	TIC (wt%)
1	0-2	1.02	0.74
2	2-4	0.92	0.46
3	4-6	1.00	0.58
4	6-8	0.96	0.58
5	8-10	1.13	0.54
6	10-12	1.29	0.56
7	12-14	1.00	0.51
8	14-16	1.42	0.50
9	16-18	1.06	0.61
10	18-20	0.81	0.46
11	20-22	0.75	0.47
12	22-24	1.15	0.36
13	24-26	1.52	0.34
14	26-28	0.94	0.43

Table S3.5 P speciation data in the sediments. ND = not determined.

Sample i.d.	Depth (cm)	P_{sorb} (wt%)	P_{Fe} (wt%)	P_{auth} (wt%)	P_{detr} (wt%)	P_{org} (wt%)
1	0-2	0.0008	0.011	0.015	0.034	0.011
2	2-4	0.0009	0.012	0.016	0.033	0.011
3	4-6	0.0015	0.015	0.020	0.029	0.010
4	6-8	0.0012	0.014	0.019	0.030	0.011
5	8-10	0.0013	0.015	0.019	0.029	0.014
6	10-12	0.0014	0.015	0.020	0.026	0.014
7	12-14	0.0011	0.013	0.016	0.032	0.011
8	14-16	0.0017	0.017	0.023	0.025	0.014
9	16-18	0.0014	0.016	0.018	0.028	0.011
10	18-20	0.0009	0.013	0.013	0.035	0.010
11	20-22	0.0014	0.015	0.015	0.035	0.008
12	22-24	0.0019	0.017	0.015	0.031	0.009
13	24-26	0.0015	0.015	0.015	0.031	0.011
14	26-28	0.0022	0.017	0.014	0.035	0.009